EPA/635/R-23/056b
External Review Draft
www.epa.gov/iris

IRIS Toxicological Review of Perfluorodecanoic Acid [PFDA, CASRN 335-76-2] and Related Salts

Supplemental Information

April 2023

Integrated Risk Information System
Center for Public Health and Environmental Assessment
Office of Research and Development
U.S. Environmental Protection Agency
Washington, DC

DISCLAIMER

This document is an external review draft for review purposes only. This information is distributed solely for the purpose of predissemination peer review under applicable information quality guidelines. It has not been formally disseminated by EPA. It does not represent and should not be construed to represent any Agency determination or policy. Mention of trade names or commercial products does not constitute endorsement or recommendation for use.

CONTENTS

TABLES

FIGURES

ABBREVIATIONS AND ACRONYMS

AC50	activity concentration at 50%
ADME	absorption, distribution, metabolism, and excretion
AIC	Akaike's information criterion
ALT	alanine aminotransferase
AOP	adverse outcome pathway
AST	aspartate aminotransferase
atm	atmosphere
ATSDR	Agency for Toxic Substances and Disease Registry
BMC	benchmark concentration
BMCL	benchmark concentration lower confidence limit
BMD	benchmark dose
BMDL	benchmark dose lower confidence limit
BMDS	Benchmark Dose Software
BMR	benchmark response
BUN	blood urea nitrogen
BW	body weight
$BW^{3/4}$	body weight scaling to the 3/4 power
CA	chromosomal aberration
CAA	Clean Air Act
CAS	Chemical Abstracts Service
CASRN	Chemical Abstracts Service registry number
CERCLA	Comprehensive Environmental Response, Compensation, and Liability Act
CHO	Chinese hamster ovary (cell line cells)
CI	confidence interval
CL	confidence limit
CNS	central nervous system
COI	conflict of interest
CPAD	Chemical and Pollutant Assessment Division
CPHEA	Center for Public Health and Environmental Assessment
CYP450	cytochrome P450
DAF	dosimetric adjustment factor
DMSO	dimethylsulfoxide
DNA	deoxyribonucleic acid
EPA	Environmental Protection Agency
ER	extra risk
FDA	Food and Drug Administration
FEV_1	forced expiratory volume of 1 second
GD	gestation day
GDH	glutamate dehydrogenase
GGT	γ-glutamyl transferase
GLP	Good Laboratory Practice
GSH	glutathione
GST	glutathione-*S*-transferase
HAP	hazardous air pollutant
HAWC	Health Assessment Workspace Collaborative
Hb/g-A	animal blood: gas partition coefficient
Hb/g-H	human blood: gas partition coefficient
HBCD	hexabromocyclododecane
HEC	human equivalent concentration
HED	human equivalent dose
HERO	Health and Environmental Research Online
i.p.	intraperitoneal
i.v.	intravenous
IAP	IRIS Assessment Plan
IARC	International Agency for Research on Cancer
IRIS	Integrated Risk Information System
IUR	inhalation unit risk
LC_{50}	median lethal concentration
LD_{50}	median lethal dose
LOAEL	lowest-observed-adverse-effect level
LOEL	lowest-observed-effect level
MeSH	Medical Subject Headings
MN	micronuclei
MNPCE	micronucleated polychromatic erythrocyte
MOA	mode of action
MTD	maximum tolerated dose
NCI	National Cancer Institute
NMD	normalized mean difference
NOAEL	no-observed-adverse-effect level
NOEL	no-observed-effect level
NTP	National Toxicology Program
NZW	New Zealand White (rabbit breed)
OAR	Office of Air and Radiation
OECD	Organization for Economic Co-operation and Development
OLEM	Office of Land and Emergency Management
ORD	Office of Research and Development
OSF	oral slope factor
PBPK	physiologically based pharmacokinetic
PECO	populations, exposures, comparators, and outcomes
PK	pharmacokinetic
PND	postnatal day
POD	point of departure
$POD_{[ADJ]}$	duration-adjusted POD
QSAR	quantitative structure-activity relationship
RD	relative deviation
RfC	inhalation reference concentration

RfD	oral reference dose
RGDR	regional gas dose ratio
RNA	ribonucleic acid
ROBINS I	Risk of Bias in Nonrandomized Studies of Interventions
SAR	structure-activity relationship
SCE	sister chromatid exchange
SD	standard deviation
SDH	sorbitol dehydrogenase
SE	standard error
SGOT	serum glutamic oxaloacetic transaminase, also known as AST
SGPT	serum glutamic pyruvic transaminase, also known as ALT
TK	toxicokinetics
TSCATS	Toxic Substances Control Act Test Submissions
TWA	time-weighted average
UF	uncertainty factor
UF_A	animal-to-human uncertainty factor
UF_D	database deficiencies uncertainty factor
UF_H	human variation uncertainty factor
UF_L	LOAEL-to-NOAEL uncertainty factor
UF_S	subchronic-to-chronic uncertainty factor
WOS	Web of Science

APPENDIX A. SYSTEMATIC REVIEW PROTOCOL FOR THE PFAS IRIS ASSESSMENTS

A single systematic review protocol was used to guide the development of five separate IRIS PFAS [per- and polyfluoroalkyl substances] assessments (i.e., perfluorobutanoic acid [PFBA], perfluorohexanoic acid [PFHxA], perfluorohexane sulfonate [PFHxS], perfluorononanoic acid [PFNA], and perfluorodecanoic acid [PFDA]). This "Systematic Review Protocol for the PFAS IRIS Assessments" was released for public comment and subsequently updated. The updated protocol and prior revisions can be found at the following location:
http://cfpub.epa.gov/ncea/iris_drafts/recordisplay.cfm?deid=345065

APPENDIX B. LITERATURE SEARCH STRATEGY AND POPULATIONS, EXPOSURES, COMPARATORS, AND OUTCOMES (PECO) CRITERIA

B.1. LITERATURE SEARCH AND SCREENING STRATEGY

Table B-1. Summary of detailed search strategies for Perfluorodecanoic Acid and Related Salts (PubMed, Web of Science, Toxline, TSCATS, Toxcenter)

Search	Search strategy	Dates of search
PubMed		
Search terms	335-76-2[rn] OR "Ndfda"[tw] OR "Nonadecafluoro-n-decanoic acid"[tw] OR "Nonadecafluorodecanoic acid"[tw] OR "Perfluoro-n-decanoic acid"[tw] OR "Perfluorodecanoic acid"[tw] OR "2,2,3,3,4,4,5,5,6,6,7,7,8,8,9,9,10,10,10-nonadecafluoro-Decanoic acid"[tw] OR "Decanoic acid, 2,2,3,3,4,4,5,5,6,6,7,7,8,8,9,9,10,10,10-nonadecafluoro-"[tw] OR "Decanoic acid, nonadecafluoro-"[tw] OR "Perfluorodecanoate"[tw] OR "PFDeA"[tw] OR "PFDcA"[tw] OR ("PFDA"[tw] AND (fluorocarbon*[tw] OR fluorotelomer*[tw] OR polyfluoro*[tw] OR perfluoro-*[tw] OR perfluoroa*[tw] OR perfluorob*[tw] OR perfluoroc*[tw] OR perfluorod*[tw] OR perfluoroe*[tw] OR perfluoroh*[tw] OR perfluoron*[tw] OR perfluoroo*[tw] OR perfluorop*[tw] OR perfluoros*[tw] OR perfluorou*[tw] OR perfluorinated[tw] OR fluorinated[tw] OR PFAS[tw] OR PFOS[tw] OR PFOA[tw]))	No date limit–7/26/2017
Literature update search terms	((335-76-2[rn] OR "Ndfda"[tw] OR "Nonadecafluoro-n-decanoic acid"[tw] OR "Nonadecafluorodecanoic acid"[tw] OR "Perfluoro-n-decanoic acid"[tw] OR "Perfluorodecanoic acid"[tw] OR "2,2,3,3,4,4,5,5,6,6,7,7,8,8,9,9,10,10,10-nonadecafluoro-Decanoic acid"[tw] OR "Decanoic acid, 2,2,3,3,4,4,5,5,6,6,7,7,8,8,9,9,10,10,10-nonadecafluoro-"[tw] OR "Decanoic acid, nonadecafluoro-"[tw] OR "Perfluorodecanoate"[tw] OR "PFDeA"[tw] OR "PFDcA"[tw] OR ("PFDA"[tw] AND (fluorocarbon*[tw] OR fluorotelomer*[tw] OR polyfluoro*[tw] OR perfluoro-*[tw] OR perfluoroa*[tw] OR perfluorob*[tw] OR perfluoroc*[tw] OR perfluorod*[tw] OR perfluoroe*[tw] OR perfluoroh*[tw] OR perfluoron*[tw] OR perfluoroo*[tw] OR perfluorop*[tw] OR perfluoros*[tw] OR perfluorou*[tw] OR perfluorinated[tw] OR fluorinated[tw] OR PFAS[tw] OR PFOS[tw] OR PFOA[tw])) AND ("2017/08/01"[Date - Publication] : "2018/03/01"[Date - Publication])	8/1/2017–2/14/2018

Search	Search strategy	Dates of search
Web of Science		
Search terms	TS="PFDeA" OR TS="PFDcA" OR TS="Ndfda" OR TS="Nonadecafluoro-n-decanoic acid" OR TS="Nonadecafluorodecanoic acid" OR TS="Perfluoro-n-decanoic acid" OR TS="Perfluorodecanoic acid" OR TS="2,2,3,3,4,4,5,5,6,6,7,7,8,8,9,9,10,10,10-nonadecafluoro-Decanoic acid" OR TS="Decanoic acid, 2,2,3,3,4,4,5,5,6,6,7,7,8,8,9,9,10,10,10-nonadecafluoro-" OR TS="Decanoic acid, nonadecafluoro-" OR TS="Perfluorodecanoate" OR (TS=PFDA AND TS=(fluorocarbon* OR fluorotelomer* OR polyfluoro* OR perfluoro-* OR perfluoroa* OR perfluorob* OR perfluoroc* OR perfluorod* OR perfluoroe* OR perfluoroh* OR perfluoron* OR perfluoroo* OR perfluorop* OR perfluoros* OR perfluorou* OR perfluorinated OR fluorinated)) OR (TS=PFDA AND TS=(fluorocarbon* OR fluorotelomer* OR polyfluoro* OR perfluoro-* OR perfluoroa* OR perfluorob* OR perfluoroc* OR perfluorod* OR perfluoroe* OR perfluoroh* OR perfluoron* OR perfluoroo* OR perfluorop* OR perfluoros* OR perfluorou* OR perfluorinated OR fluorinated OR PFAS OR PFOS OR PFOA	No date limit−7/26/2017
Literature update search terms	TS="PFDeA" OR TS="PFDcA" OR TS="Ndfda" OR TS="Nonadecafluoro-n-decanoic acid" OR TS="Nonadecafluorodecanoic acid" OR TS="Perfluoro-n-decanoic acid" OR TS="Perfluorodecanoic acid" OR TS="2,2,3,3,4,4,5,5,6,6,7,7,8,8,9,9,10,10,10-nonadecafluoro-Decanoic acid" OR TS="Decanoic acid, 2,2,3,3,4,4,5,5,6,6,7,7,8,8,9,9,10,10,10-nonadecafluoro-" OR TS="Decanoic acid, nonadecafluoro-" OR TS="Perfluorodecanoate" OR (TS=PFDA AND TS=(fluorocarbon* OR fluorotelomer* OR polyfluoro* OR perfluoro-* OR perfluoroa* OR perfluorob* OR perfluoroc* OR perfluorod* OR perfluoroe* OR perfluoroh* OR perfluoron* OR perfluoroo* OR perfluorop* OR perfluoros* OR perfluorou* OR perfluorinated OR fluorinated)) OR (TS=PFDA AND TS=(fluorocarbon* OR fluorotelomer* OR polyfluoro* OR perfluoro-* OR perfluoroa* OR perfluorob* OR perfluoroc* OR perfluorod* OR perfluoroe* OR perfluoroh* OR perfluoron* OR perfluoroo* OR perfluorop* OR perfluoros* OR perfluorou* OR perfluorinated OR fluorinated OR PFAS OR PFOS OR PFOA)) AND PY=2017-2018	2017−2018
Toxline		
Search terms	(335-76-2 [rn] OR "2,2,3,3,4,4,5,5,6,6,7,7,8,8,9,9,10,10,10-nonadecafluorodecanoic acid" OR "2,2,3,3,4,4,5,5,6,6,7,7,8,8,9,9,10,10,10-nonadecafluoro-decanoic acid" OR "decanoic acid 2,2,3,3,4,4,5,5,6,6,7,7,8,8,9,9,10,10,10-nonadecafluoro-" OR "decanoic acid nonadecafluoro-" OR "nonadecafluoro-n-decanoic acid" OR "nonadecafluorodecanoic acid" OR "perfluoro-1-nonanecarboxylic acid" OR "perfluoro-n-decanoic acid" OR "perfluorocapric acid" OR "perfluorodecanoate" OR "perfluorodecanoic acid" OR "ndfda" OR "PFDeA" OR "PFDcA" OR (pfda AND (fluorocarbon* OR fluorotelomer* OR polyfluoro* OR perfluoro* OR perfluorinated OR fluorinated OR pfas OR pfos OR pfoa))) AND (ANEUPL [org] OR BIOSIS [org] OR CIS [org] OR DART [org] OR EMIC [org] OR EPIDEM [org] OR HEEP [org] OR HMTC [org] OR IPA [org] OR RISKLINE [org] OR MTGABS [org] OR NIOSH [org] OR NTIS [org] OR PESTAB [org] OR PPBIB [org]) AND NOT PubMed [org] AND NOT pubdart [org]	No date limit−7/21/2017

Search	Search strategy	Dates of search
Literature update search terms		2017–2018
TSCATS		
Search terms	335-76-2[rn] AND TSCATS [org]	No date limit–7/21/2017

APPENDIX C. BENCHMARK DOSE MODELING RESULTS

C.1. BENCHMARK DOSE MODELING RESULTS FROM HUMAN STUDIES

The endpoints selected for benchmark dose (BMD) modeling include decreased serum antibody concentrations (Budtz-Jørgensen and Grandjean, 2018a; Grandjean et al., 2012) and decreased birth weight (Luo et al., 2021; Yao et al., 2021; Wikström et al., 2020; Valvi et al., 2017; Lenters et al., 2016). The internal doses reported in the human studies were used in the BMD modeling and then converted to human equivalent doses (HEDs) using the estimated human clearance as described in Section 3.7 of the main document, the modeling results are presented in this appendix.

C.1.1. BENCHMARK DOSE MODELING APPROACHES FOR IMMUNE EFFECTS

Modeling Results for Decreased Tetanus Antibody Concentrations at 7 Years of Age and PFDA Measured at 5 Years of Age

Budtz-Jørgensen and Grandjean (2018a) fit multivariate models of PFDA measured at age five years, against $\log_2$-transformed anti-tetanus antibody concentrations measured at the 7-year-old examination controlling for sex, exact age at the 7-year-old examination, and booster type at age 5 years. Models were evaluated with additional control for PFOS (as $\log_2$[PFOS]) and PFOA (as $\log_2$[PFOA]), and without PFOS and PFOA. Three model shapes were evaluated by Budtz-Jørgensen and Grandjean (2018a) using likelihood ratio tests: a linear model, a piecewise-linear model with a knot at the median PFDA concentration, and a logarithmic function. The logarithmic functions did not fit better than the piecewise-linear functions (Budtz-Jørgensen and Grandjean, 2018a). The piecewise-linear model did not fit better than the linear model for the PFHxS exposure without adjustment for PFOS and PFOA using a likelihood ratio test (p = 0.51; see Budtz-Jørgensen and Grandjean (2018a) Table 3), or for the model that did adjust for PFOS and PFOA ($\log_2$[PFOS] and $\log_2$[PFOA]) (p = 0.40).

Table C-1 summarizes the results from Budtz-Jørgensen and Grandjean (2018a) for PFDA at age 5 years and tetanus antibodies at age 7 years. These regression coefficients (β), their standard errors (SE), p-values, and the 90% lower confidence bounds were provided by Budtz-Jørgensen and Grandjean (2018b).

Table C-1. Results specific to the slope from the linear analyses of PFDA measured in serum at age 5 years and $\log_2$(tetanus antibody concentrations)

measured at age 7 years in a single-PFAS model and in a multi-PFAS model from (Budtz-Jørgensen and Grandjean, 2018b).

Exposure	Model shape	PFOS & PFOA adjusted	Slope (β) per ng/mL in serum	SE(β) ng/m Lin serum	Slope (β) fit	Lower bound slope (β_{LB}) per ng/mL in serum
PFDA at Age 5	Linear	No	-1.55	0.602	p = 0.01	-2.55
PFDA at Age 5	Linear	Yes	-0.98	0.681	p = 0.15	-2.10

Interpretation of results in Table C-1:

- PFDA is a significant predictor in the single-PFAS model (β = -1.55; p = 0.01)
- Effects of PFDA in the single-PFAS model are attenuated when $\log_2$[PFOS] and $\log_2$[PFOA] are included in the model (β = -0.98; p = 0.15).
- The point estimate results for PFDA (β) in the single-PFAS model are *potentially* confounded by PFOS and/or PFOA since there was a 37% reduction in the effect size for PFDA from -1.55 to -0.98 when controlling for PFOS and PFOA.
    - One explanation is that PFOS and/or PFOA was a confounder of the PFDA effect and controlling for those co-exposures removed confounding.
    - Another possibility is that controlling for co-exposures like PFOS and PFOA actually induced confounding (Weisskopf et al., 2018; Weisskopf and Webster, 2017).
    - The reasons for the change in main effect size for PFDA are not known. For this reason, there is uncertainty in knowing which point estimate is the best representation of any effect of PFDA.
- However, the lower bound on the point estimates (β_{LB}) for the single-PFAS is 21% lower than the multi-PFAS model estimate for PFDA.
    - The definition of the RfD, which is based upon the β_{LB}, includes allowing for an order of magnitude (10-fold or 1,000%) uncertainty in the estimate and the uncertainty for potential confounding in the BMD from including, or excluding, PFOS and PFOA here is about 37%, while the uncertainty for potential confounding in the BMDL is about 21%.

Selection of the Benchmark Response

The benchmark dose (BMD) approach involves dose-response modeling to obtain BMDs, i.e., dose levels corresponding to specific response levels near the low end of the observable range of the data and the lower limit of the BMD (BMDLs) to serve as potential PODs for deriving quantitative estimates below the range of observation (U.S. EPA, 2012). Selecting a BMR to estimate the BMDs and BMDLs involves making judgments about the statistical and biological characteristics of the data set and about the applications for which the resulting BMDs and BMDLs will be used. An extra risk of 10% is recommended as a standard reporting level for quantal data for toxicological data. Biological considerations may warrant the use of a BMR of 5% or lower for some types of effects as the basis of the POD for a reference value. However, a BMR of 1% has typically been used for quantal human data from epidemiology studies (U.S. EPA, 2012), although

this is more typically used for epidemiologic studies of cancer mortality within large cohorts of workers which can support the statistical estimation of small BMRs.

A blood concentration for tetanus antibodies of 0.1 IU/mL is sometimes cited in the tetanus literature as a 'protective level' and (Grandjean et al., 2017) noted that the Danish vaccine producer Statens Serum Institut recommended the 0.1 IU/mL "cutoff" level "to determine whether antibody concentrations could be considered protective"; and Galazka and Kardymowicz (1989)mentions the same concentration, but Galazka et al. (1993)argues:

> "*The amount of circulating antitoxin needed to ensure complete immunity against tetanus is not known for certain. Establishment of a fixed level of tetanus antitoxin does not take into consideration variable conditions of production and adsorption of tetanus toxin in the anaerobic area of a wound or a necrotic umbilical stump. A given serum level could be overwhelmed by a sufficiently large dose of toxin. Therefore, there is no absolute protective level of antitoxin and protection results when there is sufficient toxin-neutralizing antibody in relation to the toxin load* (Passen and Andersen, 1986)."

In the absence of a clear definition of an adverse effect for a continuous endpoint like antibody concentrations, a default BMR of one SD change from the control mean may be selected, as suggested in EPA's draft Benchmark Dose Technical Guidance Document (U.S. EPA, 2012). As noted above, a lower BMR can also be used if it can be justified on a biological and/or statistical basis. Figure C-1 replicates a figure in the Technical Guidance (page 23; (U.S. EPA, 2012) to show that in a control population where 1.4% are considered to be at risk of having an adverse effect, a downward shift in the control mean of one SD results in a ~10% extra risk of being at risk of having an adverse effect.

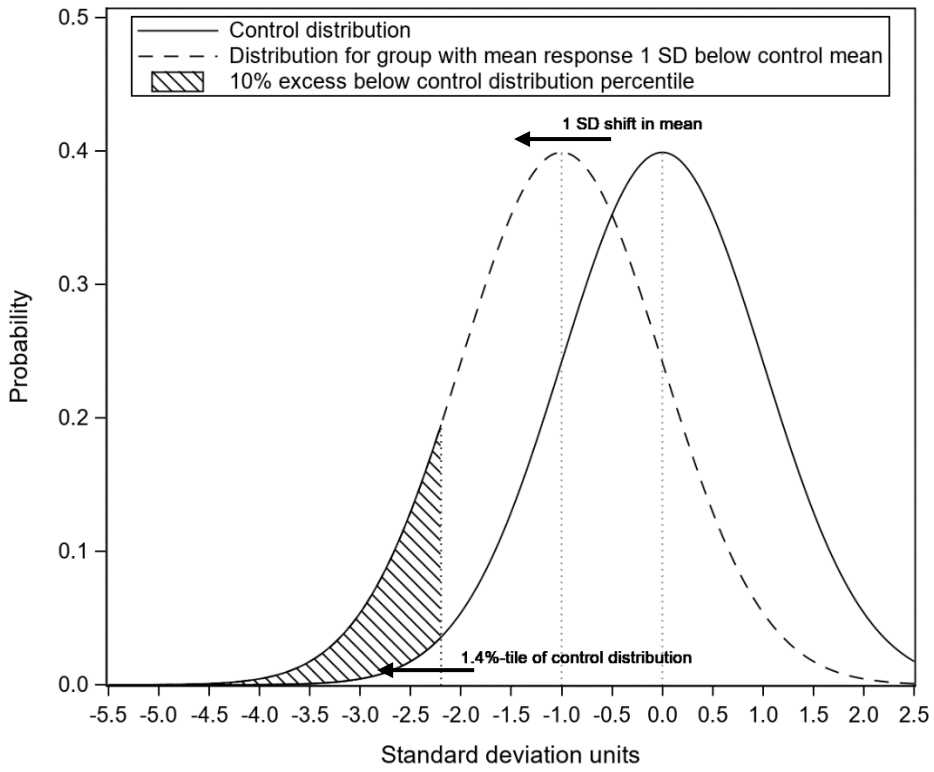

Figure C-1. Difference in population tail probabilities resulting from a one standard deviation shift in the mean from a standard normal distribution, illustrating the theoretical basis for a baseline BMR of 1 SD.

Statistically, the Technical Guidance additionally suggests that studies of developmental effects can support lower BMRs. Biologically, a BMR of ½ SD is a reasonable choice as anti-tetanus antibody concentrations prevent against tetanus, which is a rare, but severe and sometimes fatal infection, with a case-fatality rate in the U.S. of 13% during 2001–2008 (Liang et al., 2018). The case-fatality rate can be more than 80% for early lifestage cases (Patel and Mehta, 1999). Selgrade (2007) suggests that specific immuno-toxic effects observed in children may be broadly indicative of developmental immunosuppression impacting these children's ability to protect against a range of immune hazards—which has the potential to be a more adverse effect than just a single immuno-toxic effect. Thus, decrements in the ability to maintain effective levels of tetanus antitoxins following immunization may be indicative of wider immunosuppression in these children exposed to PFDA. By contrast, a BMR of one SD may be more appropriate for an effect that would be considered 'minimally adverse.' A BMR smaller than ½ SD is generally selected for severe effects (e.g., 1% extra risk of cancer mortality); decreased antibody concentrations offer diminished protection from severe effects but are not themselves severe effects.

Following the technical guidance (U.S. EPA, 2012), EPA derived BMDs and BMDLs associated with a one SD change in the distribution of $\log_2$(tetanus antibody concentrations), and ½ SD change in the distribution of $\log_2$(tetanus antibody concentrations). The SD of the $\log_2$(tetanus

antibody concentrations) at age 7 years was estimated from the distributional data presented in Grandjean et al. (2012) as follows: the interquartile range (IQR) of the tetanus antibody concentrations at age 7 years in IU/mL was (0.65, 4.6). Log_2-tranforming these values provides the IQR in log_2(IU/mL) as (-0.62, 2.20). Assuming that these log_2-transformed values are reasonably represented by a normal distribution, the width of the IQR is approximately 1.35 SDs. Thus, SD = IQR/1.35, and the SD of tetanus antibodies in log_2(IU/mL) is (2.20 – (-0.62))/1.35 = 2.09 log_2(IU/mL). To show the impact of the BMR on these results, Table E-2 presents the BMDs and BMDLs at BMRs of ½ SD and 1 SD.

While there was not a clear definition of the size of an adverse effect for a continuous endpoint like antibody concentrations, the value of 0.1 IU/mL is sometimes cited. As a check, EPA evaluated how much extra risk would have been associated with a BMR set at a cutoff value of 0.1 IU/mL. Using the observed distribution of tetanus antibodies at age seven years in log_2(IU/mL), EPA calculated that 2.8% of those values would be below the cutoff value of 0.1 IU/mL which is -3.32 log_2(IU/mL). A BMR of ½ SD resulted in 7.9% of the values being below that cutoff which is 5.1% extra risk and shows that the generic guidance that a BMR of ½ SD can provide a reasonably good estimate of 5% extra risk. Figure C-2 shows an example of this.

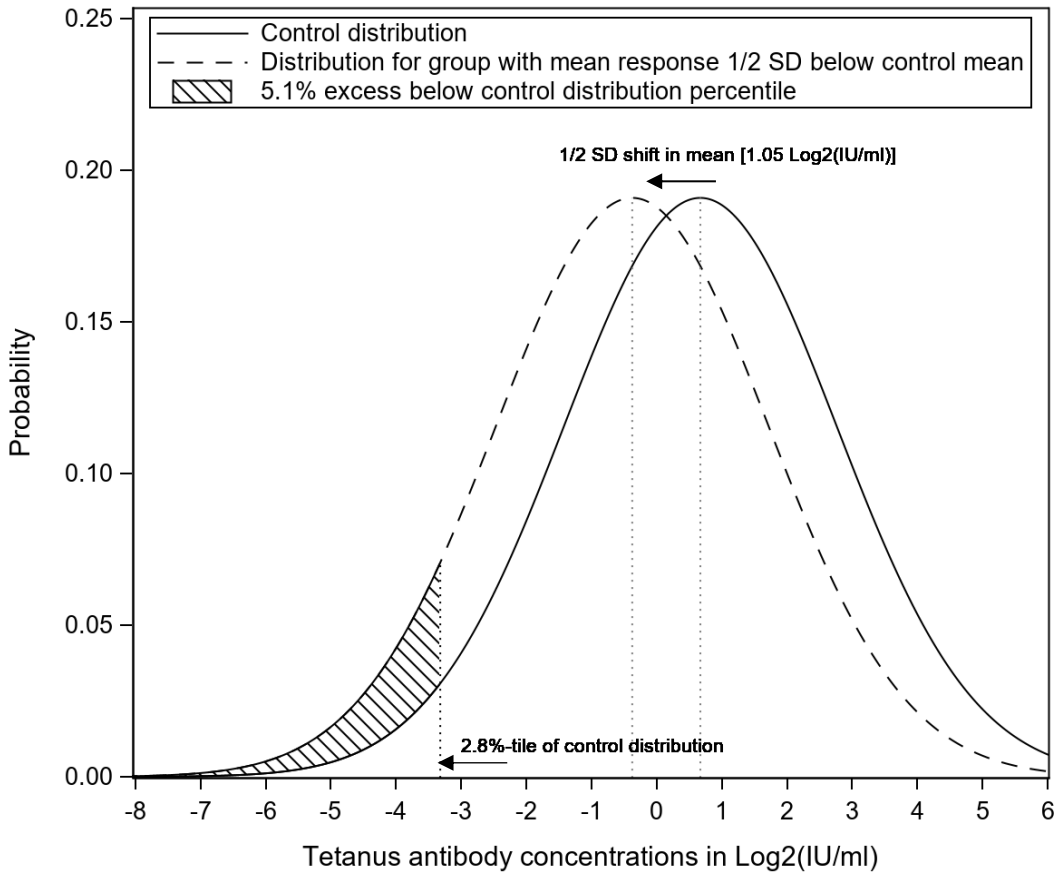

Figure C-2. Difference in population tail probabilities resulting from a ½ standard deviation shift in the mean from an estimation of the distribution of $\log_2$(tetanus antibody concentrations at age seven years).

Table C-2. BMDs and BMDLs for effect of PFDA at age five years on anti-tetanus antibody concentrations at age seven years using a BMR of ½ SD change in $\log_2$(tetanus antibodies concentration) and a BMR of 1 SD change in $\log_2$(tetanus antibodies concentration).

	Estimated without control of PFOS and PFOA		Estimated with control of PFOS and PFOA	
BMR	**BMD (ng/mL in serum)** β **= -1.55 per ng/mL**	**BMDL (ng/mL in serum)** β_{LB} **= -2.55 per ng/mL**	**BMD (ng/mL in serum)** β **= -0.98 per ng/mL**	**BMDL (ng/mL in serum)** β_{LB} **= -2.10 per ng/mL**
½ SD	0.673	**0.411**[a]	1.067	0.497
1 SD	1.346	0.821	2.135	0.994

[a] Denotes the selected POD.

The lowest serum PFDA concentration measured at age five years was 0.05 ng/mL, the 5th percentile was 0.1 ng/mL, and the 10th percentile was 0.2 ng/mL (Grandjean and Bateson, 2021) so the estimated BMDL for a BMR of ½ SD ($BMDL_{½\ SD}$) in the single-PFAS model is above the 10th

percentile of the observed distribution. No information was available to judge the fit of the model in the range of the BMDLs, but the BMD and BMDL were both within the range of observed values and the model fit PFDA well.

The $BMD_{½\ SD}$ estimate from the multi-PFAS models is 59% higher than the $BMD_{½\ SD}$ estimate from the models with just PFDA, and the $BMDL_{½\ SD}$ estimates is 21% higher. The change in BMD estimates may, or may not, reflect control for any potential confounding of the regression effect estimates. While it is not clear which PFAS model provided 'better' estimate of the point estimate of the effect of PFDA, the two $BMDL_{½\ SD}$ estimates are similar (0.411 ng/mL vs. 0.497 ng/mL) and EPA advanced the derivation based on results that did not controls for PFOS and PFOA because this model appeared to fit PFDA better (p = 0.01 vs. 0.15) and there was low uncertainty due to potential confounding in the BMDL. However, confidence was somewhat diminished by the potential confounding in the main effect—even though there was low confounding of the BMDL. Overall confidence in the BMDLs for Tetanus was judged to be medium confidence.

For immunotoxicity related to tetanus associated with PFDA exposure measured at age five years, the POD is based on a BMR of ½ SD and a $BMDL_{½\ SD}$ of 0.411 ng/mL in serum.

Modeling Results for Decreased Diphtheria Antibody Concentrations at 7 Years of Age and PFDA Measured at 5 Years of Age

Budtz-Jørgensen and Grandjean (2018a) fit multivariate models of PFDA measured at age 5 years, against log_2-transformed anti-diphtheria antibody concentrations measured at the seven-year-old examination controlling for sex, exact age at the 7-year-old examination, and booster type at age 5 years. Models were evaluated with additional control for PFOS (as log_2[PFOS]) and PFOA (as log_2[PFOA]), and without PFOS and PFOA. Three model shapes were evaluated by Budtz-Jørgensen and Grandjean (2018a) using likelihood ratio tests: a linear model of PFDA, a piecewise-linear model with a knot at the median, and a logarithmic function. The logarithmic functions did not fit better than the piecewise-linear functions (Budtz-Jørgensen and Grandjean, 2018a). The piecewise-linear model did not fit better than the linear model for the PFHxS exposure without adjustment for PFOS and PFOA using a likelihood ratio test (p = 0.55; see Budtz-Jørgensen and Grandjean (2018a) Table 3), or for the model that did adjust for PFOS and PFOA (log_2[PFOS] and log_2[PFOA]) (p = 0.73). Table C-3 summarizes the results from Budtz-Jørgensen and Grandjean (2018a) for diphtheria in this exposure window. These regression coefficients (β), their standard errors (SE), p-values, and the 90% lower confidence bounds were provided by Budtz-Jørgensen and Grandjean (2018b).

Table C-3. Results specific to the slope from the linear analyses of PFDA in serum measured at age 5 years and log_2(diphtheria antibodies) measured at age 7 years from Table 1 in a single-PFAS model and in a multi-PFAS model from (Budtz-Jørgensen and Grandjean, 2018b).

Exposure	Model shape	PFOS & PFOA adjusted	Slope (β) per ng/mL in serum	SE(β) ng/mL in serum	Slope (β) fit	Lower bound slope (β_{LB}) per ng/mL in serum
PFDA at Age 5	Linear	No	-0.894	0.561	p = 0.11	-1.82
PFDA at Age 5	Linear	Yes	-0.297	0.635	p = 0.64	-1.35

Interpretation of results in Table C-3:

- PFDA is a non-significant predictor in the single-PFAS model (β = -0.894; p = 0.11)
- Effects are attenuated when log_2[PFOS] and log_2[PFOA] are included in the model (β = -0.297; p = 0.64).
- The point estimate results for PFDA are *potentially* confounded by PFOS and/or PFOA since there was a 67% reduction in the effect size for PFDA from -0.894 to -0.297 when controlling for PFOS and PFOA.
    - One explanation is that PFOS and/or PFOA was a confounder of the PFDA effect and controlling for those co-exposures removed confounding.
    - Another possibility is that controlling for co-exposures like PFOS and PFOA actually induced confounding (Weisskopf et al., 2018; Weisskopf and Webster, 2017).
    - The reasons for the change in main effect size for PFDA are not known. For this reason, there is uncertainty in knowing which point estimate is the best representation of any effect of PFDA.
- However, the lower bound on the point estimates (β_{LB}) for the single-PFAS model is 35% lower than the multi-PFAS model estimate for PFDA.
    - The definition of the RfD, which is based upon the β_{LB}, includes allowing for an order of magnitude (10-fold or 1,000%) uncertainty in the estimate and the uncertainty for potential confounding in the BMD from including, or excluding, PFOS and PFOA here is about 67%, while the uncertainty for potential confounding in the BMDL is about 35%.

Selection of the Benchmark Response

Following the technical guidance (U.S. EPA, 2012), EPA derived BMDs and BMDLs associated with a one SD change in the distribution of log_2(diphtheria antibody concentrations), and ½ SD change in the distribution of log_2(diphtheria antibody concentrations). A blood concentration for diphtheria antibodies of 0.1 IU/mL is sometimes cited in the diphtheria literature as a 'protective level' Grandjean et al. (2017) noted that the Danish vaccine producer Statens Serum Institut recommended the 0.1 IU/mL 'cutoff' level; and Galazka et al. (1993) mentions the same concentration), but Galazka et al. (1993) argues:

> *"However, it has also been shown that there is no sharply defined level of antitoxin that gives complete protection from diphtheria (Ipsen, 1946). A certain range of variation must be*

*accepted; the same degree of antitoxin may give an unequal degree of protection in different persons. Other factors may influence the vulnerability to diphtheria including the dose and virulence of the diphtheria bacilli and the general immune status of the person infected (*Christenson and Böttiger, 1986*). Thus, an antibody concentration between 0.01 and 0.09 IU/ml may be regarded as giving basic immunity, whereas a higher titer may be needed for full protection. In some studies that used in vitro techniques, a level of 0.1 IU/ml was considered protective (*Cellesi et al., 1989*; *Galazka and Kardymowicz, 1989*)."*

Statistically, the Technical Guidance suggests that studies of developmental effects can support lower BMRs. Biologically, a BMR of ½ SD is a reasonable choice as anti-diphtheria antibody concentrations prevent against diphtheria, which is very rare in the U.S., but can cause life-threatening airway obstruction, or cardiac failure (Collier, 1975). Among 13 cases reported in the U.S. during 1996–2016, no deaths were mentioned (Liang et al., 2018). However, diphtheria remains a potentially fatal disease in other parts of the world (Galazka et al., 1993) mentions a case fatality rate of 5–10%) and PFDA-related changes in anti-diphtheria antibody concentrations cannot be considered 'minimally adverse' given the historic lethality of diphtheria in the absence of vaccination. Selgrade (2007) suggests that specific immuno-toxic effects observed in children may be broadly indicative of developmental immunosuppression impacting these children's ability to protect against a range of immune hazards—which has the potential to be a more adverse effect that just a single immuno-toxic effect.

Following the technical guidance (U.S. EPA, 2012), EPA derived BMDs and BMDLs associated with a one SD change in the distribution of $\log_2$(diphtheria antibody concentrations) as a standard reporting level, and ½ SD change in the distribution of $\log_2$(diphtheria antibody concentrations). The SD of the $\log_2$(diphtheria antibody concentrations) at age 7 years was estimated from the distributional data presented in Grandjean et al. (2012) as follows: the interquartile range (IQR) of the diphtheria antibody concentrations at age 7 years in IU/mL was (0.4, 1.6). Log_2-tranforming these values provides the IQR in $\log_2$(IU/mL) as (-1.32, 0.68). Assuming that these $\log_2$-transformed values are similar to the normal distribution, the width of the IQR is approximately 1.35 SDs, thus SD = IQR/1.35, and the SD of tetanus antibodies in $\log_2$(IU/mL) is (0.68 – (-1.32))/1.35 = 1.48 $\log_2$(IU/mL). To show the impact of the BMR on these results, Table E-4 presents the BMDs and BMDLs at BMRs of ½ SD and 1 SD.

Table C-4. BMDs and BMDLs for effect of PFDA at age 5 years on anti-diphtheria antibody concentrations at age 7 years using a BMR of ½ SD change in log_2(diphtheria antibodies concentration) and a BMR of 1 SD log_2(diphtheria antibodies concentration).

	Estimated without control of PFOS and PFOA		Estimated with control of PFOS and PFOA	
BMR	**BMD (ng/mL in serum) β = -0.894 per ng/mL**	**BMDL (ng/mL in serum) β_{LB} = -1.82 per ng/mL**	**BMD (ng/mL in serum) β = -0.297 per ng/mL**	**BMDL (ng/mL in serum) β_{LB} = -1.35 per ng/mL**
½ SD	0.827	**0.407**[a]	2.488	0.550
1 SD	1.655	0.813	4.976	1.100

[a] Denotes the selected POD.

The lowest serum PFDA concentration measured at age five years was 0.05 ng/mL, the 5th percentile was 0.1 ng/mL, and the 10th percentile was 0.2 ng/mL (Grandjean and Bateson, 2021) so the estimated BMDL for a BMR of ½ SD ($BMDL_{½\ SD}$) in the single-PFAS model is at the 10th percentile of the observed distribution. No information was available to judge the fit of the model in the range of the BMDLs, but the BMD and BMDL were both within the range of observed values and the model fit PFDA well.

The $BMD_{½\ SD}$ estimate from the multi-PFAS models is 3-fold higher than the $BMD_{½\ SD}$ estimate from the model with just PFDA, and the $BMDL_{½\ SD}$ is 35% higher. This may, or may not, reflect control for any potential confounding of the regression effect estimates. While it is not clear which PFAS model provided the 'better' estimate of the point estimate of the effect of PFDA, the two $BMDL_{½\ SD}$ estimates which serve as the PODs are comparable (0.407 ng/mL vs. 0.550 ng/mL) and EPA advanced POD based on results that did not controls for PFOS and PFOA because this model appeared to fit PFDA better (p = 0.11 vs. 0.64) and there was low uncertainty due to potential confounding in the BMDL. However, confidence was diminished by the non-significant fit for PFDA (p = 0.11) and stronger potential confounding in the main effect—even though there was low confounding of the BMDL, and overall confidence in the BMDLs for diphtheria was judged to be low confidence.

For immunotoxicity related to diphtheria, associated with PFDA measured at age 5 years, the POD is based on a BMR of ½ SD and a $BMDL_{½\ SD}$ of 0.407 ng/mL in serum.

Modeling Results for Decreased Tetanus Antibody Concentrations at 5 Years of Age and perinatal PFDA

Budtz-Jørgensen and Grandjean (2018a) fit multivariate models of PFDA measured perinatally in maternal serum, against log_2-transformed anti-tetanus antibody concentrations measured at the 5-year-old examination controlling for sex, and exact age at the 5-year-old examination, cohort, and interaction terms between cohort and sex, and between cohort and age. Models were evaluated with additional control for PFOS (as log_2[PFOS]) and PFOA (as log_2[PFOA]), and without PFOS and PFOA. Three model shapes of PFDA were evaluated by Budtz-Jørgensen and

Grandjean (2018a) using likelihood ratio tests: a linear model, a piecewise-linear model with a knot at the median, and a logarithmic function. The logarithmic functions did not fit better than the piecewise-linear functions Budtz-Jørgensen and Grandjean (2018a). Compared to the linear model, the piecewise-linear model did not fit better than the linear model for either the PFDA exposure without adjustment for PFOS and PFOA using a likelihood ratio test (p = 0.81; see Budtz-Jørgensen and Grandjean (2018a) Table 3), or for the model that did adjust for PFOS and PFOA (log_2[PFOS] and log_2[PFOA]) (p = 0.84).

Table C-5 summarizes the results from Budtz-Jørgensen and Grandjean (2018a) for tetanus in this exposure window. These regression coefficients (β), their standard errors (SE), p-values, and the 90% lower confidence bounds were provided by Budtz-Jørgensen and Grandjean (2018b).

Table C-5. Results of the linear analyses of PFDA measured perinatally in maternal serum and tetanus antibodies measured at age 5 years in a single-PFAS model and in a multi-PFAS model from (Budtz-Jørgensen and Grandjean, 2018b).

Exposure	Model shape	PFOS & PFOA adjusted	Slope (β) per ng/mL in serum	SE(β) ng/mL in serum	Slope (β) fit	Lower bound slope (β_{LB}) per ng/mL in serum
Perinatal PFDA	Linear	No	-0.343	0.462	p = 0.46	-1.103
Perinatal PFDA	Linear	Yes	0.038	0.554	p = 0.95	-0.874

Interpretation of results in Table C-5:

- PFDA is a non-significant predictor in the single-PFAS model (β = -0.34; p = 0.46).
- Effects are attenuated when log_2[PFOS] and log_2[PFOA] are included in the model (β = 0.038; p = 0.55)
- Nevertheless, these data can be used to estimate a BMDL for completeness and to allow comparisons across PFAS.

Selection of the Benchmark Response

Following the technical guidance (U.S. EPA, 2012), EPA derived BMDs and BMDLs associated with a one SD change in the distribution of log_2(tetanus antibody concentrations), and ½ SD change in the distribution of log_2(tetanus antibody concentrations). The SD of the log_2(tetanus antibody concentrations) at age 5 years was estimated from two sets of distributional data presented from two different cohorts of 5-year-olds that were pooled in Budtz-Jørgensen and Grandjean (2018a). Grandjean et al. (2012) reported on 587 5-year-olds from the cohort of children born during 1997–2000 and in Grandjean et al. (2017) reported on 349 5-year-olds from the cohort of children born during 2007–2009. The means and SDs were computed separately and then pooled to describe the common SD. The IQR of the tetanus antibody concentrations in the earlier birth cohort at age 5 years in IU/mL was (0.1, 0.51). Log_2-tranforming these values provides

the IQR in log_2(IU/mL) as (-3.32, -0.97). Assuming that these log_2-transformed values are similar to the normal distribution, the width of the IQR is approximately 1.35 SDs, thus SD = IQR/1.35, and the SD of tetanus antibodies in log_2(IU/mL) is (-0.97 – (-3.32))/1.35 = 1.74 log_2(IU/mL). The IQR of the tetanus antibody concentrations in the later birth cohort at age 5 years in IU/mL was (0.1, 0.3). Log_2-tranforming these values provides the IQR in log_2(IU/mL) as (-3.32, -1.74), and the SD of tetanus antibodies in log_2(IU/mL) is (-1.74 – (-3.32))/1.35 = 1.17 log_2(IU/mL). The pooled variance is a weighted sum of the independent SDs, and the pooled SD was estimated as 1.55 log_2(IU/mL).[1] To show the impact of the BMR on these results, Table E-6 presents the BMDs and BMDLs at BMRs of ½ SD and 1 SD.

Table C-6. BMDs and BMDLs for effect of PFDA measured perinatally and anti-tetanus antibody concentrations at age 5 years

	Estimated without control of PFOS and PFOA		Estimated with control of PFOS and PFOA	
BMR	**BMD (ng/mL in serum)** β **= -0.343 per ng/mL**	**BMDL (ng/mL in serum)** β_{LB} **= -1.103 per ng/mL**	**BMD (ng/mL in serum)** β **= 0.038 per ng/mL**	**BMDL (ng/mL in serum)** β_{LB} **= -0.874 per ng/mL**
½ SD	2.260	**0.702**[a]	-	0.886
1 SD	4.520	1.405	-	1.773

[a] Denotes the POD that corresponds to the analyses of PFDA concentrations perinatally and tetanus antibodies at age 5 years; - values can't be determined.

The lowest perinatal maternal serum PFDA concentration measured was 0.03 ng/mL, the 5th percentile was 0.1 ng/mL, and the 10th% was 0.2 ng/mL (Grandjean, 2021) so the estimated BMDLs for a BMR of ½ SD ($BMDL_{½\ SD}$ =0.702 ng/mL) in the single-PFAS model is well above the 10th% of the observed distribution. No information was available to judge the fit of the model in the range of the BMDLs, but the BMD and BMDL were both within the range of observed values and the model fit PFDA well. The $BMDL_{½\ SD}$ estimate from the single-PFAS models was 0.702 ng/mL in serum. The BMDL estimates from the multi-PFAS models were about 26% higher than for the single-PFAS model.

Low confidence in the BMDLs from the PFDA-only model (0.702 ng/mL in serum) and in the multi-PFAS model (0.886 ng/mL in serum). Confidence is diminished by the low quality of the model fit for PFDA in either model compared to the PFDA results from tetanus in the 5-year to 7-year exposure-outcome window of time and there is some uncertainty regarding potential confounding.

For immunotoxicity related to tetanus, associated with PFDA measured perinatally, the POD is based on a BMR of ½ SD and a $BMDL_{½\ SD}$ of 0.702 ng/mL in serum. Note that this result is based on a poorly fit PFDA regression parameter (β) estimated as −0.343 per ng/mL in serum (90% CI:

[1] Pooled variance for tetanus in 5-year-olds = [(502-1)(1.74)^2+ (298-1)(1.17)^2]/[502+298-2] = 2.41. The pooled SD is the square root of 2.41 which is 1.55 log_2(IU/mL).

−1.103, 0.417; p = 0.46) Budtz-Jørgensen and Grandjean (2018b), and thus this POD is identified with low confidence.

For immunotoxicity related to tetanus associated with PFDA exposure measured at age 5 years, the POD estimated for comparison purposes were based on a BMR of ½ SD and a $BMDL_{½\ SD}$ of 0.702 ng/mL in serum.

Modeling Results for Decreased Diphtheria Antibody Concentrations at 5 Years of Age and perinatal PFDA

Budtz-Jørgensen and Grandjean (2018a) fit multivariate models of PFDA measured perinatally, against log_2-transformed anti-diphtheria antibody concentrations measured at the 5-year-old examination controlling for sex and age. Models were evaluated with additional control for PFOS (as log_2[PFOS]) and PFOA (as log_2[PFOA]), and without PFOS and PFOA. Three model shapes were evaluated by Budtz-Jørgensen and Grandjean (2018a) using likelihood ratio tests: a linear model of PFDA, a piecewise-linear model with a knot at the median, and a logarithmic function. The logarithmic functions did not fit better than the piecewise-linear functions Budtz-Jørgensen and Grandjean (2018a). There was evidence that the piecewise-linear model fit better than the linear model for the PFDA exposure without adjustment for PFOS and PFOA (p = 0.05; see in Budtz-Jørgensen and Grandjean (2018a), Table 3), but not for the model that adjusted for PFOS and PFOA (log_2[PFOS] and log_2[PFOA]) (p = 0.12). Table C-7 summarizes the results from Budtz-Jørgensen and Grandjean (2018a) for diphtheria in this exposure window. These regression coefficients (β) and their standard errors (SE) were computed by EPA from the published BMDs and BMDL based on a BMR of 5% change in diphtheria antibody concentrations in Table 2 of Budtz-Jørgensen and Grandjean (2018a)[2].

[2] (Budtz-Jørgensen and Grandjean, 2018a) computed BMDs and BMDLs using a BMR of 5% decrease in the antibody concentrations. Their formula, BMD = log2(1-BMR)/β, can simply be reversed to solve for β = log2(1-BMR)/BMD. For negative dose-response where more exposure results in lower antibody concentration, the BMDL is based on the lower bound of β, (βLB). Thus, the βLB = log2(1-BMR)/BMDL. The SE(β) = (β - βLB)/1.645. The p-value is the two-sided probability that Z <= SE(β)/β.

Table C-7. Results of the analyses of PFDA measured perinatally in maternal serum and diphtheria antibodies measured at age 5 years in a single-PFAS model and in a multi-PFAS model from (Budtz-Jørgensen and Grandjean, 2018b).

Exposure	Model shape	PFOS & PFOA adjusted	Slope (β) per ng/mL in serum	SE(β)	Slope (β) fit	Lower bound slope (β_{LB}) per ng/mL in serum
Perinatal PFDA	Piecewise	No	-3.700	2.249	p = 0.100	-7.400
Perinatal PFDA	Piecewise	Yes	-2.467	0.750	p = 0.001	-3.700

Interpretation of results in Table C-7:

- PFDA is a non-significant predictor in the single-PFAS model (β = -3.700; p = 0.10)
- Effects of PFDA are attenuated when PFOA and PFOA are in the model (β = -2.467; p = 0.001).
- The point estimate results for PFDA are *potentially* confounded by PFOS and/or PFOA since there was a 33% change in the effect size for PFDA from -3.700 to -2.467 when controlling for PFOS and PFOA.
    - One explanation is that PFOS and/or PFOA was a confounder of the PFDA effect and controlling for those co-exposures removed confounding.
    - Another possibility is that controlling for co-exposures like PFOS and PFOA actually induced confounding (Weisskopf et al., 2018; Weisskopf and Webster, 2017).
    - The reasons for the change in main effect size for PFDA are not known. For this reason, there is uncertainty in knowing which point estimate is the best representation of any effect of PFDA.
- However, the lower bound on the point estimates (β_{LB}) for the single-PFAS model for PFDA is 100% lower than the multi-PFAS model effect estimate for PFDA.
    - The definition of the RfD, which is based upon the β_{LB}, includes allowing for an order of magnitude (10-fold or 1,000%) uncertainty in the estimate and the uncertainty for potential confounding in the BMD from including, or excluding, PFOS and PFOA here is about 33%, while the uncertainty for potential confounding in the BMDL is about 100%.

Selection of the Benchmark Response

Following the technical guidance (U.S. EPA, 2012), EPA derived BMDs and BMDLs associated with a one SD change in the distribution of $\log_2$(tetanus antibody concentrations) as a standard reporting level, and ½ SD change in the distribution of $\log_2$(tetanus antibody concentrations). The SD of the $\log_2$(diphtheria antibody concentrations) at age 5 years was estimated from two sets of distributional data presented from two different birth cohorts of 5-year-olds that were pooled in Budtz-Jørgensen and Grandjean (2018a). Grandjean et al. (2012) reported on 587 5-year-olds from the cohort of children born during 1997–2000 and Grandjean et al. (2017) reported on 349 5-year-olds from the cohort of children born during 2007–2009. The means and SDs were computed separately and then pooled to describe the common SD. The IQR of the diphtheria antibody concentrations in the earlier birth cohort at age 5 years in IU/mL was (0.05,

0.4). Log_2-tranforming these values provides the IQR in log_2(IU/mL) as (-4.32, -1.32). Assuming that these log_2-transformed values are similar to the normal distribution, the width of the IQR is approximately 1.35 SDs, thus SD = IQR/1.35, and the SD of diphtheria antibodies in log_2(IU/mL) is (-1.32 – (-4.32))/1.35 = 2.22 log_2(IU/mL). The IQR of the diphtheria antibody concentrations in the later birth cohort at age 5 years in IU/mL was (0.1, 0.3). Log_2-tranforming these values provides the IQR in log_2(IU/mL) as (-3.32, -1.74), and the SD of diphtheria antibodies in log_2(IU/mL) is (-1.74 – (-3.32))/1.35 = 1.17 log_2(IU/mL). The pooled variance is a weighted sum of the independent SDs, and the pooled SD was estimated as 1.90 log_2(IU/mL)[3]. To show the impact of the BMR on these results, Table C-8 presents the BMDs and BMDLs at BMRs of ½ SD and 1 SD.

Table C-8. BMDs and BMDLs for effect of PFDA measured perinatally and anti-diphtheria antibody concentrations at age 5 years.

	Estimated without control of PFOS and PFOA		Estimated with control of PFOS and PFOA	
BMR	**BMD (ng/mL in serum)** **β = -3.700 per ng/mL**	**BMDL (ng/mL in serum)** **β_{LB} = -7.400 per ng/mL**	**BMD (ng/mL in serum)** **β = -2.467 per ng/mL**	**BMDL (ng/mL in serum)** **β_{LB} = -3.700 per ng/mL**
½ SD	0.257	0.128	0.385	**0.257**[a]
1 SD	0.514	0.257	0.770	0.514

[a] Denotes the POD that corresponds to the analyses of PFDA concentrations perinatally and diphtheria antibodies at age 5 years.

The lowest serum PFDA concentration measured perinatally was 0.03 ng/mL, the 5th percentile was 0.1 ng/mL, and the 10th% was 0.2 ng/mL (Grandjean and Bateson, 2021) so the estimated BMD for a BMR of ½ SD ($BMDL_{½\ SD}$) in the single-PFAS model is well within the observed range. No information was available to judge the fit of the model in the range of the BMDLs, but the BMD and BMDL were both within the range of observed values and the model fit PFDA well.

The $BMD_{½\ SD}$ estimate from the multi-PFAS models is 50% higher than the $BMD_{½\ SD}$ estimated from the model with just PFDA, and the $BMDL_{½\ SD}$ is 100% higher. This may, or may not, reflect control for any potential confounding of the regression effect estimates. The BMDLs which serve as the PODs are two-fold different (0.128 ng/mL vs. 0.257 ng/mL) and EPA advanced the derivation based on results that did control for PFOS and PFOA because this model appeared to fit PFDA well (p = 0.001 vs. 0.10) and there was low uncertainty due to potential confounding in the BMD and moderate uncertainty in the BMDL. Medium confidence in the BMDLs from PFDA linear model (0.257 ng/mL in serum) with control of PFOS and PFOA since the model fit reasonably well and these BMDLs show moderate uncertainty about confounding.

[3] Pooled variance for diphtheria in 5-year-olds = [(502-1)(2.22)^2+ (298-1)(1.17)^2]/[502+298-2] = 3.60. The pooled SD is the square root of 2.41 which is 1.90 log2(IU/mL).

For immunotoxicity related to diphtheria, associated with PFDA measured at age 5 years, the POD is based on a BMR of ½ SD and a $BMDL_{½\ SD}$ of 0.257 ng/mL in serum.

Summary of Modeling Results for Decreased Antibody Responses in Children

Table C-9 presents the BMDs and BMDLs from Budtz-Jørgensen and Grandjean (2018a) considered for POD derivation for reduced antibody responses across different combinations of exposure timing and outcome measurement as detailed above. The BMDLs across the studies and methods ranged from 0.257–0.702 ng/mL.

Table C-9. Selected BMDs and BMDLs and associated uncertainty for effect of PFDA on decreased antibody responses in children from Budtz-Jørgensen and Grandjean (2018a)

Endpoint	$BMD_{1/2SD}$ (ng/mL)	$BMDL_{1/2SD}$ (ng/mL)	Confidence
Decreased serum tetanus antibody concentrations at 7 years of age and PFDA measured at 5 years of age[a]	0.673	0.411	Medium
Decreased serum diphtheria antibody concentrations at 7 years of age and PFDA concentrations at 5 years of age[a]	0.827	0.407	Low
Decreased serum tetanus antibody concentrations at 5 years of age and perinatal PFDA (pregnancy week 32–2 weeks postpartum)[a]	2.260	0.702	Low
Decreased serum diphtheria antibody concentrations at 5 years of age and perinatal PFDA (pregnancy week 32–2 weeks postpartum)[b]	0.385	0.257	Medium

[a]Estimated without control for PFOA and PFOS.
[b]Estimated with control for PFOA and PFOS.

C.1.2. BENCHMARK DOSE MODELING APPROACHES FOR DEVELOPMENTAL EFFECTS

Modeling Results for Decreased Birth Weight

Five *high* confidence studies (Luo et al., 2021; Yao et al., 2021; Wikström et al., 2020; Valvi et al., 2017; Division of Environmental Epidemiology et al., 2016) reported decreased birth weight in infants whose mothers were exposed to PFDA. All studies reported their exposure metric in units of ng/mL and reported the β coefficients per ln(ng/mL) or per $\log_2$(ng/mL), along with 95% confidence intervals, estimated from linear regression models. The logarithmic transformation of exposure yields a negative value for low numbers, which can result in implausible results from dose-response modeling (i.e., estimated risks are negative and unable to determine the responses at zero exposure). EPA first re-expressed the reported β coefficients in terms of per ng/mL according to Dzierlenga et al. (2020). Then EPA used the re-expressed β and the lower limit on the confidence

interval to estimate BMD and BMDL values using the general equation $y = mx + b$, where y is birth weight and x is exposure, substituting the re-expressed β values from these studies for m. The intercept b represents the baseline value of birth weight in an unexposed population and it can be estimated through $\overline{y} = m\overline{x} + b$ using an average birth weight from an external population as $\overline{y}$, an average exposure as $\overline{x}$ and re-expressed β from the studies as m.

The CDC Wonder site (https://wonder.cdc.gov/natality.html) provides vital statistics for babies born in the United States. There were 3,791,712 live births in the U.S. in 2018 according to final natality data. The mean and standard deviation for birth weight were 3,261.6 ± 590.7 g (7.19 ± 1.30 lb), with 8.27% of live births falling below the public health definition of low birth weight (i.e., <2,500 g, or 5.5 lb). The full natality data for the U.S. data on birth weight was used as it is more relevant for deriving toxicity values for the U.S. public than the study-specific birthweight data. Also, the CDC Wonder database may be queried to find the exact percentage of the population falling below the cut-off value for clinical adversity. The CDC Fourth National Report on Human Exposure to Environmental Chemicals (https://www.cdc.gov/exposurereport/index.html) provides the median of serum PFDA concentrations (0.19 ng/mL) among NHANES females in 2011–2012. These values are subsequently used in the estimation of BMD and BMDL values from the available five epidemiological studies.

(Valvi et al., 2017) reported a β coefficient of −41 g per $\log_2$(ng/mL) (95%CI: −102, 18) for the association between birth weight and maternal PFDA serum concentrations in a Denmark cohort. The reported β coefficient can be re-expressed in terms of per ng/mL according to (Dzierlenga et al., 2020). Given the reported study-specific median (0.28 ng/mL) and interquartile range (IQR) (0.22–0.38 ng/mL) of the exposure from (Valvi et al., 2017), EPA estimated the distribution of exposure by assuming the exposure follows a log-normal distribution with mean and standard deviation as:

$$\mu = ln(q_{50}) = ln(0.28) = -1.27 \quad \text{(C-1)}$$

$$\sigma = ln(q_{75}/q_{25})/1.349 = ln(0.38/0.22)/1.349 = 0.41 \quad \text{(C-2)}$$

Then, EPA estimated the 25th–75th percentiles at 10 percentile intervals of the exposure distribution and corresponding responses of reported β coefficient. The re-expressed β coefficient is determined by minimizing the sum of squared differences between the curves generated by the re-expressed β and the reported β. This resulted in a re-expressed β coefficient of −207.7 g per ng/mL (95% CI: −516.8, 91.2 g per ng/mL).

Typically, for continuous data, the preferred definition of the benchmark response (BMR) is to have a basis for what constitutes a minimal level of change in the endpoint that is biologically significant. For birth weight, there is no accepted percent change that is considered adverse. However, there is a clinical measure for what constitutes an adverse response: babies born weighing less than 2,500 g are considered to have low birth weight, and further, low birth weight is associated with a wide range of health conditions throughout life (Tian et al., 2019; Reyes and

Mañalich, 2005; Hack et al., 1995). Given this clinical cut-off for adversity and that 8.27% of live births in the U.S. in 2018 fell below this cut-off, the hybrid approach can be used to define the BMR. The hybrid approach is advantageous in that it harmonizes the definition of the BMR for continuous data with that for dichotomous data.[4] Essentially, the hybrid approach involves the estimation of the dose that increases the percentile of responses falling below (or above) some cut-off for adversity in the tail of the response distribution. Application of the hybrid approach requires the selection of an extra risk value for BMD estimation. In the case of birth weight, an extra risk of 5% is selected given that this level of response is typically used when modeling developmental responses from animal toxicology studies, and that low birthweight confers increased risk for adverse health effects throughout life, thus supporting a BMR lower than the standard BMR of 10% extra risk.

Therefore, given a background response and a BMR = 5% extra risk, the BMD would be the dose that results in 12.86% of the responses falling below the 2,500 g cut-off value:

$$Extra\ Risk(ER) = (P(d) - P(0)) \,/\, (1 - P(0)) \quad \text{(C-3)}$$

$$P(d) = ER(1 - P(0)) + P(0) = 0.05(1 - 0.0827) + 0.0827 = 0.1286 \quad \text{(C-4)}$$

Based on the mean birth weight for all births in the United States of 3,261.6 g with a standard deviation of 590.7 g, EPA calculated the mean response that would be associated with the 12.86th percentile of the distribution falling below 2,500 g. In this case, the mean birth weight would be 3,169.2 g. Given the median exposure among NHANES females as $\overline{x}$, the mean birth weight in the United States as $\overline{y}$ and the re-expressed β as m term, the intercept b can be estimated as:

$$b = \overline{y} - m\overline{x} = 3261.6\ g - \left(-207.7\ g(\tfrac{ng}{mL})^{-1}\right) 0.19\tfrac{ng}{mL} = 3301.1\ g \quad \text{(C-5)}$$

The BMD was calculated by rearranging the equation $y = mx + b$ and solving for x, using 3301.1 g for the b term and −207.7 for the m term. This resulted in a value of 0.63 ng/mL:

$$x = (y - b)/m = (3169.2\ g - 3301.1\ g)/(-207.7\ g(\tfrac{ng}{mL})^{-1}) = 0.63\ ng/mL \quad \text{(C-6)}$$

To calculate the BMDL, the method is essentially the same except that the lower limit (LL) on the re-expressed β coefficient (−516.8 g per ng/mL) is used for the m term. However, (Valvi et al., 2017) reports a two-sided 95% confidence interval for the β coefficient, meaning that the lower limit of that confidence interval corresponds to a 97.5% one-sided lower limit. The BMDL is defined as the 95% lower limit of the BMD (i.e., corresponds to a two-sided 90% confidence

[4]While the explicit application of the hybrid approach is not commonly used in IRIS dose/concentration/exposure-response analyses, the more commonly used SD-definition of the BMR for continuous data is simply one specific application of the hybrid approach. The SD-definition of the BMR assumes that the cut-off for adversity is the 1.4th percentile of a normally distributed response and that shifting the mean of that distribution by one standard deviation approximates an extra risk of 10%.

interval), so the corresponding lower limit on the re-expressed β coefficient needs to be calculated before calculating the BMDL. First, the standard error of the re-expressed β coefficient can be calculated as:

$$SE = \frac{Upper\ Limit - Lower\ Limit}{3.92} = \frac{91.2\ g(\frac{ng}{mL})^{-1} - \left(-516.8\ g(\frac{ng}{mL})^{-1}\right)}{3.92} = 155.1\ g(\frac{ng}{mL})^{-1} \quad \text{(C-7)}$$

Then the corresponding 95% one-sided lower limit on the re-expressed β coefficient is calculated as:

$$95\%\ one-sided\ LL = \beta - 1.645(SE(\beta)) = -207.7\ g(\frac{ng}{mL})^{-1} - 1.645\left(155.1\ g(\frac{ng}{mL})^{-1}\right) = -462.9 g(\frac{ng}{mL})^{-1} \quad \text{(C-8)}$$

Using this value for the m term results in a BMDL value of 0.28 ng/mL maternal serum concentration.

Valvi et al. (2017) also reported a β coefficient of −44 g per $\log_2$(ng/mL) (95%CI: −133, 44 g per $\log_2$(ng/mL) for boys and −28 g per $\log_2$(ng/mL) (95%CI: −110, 54 g per $\log_2$(ng/mL)) for girls. The re-expressed β coefficients are −222.9 g per ng/mL (95%CI: −673.9, 222.9 g per ng/mL) and −141.9 g per ng/mL (95%CI: −557.3, 273.6 g per ng/mL), and the intercepts *b* are 3,304.0 g and 3,288.6 g for boys and girls, respectively. Using these sex-specific values, the estimated BMD values are 0.60 ng/mL for boys and 0.84 ng/mL for girls.

To calculate the BMDL, the same procedure as above is used to calculate the corresponding 95% one-sided lower limit for the re-expressed β coefficient from the re-expressed lower limit on the 95% two-sided confidence interval of −673.9 g per ng/mL for boys and -557.3 g per ng/mL for girls. Using the corresponding lower limit (−599.2 g per ng/mL for boys and −490.5 g per ng/mL for girls), the BMDLs of 0.22 ng/mL for boys and 0.24 ng/mL for girls are calculated.

Division of Environmental Epidemiology et al. (2016) reported a β coefficient of −43.9 g per ln(ng/mL) (95%CI: −104.8, 17.0 g per ln(ng/mL) for the association between birth weight and maternal PFDA serum concentrations in a multi-country cohort. Given the reported study-specific geometric mean (0.25) and standard deviation of ln-transformed exposure (0.70), EPA estimated the mean (−1.41) and standard deviation (0.70) of the log normally distributed exposure. The re-expressed β coefficient is −122.2 g (95%CI: −291.5, 47.2) per ng/mL and the intercept b is 3,284.8 g. The 95% one-sided lower limits for the re-expressed β coefficient are −264.3 g per ng/mL. The values of the BMD and BMDL are 0.95 ng/mL and 0.44 ng/mL, respectively.

Luo et al. (2021) reported a β coefficient of −96.8 g per ln(ng/mL) (95%CI: −178.0, −15.5 g per ln(ng/mL)) for the association between birth weight and maternal PFDA serum concentrations in a China cohort. Given the reported study-specific median (0.48 ng/mL) and IQR (0.34–0.70 ng/mL) of the exposure, EPA estimated the mean (−0.73) and standard deviation (0.54) of the log normally distributed exposure. The re-expressed β coefficient is −195.8 g per ng/mL (95%CI: −360.2, -31.4 g per ng/mL) and the intercept *b* is 3,298.8 g. The 95% one-sided lower limits for the

re-expressed β coefficient are −333.8 g per ng/mL. The values of the BMD and BMDL are 0.66 ng/mL and 0.39 ng/mL, respectively.

Wikström et al. (2020) reported a β coefficient of −58.0 g per ln(ng/mL) (95%CI: −103.0, −13.0 g per ln(ng/mL)) for the association between birth weight and maternal PFDA serum concentrations in a Swedish cohort. Given the reported study-specific median (0.26 ng/mL) and IQR (0.19–0.34 ng/mL) of the exposure, EPA estimated the mean (−1.35) and standard deviation (0.43) of the log normally distributed exposure. The re-expressed β coefficient is −218.9 g per ng/mL (95%CI: −388.7, −49.1 g per ng/mL) and the intercept *b* is 3303.2 g. The 95% one-sided lower limits for the re-expressed β coefficient are −361.4 g per ng/mL. The values of the BMD and BMDL are 0.61 ng/mL and 0.37 ng/mL, respectively.

Wikström et al. (2020) also reported β coefficients of −47 g per ln(ng/mL) (95%CI: −112, 17 g per ln(ng/mL)) for boys and −69 g per ln(ng/mL) (95%CI: −133, -6 g per ln(ng/mL)) for girls. The re-expressed β coefficients are −177.4 g per (95%CI: −422.7, 64.2 g per ng/mL) and −260.4 g per (95%CI: −501.9, -22.6 g per ng/mL), and the intercepts *b* are 3,295.3 g and 3,311.1 g for boys and girls, respectively. Using these sex-specific values, the estimated BMD values are 0.71 ng/mL for boys and 0.54 ng/mL for girls. The corresponding 95% one-sided lower limits for the re-expressed β coefficient are −381.6 g per and −461.5 g per for boys and girls, respectively. The BMDL values are 0.33 ng/mL for boys and 0.31 ng/mL for girls.

Yao et al. (2021) reported a β coefficient of −46.3 g per ln(ng/mL) (95%CI: −131.1, 38.5 g per ln(ng/mL)) for the association between birth weight and maternal PFDA serum concentrations in a China cohort. Given the reported study-specific median (0.55 ng/mL) and IQR (0.37–0.74 ng/mL) of the exposure, EPA estimated the mean (−0.60) and standard deviation (0.51) of the log normally distributed exposure. The re-expressed β coefficient is −82.0 g per (95%CI: −232.1, 68.1 g per ng/mL) and the intercept *b* is 3277.2 g. The 95% one-sided lower limits for the re-expressed β coefficient are −208.0 g per ng/mL. The values of the BMD and BMDL are 1.32 ng/mL and 0.52 ng/mL, respectively.

For all the above calculations, EPA used the exact percentage (8.27%) of live births in the U.S. in 2018 that fell below the cut-off of 2,500 g as the tail probability to represent the probability of extreme ("adverse") response at zero dose ($P(0)$). However, this exact percentage of 8.27% was calculated without accounting for the existence of background PFDA exposure in the U.S. population (i.e., 8.27% is not the tail probability of extreme response at zero dose). Thus, EPA considers an alternative control-group response distribution ($N(\mu_c, \sigma_c)$), using the study-specific intercept *b* obtained through equation (C-5) (representing the baseline value of birth weight in an unexposed population) as μ_c and the standard deviation of the U.S. population as σ_c, to estimate the tail probability that fell below the cut-off of 2,500 g. EPA estimated the study-specific tail probability of live births falling below the public health definition of low birth weight (2,500 g) as:

$$P(0) = \frac{1}{\sigma_c\sqrt{2\pi}}\int_{-\infty}^{2500} e^{\left(-\frac{(x-b)^2}{2\sigma_c^2}\right)} dx = \frac{1}{590.7\sqrt{2\pi}}\int_{-\infty}^{2500} e^{\left(-\frac{(x-b)^2}{2*590.7^2}\right)} dx \quad \text{(C-9)}$$

$$b = \overline{y} - m\overline{x} = 3261.6 - (\beta_{re-expressed} * 0.19\frac{ng}{mL}) \quad \text{(C-10)}$$

In this alternative approach, $P(0)$ is 9.86% if there is no background exposure ($\overline{x} = 0$). By using the median serum PFDA concentrations (0.19 ng/mL) from NHANES females in 2011–2012 as background exposure ($\overline{x}$), the tail probabilities using this alternative approach were study specific and ranged from 8.48% to 9.41%. As such, the results from this alternative approach, presented under the column of "Alternative Tail Probability" in Table C-8, are very similar to the main results, presented under the column of "Exact Percentage" in Table C-8, when background exposure was not accounted for while estimating the tail probability.

Table C-8 presents the BMDs and BMDLs for all studies considered for POD derivation, with and without accounting for background exposure while estimating the percentage of the population falling below the cut-off value. The BMDLs across the studies and methods ranged from 0.22 ng/mL to 0.66 ng/mL.

Table C-10. BMDs and BMDLs for effect of PFDA on decreased birth weight, by using percentage (8.27%) of live births falling below the public health definition of low birth weight, or alternative study-specific tail probability

Study	Exposure median (IQR) or GM (SD)	Exposure distribution (μ, σ)	Reported β (95%CI)	Re-expressed β (95%CI) g/ng/mL	Intercept b	SE of β	95% one-sided LL of β	Exact percentage ($P(0)$ =8.27%)		Alternative tail probability[a]		
								BMD (ng/mL)	BMDL (ng/mL)	$P(0)$	BMD (ng/mL)	BMDL (ng/mL)
Valvi et al. (2017)	0.28 (0.22–0.38)	(−1.27, 0.41)	−41.0 (−102.0, 18.0) g/log$_2$(ng/mL)	−207.7 (−516.8, 91.2)	3301.1	155.11	−462.9	0.63	0.28	8.75%	0.70	0.31
Valvi et al. (2017) Boys	0.28 (0.22–0.38)	(−1.27, 0.41)	−44.0 (−133.0, 44.0) g/log$_2$(ng/mL)	−222.9 (−673.9, 222.9)	3304.0	228.78	−599.2	0.60	0.22*	8.67%	0.65	0.24
Valvi et al. (2017) Girls	0.28 (0.22–0.38)	(−1.27, 0.41)	−28.0 (−110.0, 54.0) g/log$_2$(ng/mL)	−141.9 (−557.3, 273.6)	3288.6	211.98	−490.5	0.84	0.24	9.09%	0.99	0.29
Division of Environmental Epidemiology et al. (2016)	0.25 (0.70)[b]	(−1.41, 0.70)	−43.9 (−104.8, 17.0) g/ln(ng/mL)	−122.2 (−291.5, 47.2)	3284.8	86.40	−264.3	0.95	0.44	9.20%	1.14	0.53
Luo et al. (2021)	0.48 (0.34–0.70)	(-0.73, 0.54)	-96.8 (-178.0, -15.5) g/ln(ng/mL)	-195.8 (-360.2, -31.4)	3298.8	83.88	-333.8	0.66	0.39	8.81%	0.73	0.43
Wikström et al. (2020)	0.26 (0.19–0.34)	(-1.35, 0.43)	-58.0 (-103.0, -13.0) g/ln(ng/mL)	-218.9 (-388.7, -49.1)	3303.2	86.64	-361.4	0.61	0.37	8.69%	0.66	0.40
Wikström et al. (2020) Boys	0.26 (0.19–0.34)	(-1.35, 0.43)	-47.0 (-112.0, 17.0) g/ln(ng/mL)	-177.4 (-422.7, 64.2)	3295.3	124.19	-381.6	0.71	0.33	8.91%	0.80	0.37
Wikström et al. (2020) Girls	0.26 (0.19–0.34)	(-1.35, 0.43)	-69.0 (-133.0, -6.0) g/ln(ng/mL)	-260.4 (-501.9, -22.6)	3311.1	122.26	-461.5	0.54	0.31	8.48%	0.57	0.32

Study	Exposure median (IQR) or GM (SD)	Exposure distribution (μ, σ)	Reported β (95%CI)	Re-expressed β (95%CI) g/ng/mL	Intercept b	SE of β	95% one-sided LL of β	Exact percentage ($P(0)$ =8.27%)		Alternative tail probability[a]		
								BMD (ng/mL)	BMDL (ng/mL)	$P(0)$	BMD (ng/mL)	BMDL (ng/mL)
Yao et al. (2021)	0.55 (0.37–0.74)	(-0.60, 0.51)	-46.3 (-131.1, 38.5) g/ln(ng/mL)	-82.0 (-232.1, 68.1)	3277.2	76.58	-208.0	1.32	0.52	9.41%	1.68	0.66

*Smallest BMDL using the five individual studies.

[a]The alternative study-specific tail probability of live births falling below the public health definition of low birth weight based on Normal distribution with intercept b as mean and standard deviation of 590.7 based on U.S. population.

[b]Division of Environmental Epidemiology et al. (2016) reports Geometric Mean (GM) and standard deviation (SD) of ln-transformed concentrations.

C.2. BENCHMARK DOSE MODELING RESULTS FROM ANIMAL STUDIES

C.2.1. BENCHMARK DOSE MODELING APPROACHES

The endpoints selected for benchmark dose (BMD) modeling are listed in Table C-11. The animal doses in the study were used in the BMD modeling and then converted to human equivalent doses (HEDs) using data-derived extrapolation factors (DDEFs) described in Section 3.1.7 of the main document; the modeling results are presented in this appendix.

Modeling Procedure for Dichotomous Noncancer Data

BMD modeling of dichotomous noncancer data was conducted using EPA's Benchmark Dose Software (BMDS, version 3.2). For these data, the Gamma, Logistic, Log-Logistic, Log-Probit, Multistage, Probit, Weibull, and Dichotomous Hill models available within the software were fit using a benchmark response (BMR) of 10% extra risk (see Toxicological Review, Section 5.2.1 for justification of selected BMRs). The Multistage model is run for all polynomial degrees up to $n - 2$, where n is the number of dose groups including control. Adequacy of model fit was judged based on χ^2 goodness-of-fit p-value ($p > 0.1$), scaled residuals at the data point (except the control) closest to the predefined benchmark response (absolute value <2.0), and visual inspection of the model fit. In the cases where no best model was found to fit to the data, a reduced data set without the high-dose group was further attempted for modeling and the result presented with that of the full data set. In cases where a model with several parameters equal to the number of dose groups was fit to the data set, all parameters were estimated, and no p-value was calculated, that model was not considered for estimating a point of departure (POD) *unless* no other model provided adequate fit. Among all models providing adequate fit, the benchmark dose lower confidence limit (BMDL) from the model with the lowest Akaike's information criterion (AIC) was selected as a potential POD when BMDL values were sufficiently close (within 3-fold). Otherwise, the lowest BMDL was selected as a potential POD.

Modeling Procedure for Continuous Noncancer Data

BMD modeling of continuous noncancer data was conducted using EPA's Benchmark Dose Software (BMDS, version 3.2). For these data, the Exponential, Hill, Polynomial, and Power models available within the software are fit using a BMR of 1 standard deviation (SD) when no toxicological information was available to determine an adverse level of response. When toxicological information was available, the BMR was based on relative deviation, as outlined in the Benchmark Dose Technical Guidance (U.S. EPA, 2012) (see Toxicological Review, Section 5.2.1 justification for using BMRs); when a BMR based on relative deviation was used, modeling results using BMRs based on SD are included for reference. An adequate fit is judged on the basis of χ^2 goodness-of-fit p-value ($p > 0.1$), scaled residuals at the data point (except the control) closest to the predefined benchmark response (absolute value <2.0), and visual inspection of the model fit. In addition to these three criteria for judging adequacy of model fit, a determination is made on whether the

variance across dose groups is homogeneous. If a homogeneous variance model is deemed appropriate on the basis of the statistical test provided by BMDS (i.e., Test 2), the final BMD results are estimated from a homogeneous variance model. If the test for homogeneity of variance is rejected ($p < 0.05$), the model is run again while modeling the variance as a power function of the mean to account for this nonhomogeneous variance. If this nonhomogeneous variance model does not adequately fit the data (i.e., Test 3; $p < 0.05$), alternative approaches are assessed on a case-by-case basis. For example, in cases where neither variance model fit, or constant variance did not fit (with adequate Test-4 *p*-value) and nonconstant variance did fit (with inadequate Test-4 *p*-value), the log-normal distribution was attempted.

In cases where a model with several parameters equal to the number of dose groups was fit to the data set, all parameters were estimated, and no *p*-value was calculated, that model was not considered for estimating a POD *unless* no other model provided adequate fit. Among all models providing adequate fit, the BMDL from the model with the lowest AIC was selected as a potential POD when BMDL estimates differed by less than 3-fold. When BMDL estimates differed by greater than 3-fold, the model with the lowest BMDL was selected to account for model uncertainty.

Modeling Procedure for Continuous Noncancer Developmental Toxicity Data

For continuous developmental toxicity data, data for individual animals were requested from the study authors when possible. The use of individual animal data allows for the correct measure of variance to be calculated. When a biological rationale for selecting a benchmark response level is lacking, a BMR equal to 0.5 SD was used. The use of 1 SD for the BMR for continuous endpoints is based on the observation that shifting the distribution of the control group by 1 SD results in ~10% of the animal data points falling beyond an adversity cutoff defined at the ~1.5 percentile (Crump, 1995). This approximates the 10% extra risk commonly used as the BMR for dichotomous endpoints. Thus, the use of 0.5 SD for continuous developmental toxicity endpoints approximates the extra risk commonly used for dichotomous developmental toxicity endpoints.

Data Used for Modeling

The source of the data used for modeling endpoints from animal studies is provided in Table C-11. These data also are included in full in the tables below.

Table C-11. Sources of data used in benchmark dose modeling of PFDA endpoints from animal studies

Endpoint/reference	Reference	HAWC link
↑ AST – M	NTP (2018)	https://hawcprd.epa.gov/ani/endpoint/100506861/
↑ AST – F	NTP (2018)	https://hawcprd.epa.gov/ani/endpoint/100506957/

Endpoint/reference	Reference	HAWC link
↑ ALP – F	NTP (2018)	https://hawcprd.epa.gov/ani/endpoint/100506956/
↑ Relative Liver weight – M	NTP (2018)	https://hawcprd.epa.gov/ani/endpoint/100506814/
↑ Relative Liver weight – F	NTP (2018)	https://hawcprd.epa.gov/ani/endpoint/100506920/
↑ Relative Liver weight – F (Histo)	Frawley et al. (2018)	https://hawcprd.epa.gov/ani/endpoint/100506676/
↑ Relative Liver weight – F (MPS)	Frawley et al. (2018)	https://hawcprd.epa.gov/ani/endpoint/100506669/
↑ Relative Liver weight – F (TDAR)	Frawley et al. (2018)	https://hawcprd.epa.gov/ani/endpoint/100506677/
↓ Fetal Body Weight (GD6–15)	Harris and Birnbaum (1989)	https://hawcprd.epa.gov/ani/endpoint/100506643/
↓ Caudal Epididymis Sperm Count	NTP (2018)	https://hawcprd.epa.gov/ani/endpoint/100506879/
↓ Absolute Testis Weight	NTP (2018)	https://hawcprd.epa.gov/ani/endpoint/100506820/
↓ Absolute Cauda Epididymis Weight	NTP (2018)	https://hawcprd.epa.gov/ani/endpoint/100506878/
↓ Absolute Whole Epididymis Weight	NTP (2018)	https://hawcprd.epa.gov/ani/endpoint/100506877/
↓ Estrus Time	NTP (2018)	https://hawcprd.epa.gov/ani/endpoint/100524936/
↑ Diestrus Time	NTP (2018)	https://hawcprd.epa.gov/ani/endpoint/100524930/
↓ Relative Uterus Weight	NTP (2018)	https://hawcprd.epa.gov/ani/endpoint/100506941/
↓ Absolute Uterus Weight	NTP (2018)	https://hawcprd.epa.gov/ani/endpoint/100506940/

C.2.2. INCREASED AST—MALE RATS (NTP, 2018)

Table C-12. Dose-response data for increased AST in male rats (NTP, 2018)

Dose (mg/kg-d)	*n*	Mean	SD
0	10	65.3	10.18
0.156	10	74	9.55
0.312	10	77.3	16.98
0.625	10	81.3	9.84
1.25	10	87.5	14.61
2.5	9	92.67	8.04

Table C-13. Benchmark dose results for increased AST in male rats—constant variance, BMR = 1 standard deviation (NTP, 2018)[1]

Models	Restriction	1 standard deviation		*p*-Value	AIC	BMDS classification	BMDS notes
		BMD	BMDL				
Constant variance							
Exponential 2 (CV—normal)	Restricted	1.3924	1.0640	0.1386	467.4755	Viable—Alternate	
Exponential 3 (CV—normal)	Restricted	1.3924	1.0640	0.1386	467.4755	Viable—Alternate	
Exponential 4 (CV—normal)	Restricted	0.3933	0.1723	0.8692	463.2441	Viable—Alternate	
Exponential 5 (CV—normal)	Restricted	0.3949	0.1723	0.8692	463.2441	Viable—Alternate	
Hill (CV—normal)	**Restricted**	**0.3266**	**0.1227**	**0.9560**	**462.8481**	**Viable—Recommended**	**Lowest BMDL**
Polynomial (5 degree) (CV—normal)	Restricted	1.2558	0.9260	0.1910	466.6376	Viable—Alternate	
Polynomial (4 degree) (CV—normal)	Restricted	1.2558	0.9260	0.1910	466.6376	Viable—Alternate	
Polynomial (3 degree) (CV—normal)	Restricted	1.2558	0.9260	0.1910	466.6376	Viable—Alternate	
Polynomial (2 degree) (CV—normal)	Restricted	1.2558	0.9260	0.1910	466.6376	Viable—Alternate	
Power (CV—normal)	Restricted	1.2558	0.9260	0.1910	466.6376	Viable—Alternate	
Linear (CV—normal)	Unrestricted	1.2558	0.9260	0.1910	466.6376	Viable—Alternate	

[1] Throughout this section, in the Benchmark Dose results table, the "Restriction" column denotes the restriction status of applied models, and the "Classification" column denotes whether a model can be considered for model selection purposes. See BMDS User Guide: https://www.epa.gov/bmds. If a model was selected as appropriately fitting the modeled data, that model's entries in the tables are in green shaded cells and the text is bolded.

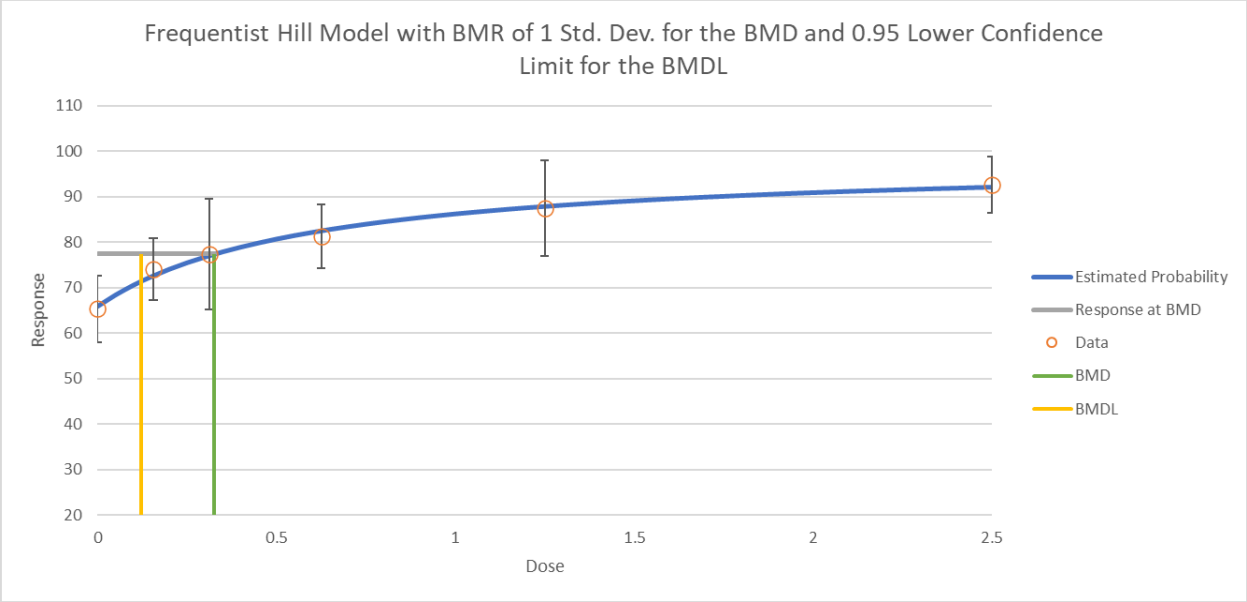

Figure C-3. Dose-response curve for the Hill model fit to increased AST in male rats (NTP, 2018).

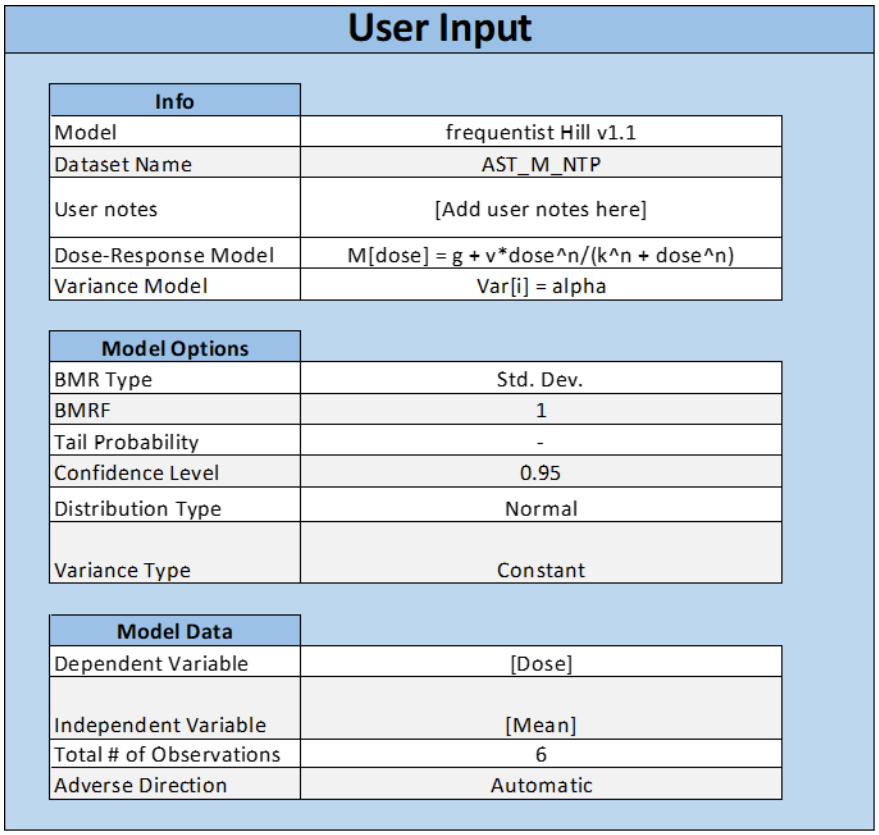

User Input

Info	
Model	frequentist Hill v1.1
Dataset Name	AST_M_NTP
User notes	[Add user notes here]
Dose-Response Model	M[dose] = g + v*dose^n/(k^n + dose^n)
Variance Model	Var[i] = alpha

Model Options	
BMR Type	Std. Dev.
BMRF	1
Tail Probability	-
Confidence Level	0.95
Distribution Type	Normal
Variance Type	Constant

Model Data	
Dependent Variable	[Dose]
Independent Variable	[Mean]
Total # of Observations	6
Adverse Direction	Automatic

Figure C-4. User Input for dose-response modeling of increased AST in male rats (NTP, 2018).

Model Results

Benchmark Dose	
BMD	0.32659537
BMDL	0.122653237
BMDU	0.926151614
AIC	462.8480778
Test 4 P-value	0.956041631
D.O.F.	3

Model Parameters	
# of Parameters	5
Variable	Estimate
g	65.96003464
v	32.30491688
k	0.59693749
n	Bounded
alpha	130.5126471

Goodness of Fit

Dose	Size	Estimated Median	Calc'd Median	Observed Mean	Estimated SD	Calc'd SD	Observed SD	Scaled Residual
0	10	65.96003464	65.3	65.3	11.4242132	10.18	10.18	-0.182700792
0.156	10	72.65324238	74	74	11.4242132	9.55	9.55	0.372789045
0.312	10	77.0489535	77.3	77.3	11.4242132	16.98	16.98	0.06949089
0.625	10	82.48344375	81.3	81.3	11.4242132	9.84	9.84	-0.327582975
1.25	10	87.82387482	87.5	87.5	11.4242132	14.61	14.61	-0.089650123
2.5	9	92.03814971	92.67	92.67	11.4242132	8.04	8.04	0.165923977

Likelihoods of Interest

Model	Log Likelihood*	# of Parameters	AIC
A1	-227.2635646	7	468.527129
A2	-223.0848415	12	470.169683
A3	-227.2635646	7	468.527129
fitted	-227.4240389	4	462.848078
R	-241.1426777	2	486.285355

* Includes additive constant of -54.21737. This constant was not included in the LL derivation prior to BMDS 3.0.

Tests of Interest

Test	-2*Log(Likelihood Ratio)	Test df	p-value
1	36.11567239	10	<0.0001
2	8.357446131	5	0.13760531
3	8.357446131	5	0.13760531
4	0.320948692	3	0.95604163

Figure C-5. Model Results for increased AST in male rats (NTP, 2018).

C.2.3. INCREASED AST—FEMALE RATS (NTP, 2018)

Table C-14. Dose-response data for increased AST in female rats (NTP, 2018)

Dose (mg/kg-d)	*n*	Mean	SD
0	10	62.6	10.75
0.156	9	60.44	6.51
0.312	10	57.9	4.11
0.625	10	63.3	5
1.25	10	81.9	8.29
2.5	7	112.57	22.54

Table C-15. Benchmark dose results for increased AST in female rats—constant variance, BMR = 1 standard deviation (NTP, 2018)

Models	Restriction	1 standard deviation		*p*-Value	AIC	BMDS classification	BMDS notes
		BMD	BMDL				
Constant variance							
Exponential 2 (CV—normal)	Restricted	0.6219	0.5312	0.1426	427.8867	Questionable	Constant variance test failed (Test 2 *p*-value < 0.05)
Exponential 3 (CV—normal)	Restricted	0.8024	0.5551	0.1375	428.5314	Questionable	Constant variance test failed (Test 2 *p*-value < 0.05)
Exponential 4 (CV—normal)	Restricted	0.5006	0.0000	0.0153	433.4316	Unusable	BMD computation failed; lower limit includes zero BMDL not estimated Constant variance test failed (Test 2 *p*-value < 0.05) Goodness of fit *p*-value < 0.1 |Residual at control| > 2
Exponential 5 (CV—normal)	Restricted	0.1055	0.1048	<0.0001	553.6193	Questionable	Constant variance test failed (Test 2 5-value < 0.05) Goodness of fit *p*-value < 0.1 |Residual at control| > 2 Modeled control response std. dev. >|1.5| actual response std. dev.
Hill (CV—normal)	Restricted	0.9445	0.6992	0.5341	426.2660	Questionable	Constant variance test failed (Test 2 *p*-value < 0.05)
Polynomial (5 degree) (CV—normal)	Restricted	0.8055	0.5285	0.1331	428.6052	Questionable	Constant variance test failed (Test 2 *p*-value < 0.05)
Polynomial (4 degree) (CV—normal)	Restricted	0.8055	0.5285	0.1331	428.6052	Questionable	Constant variance test failed (Test 2 *p*-value < 0.05)
Polynomial (3 degree) (CV—normal)	Restricted	0.8055	0.5285	0.1331	428.6052	Questionable	Constant variance test failed (Test 2 *p*-value < 0.05)

Models	Restriction	1 standard deviation		*p*-Value	AIC	BMDS classification	BMDS notes
		BMD	BMDL				
Constant variance							
Polynomial (2 degree) (CV—normal)	Restricted	0.8055	0.5285	0.1331	428.6052	Questionable	Constant variance test failed (Test 2 *p*-value < 0.05)
Power (CV—normal)	Restricted	0.8126	0.5686	0.2122	427.5127	Questionable	Constant variance test failed (Test 2 *p*-value < 0.05)
Linear (CV—normal)	Unrestricted	0.5006	0.4134	0.0339	431.4316	Questionable	Constant variance test failed (Test 2 *p*-value < 0.05) Goodness of fit *p*-value < 0.1 |Residual at control| > 2

Table C-16. Benchmark dose results for increased AST in female rats—nonconstant variance, BMR = 1 standard deviation (NTP, 2018)

Models	Restriction	1 standard deviation		*p*-Value	AIC	BMDS classification	BMDS notes
		BMD	BMDL				
Non-constant variance							
Exponential 2 (NCV—normal)	Restricted	0.4683	0.3822	0.0006	417.7886	Questionable	Nonconstant variance test failed (Test 3 *p*-value < 0.05) Goodness of fit *p*-value < 0.1 |Residual at control| > 2
Exponential 3 (NCV—normal)	Restricted	0.7433	0.5327	0.0048	413.2499	Questionable	Nonconstant variance test failed (Test 3 *p*-value < 0.05) Goodness of fit *p*-value < 0.1
Exponential 4 (NCV—normal)	Restricted	0.4044	0.3201	<0.0001	425.5227	Questionable	Nonconstant variance test failed (Test 3 *p*-value < 0.05) Goodness of fit *p*-value < 0.1 |Residual at control| > 2
Exponential 5 (NCV—normal)	Restricted	0.9173	0.6965	0.0484	408.4035	Questionable	Nonconstant variance test failed (Test 3 *p*-value < 0.05) Goodness of fit *p*-value < 0.1
Hill (NCV—normal)	Restricted	1.1570	0.6738	0.0375	408.9143	Questionable	Nonconstant variance test failed (Test 3 *p*-value < 0.05) Goodness of fit *p*-value < 0.1
Polynomial (5 degree) (NCV—normal)	Restricted	0.8488	0.5738	0.0172	410.3710	Questionable	Nonconstant variance test failed (Test 3 *p*-value < 0.05) Goodness of fit *p*-value < 0.1
Polynomial (4 degree) (NCV—normal)	Restricted	0.8488	0.5738	0.0172	410.3710	Questionable	Nonconstant variance test failed (Test 3 *p*-value < 0.05) Goodness of fit *p*-value < 0.1

Models	Restriction	1 standard deviation		*p*-Value	AIC	BMDS classification	BMDS notes
		BMD	BMDL				
Non-constant variance							
Polynomial (3 degree) (NCV—normal)	Restricted	0.8488	0.5738	0.0172	410.3710	Questionable	Nonconstant variance test failed (Test 3 *p*-value < 0.05) Goodness of fit *p*-value < 0.1
Polynomial (2 degree) (NCV—normal)	Restricted	0.8488	0.5738	0.0172	410.3710	Questionable	Nonconstant variance test failed (Test 3 *p*-value < 0.05) Goodness of fit *p*-value < 0.1
Power (NCV—normal)	Restricted	0.7553	0.5621	0.0104	411.6066	Questionable	Nonconstant variance test failed (Test 3 *p*-value < 0.05) Goodness of fit *p*-value < 0.1
Linear (NCV—normal)	Unrestricted	0.4052	0.3203	<0.0001	423.4964	Questionable	Nonconstant variance test failed (Test 3 *p*-value < 0.05) Goodness of fit *p*-value < 0.1 |Residual at control| > 2

Table C-17. Benchmark dose results for increased AST in female rats—log-normal, constant variance, BMR = 1 standard deviation (NTP, 2018)

Models	Restriction	1 standard deviation		*p*-Value	AIC	BMDS classification	BMDS notes
		BMD	BMDL				
Constant variance							
Exponential 2 (CV—log-normal)	Restricted	0.4981	0.4114	0.0353	410.1569	Questionable	Constant variance test failed (Test 2 *p*-value < 0.05) Goodness of fit *p*-value < 0.1 |Residual for Dose Group Near BMD| > 2 |Residual at control| > 2
Exponential 3 (CV— log-normal)	Restricted	0.7017	0.4707	0.0518	409.5663	Questionable	Constant variance test failed (Test 2 *p*-value < 0.05) Goodness of fit *p*-value < 0.1 |Residual for Dose Group Near BMD| > 2 |Residual at control| > 2
Exponential 4 (CV— log-normal)	Restricted	0.4173	0.0000	0.0061	414.2361	Unusable	BMD computation failed; lower limit includes zero BMDL not estimated Constant variance test failed (Test 2 *p*-value < 0.05) Goodness of fit *p*-value < 0.1 |Residual for Dose Group Near BMD| > 2 |Residual at control| > 2

Models	Restriction	1 standard deviation		*p*-Value	AIC	BMDS classification	BMDS notes
		BMD	BMDL				
Constant variance							
Exponential 5 (CV— log-normal)	Restricted	−9999.0000	0.0000	<0.0001	482.3726	Unusable	BMD computation failed; lower limit includes zero BMD not estimated BMDL not estimated Constant variance test failed (Test 2 *p*-value < 0.05) Goodness of fit *p*-value < 0.1 |Residual at control| > 2
Hill (CV— log-normal)	Restricted	0.8526	0.6413	0.4051	405.6388	Questionable	Constant variance test failed (Test 2 *p*-value < 0.05) |Residual at control| > 2
Polynomial (5 degree) (CV— log-normal)	Restricted	0.7220	0.4645	0.0501	409.6412	Questionable	Constant variance test failed (Test 2 *p*-value < 0.05) Goodness of fit *p*-value < 0.1 |Residual for Dose Group Near BMD| > 2 |Residual at control| > 2
Polynomial (4 degree) (CV— log-normal)	Restricted	0.7220	0.4645	0.0501	409.6412	Questionable	Constant variance test failed (Test 2 *p*-value < 0.05) Goodness of fit *p*-value < 0.1 |Residual for Dose Group Near BMD| > 2 |Residual at control| > 2
Polynomial (3 degree) (CV— log-normal)	Restricted	0.7220	0.4645	0.0501	409.6412	Questionable	Constant variance test failed (Test 2 *p*-value < 0.05) Goodness of fit *p*-value < 0.1 |Residual for Dose Group Near BMD| > 2 |Residual at control| > 2
Polynomial (2 degree) (CV— log-normal)	Restricted	0.7220	0.4645	0.0501	409.6412	Questionable	Constant variance test failed (Test 2 *p*-value < 0.05) Goodness of fit *p*-value < 0.1 |Residual for Dose Group Near BMD| > 2 |Residual at control| > 2
Power (CV— log-normal)	Restricted	0.7158	0.5034	0.0953	408.1933	Questionable	Constant variance test failed (Test 2 *p*-value < 0.05) Goodness of fit *p*-value < 0.1 |Residual for Dose Group Near BMD| > 2 |Residual at control| > 2
Linear (CV— log-normal)	Unrestricted	0.4170	0.3303	0.0061	414.2360	Questionable	Constant variance test failed (Test 2 *p*-value < 0.05) Goodness of fit *p*-value < 0.1 |Residual for Dose Group Near BMD| > 2 |Residual at control| > 2

C.2.4. INCREASED ALP—FEMALE RAT (NTP, 2018)

Table C-18. Dose-response data for increased ALP in female rats (NTP, 2018)

Dose (mg/kg-d)	*n*	Mean	SD
0	9	136.4	18.6
0.156	9	156.1	24
0.312	10	182.8	36.68
0.625	10	184.2	33.2
1.25	10	281.1	72.42
2.5	7	262.4	60.06

Table C-19. Benchmark dose results for increased ALP in female rats—BMR = constant variance, 1 standard deviation (NTP, 2018)

Models	Restriction	1 standard deviation		*p*-Value	AIC	BMDS classification	BMDS notes
		BMD	BMDL				
Constant variance							
Exponential 2 (CV—normal)	Restricted	1.2058	0.9747	<0.0001	598.0449	Questionable	Constant variance test failed (Test 2 *p*-value < 0.05) Goodness of fit *p*-value < 0.1 |Residual for Dose Group Near BMD| > 2 Modeled control response std. dev. >|1.5| actual response std. dev.
Exponential 3 (CV—normal)	Restricted	1.2058	0.9747	<0.0001	598.0449	Questionable	Constant variance test failed (Test 2 *p*-value < 0.05) Goodness of fit *p*-value < 0.1 |Residual for Dose Group Near BMD| > 2 Modeled control response std. dev. >|1.5| actual response std. dev.
Exponential 4 (CV—normal)	Restricted	0.3043	0.1894	0.0206	585.6900	Questionable	Constant variance test failed (Test 2 *p*-value < 0.05) Goodness of fit *p*-value < 0.1 Modeled control response std. dev. >|1.5| actual response std. dev.
Exponential 5 (CV—normal)	Restricted	0.6977	0.3389	0.0530	583.7962	Questionable	Constant variance test failed (Test 2 *p*-value < 0.05) Goodness of fit *p*-value < 0.1 Modeled control response std. dev. >|1.5| actual response std. dev.

Models	Restriction	1 standard deviation		*p*-Value	AIC	BMDS classification	BMDS notes
		BMD	BMDL				
Constant variance							
Hill (CV—normal)	Restricted	0.6547	0.6162	0.1011	582.1450	Questionable	Constant variance test failed (Test 2 *p*-value < 0.05) Modeled control response std. dev. >|1.5| actual response std. dev.
Polynomial (5 degree) (CV—normal)	Restricted	0.9018	0.6940	0.0005	594.1122	Questionable	Constant variance test failed (Test 2 *p*-value < 0.05) Goodness of fit *p*-value < 0.1 Modeled control response std. dev. >|1.5| actual response std. dev.
Polynomial (4 degree) (CV—normal)	Restricted	0.9018	0.6940	0.0005	594.1122	Questionable	Constant variance test failed (Test 2 *p*-value < 0.05) Goodness of fit *p*-value < 0.1 Modeled control response std. dev. >|1.5| actual response std. dev.
Polynomial (3 degree) (CV—normal)	Restricted	0.9018	0.6940	0.0005	594.1122	Questionable	Constant variance test failed (Test 2 *p*-value < 0.05) Goodness of fit *p*-value < 0.1 Modeled control response std. dev. >|1.5| actual response std. dev.
Polynomial (2 degree) (CV—normal)	Restricted	0.9018	0.6940	0.0005	594.1122	Questionable	Constant variance test failed (Test 2 *p*-value < 0.05) Goodness of fit *p*-value < 0.1 Modeled control response std. dev. >|1.5| actual response std. dev.
Power (CV—normal)	Restricted	0.9018	0.6941	0.0005	594.1122	Questionable	Constant variance test failed (Test 2 *p*-value < 0.05) Goodness of fit *p*-value < 0.1 Modeled control response std. dev. >|1.5| actual response std. dev.
Linear (CV—normal)	Unrestricted	0.9018	0.6940	0.0005	594.1122	Questionable	Constant variance test failed (Test 2 *p*-value < 0.05) Goodness of fit *p*-value < 0.1 Modeled control response std. dev. >|1.5| actual response std. dev.

Table C-20. Benchmark dose results for increased ALP in female rats—nonconstant variance, BMR = 1 standard deviation (NTP, 2018)

Models	Restriction	1 standard deviation		*p*-Value	AIC	BMDS classification	BMDS notes
		BMD	BMDL				
Non-constant variance							
Exponential 2 (NCV—normal)	Restricted	0.3761	0.2620	<0.0001	578.1584	Questionable	Goodness of fit *p*-value < 0.1
Exponential 3 (NCV—normal)	Restricted	0.3761	0.2620	<0.0001	578.1584	Questionable	Goodness of fit *p*-value < 0.1
Exponential 4 (NCV—normal)	Restricted	0.1191	0.0720	0.0174	565.0835	Questionable	Goodness of fit *p*-value < 0.1
Exponential 5 (NCV—normal)	Restricted	0.1556	0.0758	0.0083	566.5363	Questionable	Goodness of fit *p*-value < 0.1
Hill (NCV—normal)	Restricted	0.1501	0.0700	0.0056	567.3018	Questionable	Goodness of fit *p*-value < 0.1
Polynomial (5 degree) (NCV—normal)	Restricted	0.2457	0.1655	0.0012	570.9484	Questionable	Goodness of fit *p*-value < 0.1
Polynomial (4 degree) (NCV—normal)	Restricted	0.2457	0.1655	0.0012	570.9484	Questionable	Goodness of fit *p*-value < 0.1
Polynomial (3 degree) (NCV—normal)	Restricted	0.2457	0.1655	0.0012	570.9484	Questionable	Goodness of fit *p*-value < 0.1
Polynomial (2 degree) (NCV—normal)	Restricted	0.2457	0.1655	0.0012	570.9484	Questionable	Goodness of fit *p*-value < 0.1
Power (NCV—normal)	Restricted	0.2457	0.1655	0.0012	570.9484	Questionable	Goodness of fit *p*-value < 0.1
Linear (NCV—normal)	Unrestricted	0.2457	0.1655	0.0012	570.9484	Questionable	Goodness of fit *p*-value < 0.1

Table C-21. Benchmark dose results for increased ALP in female rats—log-normal, constant variance, BMR = 1 standard deviation (NTP, 2018)

Models	Restriction	1 standard deviation		*p*-Value	AIC	BMDS classification	BMDS notes
		BMD	BMDL				
Constant variance							
Exponential 2 (CV—log-normal)	Restricted	0.8447	0.6570	0.0001	575.0495	Questionable	Goodness of fit *p*-value < 0.1 |Residual for Dose Group Near BMD| > 2 |Residual at control| > 2
Exponential 3 (CV— log-normal)	Restricted	0.8447	0.6570	0.0001	575.0495	Questionable	Goodness of fit *p*-value < 0.1 |Residual for Dose Group Near BMD| > 2 |Residual at control| > 2
Exponential 4 (CV— log-normal)	Restricted	0.2215	0.1355	0.0337	563.1028	Questionable	Goodness of fit *p*-value < 0.1 |Residual for Dose Group Near BMD| > 2 |Residual at control| > 2
Exponential 5 (CV— log-normal)	Restricted	0.3331	0.1470	0.0200	564.2382	Questionable	Goodness of fit *p*-value < 0.1 |Residual for Dose Group Near BMD| > 2 |Residual at control| > 2
Hill (CV— log-normal)	Restricted	0.2860	0.1283	0.0121	565.2461	Questionable	Goodness of fit *p*-value < 0.1 |Residual for Dose Group Near BMD| > 2 |Residual at control| > 2
Polynomial (5 degree) (CV— log-normal)	Restricted	0.5606	0.4106	0.0017	569.7238	Questionable	Goodness of fit *p*-value < 0.1 |Residual for Dose Group Near BMD| > 2 |Residual at control| > 2
Polynomial (4 degree) (CV— log-normal)	Restricted	0.5606	0.4106	0.0017	569.7238	Questionable	Goodness of fit *p*-value < 0.1 |Residual for Dose Group Near BMD| > 2 |Residual at control| > 2
Polynomial (3 degree) (CV— log-normal)	Restricted	0.5606	0.4106	0.0017	569.7238	Questionable	Goodness of fit *p*-value < 0.1 |Residual for Dose Group Near BMD| > 2 |Residual at control| > 2
Polynomial (2 degree) (CV— log-normal)	Restricted	0.5606	0.4106	0.0017	569.7238	Questionable	Goodness of fit *p*-value < 0.1 |Residual for Dose Group Near BMD| > 2 |Residual at control| > 2
Power (CV—log-normal)	Restricted	0.5606	0.4107	0.0017	569.7238	Questionable	Goodness of fit *p*-value < 0.1 |Residual for Dose Group Near BMD| > 2 |Residual at control| > 2
Linear (CV—log-normal)	Unrestricted	0.5606	0.4106	0.0017	569.7238	Questionable	Goodness of fit *p*-value < 0.1 |Residual for Dose Group

Models	Restriction	1 standard deviation		*p*-Value	AIC	BMDS classification	BMDS notes
		BMD	BMDL				
Constant variance							
							Near BMD| > 2 |Residual at control| > 2

C.2.5. INCREASED RELATIVE LIVER WEIGHT—MALE RAT (NTP, 2018)

Table C-22. Dose-response data for increased relative liver weight in male rats (NTP, 2018)

Dose (mg/kg-d)	*n*	Mean	SD
0	10	35.5	3.07
0.156	10	39.32	1.68
0.312	10	42.61	1.77
0.625	10	45.56	2.66
1.25	10	54.77	2.15
2.5	10	67.9	3.76

Table C-23. Benchmark dose results for increased relative liver weight in male rats—constant variance, BMR = 10% relative deviation (NTP, 2018)

Models	Restriction	10% relative deviation		*p*-Value	AIC	BMDS classification	BMDS notes
		BMD	BMDL				
Constant variance							
Exponential 2 (CV—normal)	Restricted	0.4081	0.3852	<0.0001	314.8501	Questionable	Goodness of fit *p*-value < 0.1 |Residual at control| > 2
Exponential 3 (CV—normal)	Restricted	0.4081	0.3852	<0.0001	314.8501	Questionable	Goodness of fit *p*-value < 0.1 |Residual at control| > 2
Exponential 4 (CV—normal)	Restricted	0.2116	0.1764	0.2654	291.5391	Viable—Alternate	
Exponential 5 (CV—normal)	Restricted	0.2112	0.1764	0.2653	291.5398	Viable—Alternate	
Hill (CV—normal)	**Restricted**	**0.2078**	**0.1710**	**0.2774**	**291.4313**	**Viable—Recommended**	**Lowest AIC**
Polynomial (5 degree) (CV—normal)	Restricted	0.2978	0.2836	0.0115	298.5321	Questionable	Goodness of fit *p*-value < 0.1 |Residual at control| > 2
Polynomial (4 degree) (CV—normal)	Restricted	0.2978	0.2778	0.0115	298.5321	Questionable	Goodness of fit *p*-value < 0.1 |Residual at control| > 2

Models	Restriction	10% relative deviation		*p*-Value	AIC	BMDS classification	BMDS notes
		BMD	BMDL				
Constant variance							
Polynomial (3 degree) (CV—normal)	Restricted	0.2978	0.2775	0.0115	298.5321	Questionable	Goodness of fit *p*-value < 0.1 |Residual at control| > 2
Polynomial (2 degree) (CV—normal)	Restricted	0.2978	0.2775	0.0115	298.5321	Questionable	Goodness of fit *p*-value < 0.1 |Residual at control| > 2
Power (CV—normal)	Restricted	0.2978	0.2775	0.0115	298.5321	Questionable	Goodness of fit *p*-value < 0.1 |Residual at control| > 2
Linear (CV—normal)	Unrestricted	0.2978	0.2775	0.0115	298.5321	Questionable	Goodness of fit *p*-value < 0.1 |Residual at control| > 2

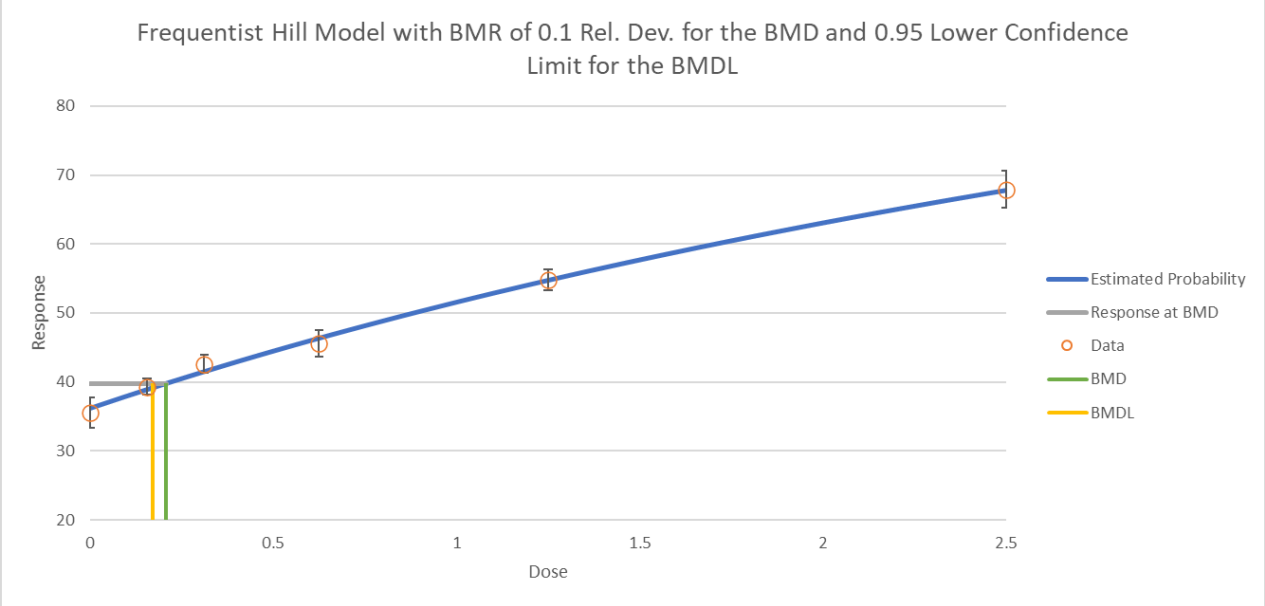

Figure C-6. Dose-response curve for the Hill model fit to increased relative liver weight in male rats (NTP, 2018).

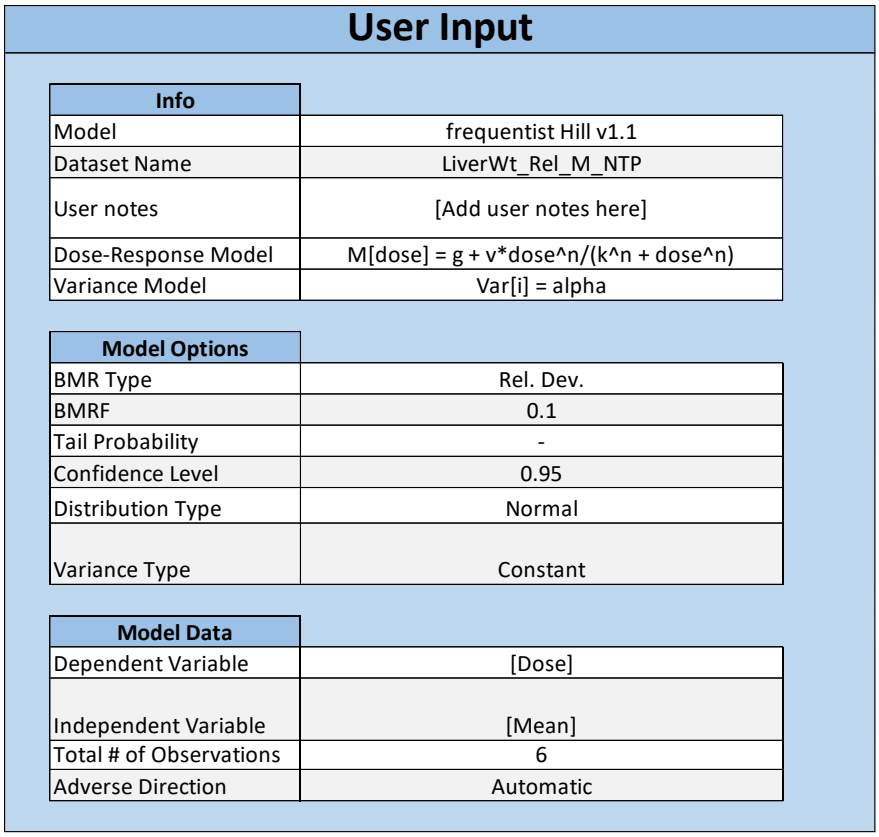

User Input

Info	
Model	frequentist Hill v1.1
Dataset Name	LiverWt_Rel_M_NTP
User notes	[Add user notes here]
Dose-Response Model	M[dose] = g + v*dose^n/(k^n + dose^n)
Variance Model	Var[i] = alpha

Model Options	
BMR Type	Rel. Dev.
BMRF	0.1
Tail Probability	-
Confidence Level	0.95
Distribution Type	Normal
Variance Type	Constant

Model Data	
Dependent Variable	[Dose]
Independent Variable	[Mean]
Total # of Observations	6
Adverse Direction	Automatic

Figure C-7. User Input for dose-response modeling of increased relative liver weight in male rats (NTP, 2018).

Model Results

Benchmark Dose	
BMD	0.207847359
BMDL	0.170963922
BMDU	0.269772648
AIC	291.4312778
Test 4 P-value	0.277392913
D.O.F.	3

Model Parameters	
# of Parameters	5
Variable	Estimate
g	36.19093843
v	106.3618737
k	5.900597337
n	Bounded
alpha	6.592795984

Goodness of Fit

Dose	Size	Estimated Median	Calc'd Median	Observed Mean	Estimated SD	Calc'd SD	Observed SD	Scaled Residual
0	10	36.19093843	35.5	35.5	2.56764405	3.07	3.07	-0.850950961
0.156	10	38.93050512	39.32	39.32	2.56764405	1.68	1.68	0.479696924
0.312	10	41.53248929	42.61	42.61	2.56764405	1.77	1.77	1.32704845
0.625	10	46.37792479	45.56	45.56	2.56764405	2.66	2.66	-1.007345743
1.25	10	54.78411826	54.77	54.77	2.56764405	2.15	2.15	-0.017387866
2.5	10	67.84400709	67.9	67.9	2.56764405	3.76	3.76	0.068960153

Likelihoods of Interest

Model	Log Likelihood*	# of Parameters	AIC
A1	-139.7874356	7	293.574871
A2	-134.7721348	12	293.54427
A3	-139.7874356	7	293.574871
fitted	-141.7156389	4	291.431278
R	-229.7698577	2	463.539715

* Includes additive constant of -55.13631. This constant was not included in the LL derivation prior to BMDS 3.0.

Tests of Interest

Test	-2*Log(Likelihood Ratio)	Test df	p-value
1	189.9954459	10	<0.0001
2	10.03060162	5	0.07437279
3	10.03060162	5	0.07437279
4	3.856406652	3	0.27739291

Figure C-8. Model Results for increased relative liver weight in male rats (NTP, 2018).

Table C-24. Benchmark dose results for increased relative liver weight in male rats—constant variance, BMR = 1 standard deviation (NTP, 2018)

Models	Restriction	10% relative deviation		*p*-Value	AIC	BMDS classification	BMDS notes
		BMD	BMDL				
Constant variance							
Exponential 2 (CV—normal)	Restricted	0.3381	0.2930	<0.0001	314.8501	Questionable	Goodness of fit *p*-value < 0.1 |Residual at control| > 2
Exponential 3 (CV—normal)	Restricted	0.3381	0.2930	<0.0001	314.8501	Questionable	Goodness of fit *p*-value < 0.1 |Residual at control| > 2
Exponential 4 (CV—normal)	Restricted	0.1486	0.1209	0.2654	291.5391	Viable—Alternate	
Exponential 5 (CV—normal)	Restricted	0.1485	0.1209	0.2653	291.5398	Viable—Alternate	
Hill (CV—normal)	**Restricted**	**0.1460**	**0.1169**	**0.2774**	**291.4313**	**Viable—Recommended**	**Lowest AIC**
Polynomial (5 degree) (CV—normal)	Restricted	0.2202	0.1909	0.0115	298.5321	Questionable	Goodness of fit *p*-value < 0.1 |Residual at control| > 2
Polynomial (4 degree) (CV—normal)	Restricted	0.2202	0.1976	0.0115	298.5321	Questionable	Goodness of fit *p*-value < 0.1 |Residual at control| > 2
Polynomial (3 degree) (CV—normal)	Restricted	0.2202	0.1894	0.0115	298.5321	Questionable	Goodness of fit *p*-value < 0.1 |Residual at control| > 2
Polynomial (2 degree) (CV—normal)	Restricted	0.2202	0.1894	0.0115	298.5321	Questionable	Goodness of fit *p*-value < 0.1 |Residual at control| > 2
Power (CV—normal)	Restricted	0.2202	0.1894	0.0115	298.5321	Questionable	Goodness of fit *p*-value < 0.1 |Residual at control| > 2
Linear (CV—normal)	Unrestricted	0.2202	0.1894	0.0115	298.5321	Questionable	Goodness of fit *p*-value < 0.1 |Residual at control| > 2

C.2.6. INCREASED RELATIVE LIVER WEIGHT—FEMALE RAT (NTP, 2018)

Table C-25. Dose-response data for increased relative liver weight in female rats (NTP, 2018)

Dose (mg/kg-d)	*n*	Mean	SD
0	10	33.52	2.37
0.156	10	37.66	2.81
0.312	10	40.08	1.77
0.625	10	44.25	2.59
1.25	10	50.84	2.12
2.5	10	67.75	2.85

Table C-26. Benchmark dose results for increased relative liver weight in female rats—BMR = constant variance, 10% relative deviation (NTP, 2018)

Models	Restriction	10% relative deviation		*p*-Value	AIC	BMDS classification	BMDS notes
		BMD	BMDL				
Constant variance							
Exponential 2 (CV—normal)	Restricted	0.3761	0.3585	0.0005	297.3583	Questionable	Goodness of fit *p*-value < 0.1 |Residual at control| > 2
Exponential 3 (CV—normal)	Restricted	0.3761	0.3585	0.0005	297.3583	Questionable	Goodness of fit *p*-value < 0.1 |Residual at control| > 2
Exponential 4 (CV—normal)	Restricted	0.2457	0.2042	0.0512	287.1715	Questionable	Goodness of fit *p*-value < 0.1
Exponential 5 (CV—normal)	Restricted	0.2456	0.2042	0.0512	287.1717	Questionable	Goodness of fit *p*-value < 0.1
Hill (CV—normal)	Restricted	0.2446	0.2018	0.0518	287.1453	Questionable	Goodness of fit *p*-value < 0.1
Polynomial (5 degree) (CV—normal)	Restricted	0.2688	0.2545	0.0764	285.8573	Questionable	Goodness of fit *p*-value < 0.1 |Residual at control| > 2
Polynomial (4 degree) (CV—normal)	Restricted	0.2688	0.2528	0.0764	285.8573	Questionable	Goodness of fit *p*-value < 0.1 |Residual at control| > 2
Polynomial (3 degree) (CV—normal)	Restricted	0.2688	0.2524	0.0764	285.8573	Questionable	Goodness of fit *p*-value < 0.1 |Residual at control| > 2
Polynomial (2 degree) (CV—normal)	Restricted	0.2688	0.2524	0.0764	285.8573	Questionable	Goodness of fit *p*-value < 0.1 |Residual at control| > 2
Power (CV—normal)	Restricted	0.2688	0.2524	0.0764	285.8573	Questionable	Goodness of fit *p*-value < 0.1 |Residual at control| > 2
Linear (CV—normal)	Unrestricted	0.2688	0.2524	0.0764	285.8573	Questionable	Goodness of fit *p*-value < 0.1 |Residual at control| > 2

Table C-27. Benchmark dose results for increased relative liver weight in female rats—nonconstant variance, BMR = 10% relative deviation (NTP, 2018)

Models	Restriction	10% relative deviation		*p*-Value	AIC	BMDS classification	BMDS notes
		BMD	BMDL				
Non-constant variance							
Exponential 2 (NCV—normal)	Restricted	0.3779	0.3586	0.0005	299.1741	Questionable	Goodness of fit *p*-value < 0.1 |Residual at control| > 2
Exponential 3 (NCV—normal)	Restricted	0.3779	0.3586	0.0005	299.1741	Questionable	Goodness of fit *p*-value < 0.1 |Residual at control| > 2
Exponential 4 (NCV—normal)	Restricted	0.2443	0.2017	0.0468	289.1376	Questionable	Goodness of fit *p*-value < 0.1
Exponential 5 (NCV—normal)	Restricted	0.2464	0.2016	0.0466	289.1432	Questionable	Goodness of fit *p*-value < 0.1
Hill (NCV—normal)	Restricted	0.2431	0.1997	0.0474	289.1075	Questionable	Goodness of fit *p*-value < 0.1
Polynomial (5 degree) (NCV—normal)	Restricted	0.2688	0.2519	0.0695	287.8570	Questionable	Goodness of fit *p*-value < 0.1 |Residual at control| > 2
Polynomial (4 degree) (NCV—normal)	Restricted	0.2688	0.2519	0.0695	287.8570	Questionable	Goodness of fit *p*-value < 0.1 |Residual at control| > 2
Polynomial (3 degree) (NCV—normal)	Restricted	0.2688	0.2521	0.0695	287.8570	Questionable	Goodness of fit *p*-value < 0.1 |Residual at control| > 2
Polynomial (2 degree) (NCV—normal)	Restricted	0.2688	0.2521	0.0695	287.8570	Questionable	Goodness of fit *p*-value < 0.1 |Residual at control| > 2
Power (NCV—normal)	Restricted	0.2688	0.2521	0.0695	287.8570	Questionable	Goodness of fit *p*-value < 0.1 |Residual at control| > 2
Linear (NCV—normal)	Unrestricted	0.2688	0.2521	0.0695	287.8570	Questionable	Goodness of fit *p*-value < 0.1 |Residual at control| > 2

Table C-28. Benchmark dose results for increased relative liver weight in female rats—log-normal, constant variance, BMR = 10% relative deviation (NTP, 2018)

Models	Restriction	10% relative deviation		*p*-Value	AIC	BMDS classification	BMDS notes
		BMD	BMDL				
Constant variance							
Exponential 2 (CV—log-normal)	Restricted	0.3617	0.3404	<0.0001	304.9243	Questionable	Constant variance test failed (Test 2 *p*-value < 0.05) Goodness of fit *p*-value < 0.1 |Residual for Dose Group Near BMD| > 2 |Residual at control| > 2
Exponential 3 (CV— log-normal)	Restricted	0.3617	0.3404	<0.0001	304.9243	Questionable	Constant variance test failed (Test 2 *p*-value < 0.05) Goodness of fit *p*-value < 0.1 |Residual for Dose Group Near BMD| > 2 |Residual at control| > 2
Exponential 4 (CV— log-normal)	Restricted	0.2228	0.1850	<0.0001	291.5746	Questionable	Constant variance test failed (Test 2 *p*-value < 0.05) Goodness of fit *p*-value < 0.1 |Residual for Dose Group Near BMD| > 2 |Residual at control| > 2
Exponential 5 (CV— log-normal)	Restricted	0.2228	0.1850	<0.0001	291.5746	Questionable	Constant variance test failed (Test 2 *p*-value < 0.05) Goodness of fit *p*-value < 0.1 |Residual for Dose Group Near BMD| > 2 |Residual at control| > 2
Hill (CV— log-normal)	Restricted	0.2200	0.1800	<0.0001	291.4503	Questionable	Constant variance test failed (Test 2 *p*-value < 0.05) Goodness of fit *p*-value < 0.1 |Residual for Dose Group Near BMD| > 2 |Residual at control| > 2
Polynomial (5 degree) (CV— log-normal)	Restricted	0.2622	0.2441	<0.0001	291.8437	Questionable	Constant variance test failed (Test 2 *p*-value < 0.05) Goodness of fit *p*-value < 0.1 |Residual for Dose Group Near BMD| > 2 |Residual at control| > 2
Polynomial (4 degree) (CV— log-normal)	Restricted	0.2622	0.2454	<0.0001	291.8437	Questionable	Constant variance test failed (Test 2 *p*-value < 0.05) Goodness of fit *p*-value < 0.1 |Residual for Dose Group Near BMD| > 2 |Residual at control| > 2

Models	Restriction	10% relative deviation		*p*-Value	AIC	BMDS classification	BMDS notes
		BMD	BMDL				
Constant variance							
Polynomial (3 degree) (CV— log-normal)	Restricted	0.2622	0.2433	<0.0001	291.8437	Questionable	Constant variance test failed (Test 2 *p*-value < 0.05) Goodness of fit *p*-value < 0.1 |Residual for Dose Group Near BMD| > 2 |Residual at control| > 2
Polynomial (2 degree) (CV— log-normal)	Restricted	0.2622	0.2433	<0.0001	291.8437	Questionable	Constant variance test failed (Test 2 *p*-value < 0.05) Goodness of fit *p*-value < 0.1 |Residual for Dose Group Near BMD| > 2 |Residual at control| > 2
Power (CV— log-normal)	Restricted	0.2622	0.2433	<0.0001	291.8437	Questionable	Constant variance test failed (Test 2 *p*-value < 0.05) Goodness of fit *p*-value < 0.1 |Residual for Dose Group Near BMD| > 2 |Residual at control| > 2
Linear (CV— log-normal)	Unrestricted	0.2622	0.2433	<0.0001	291.8437	Questionable	Constant variance test failed (Test 2 *p*-value < 0.05) Goodness of fit *p*-value < 0.1 |Residual for Dose Group Near BMD| > 2 |Residual at control| > 2

Table C-29. Benchmark dose results for increased relative liver weight in female rats, high dose dropped—BMR = constant variance, 10% relative deviation (NTP, 2018)

Models	Restriction	10% relative deviation		*p*-Value	AIC	BMDS classification	BMDS notes
		BMD	BMDL				
Constant variance							
Exponential 2 (CV—normal)	Restricted	0.3195	0.2902	0.0031	242.3745	Questionable	Goodness of fit *p*-value < 0.1 |Residual at control| > 2
Exponential 3 (CV—normal)	Restricted	0.3195	0.2902	0.0031	242.3745	Questionable	Goodness of fit *p*-value < 0.1 |Residual at control| > 2
Exponential 4 (CV—normal)	Restricted	0.1611	0.1214	0.5849	231.5654	Viable—Alternate	
Exponential 5 (CV—normal)	Restricted	0.1610	0.1214	0.5849	231.5654	Viable—Alternate	
Hill (CV—normal)	**Restricted**	**0.1544**	**0.1117**	**0.6566**	**231.3342**	**Viable—Recommended**	**Lowest AIC**

Models	Restriction	10% relative deviation		*p*-Value	AIC	BMDS classification	BMDS notes
		BMD	BMDL				
Constant variance							
Polynomial (5 degree) (CV—normal)	Restricted	0.2659	0.2374	0.0308	237.3809	Questionable	Goodness of fit *p*-value < 0.1 |Residual at control| > 2
Polynomial (4 degree) (CV—normal)	Restricted	0.2659	0.2374	0.0308	237.3809	Questionable	Goodness of fit *p*-value < 0.1 |Residual at control| > 2
Polynomial (3 degree) (CV—normal)	Restricted	0.2659	0.2374	0.0308	237.3809	Questionable	Goodness of fit *p*-value < 0.1 |Residual at control| > 2
Polynomial (2 degree) (CV—normal)	Restricted	0.2659	0.2374	0.0308	237.3809	Questionable	Goodness of fit *p*-value < 0.1 |Residual at control| > 2
Power (CV—normal)	Restricted	0.2659	0.2374	0.0308	237.3809	Questionable	Goodness of fit *p*-value < 0.1 |Residual at control| > 2
Linear (CV—normal)	Unrestricted	0.3195	0.2902	0.0031	242.3745	Questionable	Goodness of fit *p*-value < 0.1 |Residual at control| > 2

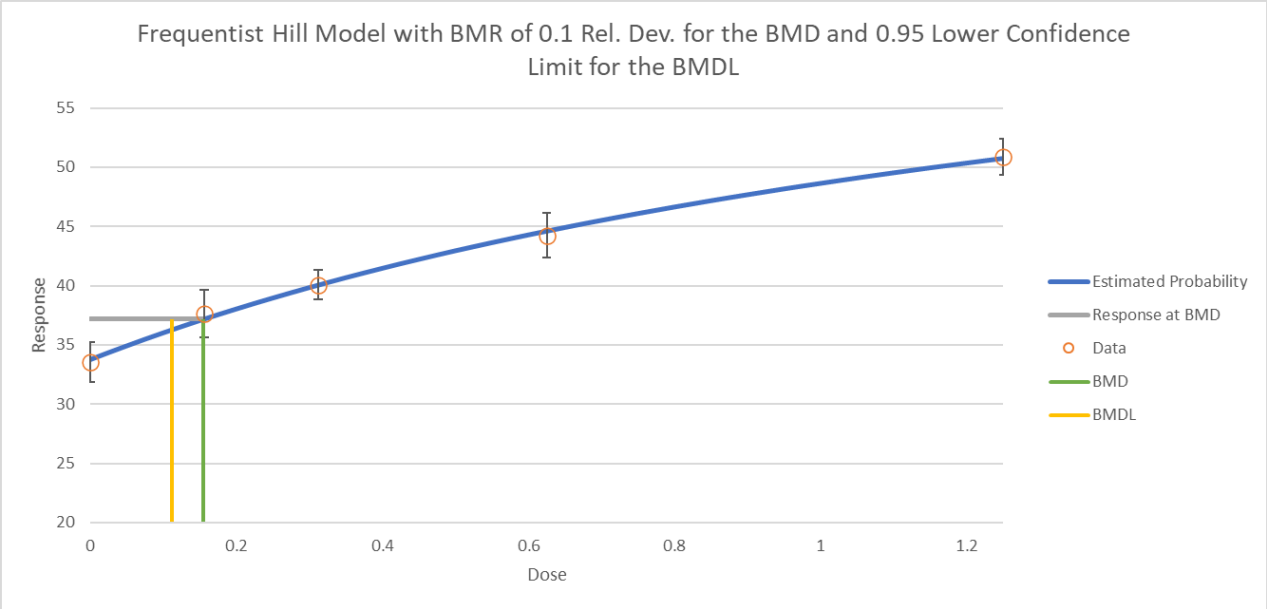

Figure C-9. Dose-response curve for the Hill model fit to increased relative liver weight in female rats with the highest dose dropped (NTP, 2018).

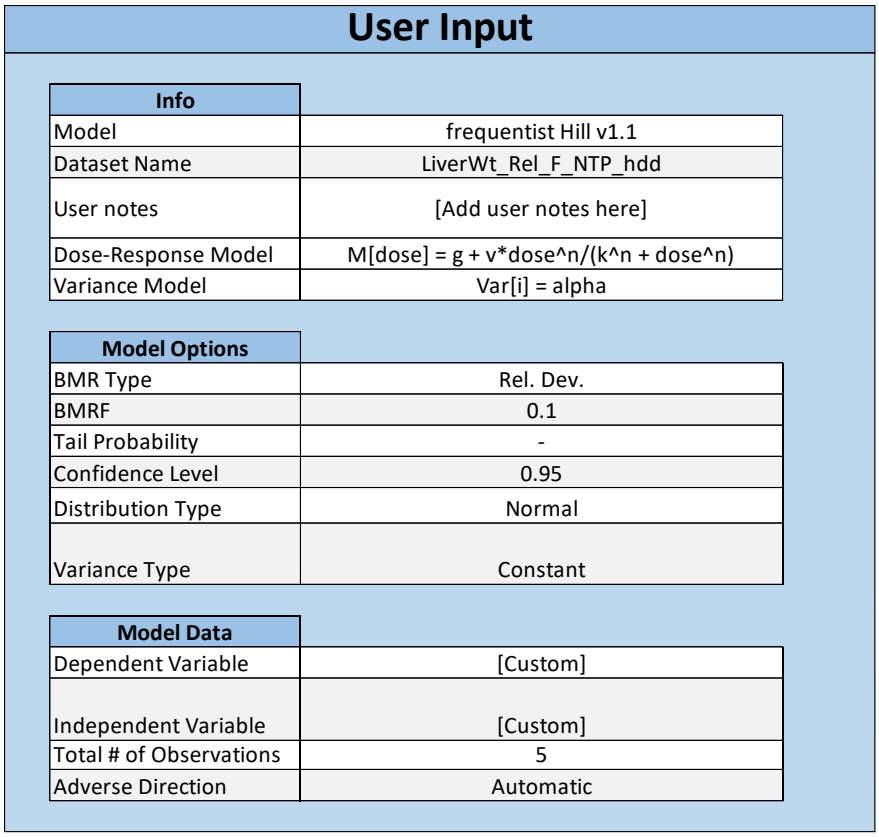

User Input

Info	
Model	frequentist Hill v1.1
Dataset Name	LiverWt_Rel_F_NTP_hdd
User notes	[Add user notes here]
Dose-Response Model	M[dose] = g + v*dose^n/(k^n + dose^n)
Variance Model	Var[i] = alpha

Model Options	
BMR Type	Rel. Dev.
BMRF	0.1
Tail Probability	-
Confidence Level	0.95
Distribution Type	Normal
Variance Type	Constant

Model Data	
Dependent Variable	[Custom]
Independent Variable	[Custom]
Total # of Observations	5
Adverse Direction	Automatic

Figure C-10. User input for dose-response modeling of increased relative liver weight in females rats with highest dose dropped (NTP, 2018).

Model Results

Benchmark Dose	
BMD	0.154369377
BMDL	0.111740633
BMDU	0.218901711
AIC	231.3341743
Test 4 P-value	0.656565161
D.O.F.	2

Model Parameters	
# of Parameters	5
Variable	Estimate
g	33.78210999
v	38.98056451
k	1.626870887
n	Bounded
alpha	5.097775081

Goodness of Fit

Dose	Size	Estimated Median	Calc'd Median	Observed Mean	Estimated SD	Calc'd SD	Observed SD	Scaled Residual
0	10	33.78210999	33.52	33.52	2.2578253	2.37	2.37	-0.367107486
0.156	10	37.19288309	37.66	37.66	2.2578253	2.81	2.81	0.654237225
0.312	10	40.05480005	40.08	40.08	2.2578253	1.77	1.77	0.035294693
0.625	10	44.60104858	44.25	44.25	2.2578253	2.59	2.59	-0.491673589
1.25	10	50.71915985	50.84	50.84	2.2578253	2.12	2.12	0.169246978

Likelihoods of Interest

Model	Log Likelihood*	# of Parameters	AIC
A1	-111.2463538	6	234.492708
A2	-110.0141933	10	240.028387
A3	-111.2463538	6	234.492708
fitted	-111.6670871	4	231.334174
R	-163.1738575	2	330.347715

* Includes additive constant of -45.94693. This constant was not included in the LL derivation prior to BMDS 3.0.

Tests of Interest

Test	-2*Log(Likelihood Ratio)	Test df	p-value
1	106.3193285	8	<0.0001
2	2.464321029	4	0.65103586
3	2.464321029	4	0.65103586
4	0.84146667	2	0.65656516

Figure C-11. Model results for increased relative liver weight in female rats with highest dose dropped (NTP, 2018).

Table C-30. Benchmark dose results for increased relative liver weight in female rats, high dose dropped—constant variance, BMR = 1 standard deviation (NTP, 2018)

Models	Restriction	10% relative deviation		*p*-Value	AIC	BMDS classification	BMDS notes
		BMD	BMDL				
Constant variance							
Exponential 2 (CV—normal)	Restricted	0.2341	0.1980	0.0031	242.3745	Questionable	Goodness of fit *p*-value < 0.1 |Residual at control| > 2
Exponential 3 (CV—normal)	Restricted	0.2341	0.1980	0.0031	242.3745	Questionable	Goodness of fit *p*-value < 0.1 |Residual at control| > 2
Exponential 4 (CV—normal)	Restricted	0.1050	0.0785	0.5849	231.5654	Viable—Alternate	
Exponential 5 (CV—normal)	Restricted	0.1049	0.0785	0.5849	231.5654	Viable—Alternate	
Hill (CV—normal)	**Restricted**	**0.1000**	**0.0722**	**0.6566**	**231.3342**	**Viable—Recommended**	**Lowest AIC**
Polynomial (5 degree) (CV—normal)	Restricted	0.1854	0.1675	0.0308	237.3809	Questionable	Goodness of fit *p*-value < 0.1 |Residual at control| > 2
Polynomial (4 degree) (CV—normal)	Restricted	0.1854	0.1553	0.0308	237.3809	Questionable	Goodness of fit *p*-value < 0.1 |Residual at control| > 2
Polynomial (3 degree) (CV—normal)	Restricted	0.1854	0.1553	0.0308	237.3809	Questionable	Goodness of fit *p*-value < 0.1 |Residual at control| > 2
Polynomial (2 degree) (CV—normal)	Restricted	0.1854	0.1553	0.0308	237.3809	Questionable	Goodness of fit *p*-value < 0.1 |Residual at control| > 2
Power (CV—normal)	Restricted	0.1854	0.1553	0.0308	237.3809	Questionable	Goodness of fit *p*-value < 0.1 |Residual at control| > 2
Linear (CV—normal)	Unrestricted	0.2341	0.1980	0.0031	242.3745	Questionable	Goodness of fit *p*-value < 0.1 |Residual at control| > 2

C.2.7. INCREASED RELATIVE LIVER WEIGHT (HISTO)—FEMALE RATS (Frawley et al., 2018)

Table C-31. Dose-response data for increased relative liver weight (Histo) in female rats (Frawley et al., 2018)

Dose (mg/kg-d)	*n*	Mean	SD
0	8	4.02	0.28
0.125	8	4.06	0.28
0.25	8	4.35	0.28
0.5	8	4.68	0.34

Table C-32. Benchmark dose results for increased relative liver weight (Histo) in female rats—constant variance, BMR = 10% relative deviation (Frawley et al., 2018)

Models	Restriction	10% Relative deviation		*p*-Value	AIC	BMDS classification	BMDS notes
		BMD	BMDL				
Constant variance							
Exponential 2 (CV—normal)	**Restricted**	**0.2929**	**0.2224**	**0.6024**	**15.6701**	**Viable—Recommended**	**Lowest AIC**
Exponential 3 (CV—normal)	Restricted	0.3215	0.2240	0.3551	17.5116	Viable—Alternate	
Exponential 4 (CV—normal)	Restricted	0.2823	0.1647	0.2944	17.7557	Viable—Alternate	
Exponential 5 (CV—normal)	Restricted	0.2729	0.1840	NA	18.6564	Questionable	d.f. = 0, saturated model (Goodness of fit test cannot be calculated)
Hill (CV—normal)	Restricted	0.2777	0.1901	NA	18.6564	Questionable	d.f. = 0, saturated model (Goodness of fit test cannot be calculated)
Polynomial (3 degree) (CV—normal)	Restricted	0.3170	0.2099	0.3338	17.5904	Viable—Alternate	
Polynomial (2 degree) (CV—normal)	Restricted	0.3170	0.2099	0.3338	17.5904	Viable—Alternate	
Power (CV—normal)	Restricted	0.3195	0.2113	0.3675	17.4686	Viable—Alternate	
Linear (CV—normal)	Unrestricted	0.2824	0.2081	0.5775	15.7543	Viable—Alternate	

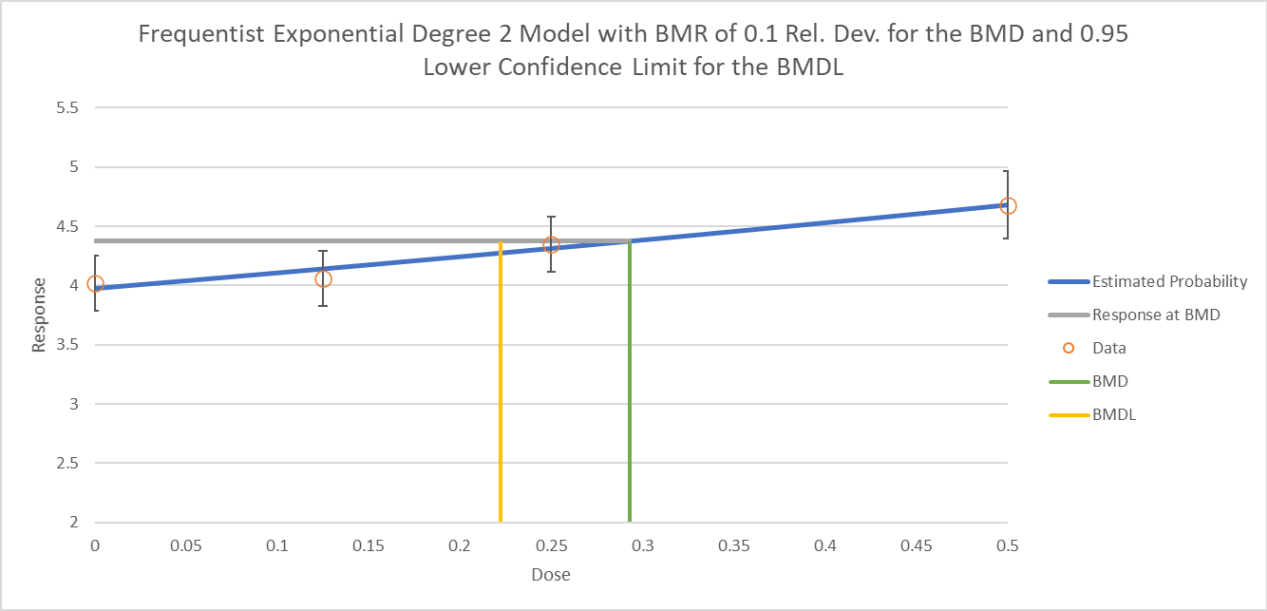

Figure C-12. Dose-response curve for the Exponential 2 model fit to increased relative liver weight (Histo) in female rats (Frawley et al., 2018).

User Input

Info	
Model	frequentist Exponential degree 2 v1.1
Dataset Name	LiverWt_Rel_Frawley_Histo
User notes	[Add user notes here]
Dose-Response Model	M[dose] = a * exp(±1 * b * dose)
Variance Model	Var[i] = alpha

Model Options	
BMR Type	Rel. Dev.
BMRF	0.1
Tail Probability	-
Confidence Level	0.95
Distribution Type	Normal
Variance Type	Constant

Model Data	
Dependent Variable	[Dose]
Independent Variable	[Mean]
Total # of Observations	4
Adverse Direction	Automatic

Figure C-13. User input for dose-response modeling of increased relative liver weight (Histo) in female rats (Frawley et al., 2018).

Model Results

Benchmark Dose	
BMD	0.292874336
BMDL	0.222375421
BMDU	0.429901615
AIC	15.67013988
Test 4 P-value	0.602376128
D.O.F.	2

Model Parameters	
# of Parameters	3
Variable	Estimate
a	3.97629556
b	0.325430373
log-alpha	-2.536765652

Goodness of Fit

Dose	Size	Estimated Median	Calc'd Median	Observed Mean	Estimated SD	Calc'd SD	Observed SD	Scaled Residual
0	8	3.97629556	4.02	4.02	0.28128614	0.28	0.28	0.439462902
0.125	8	4.141381462	4.06	4.06	0.28128614	0.28	0.28	-0.818318074
0.25	8	4.31332132	4.35	4.35	0.28128614	0.28	0.28	0.368816506
0.5	8	4.678912956	4.68	4.68	0.28128614	0.34	0.34	0.01093059

Likelihoods of Interest

Model	Log Likelihood*	# of Parameters	AIC
A1	-4.328196707	5	18.6563934
A2	-4.087877276	8	24.1757546
A3	-4.328196707	5	18.6563934
fitted	-4.835069939	3	15.6701399
R	-14.72410737	2	33.4482147

* Includes additive constant of -29.40603. This constant was not included in the LL derivation prior to BMDS 3.0.

Tests of Interest

Test	-2*Log(Likelihood Ratio)	Test df	p-value
1	21.2724602	6	0.00163883
2	0.480638862	3	0.92312391
3	0.480638862	3	0.92312391
4	1.013746464	2	0.60237613

Figure C-14. Model results for increased relative liver weight (Histo) in female rats (Frawley et al., 2018).

Table C-33. Benchmark dose results for increased relative liver weight (Histo) in female rats—constant variance, BMR = 1 standard deviation (Frawley et al., 2018)

Models	Restriction	1 standard deviation		*p*-Value	AIC	BMDS classification	BMDS notes
		BMD	BMDL				
Constant variance							
Exponential 2 (CV—normal)	**Restricted**	**0.2100**	**0.1561**	**0.6024**	**15.6701**	**Viable—Recommended**	**Lowest AIC**
Exponential 3 (CV—normal)	Restricted	0.2405	0.1572	0.3551	17.5116	Viable—Alternate	
Exponential 4 (CV—normal)	Restricted	0.2003	0.1453	0.2944	17.7557	Viable—Alternate	

Models	Restriction	1 standard deviation		*p*-Value	AIC	BMDS classification	BMDS notes
		BMD	BMDL				
Constant variance							
Exponential 5 (CV—normal)	Restricted	0.2332	0.1314	NA	18.6564	Questionable	d.f. = 0, saturated model (Goodness of fit test cannot be calculated)
Hill (CV—normal)	Restricted	0.2310	0.1312	NA	18.6564	Questionable	d.f. = 0, saturated model (Goodness of fit test cannot be calculated)
Polynomial (3 degree) (CV—normal)	Restricted	0.2343	0.1467	0.3338	17.5904	Viable—Alternate	
Polynomial (2 degree) (CV—normal)	Restricted	0.2343	0.1467	0.3338	17.5904	Viable—Alternate	
Power (CV—normal)	Restricted	0.2394	0.1476	0.3675	17.4686	Viable—Alternate	
Linear (CV—normal)	Unrestricted	0.2005	0.1455	0.5775	15.7543	Viable—Alternate	

C.2.8. INCREASED RELATIVE LIVER WEIGHT (MPS)—FEMALE RATS (Frawley et al., 2018)

Table C-34. Dose-response data for increased relative liver weight (MPS) in female rats (Frawley et al., 2018)

Dose (mg/kg-d)	*n*	Mean	SD
0	8	3.42	0.26
0.125	8	3.77	0.28
0.25	8	3.86	0.26
0.5	8	4.19	0.17

Table C-35. Benchmark dose results for increased relative liver weight (Histo) in female rats—constant variance, BMR = 10% relative deviation (Frawley et al., 2018)

Models	Restriction	10% Relative deviation		*p*-Value	AIC	BMDS classification	BMDS notes
		BMD	BMDL				
Constant variance							
Exponential 2 (CV—normal)	Restricted	0.2575	0.2036	0.2714	5.4499	Viable—Alternate	
Exponential 3 (CV—normal)	Restricted	0.2575	0.2044	0.2714	5.4499	Viable—Alternate	
Exponential 4 (CV—normal)	Restricted	0.1644	0.0852	0.3121	5.8634	Viable—Alternate	

Models	Restriction	10% Relative deviation		*p*-Value	AIC	BMDS classification	BMDS notes
		BMD	BMDL				
Exponential 5 (CV—normal)	Restricted	0.1646	0.0851	0.3121	5.8634	Viable—Alternate	
Hill (CV—normal)	Restricted	0.1587	0.0730	0.3336	5.7766	Viable—Alternate	
Polynomial (3 degree) (CV—normal)	Restricted	0.2419	0.1864	0.3283	5.0691	Viable—Alternate	
Polynomial (2 degree) (CV—normal)	Restricted	0.2419	0.1864	0.3283	5.0691	Viable—Alternate	
Power (CV—normal)	Restricted	0.2419	0.1864	0.3283	5.0691	Viable—Alternate	
Linear (CV—normal)	**Unrestricted**	**0.2419**	**0.1864**	**0.3283**	**5.0691**	**Viable—Recommended**	**Lowest AIC**

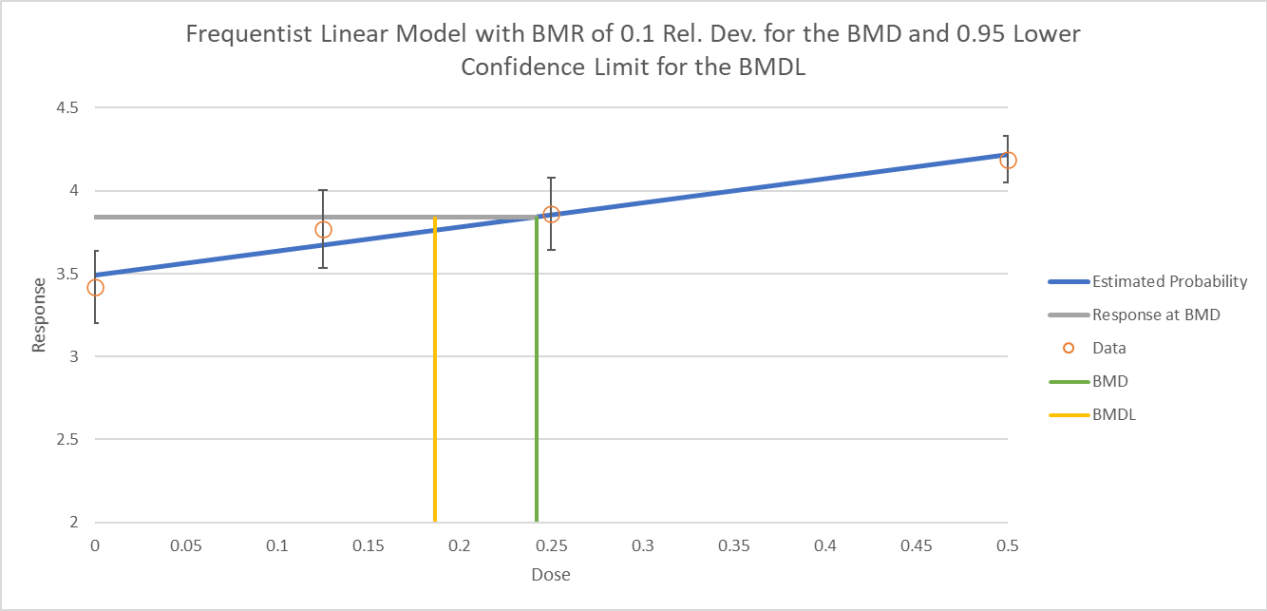

Figure C-15. Dose-response curve for the Linear model fit to increased relative liver weight (MPS) in female rats (Frawley et al., 2018).

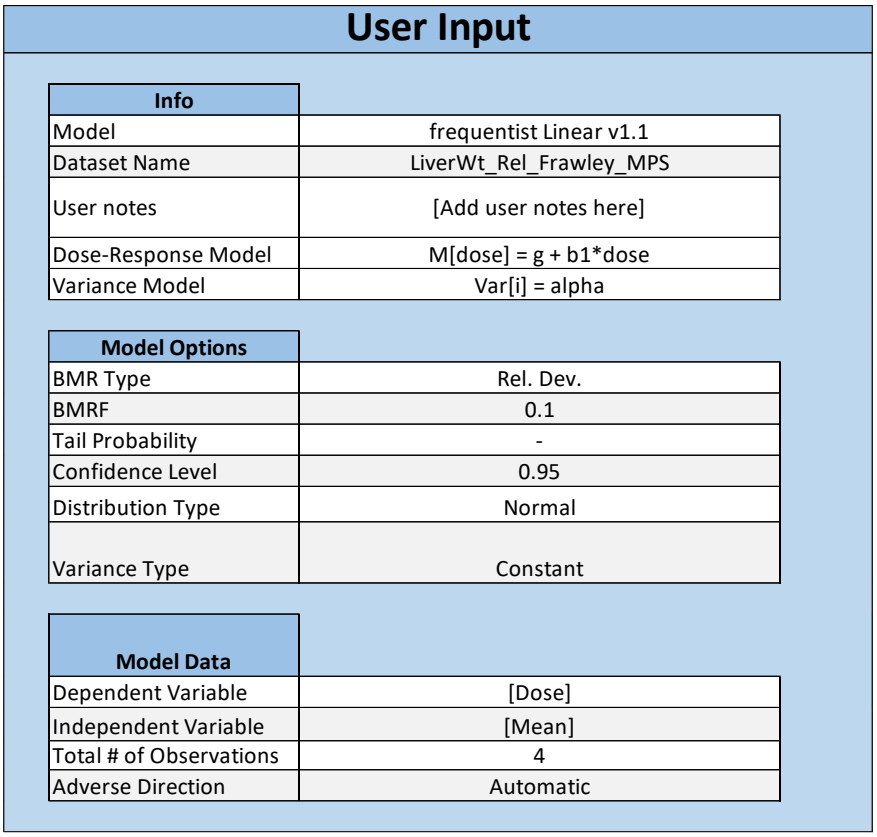

User Input

Info	
Model	frequentist Linear v1.1
Dataset Name	LiverWt_Rel_Frawley_MPS
User notes	[Add user notes here]
Dose-Response Model	M[dose] = g + b1*dose
Variance Model	Var[i] = alpha

Model Options	
BMR Type	Rel. Dev.
BMRF	0.1
Tail Probability	-
Confidence Level	0.95
Distribution Type	Normal
Variance Type	Constant

Model Data	
Dependent Variable	[Dose]
Independent Variable	[Mean]
Total # of Observations	4
Adverse Direction	Automatic

Figure C-16. User input for dose-response modeling of increased relative liver weight (MPS) in female rats (Frawley et al., 2018).

Model Results

Benchmark Dose	
BMD	0.24187088
BMDL	0.186409723
BMDU	0.337253407
AIC	5.069125072
Test 4 P-value	0.328309463
D.O.F.	2

Model Parameters	
# of Parameters	3
Variable	Estimate
g	3.49399996
beta1	1.444571613
alpha	0.05687116

Goodness of Fit

Dose	Size	Estimated Median	Calc'd Median	Observed Mean	Estimated SD	Calc'd SD	Observed SD	Scaled Residual
0	8	3.49399996	3.42	3.42	0.23847675	0.26	0.26	-0.877668349
0.125	8	3.674571412	3.77	3.77	0.23847675	0.28	0.28	1.13182022
0.25	8	3.855142863	3.86	3.86	0.23847675	0.26	0.26	0.057607531
0.5	8	4.216285767	4.19	4.19	0.23847675	0.17	0.17	-0.31175943

Likelihoods of Interest

Model	Log Likelihood*	# of Parameters	AIC
A1	1.579236095	5	6.84152781
A2	2.643027712	8	10.7139446
A3	1.579236095	5	6.84152781
fitted	0.465437464	3	5.06912507
R	-12.53902329	2	29.0780466

* Includes additive constant of -29.40603. This constant was not included in the LL derivation prior to BMDS 3.0.

Tests of Interest

Test	-2*Log(Likelihood Ratio)	Test df	p-value
1	30.364102	6	<0.0001
2	2.127583234	3	0.54635267
3	2.127583234	3	0.54635267
4	2.227597262	2	0.32830946

Figure C-17. Model results for increased relative liver weight (MPS) in female rats (Frawley et al., 2018).

Table C-36. Benchmark dose results for increased relative liver weight (MPS) in female rats – constant variance, BMR = 1 standard deviation (Frawley et al., 2018)

Models	Restriction	1 standard deviation		*p*-Value	AIC	BMDS classification	BMDS notes
		BMD	BMDL				
Constant variance							
Exponential 2 (CV—normal)	Restricted	0.1788	0.1367	0.2714	5.4499	Viable—Alternate	
Exponential 3 (CV—normal)	Restricted	0.1788	0.1367	0.2714	5.4499	Viable—Alternate	

Models	Restriction	1 standard deviation		*p*-Value	AIC	BMDS classification	BMDS notes
		BMD	BMDL				
Constant variance							
Exponential 4 (CV—normal)	Restricted	0.1046	0.0549	0.3121	5.8634	Viable—Alternate	
Exponential 5 (CV—normal)	Restricted	0.1048	0.0549	0.3121	5.8634	Viable—Alternate	
Hill (CV—normal)	**Restricted**	**0.0994**	**0.0450**	**0.3336**	**5.7766**	**Viable—Recommended**	**Lowest BMDL**
Polynomial (3 degree) (CV—normal)	Restricted	0.1651	0.1238	0.3283	5.0691	Viable—Alternate	
Polynomial (2 degree) (CV—normal)	Restricted	0.1651	0.1238	0.3283	5.0691	Viable—Alternate	
Power (CV—normal)	Restricted	0.1651	0.1238	0.3283	5.0691	Viable—Alternate	
Linear (CV—normal)	Unrestricted	0.1651	0.1238	0.3283	5.0691	Viable—Alternate	

C.2.9. INCREASED RELATIVE LIVER WEIGHT (TDAR)—FEMALE RATS (Frawley et al., 2018)

Table C-37. Dose-response data for increased relative liver weight (TDAR) in female rats (Frawley et al., 2018)

Dose (mg/kg-d)	*n*	Mean	SD
0	8	3.85	0.14
0.125	8	3.94	0.11
0.25	8	4.6	0.37
0.5	8	5.21	0.28

Table C-38. Benchmark dose results for increased relative liver weight (TDAR) in female rats—constant variance, BMR = 10% relative deviation (Frawley et al., 2018)

Models	Restriction	10% Relative deviation		*p*-Value	AIC	BMDS classification	BMDS notes
		BMD	BMDL				
Constant variance							
Exponential 2 (CV—normal)	Restricted	0.1478	0.1295	0.0284	10.5539	Questionable	Constant variance test failed (Test 2 *p*-value < 0.05) Goodness of fit *p*-value < 0.1 Modeled control response std. dev. >|1.5| actual response std. dev.

Models	Restriction	10% Relative deviation		*p*-Value	AIC	BMDS classification	BMDS notes
		BMD	BMDL				
Constant variance							
Exponential 3 (CV—normal)	Restricted	0.1541	0.1297	0.0077	12.5248	Questionable	Constant variance test failed (Test 2 *p*-value < 0.05) Goodness of fit *p*-value < 0.1 Modeled control response std. dev. >|1.5| actual response std. dev.
Exponential 4 (CV—normal)	Restricted	0.1294	0.0935	0.0073	12.6257	Questionable	Constant variance test failed (Test 2 *p*-value < 0.05) Goodness of fit *p*-value < 0.1 |Residual for Dose Group Near BMD| > 2 Modeled control response std. dev. >|1.5| actual response std. dev.
Exponential 5 (CV—normal)	Restricted	0.1951	0.1458	NA	7.4299	Questionable	Constant variance test failed (Test 2 *p*-value < 0.05) Modeled control response std. dev. >|1.5| actual response std. dev. d.f. = 0, saturated model (Goodness of fit test cannot be calculated)
Hill (CV—normal)	Restricted	0.1904	0.1497	NA	7.4299	Questionable	Constant variance test failed (Test 2 *p*-value < 0.05) Modeled control response std. dev. >|1.5| actual response std. dev. d.f. = 0, saturated model (Goodness of fit test cannot be calculated)
Polynomial (3 degree) (CV—normal)	Restricted	0.1419	0.1108	0.0079	12.4766	Questionable	Constant variance test failed (Test 2 *p*-value < 0.05) Goodness of fit *p*-value < 0.1 Modeled control response std. dev. >|1.5| actual response std. dev.
Polynomial (2 degree) (CV—normal)	Restricted	0.1419	0.1108	0.0079	12.4766	Questionable	Constant variance test failed (Test 2 *p*-value < 0.05) Goodness of fit *p*-value < 0.1 Modeled control response std. dev. >|1.5| actual response std. dev.
Power (CV—normal)	Restricted	0.1556	0.1124	0.0103	12.0114	Questionable	Constant variance test failed (Test 2 *p*-value < 0.05) Goodness of fit *p*-value < 0.1 Modeled control response std. dev. >|1.5| actual response std. dev.

Models	Restriction	10% Relative deviation		*p*-Value	AIC	BMDS classification	BMDS notes
		BMD	BMDL				
Constant variance							
Linear (CV—normal)	Unrestricted	0.1295	0.1103	0.0274	10.6256	Questionable	Constant variance test failed (Test 2 *p*-value < 0.05) Goodness of fit *p*-value < 0.1 |Residual for Dose Group Near BMD| > 2 Modeled control response std. dev. >|1.5| actual response std. dev.

Table C-39. Benchmark dose results for increased relative liver weight (TDAR) in female rats—non-constant variance, BMR = 10% relative deviation (Frawley et al., 2018)

Models	Restriction	10% Relative deviation		*p*-Value	AIC	BMDS classification	BMDS notes
		BMD	BMDL				
Non-constant variance							
Exponential 2 (NCV—normal)	Restricted	0.1478	0.1284	0.0012	10.0543	Questionable	Goodness of fit *p*-value < 0.1 |Residual for Dose Group Near BMD| > 2
Exponential 3 (NCV—normal)	Restricted	0.1607	0.1292	0.0003	11.8202	Questionable	Goodness of fit *p*-value < 0.1 |Residual for Dose Group Near BMD| > 2
Exponential 4 (NCV—normal)	Restricted	0.1333	0.1030	0.0002	12.4411	Questionable	Goodness of fit *p*-value < 0.1 |Residual for Dose Group Near BMD| > 2
Exponential 5 (NCV—normal)	Restricted	0.1937	0.1654	NA	0.5572	Questionable	d.f. = 0, saturated model (Goodness of fit test cannot be calculated)
Hill (NCV—normal)	Restricted	0.1880	0.1653	NA	0.5577	Questionable	d.f. = 0, saturated model (Goodness of fit test cannot be calculated)
Polynomial (3 degree) (NCV—normal)	Restricted	0.1507	0.1144	0.0002	11.9784	Questionable	Goodness of fit *p*-value < 0.1 |Residual for Dose Group Near BMD| > 2
Polynomial (2 degree) (NCV—normal)	Restricted	0.1507	0.1144	0.0002	11.9784	Questionable	Goodness of fit *p*-value < 0.1 |Residual for Dose Group Near BMD| > 2
Power (NCV—normal)	Restricted	0.1628	0.1183	0.0004	11.0771	Questionable	Goodness of fit *p*-value < 0.1
Linear (NCV—normal)	Unrestricted	0.1334	0.1127	0.0010	10.4397	Questionable	Goodness of fit *p*-value < 0.1 |Residual for Dose Group Near BMD| > 2

Table C-40. Benchmark dose results for increased relative liver weight (TDAR) in female rats—log-normal, constant variance, BMR = 10% relative deviation (Frawley et al., 2018)

Models	Restriction	10% Relative deviation		*p*-Value	AIC	BMDS classification	BMDS notes
		BMD	BMDL				
Log-normal Constant variance							
Exponential 2 (CV—log-normal)	Restricted	0.1478	0.1295	0.0172	7.4633	Questionable	Constant variance test failed (Test 2 *p*-value < 0.05) Goodness of fit *p*-value < 0.1 Modeled control response std. dev. >|1.5| actual response std. dev.
Exponential 3 (CV— log-normal)	Restricted	0.1639	0.1304	0.0050	9.2051	Questionable	Constant variance test failed (Test 2 *p*-value < 0.05) Goodness of fit *p*-value < 0.1 Modeled control response std. dev. >|1.5| actual response std. dev.
Exponential 4 (CV— log-normal)	Restricted	0.1315	0.1026	0.0033	9.9692	Questionable	Constant variance test failed (Test 2 *p*-value < 0.05) Goodness of fit *p*-value < 0.1 Modeled control response std. dev. >|1.5| actual response std. dev.
Exponential 5 (CV— log-normal)	Restricted	0.1644	0.1111	NA	10.6210	Questionable	Constant variance test failed (Test 2 *p*-value < 0.05) Modeled control response std. dev. >|1.5| actual response std. dev. d.f. = 0, saturated model (Goodness of fit test cannot be calculated)
Hill (CV— log-**normal)**	Restricted	0.1918	0.1692	NA	3.3425	Questionable	Constant variance test failed (Test 2 *p*-value < 0.05) Modeled control response std. dev. >|1.5| actual response std. dev. d.f. = 0, saturated model (Goodness of fit test cannot be calculated)
Polynomial (3 degree) (CV— log-normal)	Restricted	0.1541	0.1143	0.0046	9.3729	Questionable	Constant variance test failed (Test 2 *p*-value < 0.05) Goodness of fit *p*-value < 0.1 Modeled control response std. dev. >|1.5| actual response std. dev.

Models	Restriction	10% Relative deviation		*p*-Value	AIC	BMDS classification	BMDS notes
		BMD	BMDL				
Log-normal Constant variance							
Polynomial (2 degree) (CV— log-normal)	Restricted	0.1541	0.1143	0.0046	9.3729	Questionable	Constant variance test failed (Test 2 *p*-value < 0.05) Goodness of fit *p*-value < 0.1 Modeled control response std. dev. >|1.5| actual response std. dev.
Power (CV— log-normal)	Restricted	0.1649	0.1176	0.0070	8.6207	Questionable	Constant variance test failed (Test 2 *p*-value < 0.05) Goodness of fit *p*-value < 0.1 Modeled control response std. dev. >|1.5| actual response std. dev.
Linear (CV— log-normal)	Unrestricted	0.1315	0.1122	0.0134	7.9687	Questionable	Constant variance test failed (Test 2 *p*-value < 0.05) Goodness of fit *p*-value < 0.1 Modeled control response std. dev. >|1.5| actual response std. dev.

C.2.10. DECREASED FETAL WEIGHT—MALE AND FEMALE RATS (Harris and Birnbaum, 1989)

Table C-41. Dose-response data for decreased fetal weight in male and female rats (Harris and Birnbaum, 1989)

Dose (mg/kg-d)	*n*	Mean	SD
0	86.4	1.17	0.09
0.03	85.8	1.16	0.02
0.1	94.8	1.13	0.2
0.3	102	1.16	0.3
1	103.6	1.12	0.2
3	87.6	1.1	0.09
6.4	75.4	0.9	0.26
12.8	32.2	0.59	0.11

Table C-42. Benchmark dose results for decreased fetal weight in male and female rats—constant variance, BMR = 5% relative deviation (Harris and Birnbaum, 1989)

Models	Restriction	5% relative deviation		*p*-Value	AIC	BMDS classification	BMDS notes
		BMD	BMDL				
Constant variance							
Exponential 2 (CV—normal)	Restricted	1.1862	1.0702	0.0010	−303.6182	Questionable	Constant variance test failed (Test 2 *p*-value < 0.05) Goodness of fit *p*-value < 0.1 Modeled control response std. dev. >|1.5| actual response std. dev.
Exponential 3 (CV—normal)	Restricted	2.4486	1.8922	0.3529	−318.5263	Questionable	Constant variance test failed (Test 2 *p*-value < 0.05) Modeled control response std. dev. >|1.5| actual response std. dev.
Exponential 4 (CV—normal)	Restricted	1.1862	1.0702	0.0010	−303.6182	Questionable	Constant variance test failed (Test 2 *p*-value < 0.05) Goodness of fit *p*-value < 0.1 Modeled control response std. dev. >|1.5| actual response std. dev.
Exponential 5 (CV—normal)	Restricted	3.0401	2.0145	0.3470	−317.6098	Questionable	Constant variance test failed (Test 2 *p*-value < 0.05) Modeled control response std. dev. >|1.5| actual response std. dev.
Hill (CV—normal)	Restricted	3.0451	2.0215	0.3383	−317.5367	Questionable	Constant variance test failed (Test 2 *p*-value < 0.05) Modeled control response std. dev. >|1.5| actual response std. dev.
Polynomial (7 degree) (CV—normal)	Restricted	1.9190	1.4664	0.1942	−316.6978	Questionable	Constant variance test failed (Test 2 *p*-value < 0.05) Modeled control response std. dev. >|1.5| actual response std. dev.
Polynomial (6 degree) (CV—normal)	Restricted	1.9190	1.4668	0.1942	−316.6978	Questionable	Constant variance test failed (Test 2 *p*-value < 0.05) Modeled control response std. dev. >|1.5| actual response std. dev.
Polynomial (5 degree) (CV—normal)	Restricted	1.9190	1.4667	0.1942	−316.6978	Questionable	Constant variance test failed (Test 2 *p*-value < 0.05) Modeled control response std. dev. >|1.5| actual response std. dev.

Models	Restriction	5% relative deviation		*p*-Value	AIC	BMDS classification	BMDS notes
		BMD	BMDL				
Constant variance							
Polynomial (4 degree) (CV—normal)	Restricted	1.9190	1.4667	0.1942	−316.6978	Questionable	Constant variance test failed (Test 2 *p*-value < 0.05) Modeled control response std. dev. >|1.5| actual response std. dev.
Polynomial (3 degree) (CV—normal)	Restricted	1.9190	1.4681	0.1942	−316.6978	Questionable	Constant variance test failed (Test 2 *p*-value < 0.05) Modeled control response std. dev. >|1.5| actual response std. dev.
Polynomial (2 degree) (CV—normal)	Restricted	1.9190	1.4884	0.1942	−316.6978	Questionable	Constant variance test failed (Test 2 *p*-value < 0.05) Modeled control response std. dev. >|1.5| actual response std. dev.
Power (CV—normal)	Restricted	2.1795	1.6300	0.2568	−317.5277	Questionable	Constant variance test failed (Test 2 *p*-value < 0.05) Modeled control response std. dev. >|1.5| actual response std. dev.
Linear (CV—normal)	Unrestricted	1.3815	1.2741	0.0441	−313.1368	Questionable	Constant variance test failed (Test 2 *p*-value < 0.05) Goodness of fit *p*-value < 0.1 Modeled control response std. dev. >|1.5| actual response std. dev.

Table C-43. Benchmark dose results for decreased fetal weight in male and female rats—nonconstant variance, BMR = 5% relative deviation (Harris and Birnbaum, 1989)

Models	Restriction	5% relative deviation		*p*-Value	AIC	BMDS classification	BMDS notes
		BMD	BMDL				
Non-constant variance							
Exponential 2 (NCV— normal)	Restricted	1.2032	1.0775	0.0012	−302.0911	Questionable	Nonconstant variance test failed (Test 3 *p*-value < 0.05) Goodness of fit *p*-value < 0.1 Modeled control response std. dev. >|1.5| actual response std. dev.
Exponential 3 (NCV— normal)	Restricted	2.4989	1.9388	0.4468	−317.3295	Questionable	Nonconstant variance test failed (Test 3 *p*-value < 0.05) Modeled control response std. dev. >|1.5| actual response std. dev.

Models	Restriction	5% relative deviation		*p*-Value	AIC	BMDS classification	BMDS notes
		BMD	BMDL				
Non-constant variance							
Exponential 4 (NCV— normal)	Restricted	1.2031	1.0775	0.0012	−302.0911	Questionable	Nonconstant variance test failed (Test 3 *p*-value < 0.05) Goodness of fit *p*-value < 0.1 Modeled control response std. dev. >|1.5| actual response std. dev.
Exponential 5 (NCV— normal)	Restricted	2.4942	1.9392	0.3140	−315.3322	Questionable	Nonconstant variance test failed (Test 3 *p*-value < 0.05) Modeled control response std. dev. >|1.5| actual response std. dev.
Hill (NCV— normal)	Restricted	2.9282	1.9155	0.3696	−315.8031	Questionable	Nonconstant variance test failed (Test 3 *p*-value < 0.05) Modeled control response std. dev. >|1.5| actual response std. dev.
Polynomial (7 degree) (NCV— normal)	Restricted	1.9751	1.6128	0.2753	−315.7500	Questionable	Nonconstant variance test failed (Test 3 *p*-value < 0.05) Modeled control response std. dev. >|1.5| actual response std. dev.
Polynomial (6 degree) (NCV— normal)	Restricted	1.9716	1.4955	0.2749	−315.7461	Questionable	Nonconstant variance test failed (Test 3 *p*-value < 0.05) Modeled control response std. dev. >|1.5| actual response std. dev.
Polynomial (5 degree) (NCV— normal)	Restricted	1.9712	1.4921	0.2749	−315.7460	Questionable	Nonconstant variance test failed (Test 3 *p*-value < 0.05) Modeled control response std. dev. >|1.5| actual response std. dev.
Polynomial (4 degree) (NCV— normal)	Restricted	1.9751	1.4965	0.2753	−315.7500	Questionable	Nonconstant variance test failed (Test 3 *p*-value < 0.05) Modeled control response std. dev. >|1.5| actual response std. dev.
Polynomial (3 degree) (NCV— normal)	Restricted	1.9751	1.4973	0.2753	−315.7500	Questionable	Nonconstant variance test failed (Test 3 *p*-value < 0.05) Modeled control response std. dev. >|1.5| actual response std. dev.
Polynomial (2 degree) (NCV— normal)	Restricted	1.9751	1.5263	0.2753	−315.7500	Questionable	Nonconstant variance test failed (Test 3 *p*-value < 0.05) Modeled control response std. dev. >|1.5| actual response std. dev.

Models	Restriction	5% relative deviation		*p*-Value	AIC	BMDS classification	BMDS notes
		BMD	BMDL				
Non-constant variance							
Power (NCV—normal)	Restricted	2.2422	1.6842	0.3562	−316.5655	Questionable	Nonconstant variance test failed (Test 3 *p*-value < 0.05) Modeled control response std. dev. >|1.5| actual response std. dev.
Linear (NCV—normal)	Unrestricted	1.3772	1.2719	0.0450	−311.2042	Questionable	Nonconstant variance test failed (Test 3 *p*-value < 0.05) Goodness of fit *p*-value < 0.1 Modeled control response std. dev. >|1.5| actual response std. dev.

Table C-44. Benchmark dose results for decreased fetal weight in male and female rats—log-normal, constant variance, BMR = 5% relative deviation (Harris and Birnbaum, 1989)

Models	Restriction	5% relative deviation		*p*-Value	AIC	BMDS classification	BMDS notes
		BMD	BMDL				
Log-normal, constant variance							
Exponential 2 (CV—log-normal)	Restricted	1.0479	0.9755	<0.0001	−307.8546	Questionable	Constant variance test failed (Test 2 *p*-value < 0.05) Goodness of fit *p*-value < 0.1 Modeled control response std. dev. >|1.5| actual response std. dev.
Exponential 3 (CV— log-normal)	Restricted	2.1631	1.7042	0.0286	−326.0092	Questionable	Constant variance test failed (Test 2 *p*-value < 0.05) Goodness of fit *p*-value < 0.1 Modeled control response std. dev. >|1.5| actual response std. dev.
Exponential 4 (CV— log-normal)	Restricted	1.0479	0.9755	<0.0001	−307.8546	Questionable	Constant variance test failed (Test 2 *p*-value < 0.05) Goodness of fit *p*-value < 0.1 Modeled control response std. dev. >|1.5| actual response std. dev.
Exponential 5 (CV— log-normal)	Restricted	3.4280	2.4438	0.1216	−329.2234	Questionable	Constant variance test failed (Test 2 *p*-value < 0.05) Modeled control response std. dev. >|1.5| actual response std. dev.

Models	Restriction	5% relative deviation		*p*-Value	AIC	BMDS classification	BMDS notes
		BMD	BMDL				
Log-normal, constant variance							
Hill (CV— log-normal)	Restricted	-	-	-	-	Unusable	BMD computation failed Model was not run. Adverse direction "down" not compatible with lognormal distribution
Polynomial (7 degree) (CV— log-normal)	Restricted	-	-	-	-	Unusable	BMD computation failed Model was not run. Adverse direction "down" not compatible with lognormal distribution
Polynomial (6 degree) (CV— log-normal)	Restricted	-	-	-	-	Unusable	BMD computation failed Model was not run. Adverse direction "down" not compatible with lognormal distribution
Polynomial (5 degree) (CV— log-normal)	Restricted	-	-	-	-	Unusable	BMD computation failed Model was not run. Adverse direction "down" not compatible with lognormal distribution
Polynomial (4 degree) (CV— log-normal)	Restricted	-	-	-	-	Unusable	BMD computation failed Model was not run. Adverse direction "down" not compatible with lognormal distribution
Polynomial (3 degree) (CV— log-normal)	Restricted	-	-	-	-	Unusable	BMD computation failed Model was not run. Adverse direction "down" not compatible with lognormal distribution
Polynomial (2 degree) (CV— log-normal)	Restricted	-	-	-	-	Unusable	BMD computation failed Model was not run. Adverse direction "down" not compatible with lognormal distribution
Power (CV— log-normal)	Restricted	-	-	-	-	Unusable	BMD computation failed Model was not run. Adverse direction "down" not compatible with lognormal distribution
Linear (CV— log-normal)	Unrestricted	-	-	-	-	Unusable	BMD computation failed Model was not run. Adverse direction "down" not compatible with lognormal distribution

C.2.11. DECREASED SPERM COUNT—MALE RATS (NTP, 2018)

Table C-45. Dose-response data for decreased sperm counts in male rats (NTP, 2018)

Dose (mg/kg-d)	*n*	Mean	SD
0	10	136.3	32.26
0.625	10	120.8	17.39
1.25	10	112.9	23.09
2.5	10	95.7	36.37

Table C-46. Benchmark dose results for decreased sperm counts in male rats, BMR = 1 standard deviation (NTP, 2018)

Models	Restriction	1 standard deviation		*p*-Value	AIC	BMDS classification	BMDS notes
		BMD	BMDL				
Constant variance							
Exponential 2 (CV—normal)	**Restricted**	**1.5928**	**0.9634**	**0.9331**	**382.8116**	**Viable—Recommended**	**Lowest AIC**
Exponential 3 (CV—normal)	Restricted	1.5928	0.9634	0.9331	382.8116	Viable—Recommended	Lowest AIC
Exponential 4 (CV—normal)	Restricted	1.4241	0.5083	0.8023	384.7359	Viable—Alternate	
Exponential 5 (CV—normal)	Restricted	1.4241	0.5083	0.8023	384.7359	Viable—Alternate	
Hill (CV—normal)	Restricted	1.4208	0.4347	0.8120	384.7298	Viable—Alternate	
Polynomial (3 degree) (CV—normal)	Restricted	1.7202	1.1328	0.8756	382.9388	Viable—Alternate	
Polynomial (2 degree) (CV—normal)	Restricted	1.7202	1.1328	0.8756	382.9388	Viable—Alternate	
Power (CV—normal)	Restricted	1.7202	1.1329	0.8756	382.9388	Viable—Alternate	
Linear (CV—normal)	Unrestricted	1.7202	1.1328	0.8756	382.9388	Viable—Alternate	

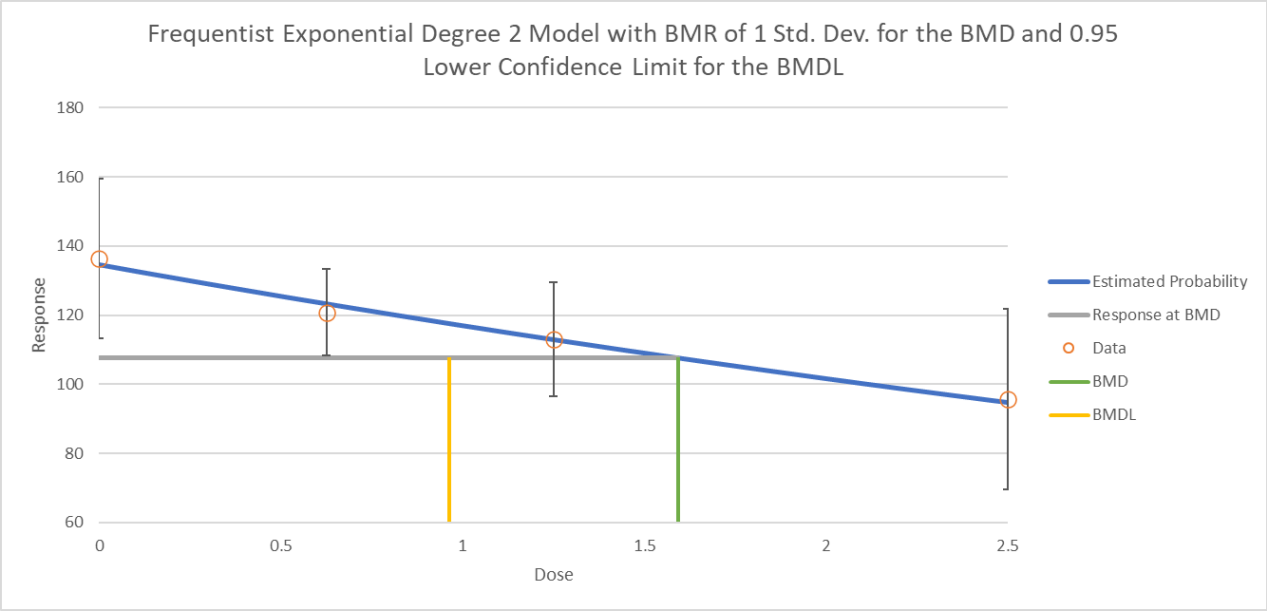

Figure C-18. Dose-response curve for the Exponential 2 model fit to decreased sperm counts in male rats (NTP, 2018).

User Input

Info	
Model	frequentist Exponential degree 2 v1.1
Dataset Name	Sperm_Count_NTP
User notes	[Add user notes here]
Dose-Response Model	M[dose] = a * exp(±1 * b * dose)
Variance Model	Var[i] = alpha

Model Options	
BMR Type	Std. Dev.
BMRF	1
Tail Probability	-
Confidence Level	0.95
Distribution Type	Normal
Variance Type	Constant

Model Data	
Dependent Variable	[Dose]
Independent Variable	[Mean]
Total # of Observations	4
Adverse Direction	Automatic

Figure C-19. User input for dose-response modeling of decreased sperm counts in male counts (NTP, 2018).

Model Results

Benchmark Dose	
BMD	1.592768431
BMDL	0.963412903
BMDU	3.624046063
AIC	382.8116246
Test 4 P-value	0.933123027
D.O.F.	2

Model Parameters	
# of Parameters	3
Variable	Estimate
a	134.5572517
b	0.139886976
log-alpha	6.582413542

Goodness of Fit

Dose	Size	Estimated Median	Calc'd Median	Observed Mean	Estimated SD	Calc'd SD	Observed SD	Scaled Residual
0	10	134.5572517	136.3	136.3	26.8752764	32.26	32.26	0.205060364
0.625	10	123.2926024	120.8	120.8	26.8752764	17.39	17.39	-0.293291902
1.25	10	112.9709891	112.9	112.9	26.8752764	23.09	23.09	-0.008352922
2.5	10	94.84768903	95.7	95.7	26.8752764	36.37	36.37	0.100287116

Likelihoods of Interest

Model	Log Likelihood*	# of Parameters	AIC
A1	-188.3365941	5	386.673188
A2	-185.2790038	8	386.558008
A3	-188.3365941	5	386.673188
fitted	-188.4058123	3	382.811625
R	-193.5430425	2	391.086085

* Includes additive constant of -36.75754. This constant was not included in the LL derivation prior to BMDS 3.0.

Tests of Interest

Test	-2*Log(Likelihood Ratio)	Test df	p-value
1	16.52807739	6	0.01118344
2	6.115180405	3	0.10613895
3	6.115180405	3	0.10613895
4	0.138436451	2	0.93312303

Figure C-20. Model results for decreased sperm counts in rat males (NTP, 2018).

C.2.12. DECREASED ABSOLUTE TESTIS WEIGHT IN MALE RATS (NTP, 2018)

Table C-47. Dose-response data for decreased absolute testis weight in male rats (NTP, 2018)

Dose (mg/kg-d)	*n*	Mean	SD
0	9	1.777	0.17
0.156	10	1.797	0.15
0.312	10	1.742	0.12
0.625	10	1.74	0.1
1.25	10	1.695	0.11
2.5	10	1.553	0.2

Table C-48. Benchmark dose results for decreased absolute testis weight in male rats—constant variance, BMR = 1 standard deviation (NTP, 2018)

Models	Restriction	1 standard deviation		*p*-Value	AIC	BMDS classification	BMDS notes
		BMD	BMDL				
Constant variance							
Exponential 2 (CV—normal)	Restricted	1.4763	1.0220	0.9324	−59.4936	Viable—Alternate	
Exponential 3 (CV—normal)	Restricted	1.7052	1.0373	0.8973	−57.7417	Viable—Alternate	
Exponential 4 (CV—normal)	Restricted	1.4763	1.0220	0.9324	−59.4936	Viable—Alternate	
Exponential 5 (CV—normal)	Restricted	1.7049	0.8202	0.7420	−55.7409	Viable—Alternate	
Hill (CV—normal)	Restricted	1.7088	0.8010	0.7448	−55.7486	Viable—Alternate	
Polynomial (5 degree) (CV—normal)	Restricted	1.7976	1.0880	0.9114	−57.8041	Viable—Alternate	
Polynomial (4 degree) (CV—normal)	Restricted	1.7750	1.0878	0.9107	−57.8008	Viable—Alternate	
Polynomial (3 degree) (CV—normal)	Restricted	1.7482	1.0873	0.9089	−57.7926	Viable—Alternate	
Polynomial (2 degree) (CV—normal)	Restricted	1.7214	1.0861	0.9046	−57.7738	Viable—Alternate	
Power (CV—normal)	Restricted	1.7089	1.0848	0.8995	−57.7514	Viable—Alternate	
Linear (CV—normal)	**Unrestricted**	**1.5110**	**1.0742**	**0.9430**	**−59.5723**	**Viable—Recommended**	**Lowest AIC**

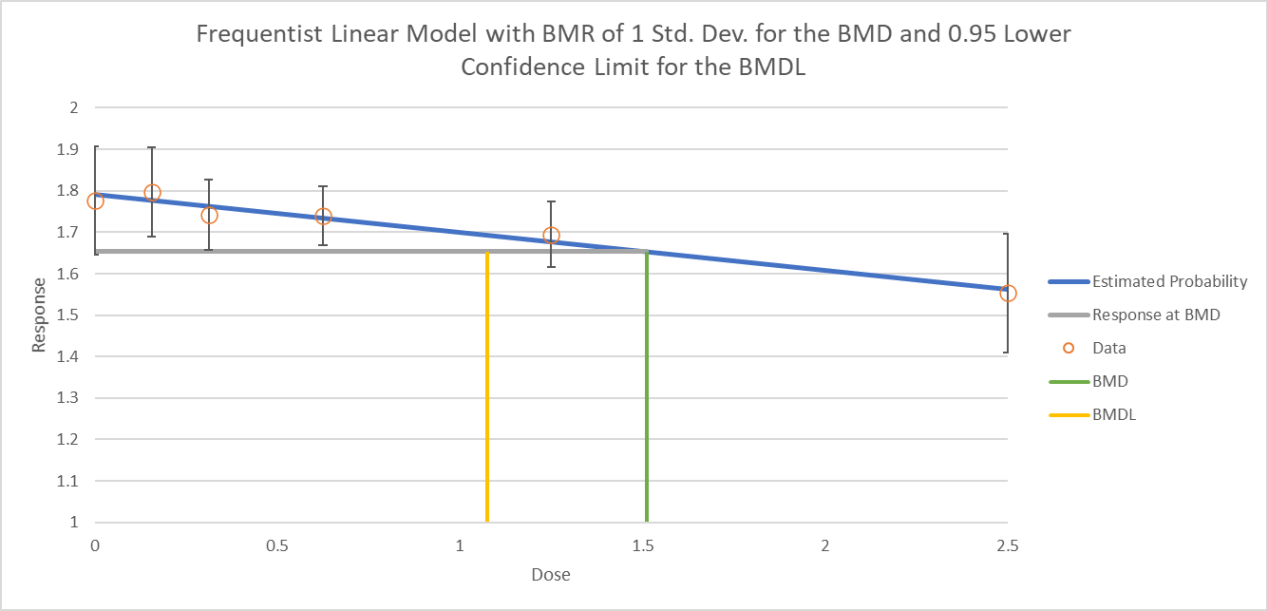

Figure C-21. Dose-response curve for the Linear model fit to decreased absolute testis weight in male rats (NTP, 2018).

User Input

Info	
Model	frequentist Linear v1.1
Dataset Name	TestisWt_Abs_NTP
User notes	[Add user notes here]
Dose-Response Model	M[dose] = g + b1*dose
Variance Model	Var[i] = alpha

Model Options	
BMR Type	Std. Dev.
BMRF	1
Tail Probability	-
Confidence Level	0.95
Distribution Type	Normal
Variance Type	Constant

Model Data	
Dependent Variable	[Dose]
Independent Variable	[Mean]
Total # of Observations	6
Adverse Direction	Automatic

Figure C-22. User input for dose-response modeling of decreased absolute testis weight in male rats (NTP, 2018).

Model Results

Benchmark Dose	
BMD	1.511042118
BMDL	1.074196873
BMDU	2.542202182
AIC	-59.57226688
Test 4 P-value	0.943009409
D.O.F.	4

Model Parameters	
# of Parameters	3
Variable	Estimate
g	1.791729181
beta1	-0.091864992
alpha	0.019268735

Goodness of Fit

Dose	Size	Estimated Median	Calc'd Median	Observed Mean	Estimated SD	Calc'd SD	Observed SD	Scaled Residual
0	9	1.791729181	1.777	1.777	0.13881187	0.17	0.17	-0.318326837
0.156	10	1.777398242	1.797	1.797	0.13881187	0.15	0.15	0.446548271
0.312	10	1.763067304	1.742	1.742	0.13881187	0.12	0.12	-0.479934917
0.625	10	1.734313561	1.74	1.74	0.13881187	0.1	0.1	0.129542952
1.25	10	1.676897941	1.695	1.695	0.13881187	0.11	0.11	0.412383595
2.5	10	1.5620667	1.553	1.553	0.13881187	0.2	0.2	-0.206548786

Likelihoods of Interest

Model	Log Likelihood*	# of Parameters	AIC
A1	33.16889532	7	-52.3377906
A2	36.76108906	12	-49.5221781
A3	33.16889532	7	-52.3377906
fitted	32.78613344	3	-59.5722669
R	24.53190731	2	-45.0638146

* Includes additive constant of -54.21737. This constant was not included in the LL derivation prior to BMDS 3.0.

Tests of Interest

Test	-2*Log(Likelihood Ratio)	Test df	p-value
1	24.4583635	10	0.0064724
2	7.184387472	5	0.20728439
3	7.184387472	5	0.20728439
4	0.765523758	4	0.94300941

Figure C-23. Model results for decreased absolute testis weight in male rats (NTP, 2018).

C.2.13. DECREASED ABSOLUTE CAUDAL EPIDIDYMIS WEIGHT IN MALE RATS (NTP, 2018)

Table C-49. Dose-response data for decreased absolute caudal epididymis weight in male rats (NTP, 2018)

Dose (mg/kg-d)	*n*	Mean	SD
0	10	0.184	0.02
0.625	10	0.178	0.01
1.25	10	0.164	0.02
2.5	10	0.138	0.03

Table C-50. Benchmark dose results for decreased absolute caudal epididymis weight in male rats—constant variance, BMR = 1 standard deviation (NTP, 2018)

Models	Restriction	1 standard deviation		*p*-Value	AIC	BMDS classification	BMDS notes
		BMD	BMDL				
Constant variance							
Exponential 2 (CV—normal)	Restricted	0.9906	0.7014	0.6614	−192.1231	Questionable	Constant variance test failed (Test 2 *p*-value < 0.05)
Exponential 3 (CV—normal)	Restricted	1.2840	0.7347	0.7934	−190.8813	Questionable	Constant variance test failed (Test 2 *p*-value < 0.05)
Exponential 4 (CV—normal)	Restricted	0.9906	0.7014	0.6614	−192.1231	Questionable	Constant variance test failed (Test 2 *p*-value < 0.05)
Exponential 5 (CV—normal)	Restricted	1.2550	0.6841	NA	−188.9499	Questionable	Constant variance test failed (Test 2 *p*-value < 0.05) d.f. = 0, saturated model (Goodness of fit test cannot be calculated)
Hill (CV—normal)	Restricted	1.2551	0.6802	NA	−188.9499	Questionable	Constant variance test failed (Test 2 *p*-value < 0.05) d.f. = 0, saturated model (Goodness of fit test cannot be calculated)
Polynomial (3 degree) (CV—normal)	Restricted	1.2961	0.8004	0.6972	−190.7984	Questionable	Constant variance test failed (Test 2 *p*-value < 0.05)
Polynomial (2 degree) (CV—normal)	Restricted	1.2961	0.8004	0.6972	−190.7984	Questionable	Constant variance test failed (Test 2 *p*-value < 0.05)
Power (CV—normal)	Restricted	1.2924	0.8027	0.7563	−190.8535	Questionable	Constant variance test failed (Test 2 *p*-value < 0.05)
Linear (CV—normal)	Unrestricted	1.0647	0.7868	0.7835	−192.4618	Questionable	Constant variance test failed (Test 2 *p*-value < 0.05)

Table C-51. Benchmark dose results for decreased absolute caudal epididymis weight in male rats—nonconstant variance, BMR = 1 standard deviation (NTP, 2018)

Models	Restriction	1 standard deviation		*p*-Value	AIC	BMDS classification	BMDS notes
		BMD	BMDL				
Constant variance							
Exponential 2 (NCV—normal)	Restricted	0.7898	0.5327	0.3071	−193.9474	Viable—Alternate	
Exponential 3 (NCV—normal)	Restricted	1.1440	0.6331	0.5123	−193.8789	Viable—Alternate	
Exponential 4 (NCV—normal)	Restricted	0.7902	0.5326	0.3070	−193.9463	Viable—Alternate	
Exponential 5 (NCV—normal)	Restricted	1.1558	0.6708	NA	−192.3083	Questionable	d.f. = 0, saturated model (Goodness of fit test cannot be calculated)
Hill (NCV—normal)	Restricted	1.1495	0.6702	NA	−192.3080	Questionable	d.f. = 0, saturated model (Goodness of fit test cannot be calculated)
Polynomial (3 degree) (NCV—normal)	Restricted	1.1618	0.6304	0.4150	−193.6438	Viable—Alternate	
Polynomial (2 degree) (NCV—normal)	Restricted	1.1618	0.6304	0.4150	−193.6438	Viable—Alternate	
Power (NCV—normal)	Restricted	1.1497	0.6390	0.4771	−193.8028	Viable—Alternate	
Linear (NCV—normal)	**Unrestricted**	**0.8363**	**0.5824**	**0.4086**	**−194.5183**	**Viable—Recommended**	**Lowest AIC**

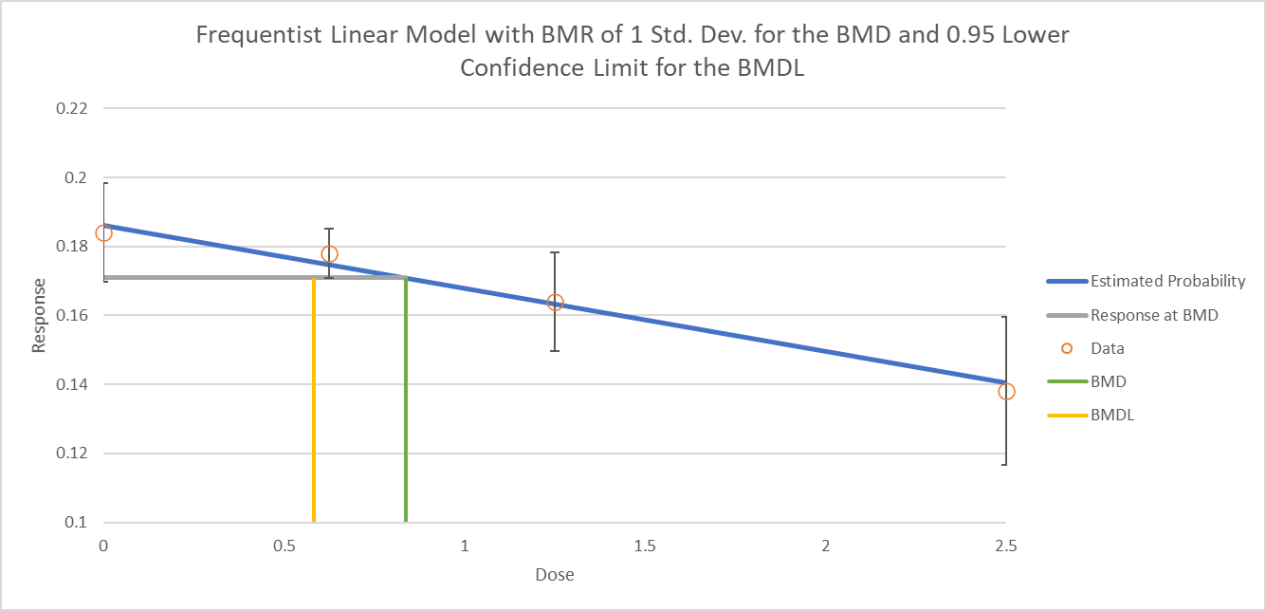

Figure C-24. Dose-response curve for the Linear model fit to decreased absolute caudal epididymis weight in male rats (NTP, 2018).

User Input

Info	
Model	frequentist Linear v1.1
Dataset Name	CaudaEpiWt_Abs_NTP
User notes	[Add user notes here]
Dose-Response Model	M[dose] = g + b1*dose
Variance Model	Var[i] = alpha * mean[i] ^ rho

Model Options	
BMR Type	Std. Dev.
BMRF	1
Tail Probability	-
Confidence Level	0.95
Distribution Type	Normal
Variance Type	Non-Constant

Model Data	
Dependent Variable	[Dose]
Independent Variable	[Mean]
Total # of Observations	4
Adverse Direction	Automatic

Figure C-25. User Input for dose-response modeling of decreased caudal epididymis weight in male rats (NTP, 2018).

Model Results

Benchmark Dose	
BMD	0.836267471
BMDL	0.582449886
BMDU	1.345231202
AIC	-194.5182635
Test 4 P-value	0.408601663
D.O.F.	2

Model Parameters	
# of Parameters	4
Variable	Estimate
g	0.186188825
beta1	-0.018332295
rho	-3.81191884
alpha	-14.76361024

Goodness of Fit

Dose	Size	Estimated Median	Calc'd Median	Observed Mean	Estimated SD	Calc'd SD	Observed SD	Scaled Residual
0	10	0.186188825	0.184	0.184	0.01533068	0.02	0.02	-0.451491469
0.625	10	0.174731141	0.178	0.178	0.01730351	0.01	0.01	0.59739552
1.25	10	0.163273457	0.164	0.164	0.01969127	0.02	0.02	0.116677641
2.5	10	0.140358089	0.138	0.138	0.02626961	0.03	0.03	-0.283861514

Likelihoods of Interest

Model	Log Likelihood*	# of Parameters	AIC
A1	99.47492849	5	-188.949857
A2	104.7074099	8	-193.41482
A3	102.1541463	6	-192.308293
fitted	101.2591317	4	-194.518263
R	87.99544268	2	-171.990885

* Includes additive constant of -36.75754. This constant was not included in the LL derivation prior to BMDS 3.0.

Tests of Interest

Test	-2*Log(Likelihood Ratio)	Test df	p-value
1	33.42393448	6	<0.0001
2	10.46496286	3	0.01500047
3	5.106527298	2	0.07782725
4	1.790029051	2	0.40860166

Figure C-26. Model results for decreased caudal epididymis weight in male rats (NTP, 2018).

C.2.14. DECREASED ABSOLUTE WHOLE EPIDIDYMIS WEIGHT IN MALE RATS (NTP, 2018)

Table C-52. Dose-response data for decreased absolute whole epididymis weight in male rats (NTP, 2018)

Dose (mg/kg-d)	*n*	Mean	SD
0	10	0.528	0.05
0.625	10	0.508	0.03
1.25	10	0.474	0.04
2.5	10	0.407	0.08

Table C-53. Benchmark dose results for decreased whole caudal epididymis weight in male rats—constant variance, BMR = 1 standard deviation (NTP, 2018)

Models	Restriction	1 standard deviation		*p*-Value	AIC	BMDS classification	BMDS notes
		BMD	BMDL				
Constant variance							
Exponential 2 (CV—normal)	Restricted	0.9572	0.6866	0.7614	−118.5715	Questionable	Constant variance test failed (Test 2 *p*-value < 0.05)
Exponential 3 (CV—normal)	Restricted	1.2024	0.7076	0.8891	−117.0973	Questionable	Constant variance test failed (Test 2 *p*-value < 0.05)
Exponential 4 (CV—normal)	Restricted	0.9572	0.6866	0.7614	−118.5715	Questionable	Constant variance test failed (Test 2 *p*-value < 0.05)
Exponential 5 (CV—normal)	Restricted	1.2024	0.7076	0.8891	−117.0973	Questionable	Constant variance test failed (Test 2 *p*-value < 0.05)
Hill (CV—normal)	Restricted	1.1911	0.6254	NA	−115.1168	Questionable	Constant variance test failed (Test 2 *p*-value < 0.05) d.f. = 0, saturated model (Goodness of fit test cannot be calculated)
Polynomial (3 degree) (CV—normal)	Restricted	1.2061	0.7720	0.7980	−117.0513	Questionable	Constant variance test failed (Test 2 *p*-value < 0.05)
Polynomial (2 degree) (CV—normal)	Restricted	1.2061	0.7720	0.7980	−117.0513	Questionable	Constant variance test failed (Test 2 *p*-value < 0.05)
Power (CV—normal)	Restricted	1.2076	0.7732	0.8530	−117.0825	Questionable	Constant variance test failed (Test 2 *p*-value < 0.05)
Linear (CV—normal)	Unrestricted	1.0266	0.7639	0.8678	−118.8333	Questionable	Constant variance test failed (Test 2 p-value < 0.05)

Table C-54. Benchmark dose results for decreased absolute whole epididymis weight in male rats—nonconstant variance, BMR = 1 standard deviation (NTP, 2018)

Models	Restriction	1 standard deviation		*p*-Value	AIC	BMDS classification	BMDS notes
		BMD	BMDL				
Constant variance							
Exponential 2 (NCV— normal)	Restricted	0.7358	0.5033	0.3609	−121.3235	Viable—Alternate	
Exponential 3 (NCV— normal)	Restricted	1.0959	0.5980	0.7979	−121.2963	Viable—Alternate	
Exponential 4 (NCV— normal)	Restricted	0.7360	0.5033	0.3609	−121.3235	Viable—Alternate	

Models	Restriction	1 standard deviation		*p*-Value	AIC	BMDS classification	BMDS notes
		BMD	BMDL				
Constant variance							
Exponential 5 (NCV— normal)	Restricted	1.0960	0.5986	NA	−119.2989	Questionable	d.f. = 0, saturated model (Goodness of fit test cannot be calculated)
Hill (NCV— normal)	Restricted	1.1035	0.6011	NA	−119.3619	Questionable	d.f. = 0, saturated model (Goodness of fit test cannot be calculated)
Polynomial (3 degree) (NCV— normal)	Restricted	1.1012	0.5975	0.6702	−121.1805	Viable— Alternate	
Polynomial (2 degree) (NCV— normal)	Restricted	1.1012	0.5974	0.6702	−121.1805	Viable— Alternate	
Power (NCV— normal)	Restricted	1.0965	0.6018	0.7557	−121.2651	Viable— Alternate	
Linear (NCV— normal)	**Unrestricted**	**0.7766**	**0.5458**	**0.4809**	**−121.8975**	**Viable— Recommended**	**Lowest AIC**

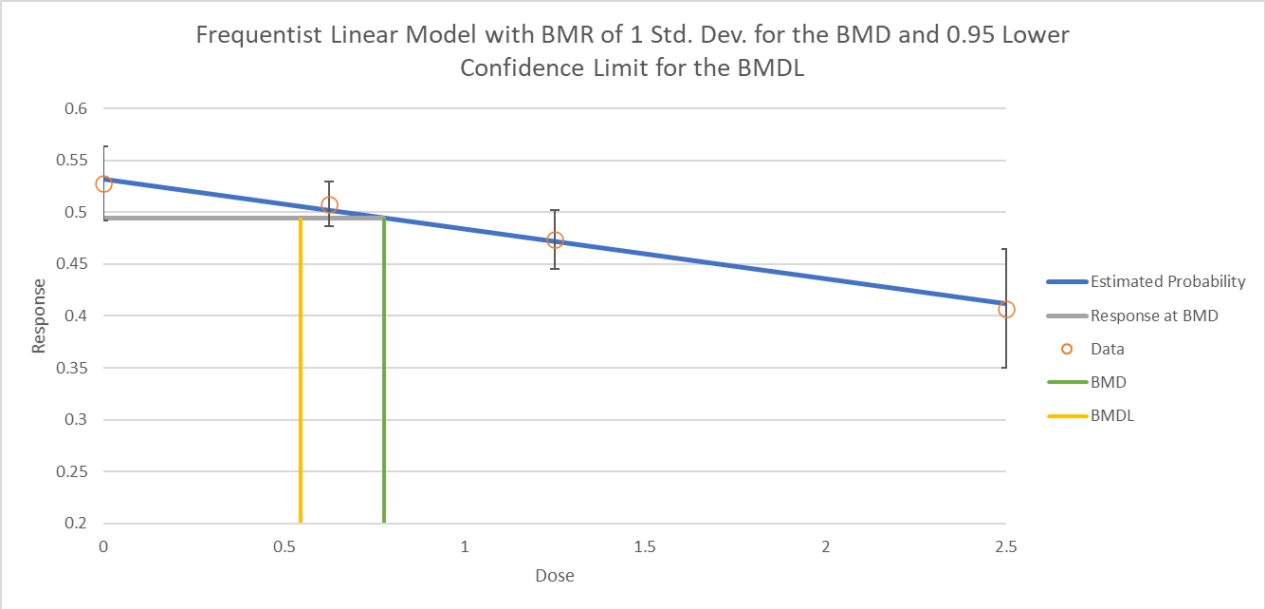

Figure C-27. Dose-response curve for the Linear model fit to decreased absolute whole epididymis weight in male rats (NTP, 2018).

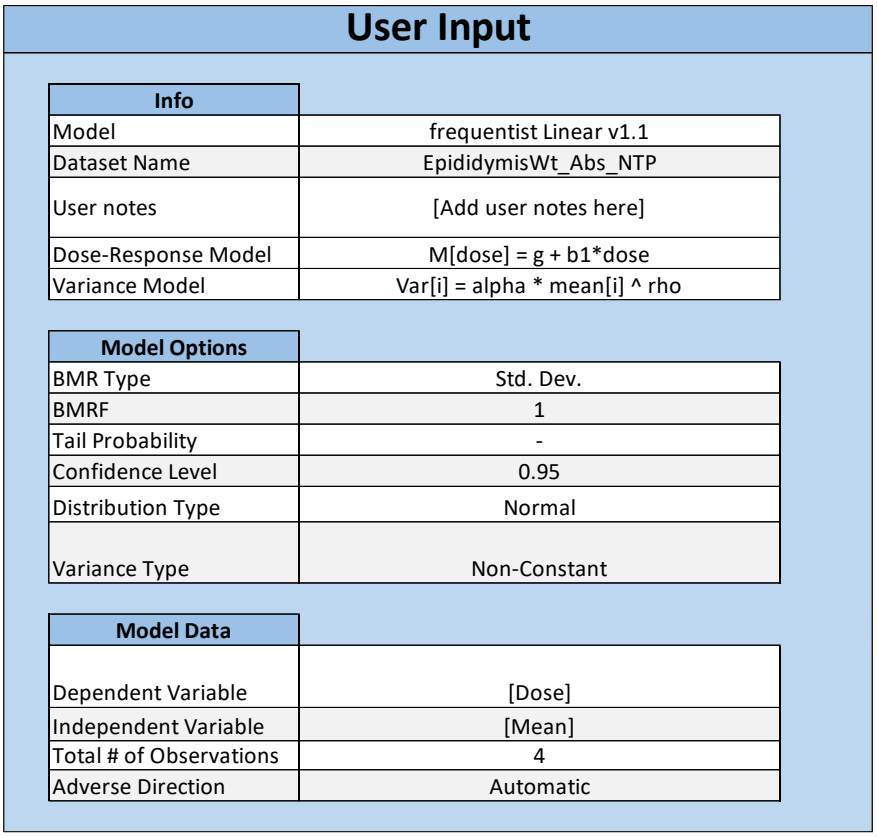

User Input

Info	
Model	frequentist Linear v1.1
Dataset Name	EpididymisWt_Abs_NTP
User notes	[Add user notes here]
Dose-Response Model	M[dose] = g + b1*dose
Variance Model	Var[i] = alpha * mean[i] ^ rho

Model Options	
BMR Type	Std. Dev.
BMRF	1
Tail Probability	-
Confidence Level	0.95
Distribution Type	Normal
Variance Type	Non-Constant

Model Data	
Dependent Variable	[Dose]
Independent Variable	[Mean]
Total # of Observations	4
Adverse Direction	Automatic

Figure C-28. User input for dose-response modeling of decreased absolute whole epididymis weight in male rats (NTP, 2018).

Model Results

Benchmark Dose	
BMD	0.776560307
BMDL	0.545815255
BMDU	1.227214732
AIC	-121.8975001
Test 4 P-value	0.48085367
D.O.F.	2

Model Parameters	
# of Parameters	4
Variable	Estimate
g	0.532146909
beta1	-0.048115367
rho	-4.500456294
alpha	-9.413118476

Goodness of Fit

Dose	Size	Estimated Median	Calc'd Median	Observed Mean	Estimated SD	Calc'd SD	Observed SD	Scaled Residual
0	10	0.532146909	0.528	0.528	0.03736447	0.05	0.05	-0.350966522
0.625	10	0.502074805	0.508	0.508	0.0425899	0.03	0.03	0.439942633
1.25	10	0.472002701	0.474	0.474	0.0489403	0.04	0.04	0.129055502
2.5	10	0.411858493	0.407	0.407	0.06650773	0.08	0.08	-0.231009273

Likelihoods of Interest

Model	Log Likelihood*	# of Parameters	AIC
A1	62.55839468	5	-115.116789
A2	67.81861539	8	-119.637231
A3	65.68094232	6	-119.361885
fitted	64.94875004	4	-121.8975
R	50.54148697	2	-97.0829739

* Includes additive constant of -36.75754. This constant was not included in the LL derivation prior to BMDS 3.0.

Tests of Interest

Test	-2*Log(Likelihood Ratio)	Test df	p-value
1	34.55425682	6	<0.0001
2	10.52044141	3	0.01462287
3	4.275346136	2	0.11792894
4	1.46438455	2	0.48085367

Figure C-29. Model Results for decreased absolute whole epididymis weight in male rats (NTP, 2018).

C.2.15. DECREASED DAYS IN ESTRUS—FEMALE RATS (Butenhoff et al., 2012; van Otterdijk, 2007)

Table C-55. Dose-response data for decreased days in estrus in female rats (Butenhoff et al., 2012; van Otterdijk, 2007)

Dose (mg/kg-d)	*n*	Mean	SD
0	10	5.5	1.5092
0.625	10	4.3	2.0575
1.25	10	3.2	1.8136
2.5	10	0.9	0.9944

Table C-56. Benchmark dose results for decreased days in estrus in female rats—constant variance, BMR = 5% relative deviation (Butenhoff et al., 2012; van Otterdijk, 2007)

Models	Restriction	5% relative deviation		*p*-Value	AIC	BMDS classification	BMDS notes
		BMD	BMDL				
Constant variance							
Exponential 2 (CV—normal)	Restricted	0.0923	0.0687	0.3592	157.0377	Viable—Alternate	BMD 3× lower than lowest non-zero dose BMDL 3× lower than lowest non-zero dose
Exponential 3 (CV—normal)	Restricted	0.2611	0.0778	0.6119	157.2473	Viable—Alternate	BMDL 3× lower than lowest non-zero dose
Exponential 4 (CV—normal)	Restricted	0.0923	0.0687	0.3592	157.0377	Viable—Alternate	BMD 3× lower than lowest non-zero dose BMDL 3× lower than lowest non-zero dose
Exponential 5 (CV—normal)	Restricted	0.2608	0.0776	0.6119	157.2473	Viable—Alternate	BMDL 3× lower than lowest non-zero dose
Hill (CV—normal)	Restricted	0.1487	0.0739	NA	158.9967	Questionable	BMD 3× lower than lowest non-zero dose BMDL 3× lower than lowest non-zero dose d.f. = 0, saturated model (Goodness of fit test cannot be calculated)
Polynomial (3 degree) (CV—normal)	Restricted	0.1495	0.1283	0.9965	154.9969	Viable—Alternate	BMD 3× lower than lowest non-zero dose BMDL 3× lower than lowest non-zero dose
Polynomial (2 degree) (CV—normal)	**Restricted**	**0.1495**	**0.1283**	**0.9965**	**154.9969**	**Viable—Recommended**	**Lowest AIC BMD 3× lower than lowest non-zero dose BMDL 3× lower than lowest non-zero dose**
Power (CV—normal)	Restricted	0.1495	0.1283	0.9965	154.9969	Viable—Alternate	BMD 3× lower than lowest non-zero dose BMDL 3× lower than lowest non-zero dose
Linear (CV—normal)	Unrestricted	0.1495	0.1283	0.9965	154.9969	Viable—Alternate	BMD 3× lower than lowest non-zero dose BMDL 3× lower than lowest non-zero dose

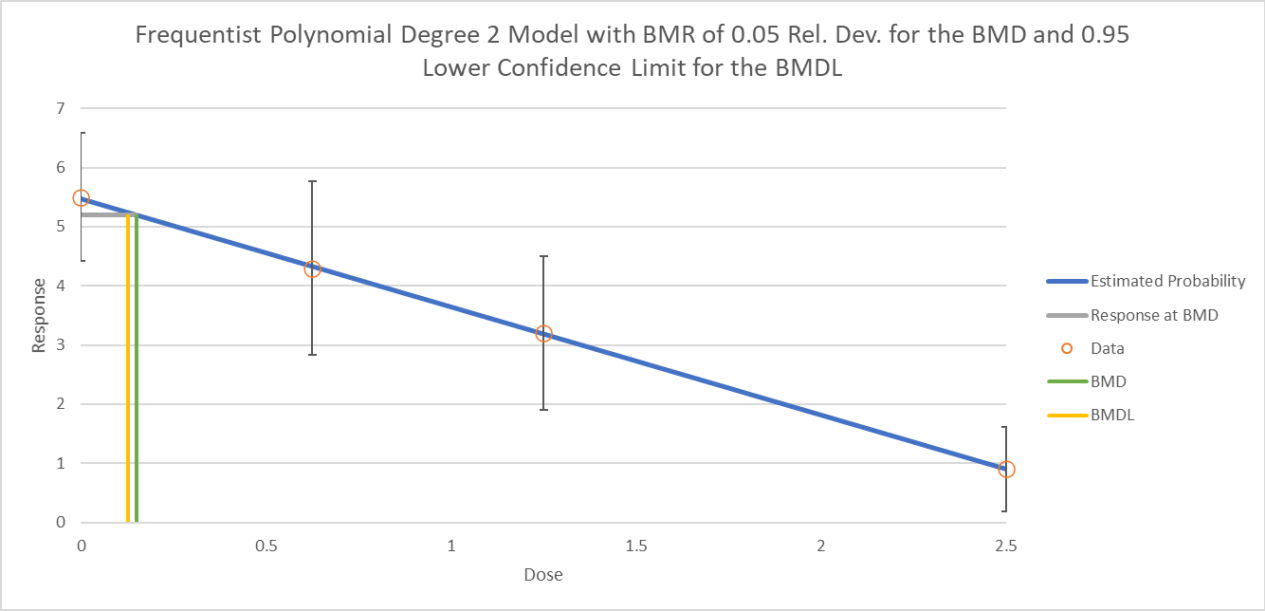

Figure C-30. Dose-response curve for the Polynomial 2 model fit to decreased days in estrus in female rats (Butenhoff et al., 2012; van Otterdijk, 2007).

User Input

Info	
Model	frequentist Polynomial degree 2 v1.1
Dataset Name	Estrus_Days_NTP
User notes	[Add user notes here]
Dose-Response Model	M[dose] = g + b1*dose + b2*dose^2 + ...
Variance Model	Var[i] = alpha

Model Options	
BMR Type	Rel. Dev.
BMRF	0.05
Tail Probability	-
Confidence Level	0.95
Distribution Type	Normal
Variance Type	Constant

Model Data	
Dependent Variable	[Dose]
Independent Variable	[Mean]
Total # of Observations	4
Adverse Direction	Automatic

Figure C-31. User input for dose-response modeling of decreased days in estrus in female rats (NTP, 2018).

Model Results

Benchmark Dose	
BMD	0.149469972
BMDL	0.128321644
BMDU	0.470941256
AIC	154.9969111
Test 4 P-value	0.996475595
D.O.F.	2

Model Parameters	
# of Parameters	4
Variable	Estimate
g	5.479999986
beta1	-1.833142847
beta2	Bounded
alpha	2.427946195

Goodness of Fit

Dose	Size	Estimated Median	Calc'd Median	Observed Mean	Estimated SD	Calc'd SD	Observed SD	Scaled Residual
0	10	5.479999986	5.5	5.5	1.55818683	1.5092	1.5092	0.040589227
0.625	10	4.334285706	4.3	4.3	1.55818683	2.0575	2.0575	-0.069581465
1.25	10	3.188571426	3.2	3.2	1.55818683	1.8136	1.8136	0.023193832
2.5	10	0.897142867	0.9	0.9	1.55818683	0.9944	0.9944	0.005798436

Likelihoods of Interest

Model	Log Likelihood*	# of Parameters	AIC
A1	-74.49492494	5	158.98985
A2	-71.87802546	8	159.756051
A3	-74.49492494	5	158.98985
fitted	-74.49845557	3	154.996911
R	-90.10938562	2	184.218771

* Includes additive constant of -36.75754. This constant was not included in the LL derivation prior to BMDS 3.0.

Tests of Interest

Test	-2*Log(Likelihood Ratio)	Test df	p-value
1	36.46272031	6	<0.0001
2	5.233798961	3	0.15545622
3	5.233798961	3	0.15545622
4	0.007061261	2	0.9964756

Figure C-32. Model results for decreased days in estrus in female rats (NTP, 2018).

Table C-57. Benchmark dose results for decreased days in estrus in female rats—constant variance, BMR = 1 standard deviation (Butenhoff et al., 2012; van Otterdijk, 2007)

Models	Restriction	1 standard deviation		*p*-Value	AIC	BMDS classification	BMDS notes
		BMD	BMDL				
Constant variance							
Exponential 2 (CV—normal)	Restricted	0.5895	0.3889	0.3592	157.0377	Viable—Alternate	

Models	Restriction	1 standard deviation		*p*-Value	AIC	BMDS classification	BMDS notes
		BMD	BMDL				
Constant variance							
Exponential 3 (CV—normal)	Restricted	0.8806	0.4576	0.6119	157.2473	Viable—Alternate	
Exponential 4 (CV—normal)	Restricted	0.5895	0.3889	0.3592	157.0377	Viable—Alternate	
Exponential 5 (CV—normal)	Restricted	0.8804	0.4576	0.6119	157.2473	Viable—Alternate	
Hill (CV—normal)	Restricted	0.8393	0.4491	NA	158.9967	Questionable	d.f. = 0, saturated model (Goodness of fit test cannot be calculated)
Polynomial (3 degree) (CV—normal)	Restricted	0.8500	0.6520	0.9965	154.9969	Viable—Alternate	
Polynomial (2 degree) (CV—normal)	**Restricted**	**0.8500**	**0.6520**	**0.9965**	**154.9969**	**Viable—Recommended**	**Lowest AIC**
Power (CV—normal)	Restricted	0.8500	0.6520	0.9965	154.9969	Viable—Alternate	
Linear (CV—normal)	Unrestricted	0.8500	0.6520	0.9965	154.9969	Viable—Alternate	

C.2.16. INCREASED DAYS IN DIESTRUS—FEMALE RATS (Butenhoff et al., 2012; van Otterdijk, 2007)

Table C-58. Dose-response data for increased days in diestrus in female rats (Butenhoff et al., 2012; van Otterdijk, 2007)

Dose (mg/kg-d)	*n*	Mean	SD
0	10	9.2	1.874
0.625	10	10.1	2.1833
1.25	10	11.7	2.2632
2.5	10	15	1.0541

Table C-59. Benchmark dose results for increased days in diestrus in female rats—constant variance, BMR = 5% relative deviation (Butenhoff et al., 2012; van Otterdijk, 2007)

Models	Restriction	5% relative deviation		*p*-Value	AIC	BMDS classification	BMDS notes
		BMD	BMDL				
Constant variance							
Exponential 2 (CV—normal)	**Restricted**	**0.2430**	**0.2000**	**0.9231**	**167.0076**	**Viable—Recommended**	**Lowest AIC BMDL 3× lower than lowest non-zero dose**
Exponential 3 (CV—normal)	Restricted	0.2891	0.2006	0.7433	168.9548	Viable—Alternate	BMDL 3× lower than lowest non-zero dose
Exponential 4 (CV—normal)	Restricted	0.1870	0.1136	0.4064	169.5368	Viable—Alternate	BMD 3× lower than lowest non-zero dose BMDL 3× lower than lowest non-zero dose
Exponential 5 (CV—normal)	Restricted	0.4063	0.1241	NA	170.8476	Questionable	BMDL 3× lower than lowest non-zero dose d.f. = 0, saturated model (Goodness of fit test cannot be calculated)
Hill (CV—normal)	Restricted	0.4079	0.1226	NA	170.8476	Questionable	BMDL 3× lower than lowest non-zero dose d.f. = 0, saturated model (Goodness of fit test cannot be calculated)
Polynomial (3 degree) (CV—normal)	Restricted	0.2770	0.1470	0.7388	168.9588	Viable—Alternate	BMDL 3× lower than lowest non-zero dose
Polynomial (2 degree) (CV—normal)	Restricted	0.2770	0.1470	0.7388	168.9588	Viable—Alternate	BMDL 3× lower than lowest non-zero dose
Power (CV—normal)	Restricted	0.3283	0.1475	0.8200	168.8993	Viable—Alternate	BMDL 3× lower than lowest non-zero dose
Linear (CV—normal)	Unrestricted	0.1872	0.1427	0.7099	167.5330	Viable—Alternate	BMD 3× lower than lowest non-zero dose BMDL 3× lower than lowest non-zero dose

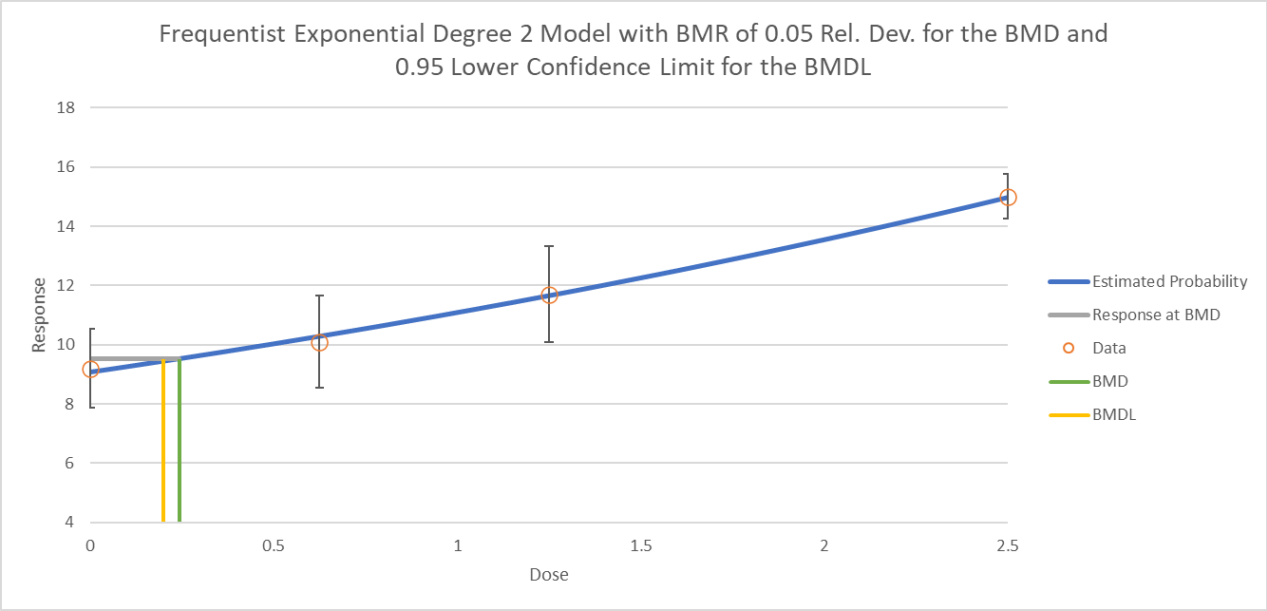

Figure C-33. Dose-response curve for the Exponential 2 model fit to increased days in diestrus in female rats (Butenhoff et al., 2012; van Otterdijk, 2007).

User Input

Info	
Model	frequentist Exponential degree 2 v1.1
Dataset Name	Diestrus_Days_NTP
User notes	[Add user notes here]
Dose-Response Model	M[dose] = a * exp(±1 * b * dose)
Variance Model	Var[i] = alpha

Model Options	
BMR Type	Rel. Dev.
BMRF	0.05
Tail Probability	-
Confidence Level	0.95
Distribution Type	Normal
Variance Type	Constant

Model Data	
Dependent Variable	[Dose]
Independent Variable	[Mean]
Total # of Observations	4
Adverse Direction	Automatic

Figure C-34. User input for dose-response modeling of increased days in diestrus in female rats (NTP, 2018).

Model Results

Benchmark Dose	
BMD	0.242986679
BMDL	0.200009167
BMDU	0.309079273
AIC	167.0076126
Test 4 P-value	0.923101914
D.O.F.	2

Model Parameters	
# of Parameters	3
Variable	Estimate
a	9.070650097
b	0.200793313
log-alpha	1.187317248

Goodness of Fit

Dose	Size	Estimated Median	Calc'd Median	Observed Mean	Estimated SD	Calc'd SD	Observed SD	Scaled Residual
0	10	9.070650097	9.2	9.2	1.81060062	1.874	1.874	0.225914154
0.625	10	10.28349063	10.1	10.1	1.81060062	2.1833	2.1833	-0.320472836
1.25	10	11.65850059	11.7	11.7	1.81060062	2.2632	2.2632	0.072480181
2.5	10	14.98466312	15	15	1.81060062	1.0541	1.0541	0.026786401

Likelihoods of Interest

Model	Log Likelihood*	# of Parameters	AIC
A1	-80.42379068	5	170.847581
A2	-77.43412842	8	170.868257
A3	-80.42379068	5	170.847581
fitted	-80.50380632	3	167.007613
R	-98.71832217	2	201.436644

* Includes additive constant of -36.75754. This constant was not included in the LL derivation prior to BMDS 3.0.

Tests of Interest

Test	-2*Log(Likelihood Ratio)	Test df	p-value
1	42.56838749	6	<0.0001
2	5.97932452	3	0.11262048
3	5.97932452	3	0.11262048
4	0.160031269	2	0.92310191

Figure C-35. Model results for increased days in diestrus in female rats (NTP, 2018).

Table C-60. Benchmark dose results for increased days in diestrus in female rats—constant variance, BMR = 1 standard deviation (Butenhoff et al., 2012; van Otterdijk, 2007)

Models	Restriction	1 standard deviation		*p*-Value	AIC	BMDS classification	BMDS notes
		BMD	BMDL				
Constant variance							
Exponential 2 (CV—normal)	**Restricted**	**0.9064**	**0.7377**	**0.9231**	**167.0076**	**Viable—Recommended**	**Lowest AIC**
Exponential 3 (CV—normal)	Restricted	0.9766	0.7391	0.7433	168.9548	Viable—Alternate	
Exponential 4 (CV—normal)	Restricted	0.7661	0.5970	0.4064	169.5368	Viable—Alternate	
Exponential 5 (CV—normal)	Restricted	0.9947	0.5599	NA	170.8476	Questionable	d.f. = 0, saturated model (Goodness of fit test cannot be calculated)
Hill (CV—normal)	Restricted	0.9936	0.5580	NA	170.8476	Questionable	d.f. = 0, saturated model (Goodness of fit test cannot be calculated)
Polynomial (3 degree) (CV—normal)	Restricted	0.9687	0.6117	0.7388	168.9588	Viable—Alternate	
Polynomial (2 degree) (CV—normal)	Restricted	0.9687	0.6117	0.7388	168.9588	Viable—Alternate	
Power (CV—normal)	Restricted	0.9805	0.6134	0.8200	168.8993	Viable—Alternate	
Linear (CV—normal)	Unrestricted	0.7667	0.5963	0.7099	167.5330	Viable—Alternate	

C.2.17. DECREASED RELATIVE UTERINE WEIGHT—FEMALE RATS (Butenhoff et al., 2012; van Otterdijk, 2007)

Table C-61. Dose-response data for decreased relative uterine weight in female rats (Butenhoff et al., 2012; van Otterdijk, 2007))

Dose (mg/kg-d)	*n*	Mean	SD
0	10	3.26	1.3
0.156	10	2.73	0.41
0.312	10	2.94	0.79
0.625	10	3.65	1.68
1.25	10	2.05	0.61
2.5	10	1.81	0.32

Table C-62. Benchmark dose results for decreased relative uterine weight in female rats—BMR = constant variance, 1 standard deviation (Butenhoff et al., 2012; van Otterdijk, 2007)

Models	Restriction	1 standard deviation		*p*-Value	AIC	BMDS Classification	BMDS notes
		BMD	BMDL				
Constant variance							
Exponential 2 (CV—normal)	Restricted	1.6357	0.9728	0.0296	178.4420	Questionable	Constant variance test failed (Test 2 *p*-value < 0.05) Goodness of fit *p*-value < 0.1
Exponential 3 (CV—normal)	Restricted	1.8431	1.0220	0.0170	179.8915	Questionable	Constant variance test failed (Test 2 *p*-value < 0.05) Goodness of fit *p*-value < 0.1
Exponential 4 (CV—normal)	Restricted	1.6357	0.9728	0.0296	178.4420	Questionable	Constant variance test failed (Test 2 *p*-value < 0.05) Goodness of fit *p*-value < 0.1
Exponential 5 (CV—normal)	Restricted	1.2312	0.7036	0.1496	175.0232	Questionable	Constant variance test failed (Test 2 *p*-value < 0.05)
Hill (CV—normal)	Restricted	1.2139	0.7285	0.1496	175.0233	Questionable	Constant variance test failed (Test 2 *p*-value < 0.05)
Polynomial (5 degree) (CV—normal)	Restricted	1.8244	1.2032	0.0147	180.2109	Questionable	Constant variance test failed (Test 2 *p*-value < 0.05) Goodness of fit *p*-value < 0.1
Polynomial (4 degree) (CV—normal)	Restricted	1.8244	1.2032	0.0147	180.2109	Questionable	Constant variance test failed (Test 2 *p*-value < 0.05) Goodness of fit *p*-value < 0.1
Polynomial (3 degree) (CV—normal)	Restricted	1.8244	1.2032	0.0147	180.2109	Questionable	Constant variance test failed (Test 2 *p*-value < 0.05) Goodness of fit *p*-value < 0.1
Polynomial (2 degree) (CV—normal)	Restricted	1.8244	1.2032	0.0147	180.2109	Questionable	Constant variance test failed (Test 2 *p*-value < 0.05) Goodness of fit *p*-value < 0.1
Power (CV—normal)	Restricted	1.8813	1.2094	0.0153	180.1247	Questionable	Constant variance test failed (Test 2 *p*-value < 0.05) Goodness of fit *p*-value < 0.1
Linear (CV—normal)	Unrestricted	1.7547	1.2018	0.0324	178.2308	Questionable	Constant variance test failed (Test 2 *p*-value < 0.05) Goodness of fit *p*-value < 0.1

Table C-63. Benchmark dose results for decreased relative uterine weight in female rats — nonconstant variance, BMR = 1 standard deviation (Butenhoff et al., 2012; van Otterdijk, 2007)

Models	Restriction	1 standard deviation		*p*-Value	AIC	BMDS classification	BMDS notes
		BMD	BMDL				
Non-constant variance							
Exponential 2 (NCV— normal)	Restricted	2.3599	1.4658	<0.0001	168.8763	Questionable	Goodness of fit *p*-value < 0.1
Exponential 3 (NCV— normal)	Restricted	2.4946	1.8929	<0.0001	167.1138	Questionable	Goodness of fit *p*-value < 0.1
Exponential 4 (NCV— normal)	Restricted	2.3592	1.4658	<0.0001	168.8763	Questionable	Goodness of fit *p*-value < 0.1
Exponential 5 (NCV— normal)	Restricted	1.2787	1.1724	0.0011	157.4375	Questionable	Goodness of fit *p*-value < 0.1
Hill (NCV— normal)	Restricted	1.3094	1.1258	0.0011	157.4376	Questionable	Goodness of fit *p*-value < 0.1
Polynomial (5 degree) (NCV— normal)	Restricted	2.5118	1.9996	<0.0001	165.4887	Questionable	Goodness of fit *p*-value < 0.1 BMD higher than maximum dose
Polynomial (4 degree) (NCV— normal)	Restricted	2.5118	1.9997	<0.0001	165.4887	Questionable	Goodness of fit *p*-value < 0.1 BMD higher than maximum dose
Polynomial (3 degree) (NCV— normal)	Restricted	2.5118	1.9997	<0.0001	165.4887	Questionable	Goodness of fit *p*-value < 0.1 BMD higher than maximum dose
Polynomial (2 degree) (NCV— normal)	Restricted	2.5118	1.9997	<0.0001	165.4887	Questionable	Goodness of fit *p*-value < 0.1 BMD higher than maximum dose
Power (NCV— normal)	Restricted	2.5092	1.9643	<0.0001	167.4725	Questionable	Goodness of fit *p*-value < 0.1 BMD higher than maximum dose
Linear (NCV— normal)	Unrestricted	2.4008	1.7105	<0.0001	167.5269	Questionable	Goodness of fit *p*-value < 0.1

Table C-64. Benchmark dose results for decreased relative uterine weight in female rats—log-normal, constant variance, BMR = 1 standard deviation (Butenhoff et al., 2012; van Otterdijk, 2007)

Models	Restriction	1 standard deviation		*p*-Value	AIC	BMDS classification	BMDS notes
		BMD	BMDL				
Constant variance							
Exponential 2 (CV—log-normal)	Restricted	1.9961	0.9991	0.0518	147.6232	Questionable	Constant variance test failed (Test 2 *p*-value < 0.05) Goodness of fit *p*-value < 0.1

Models	Restriction	1 standard deviation		*p*-Value	AIC	BMDS classification	BMDS notes
		BMD	BMDL				
Constant variance							
Exponential 3 (CV— log-normal)	Restricted	2.0457	1.0012	0.0249	149.5811	Questionable	Constant variance test failed (Test 2 *p*-value < 0.05) Goodness of fit *p*-value < 0.1
Exponential 4 (CV— log-normal)	Restricted	1.9491	0.6763	0.0246	149.6001	Questionable	Constant variance test failed (Test 2 *p*-value < 0.05) Goodness of fit *p*-value < 0.1
Exponential 5 (CV— log-normal)	Restricted	1.2532	0.6896	0.2457	145.0275	Questionable	Constant variance test failed (Test 2 *p*-value < 0.05)
Hill (CV— log-normal)	Restricted	-	-	-	-	Unusable	BMD computation failed Model was not run. Adverse direction "down" not compatible with lognormal distribution
Polynomial (5 degree) (CV— log-normal)	Restricted	-	-	-	-	Unusable	BMD computation failed Model was not run. Adverse direction "down" not compatible with lognormal distribution
Polynomial (4 degree) (CV— log-normal)	Restricted	-	-	-	-	Unusable	BMD computation failed Model was not run. Adverse direction "down" not compatible with lognormal distribution
Polynomial (3 degree) (CV— log-normal)	Restricted	-	-	-	-	Unusable	BMD computation failed Model was not run. Adverse direction "down" not compatible with lognormal distribution
Polynomial (2 degree) (CV— log-normal)	Restricted	-	-	-	-	Unusable	BMD computation failed Model was not run. Adverse direction "down" not compatible with lognormal distribution
Power (CV— log-normal)	Restricted	-	-	-	-	Unusable	BMD computation failed Model was not run. Adverse direction "down" not compatible with lognormal distribution
Linear (CV— log-normal)	Unrestricted	-	-	-	-	Unusable	BMD computation failed Model was not run. Adverse direction "down" not compatible with lognormal distribution

C.2.18. DECREASED ABSOLUTE UTERINE WEIGHT—FEMALE RAT (Butenhoff et al., 2012; van Otterdijk, 2007)

Table C-65. Dose-response data for decreased absolute uterine weight in female rats (NTP, 2018)

Dose (mg/kg-d)	*n*	Mean	SD
0	10	0.731	0.27
0.156	10	0.646	0.09
0.312	10	0.691	0.18
0.625	10	0.818	0.35
1.25	10	0.409	0.13
2.5	10	0.26	0.03

Table C-66. Benchmark dose results for decreased absolute uterine weight in female rats—BMR = constant variance, 1 standard deviation (Butenhoff et al., 2012; van Otterdijk, 2007)

Models	Restriction	1 standard deviation		*p*-Value	AIC	BMDS classification	BMDS notes
		BMD	BMDL				
Constant variance							
Exponential 2 (CV—normal)	Restricted	0.8877	0.5920	0.0083	−6.1338	Questionable	Constant variance test failed (Test 2 *p*-value < 0.05) Goodness of fit *p*-value < 0.1 |Residual for Dose Group Near BMD| > 2
Exponential 3 (CV—normal)	Restricted	1.2592	0.7971	0.0140	−7.2318	Questionable	Constant variance test failed (Test 2 *p*-value < 0.05) Goodness of fit *p*-value < 0.1
Exponential 4 (CV—normal)	Restricted	0.8877	0.5920	0.0083	−6.1338	Questionable	Constant variance test failed (Test 2 *p*-value < 0.05) Goodness of fit *p*-value < 0.1 |Residual for Dose Group Near BMD| > 2
Exponential 5 (CV—normal)	Restricted	1.2039	0.9713	0.2538	−13.7789	Questionable	Constant variance test failed (Test 2 *p*-value < 0.05)
Hill (CV—normal)	Restricted	1.1828	0.8675	0.1306	−11.7788	Questionable	Constant variance test failed (Test 2 *p*-value < 0.05)
Polynomial (5 degree) (CV—normal)	Restricted	1.2569	0.8354	0.0076	−5.9234	Questionable	Constant variance test failed (Test 2 *p*-value < 0.05) Goodness of fit *p*-value < 0.1
Polynomial (4 degree) (CV—normal)	Restricted	1.2569	0.8354	0.0076	−5.9234	Questionable	Constant variance test failed (Test 2 *p*-value < 0.05) Goodness of fit *p*-value < 0.1

Models	Restriction	1 standard deviation		*p*-Value	AIC	BMDS classification	BMDS notes
		BMD	BMDL				
Constant variance							
Polynomial (3 degree) (CV—normal)	Restricted	1.2569	0.8354	0.0076	−5.9234	Questionable	Constant variance test failed (Test 2 *p*-value < 0.05) Goodness of fit *p*-value < 0.1
Polynomial (2 degree) (CV—normal)	Restricted	1.2569	0.8354	0.0076	−5.9234	Questionable	Constant variance test failed (Test 2 *p*-value < 0.05) Goodness of fit *p*-value < 0.1
Power (CV—normal)	Restricted	1.3086	0.8477	0.0088	−6.2298	Questionable	Constant variance test failed (Test 2 *p*-value < 0.05) Goodness of fit *p*-value < 0.1
Linear (CV—normal)	Unrestricted	1.0823	0.8275	0.0163	−7.7099	Questionable	Constant variance test failed (Test 2 *p*-value < 0.05) Goodness of fit *p*-value < 0.1

Table C-67. Benchmark dose results for decreased absolute uterine weight in female rats—nonconstant variance, BMR = 1 standard deviation (Butenhoff et al., 2012; van Otterdijk, 2007)

Models	Restriction	1 standard deviation		*p*-Value	AIC	BMDS classification	BMDS notes
		BMD	BMDL				
Non-constant variance							
Exponential 2 (NCV—normal)	Restricted	1.3500	0.9186	<0.0001	−25.2943	Questionable	Nonconstant variance test failed (Test 3 *p*-value < 0.05) Goodness of fit *p*-value < 0.1
Exponential 3 (NCV—normal)	Restricted	1.8175	1.3964	<0.0001	−33.2616	Questionable	Nonconstant variance test failed (Test 3 *p*-value < 0.05) Goodness of fit *p*-value < 0.1 |Residual for Dose Group Near BMD| > 2
Exponential 4 (NCV—normal)	Restricted	1.3502	0.9186	<0.0001	−25.2943	Questionable	Nonconstant variance test failed (Test 3 *p*-value < 0.05) Goodness of fit *p*-value < 0.1
Exponential 5 (NCV—normal)	Restricted	1.2424	1.1367	0.0036	−42.1526	Questionable	Nonconstant variance test failed (Test 3 *p*-value < 0.05) Goodness of fit *p*-value < 0.1
Hill (NCV—normal)	Restricted	1.2387	1.1069	0.0103	−44.1525	Questionable	Nonconstant variance test failed (Test 3 *p*-value < 0.05) Goodness of fit *p*-value < 0.1
Polynomial (5 degree) (NCV—normal)	Restricted	2.0088	1.5693	0.0001	−33.9754	Questionable	Nonconstant variance test failed (Test 3 *p*-value < 0.05) Goodness of fit *p*-value < 0.1

Models	Restriction	1 standard deviation		*p*-Value	AIC	BMDS classification	BMDS notes
		BMD	BMDL				
Non-constant variance							
Polynomial (4 degree) (NCV—normal)	Restricted	2.0088	1.5692	0.0001	−33.9754	Questionable	Nonconstant variance test failed (Test 3 *p*-value < 0.05) Goodness of fit *p*-value < 0.1
Polynomial (3 degree) (NCV—normal)	Restricted	2.0088	1.5692	0.0001	−33.9754	Questionable	Nonconstant variance test failed (Test 3 *p*-value < 0.05) Goodness of fit *p*-value < 0.1
Polynomial (2 degree) (NCV—normal)	Restricted	2.0088	1.5692	0.0001	−33.9754	Questionable	Nonconstant variance test failed (Test 3 *p*-value < 0.05) Goodness of fit *p*-value < 0.1
Power (NCV—normal)	Restricted	1.9555	1.5188	<0.0001	−32.0845	Questionable	Nonconstant variance test failed (Test 3 *p*-value < 0.05) Goodness of fit *p*-value < 0.1
Linear (NCV—normal)	Unrestricted	1.6526	1.2761	<0.0001	−30.8879	Questionable	Nonconstant variance test failed (Test 3 *p*-value < 0.05) Goodness of fit *p*-value < 0.1 |Residual for Dose Group Near BMD| > 2

Table C-68. Benchmark dose results for decreased absolute uterine weight in female rats—log-normal, constant variance, BMR = 1 standard deviation (Butenhoff et al., 2012; van Otterdijk, 2007)

Models	Restriction	1 standard deviation		*p*-Value	AIC	BMDS classification	BMDS notes
		BMD	BMDL				
Constant variance							
Exponential 2 (CV—log-normal)	Restricted	1.0282	0.5795	0.0129	−43.7584	Questionable	Constant variance test failed (Test 2 *p*-value < 0.05) Goodness of fit *p*-value < 0.1 Modeled control response std. dev. >|1.5| actual response std. dev.
Exponential 3 (CV— log-normal)	Restricted	1.2617	0.6141	0.0101	−43.1248	Questionable	Constant variance test failed (Test 2 *p*-value < 0.05) Goodness of fit *p*-value < 0.1 Modeled control response std. dev. >|1.5| actual response std. dev.
Exponential 4 (CV— log-normal)	Restricted	1.0282	1.0189	0.0129	−43.7584	Questionable	Constant variance test failed (Test 2 *p*-value < 0.05) Goodness of fit *p*-value < 0.1 Modeled control response

Models	Restriction	1 standard deviation		*p*-Value	AIC	BMDS classification	BMDS notes
		BMD	BMDL				
Constant variance							
							std. dev. >|1.5| actual response std. dev.
Exponential 5 (CV— log-normal)	Restricted	1.2149	0.9197	0.3929	−50.5863	Questionable	Constant variance test failed (Test 2 *p*-value < 0.05) Modeled control response std. dev. >|1.5| actual response std. dev.
Hill (CV— log-normal)	Restricted	-	-	-	-	Unusable	BMD computation failed Model was not run. Adverse direction "down" not compatible with lognormal distribution
Polynomial (5 degree) (CV— log-normal)	Restricted	-	-	-	-	Unusable	BMD computation failed Model was not run. Adverse direction "down" not compatible with lognormal distribution
Polynomial (4 degree) (CV— log-normal)	Restricted	-	-	-	-	Unusable	BMD computation failed Model was not run. Adverse direction "down" not compatible with lognormal distribution
Polynomial (3 degree) (CV— log-normal)	Restricted	-	-	-	-	Unusable	BMD computation failed Model was not run. Adverse direction "down" not compatible with lognormal distribution
Polynomial (2 degree) (CV— log-normal)	Restricted	-	-	-	-	Unusable	BMD computation failed Model was not run. Adverse direction "down" not compatible with lognormal distribution
Power (CV— log-normal)	Restricted	-	-	-	-	Unusable	BMD computation failed Model was not run. Adverse direction "down" not compatible with lognormal distribution
Linear (CV— log-normal)	Unrestricted	-	-	-	-	Unusable	BMD computation failed Model was not run. Adverse direction "down" not compatible with lognormal distribution

1

APPENDIX D. ADVERSE OUTCOME PATHWAY/ MODE OF ACTION(AOP/MOA)-BASED APPROACH FOR EVALUATING PFDA-INDUCED MECHANISM OF HEPATOXITY

D.1. OBJECTIVE AND METHODOLOGY

The goal of the qualitative analysis described here is to evaluate the available mechanistic evidence for PFDA-induced liver effects to assess the biological plausibility of effects observed in animal models and identify mechanistic pathways that are conserved across species and strains of animals and liver cell culture models and are therefore more relevant to human health. The available mechanistic and toxicological evidence was organized and evaluated in concordance with the frameworks used for mode of action (MOA) analysis for non-cancer effects and development of adverse outcome pathways (AOP)[1] (Edwards et al., 2016; Boobis et al., 2008; IPCS, 2007). PFDA-induced hepatic effects reported in in vivo and cell culture studies were organized according to the following levels of biological organization: molecular interactions, cellular effects, organ effects, and organism effects. The analysis described here was focused on the concordance of key events and adverse responses across species to obtain clarification on the relevance of animal studies to human health.

In addition to analyzing the available evidence published in the peer-reviewed literature, EPA also considered mechanistic evidence from in vitro high throughput screening (HTS) assays on PFDA available from the EPA's CompTox Chemicals Dashboard (https://comptox.epa.gov/dashboard) (U.S. EPA, 2019). Bioactivity data from the ToxCast and Tox21 collaborative projects were also considered at the same levels of biological organization described below. A more detailed description of the HTS analysis and results is provided in Appendix E.

[1]Although the World Health Organization (WHO)-International Programme on Chemical Safety (IPCS)-MOA and the Organization for Economic Co-operation and Development (OECD)-AOP frameworks are similar in the identification and analysis of key events following modified Bradford-Hill criteria (Meek et al., 2014), AOPs are chemically agnostic, whereas MOA analyses are intended to inform health assessments of individual (or groups of) chemical(s) (Edwards et al., 2016).

D.2. PROPOSED MOA/AOP APPROACH FOR EVALUATING PFAS-INDUCED LIVER TOXICITY

The proposed MOA displayed in Figure D-1 is based on molecular initiating events, key events, and adverse outcomes identified in previous mechanistic evaluations and reviews on PFOS and PFOA (ATSDR, 2018; Li et al., 2017; U.S. EPA, 2016a, b), which are structurally related to PFDA and among the most well-studied PFAS. Additional reviews on biological pathways associated with chemical-induced cancer and noncancer liver effects were also consulted (see citations below). A summary of the MOA is presented below.

At the molecular level, experimental studies using in vivo and cell culture models have shown that perfluorinated compounds such as PFOS and PFOA can activate several nuclear receptor pathways including the constitutive androstane receptor (CAR), the pregnane X receptor (PXR), the farnesoid X receptor (FXR), the peroxisome proliferator activated receptor alpha (PPARα) and gamma (PPARγ), estrogen receptor alpha (ERα) and other receptor-independent cell signaling pathways (e.g., phosphatidylinositol 3-kinase-serine/threonine protein kinase (PI3K-Akt) signal transduction pathway, and the nuclear factor kappa B pathway [NFκB]) (ATSDR, 2018; Li et al., 2017; U.S. EPA, 2016a, b). PFOS- and PFOA-induced activation of PPARα is associated with hepatocellular hypertrophy caused by peroxisome proliferation, and increased peroxisomal fatty acid β oxidation and cytochrome P450 4A (CYP4A) expression and activity (ATSDR, 2018; U.S. EPA, 2016a, b), and altered cholesterol metabolism (Li et al., 2017). Increased PPARα activity can lead to oxidative stress via induction of acyl CoA oxidase expression and activity and to H_2O_2 production in peroxisomes (Hall et al., 2012). Several studies have used genetically modified animal and cell culture models and immortalized human cell lines to evaluate potential PFOS or PFOA activation of the human PPARα. COS-1 cells transfected with the murine or human PPARα were responsive to PFAS exposure (U.S. EPA, 2016a, b), and F1 generation PPARα-humanized mice were responsive to PFOA-induced expression responsive genes on GD 18, but unlike wild type animals this response was not apparent on PND 20 (U.S. EPA, 2016b; Takacs and Abbott, 2007). Studies using human liver cell lines or humanized animal models suggest that humans are less sensitive to PPARα activation by the perfluorinated compounds PFOS and PFOA (reviewed in Li et al. (2017) and U.S. EPA (2016a)). PPARα has also been shown to be activated by exposure to several PFAS, including PFOS, PFOA, PFNA, and PFHxS (ATSDR, 2018; Li et al., 2017). Although PPARα is not expressed in high levels in the liver, its activation by pharmaceuticals and xenobiotic compounds has been proposed to be associated with hepatic steatosis caused by lipid accumulation (Angrish et al., 2016; Mellor et al., 2016).

As described above, exposure to perfluorinated compounds such as PFOS and PFOA has also been shown to activate other nuclear receptor and cell signaling pathways including the CAR, PXR, FXR, ERα, NFκB, and the oxidative stress responsive nuclear factor erythroid 2 related factor 2 (Nrf2) (ATSDR, 2018; Li et al., 2017; U.S. EPA, 2016a). Furthermore, experiments using null animal models exposed to several PFAS suggest that activation of CAR/PXR occurs independently of PPARα

(ATSDR, 2018; Li et al., 2017). Previous analyses of chemical-induced hepatotoxicity suggest that activation of these cell signaling pathways in experimental models is associated with increased expression and activity of xenobiotic metabolizing enzymes (XMEs) (Joshi-Barve et al., 2015; Hall et al., 2012), formation of reactive metabolites, alterations in cellular lipid metabolism (Angrish et al., 2016), and endoplasmic reticulum damage (Joshi-Barve et al., 2015).

At the cellular level, exposure to PFAS such as PFOS and PFOA has been shown to increase reactive oxygen species production and oxidative damage to cellular macromolecules (ATSDR, 2018; Li et al., 2017; U.S. EPA, 2016a); promote mitochondrial damage, inhibit mitochondrial function, activate mitochondrial-mediated cell death (Li et al., 2017; U.S. EPA, 2016b); increase endoplasmic reticulum stress (U.S. EPA, 2016b); induce DNA damage (ATSDR, 2018; U.S. EPA, 2016b); disrupt intercellular gap junction communication (ATSDR, 2018); elevate production/levels of proinflammatory cytokines (U.S. EPA, 2016b); alter lipid and glucose metabolism and bile acid biosynthesis (U.S. EPA, 2016a, b); and increase hepatocellular death (Li et al., 2017; U.S. EPA, 2016a). These pathways/mechanisms are associated with toxicant-induced liver disease and can promote steatohepatitis and fibrosis (Angrish et al., 2016; Cao et al., 2016; Joshi-Barve et al., 2015; Wahlang et al., 2013).

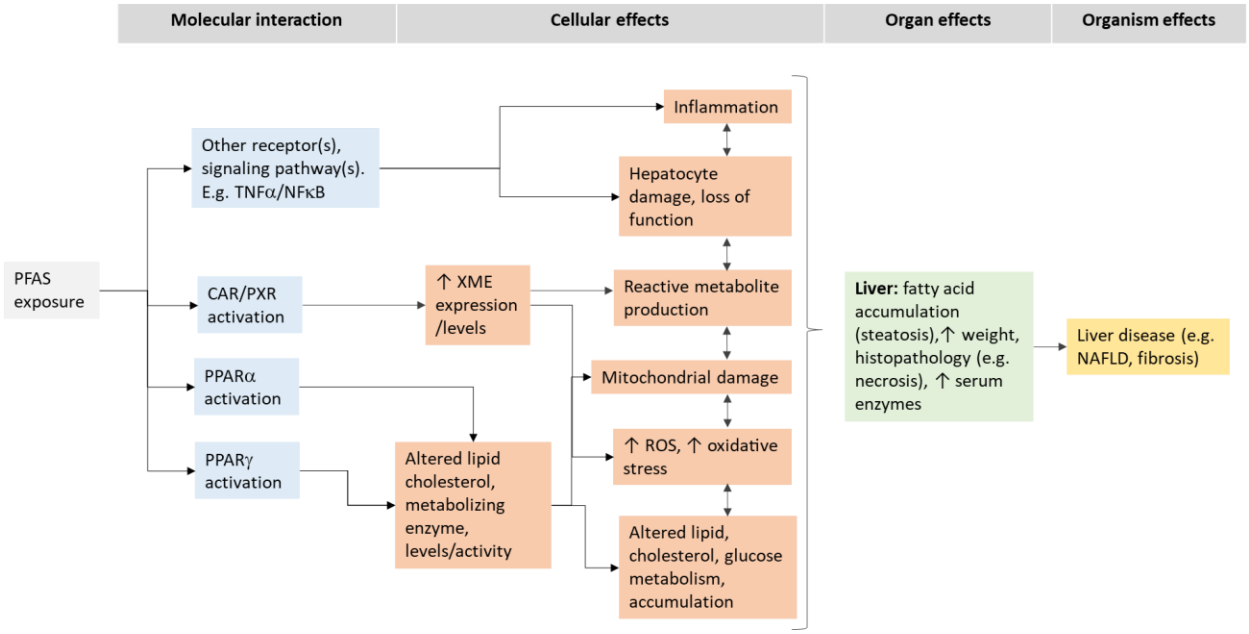

Figure D-1. This proposed MOA is based on previous analyses on PFAS-induced (e.g., PFOA/PFOS) liver toxicity and the role of nuclear receptor pathways in hepatotoxicity.

D.3. SYNTHESIS OF MECHANISTIC STUDIES AND SUPPLEMENTAL INFORMATION FOR PFDA

As mentioned previously, mechanistic evidence from peer-reviewed studies and HTS assays from EPA's ToxCast/Tox21 database were organized and evaluated according to the proposed MOA for the noncancer-liver effects associated with exposure to PFAS (see Figure D-1). The evidence consists primarily of in vitro and in vivo studies conducted in liver tissues derived from human and animal models. When available, cell-free receptor binding studies and gene reporter assays profiling different key events in receptor signaling pathways in other cell tissue models (e.g., receptor dimerization, cofactor recruitment, DNA binding and gene transactivation) were included in the analysis to provide additional information on the activation of nuclear receptor pathways and on potential species-specific differences in receptor sensitivity relevant to the mechanisms of liver toxicity for PFDA and other PFAS.

D.3.1. MOLECULAR INITIATING EVENTS

As discussed below, the available studies have examined several nuclear receptor and cell signaling pathways associated with chemical-induced liver toxicity.

PPARα

PPARα is involved in a variety of processes, including nutrient metabolism, tissue development, cell differentiation, xenobiotic biotransformation and inflammation (Li et al., 2017). Induction of PPARα activity is primarily associated with increased CYP450 activity, peroxisomal proliferation and hepatomegaly (liver enlargement) (Hall et al., 2012) and has been implicated in the mechanisms of hepatotoxicity of PFAS such as PFOA and PFOS (ATSDR, 2018; U.S. EPA, 2016a). Several experimental studies have evaluated PFDA-induced activation of the PPARα in vivo in the rat and mouse liver, and in human and rodent hepatocyte cell cultures. PFDA exposure was associated with increased hepatic expression of PPARα-responsive genes in Sprague Dawley rats (NTP, 2018; Sterchele et al., 1996), C57BL/6J mice (Abe et al., 2017; Cheng and Klaassen, 2008a, b; Maher et al., 2008) and SV129 mice (Luo et al., 2017). PFDA treatment has also been shown to increase hepatic PPARα mRNA levels (Sterchele et al., 1996) and activity of the PPARα-responsive enzyme acyl-CoA oxidase in Sprague Dawley rats (NTP, 2018). Chinje et al. (1994) exposed male Wistar rats and Harley Guinea pigs to PFDA and reported increased CYP4A1 mRNA levels (indicative of PPARα activation) in rats, but no effects in Guinea pigs. These findings are consistent with analyses, which conclude that Guinea pigs, along with Syrian hamsters and non-human primates, are less responsive to PPARα activation than other rodent models (Corton et al., 2018; Hall et al., 2012).

Several cell culture and in vitro studies also report evidence considered supportive of the in vivo findings. PFDA exposure increased mRNA levels of PPARα and PPARα-responsive genes in rat hepatoma FaO cells (Sterchele et al., 1996). Two studies evaluated PFDA-induced effects on

PPARα-responsive genes in human hepatic progenitor cells (HepaRG). One study was unable to measure activation of PPARα or other nuclear receptors due to PFDA exposure associated with cytotoxicity (100 μM) but detected gene reported activity in non-human primate kidney cells transfected with the mouse PPARα (COS-1) (Abe et al., 2017). The other study that tested a lower PFDA concentration (45 μM) confirmed PPARα activation (Lim et al., 2021). Rosen et al. (2013) analyzed gene expression changes in response to PFDA treatment and reported higher transcriptional activity in cultured primary human versus mouse hepatocytes, including the induction of PPARα-dependent and PPARα-independent genes. The lower than expected pattern of transcriptional activity for PFDA and other PFAS in cultured primary mouse hepatocytes compared to previous in vivo studies was attributed to cell culture conditions and the absence of hepatic non-parenchymal cells (Rosen et al., 2013). The authors also noted inconsistencies in the dose-response patterns of transcriptional activity in human hepatocytes across PFAS that could be due to interindividual variation in donor cells or inherent differences in the pattern of gene expression of tested chemicals (Rosen et al., 2013). PPARα-dependent reporter gene expression was also induced after PFDA treatment in human hepatoma HepG2 cells (Rosenmai et al., 2018) and human embryonic kidney HEK293 cells (Buhrke et al., 2013). HTS assays showed induction of PPARα transactivation in HepG2 cells but no activity in a binding reporter assay for the human PPARα (see Table E-2). However, a recent in vitro study in the peer-reviewed literature reported that PFDA can bind to the human PPARα ligand binding domain, albeit with lower affinity than the Baikal seal PPARα (Ishibashi et al., 2019). Potential interspecies differences in PPARα activation were also described by Routti et al. (2019); Wolf et al. (2012); Wolf et al. (2008), showing induction of transcriptional activity of the mouse and polar PPARα isoforms but minimal or no activity towards the human PPARα in non-human primate kidney cells (COS-1 and COS-7) exposed to PFDA.

Overall, the available evidence suggests that PFDA can activate hepatic PPARα in rats and mice in vivo and in cell culture models. There are inconsistencies with respect to the activation of PPARα in in vitro human models possibly due to differences in experimental design and/or potential confounding with PFDA-induced cytotoxicity. However, some evidence indicates that PFDA interacts with the human PPARα in immortalized and primary cells derived from liver tissue. The data also suggest potential species differences in the binding affinity and activity of PPARα with the human isoform being potentially less sensitive compared to other mammalian species. In vivo studies with genetically modified animals in which the gene encoding PPARα is inactivated are needed to further characterize these differences.

Other PPARs (PPARγ and PPARβ/δ)

Two other PPAR subtypes have been characterized, PPARγ and PPARβ/δ, that play an essential role in energy homeostasis and metabolism. PPARγ is known to regulate adipogenesis, lipid and glucose metabolism and inflammatory pathways and its hepatic upregulation has been proposed as a key mechanism in the pathogenesis of non-alcoholic fatty liver disease (NAFLD) (Al Sharif et al., 2014). PFDA-induced transactivation of human PPARγ was observed in HEK263

(Buhrke et al., 2013) and HepG2 cells (Zhang et al., 2014) and HTS results from the EPA's ToxCast/Tox21 database displayed in Table F-2). PFDA also showed affinity for the human PPARγ in receptor-ligand binding assays (Zhang et al. (2014) and Table E-2) but displayed no activity in agonist/antagonist or cofactor recruitment assays related to this receptor conducted in HEK293T cells (see Table E-2). Further, PFDA upregulated the expression of the PPARγ gene in primary human hepatocytes (Rosen et al., 2013).

PPARβ/δ is involved in fatty acid metabolism and suppression of macrophage-derived inflammation (Barish et al., 2006). Studies examining potential interaction between PFAS and PPARβ/δ are limited. In vitro evidence showed that PFDA is capable of binding to the human PPARβ/δ and activating its transcriptional activity in HEK293 cells at non-cytotoxic concentrations (< 100 μM) (Li et al., 2019). In contrast, PFDA was inactive in ToxCast/Tox21 assays (see Table F-2), evaluating human PPARβ/δ transactivation in HEK293 and HepG2 cells at concentrations up to 200 μM. Differences in experimental design (e.g., reporter system) could account for discrepancies in the results.

There is in vitro evidence that suggests potential activation of other human PPAR subtypes after PFDA treatment, primarily PPARγ and possibly PPARβ/δ. Experimental studies in animals and humanized models would be critical to confirming and better characterizing the potential role of these receptors in the mechanism(s) of hepatotoxicity from PFDA exposure.

CAR/PXR

Chemical-induced activation of CAR and PXR leads to increased expression and activity of xenobiotic metabolizing enzymes (XMEs) (Li et al., 2017; Hall et al., 2012) and drug transport proteins (Mackowiak et al., 2018). In addition to metabolism and excretion of xenobiotic compounds (and endogenous substrates such as steroids and fatty acids), CAR/PXR-induced xenobiotic enzyme activities have been proposed to promote formation of reactive metabolites (Wang et al., 2014; Li et al., 2012), alter drug interactions (Mackowiak et al., 2018), and increase oxidative stress, immune responses, and mitochondrial disfunction (Wang et al., 2014). CAR/PXR activation can also alter lipid homeostasis and promote hepatic steatosis (Mackowiak et al., 2018; Mellor et al., 2016).

Experimental studies have evaluated PFDA-mediated activation of CAR and PXR in rodents. PFDA exposure led to increase in CAR mRNA levels, nuclear translocation of CAR, and increased mRNA and/or protein levels of CAR- and PXR-responsive genes such as Cyp2B10 and Cyp3A11 in C57BL6/6J mice (Abe et al., 2017; Cheng and Klaassen, 2008b). NTP (2018) also reported increased in the mRNA levels of CAR-responsive genes, Cyp1B1 and cyp1B2, in Sprague-Dawley rats. Further evaluation of the effects of PFDA on CYP450s in genetically modified mice devoid of function of specific nuclear receptors revealed that PFDA-mediated Cyp2B10 mRNA expression is regulated by CAR and independent of PPARα, PXR or FXR (Cheng and Klaassen, 2008b). PXR was also not required for the induction of Cyp3A11 mRNA after PFDA exposure (Cheng and Klaassen, 2008b).

Cell culture studies and HTS assays from the ToxCast database have also evaluated PFDA-induced activation of CAR and PXR. PFDA exposure resulted in increased mRNA and protein levels of PXR but did not affect the expression of the PXR target gene, Cyp3A23, in primary rat hepatocytes (Ma et al., 2005). PXR-dependent CYP3A4 activation by PFDA was reported in HepG2 cells transfected with the human PXR (Zhang et al., 2017), and increased mRNA levels of CAR/PXR-responsive genes, CYP2B6 and CYP3A4, were detected in primary human hepatocytes after PFDA treatment (Rosen et al., 2013). In primary mouse hepatocytes, PFDA treatment had no effect on CAR-responsive genes, but according to the study authors this may have been caused by cell culture conditions and time in culture before and during exposure (Rosen et al., 2013). An additional study reported no effects on the induction of the mouse or human CAR in gene reporter assays using nonhuman primate kidney COS-1 cells but failed to assess PFDA-induced expression of CAR-responsive genes in HepaRG cells due to increased cytotoxicity after chemical exposure (100 μM) (Abe et al., 2017). Using a lower PFDA concentration (45 μM), Lim et al. (2021) showed upregulation of the CAR-target gene, CYP2B6. Gene reporter activity measured in HTS assays conducted in HepG2 cells revealed PFDA-induced activation of the human PXR in 1 of 3 assays but no activation of the human CAR across 4 assays (see Table E-2). PFDA also demonstrated binding activity for the human PXR (see Table E-2).

Overall, the available evidence suggests that PFDA exposure can activate the murine CAR resulting in altered levels of CYP450s in vivo and, although not all of the available experiments were clearly positive, PFDA appears to interact with PXR in in vitro rodent and human model systems. Future studies focusing on the potential involvement of these receptors in the mechanisms of PFDA-induced liver effects would be informative.

FXR

FXR is a key regulator of bile acid synthesis and lipid metabolism (Russell, 2003). Deletion of the mouse FXR gene (Nr1h4) leads to fatty liver and insulin resistance (Ma et al., 2006) and exacerbation of chemical-induced acute liver injury (Takahashi et al., 2017), while activation of FXR in response to liver injury and disease may have a protective role (Han, 2018). PFDA was evaluated in HTS from EPA's ToxCast/Tox21 database (see Analysis of relevant high throughput screening assays from the EPA's CompTox Chemicals Dashboard in Appendix E for more details). No FXR activity was detected in assays related to receptor/cofactor interaction or agonist/antagonist transactivation in human embryonic kidney HEK293 cells (see Table E-2). Conversely, PFDA displayed agonist activity in a cell-free receptor-ligand binding assay and was active in one of two assays profiling transcriptional activity of this receptor in a human liver cell line (HepG2) (see Table E-2). Importantly, PFDA exhibited high potency for the human FXR compared to other nuclear receptors (e.g., PPARα/γ and CAR/PXR) based on estimated effective concentrations (i.e., AC50 values) (see Figure F-2B). In summary, FXR appears to be a sensitive target of PFDA in HTS assays and thus, similar to CAR above, experiments specifically targeting the potential role of this receptor in the liver effects of PFDA would be informative.

Other Pathways

Additional cell signaling pathways have been evaluated in vivo and in liver cells in vitro. In Wistar rats and SV129 mice, PFDA exposure had no effects on mRNA levels of c-Jun/c-Fos (Luo et al., 2017) (Oguro et al., 1998). Similarly, PFDA exposure had no significant effects on aryl hydrocarbon receptor (AHR)-inducible P450 activity in C57BL/6J mice (Brewster and Birnbaum, 1989) or mRNA expression of AHR-responsive genes (Cyp1A1/2) in C57BL/6J mice (Cheng and Klaassen, 2008b) and HepaRG cells (Lim et al., 2021). However, PFDA increased 2,3,7,8-Tetrachlorodibenzo-p-dioxin (TCDD)-induced AHR transactivation in an antagonist assay conducted in mouse hepatoma Hepa 1.12cR cells (Long et al., 2013). Effects on inflammatory and oxidative/cellular stress signaling involving the nuclear factor erythroid 2 related factor 2 (Nrf2), nuclear factor kappa B pathway (NFκB), tumor necrosis factor alpha (TNFα), c-Jun-N-terminal kinase (JNK) and activating transcription factor 2 (ATF-2) were reported following PFDA exposure in rodents (see synthesis on Inflammation and Cellular Stress for more details).

In vitro HTS assays from ToxCast/Tox21 showed induction of target gene pathways in HepG2 and HepaRG cells (measured as gene reporter activity) (see Table F-1), including several nuclear receptors discussed previously. According to estimated AC50 values (concentration at half maximal response), gene-specific activities occurred upstream but were closely associated with responses indicative of cellular stress/cytotoxicity (see Figure E-1). Specifically, PFDA was active in all three assays measuring Nrf2 transcriptional or agonist activity but was inactive in transactivation assays for NFκB and AHR in HepG2 and HepRG cells (see Table E-1). Induction of transcriptional activity for JUN/FOS was demonstrated in HepaRG cells but not HepG2 cells with PFDA exposure (see Table F-1).

Overall, the available experimental studies suggest that in addition to activation of PPARα and CAR/PXR nuclear receptor pathways (and possibly PPARγ and FXR based on limited in vitro studies in human cells), exposure to PFDA may also promote activation of other cell signaling pathways associated with inflammatory and oxidative/cellular stress responses (see synthesis on Inflammation and Cellular stress in this Appendix for more details).

D.3.2. CELLULAR EFFECTS

As discussed below, the available studies provide evidence on potential PFDA-induced alterations in hepatic expression and/or activity of XMEs, oxidative stress, cell and mitochondrial damage, inflammation, and alterations in liver metabolic functions.

Expression and Activity of XMEs

Several in vivo studies have evaluated PFDA-induced effects on the expression and activity of XMEs. In Wistar rats, PFDA exposure was associated with increased cytochrome P450 content and activity of NADPH-cytochrome c (P-450) reductase (Yamamoto and Kawashima, 1997) and decreased GST protein levels and activity (Oguro et al., 1998; Kawashima et al., 1995; Schramm et

al., 1989). Furthermore, PFDA exposure altered bilirubin glucuronosyltransferase activities and bilirubin, morphine, testosterone, and naphthol glucuronidation (Arand et al., 1991). In Fischer rats, PFDA treatment resulted in decreased sulfotransferase protein levels (Witzmann et al., 1996) and microsomal carboxylesterase activity (Derbel et al., 1996). A study using SV129 mice found that PFDA exposure decreased hepatic mRNA levels of CYP450s, and organic-anion-transporting polypeptides (OATPs) involved in the bile acid synthesis and uptake, while increasing mRNA levels of UDP-glucuronosyltransferases (UGT) enzymes (Luo et al., 2017). PPARα-null mice were mostly resistant to these effects (Luo et al., 2017). Similarly, Cheng and Klaassen (2008b) reported that PFDA-mediated downregulation of hepatic bile acid uptake transporters (OATPs and the Na+-taurocholate cotransporting peptide) is notably disrupted in PPARα-null mice but not in CAR-, PXR-, Nrf2- or FXR- null counterparts. As such, PPARα appears to be involved in the modulation of metabolizing enzymes and transport mechanisms important for bile acid homeostasis.

Several in vivo studies evaluated the effects of PFDA exposure on multidrug resistance proteins, which play important roles in hepatic metabolic and detoxifying functions, including bile acid excretion (Roth et al., 2019; Yang et al., 2014). In Sprague Dawley rats, PFDA exposure was associated with decreased mRNA and protein levels of the hepatic multidrug resistance protein 2 (Mrp2), albeit effects were not statically significant (Johnson and Klaassen, 2002). A separate study reported that PFDA exposure significantly increased Mrp2 mRNA levels in SV129 mice and that PPARα-null animals were resistant to this effect (Luo et al., 2017). Two studies using wild type and PPARα-null mice evaluated PFDA-induced changes in hepatic levels of Mrp3 and Mrp4 (Luo et al., 2017; Maher et al., 2008). Both studies report that PFDA treatment increased Mrp4 mRNA levels in wild type SV129 or C57BL/6J mice, but the responses in PPARα-null animals differed: Maher et al. (2008) observed that elimination of PPARα ameliorated this effect, while Luo et al. (2017) reported that PPARα-nulls were as responsive as wild type animals. Maher et al. (2008) observed that unlike wild type mice, PPARα-null animals were resistant to PFDA induction of Mrp3, and Luo et al. (2017) reported no exposure-related effects on Mrp3 levels in either wild type or null animals. Luo et al. (2017) and Maher et al. (2008) used a similar dose regimen (single i.p. injection of 80 mg/kg) but Luo et al. (2017) sampled animals on day 5 post exposure whereas Maher et al. (2008) sampled animals 48 hours post exposure) and test mouse strain (SV129 and C57BL/6, respectively) differed between studies. These differences in experimental model and/or design features could account for the perceived discrepancies in the results. Maher et al. (2008) also reported that Nrf2-null mice were resistant to PFDA-induced expression of Mrp3 and Mrp4, and that pretreatment with gadolinium chloride ameliorated PFDA-induction of Mrp4 mRNA levels but had no effect on Mrp3. Overall, the results suggest that PPARα and other signaling pathways (i.e., Nrf2 and Kupffer cell activation) participate in PFDA-mediated disruption of hepatic efflux Mrp transporters.

A study evaluating transcriptomic changes in HepaRG cells with exposure to PFDA and other long-chain PFAS observed enrichment of gene pathways involved in phase I and phase II metabolism, transporters, bile acid metabolism, amino acid metabolism and carbohydrate

metabolism (Lim et al., 2021). An increase in transcriptomic response was reported with increasing carbon chain length with PFDA being the most potent PFAS tested. Specifically with respect to transporters, PFDA exposure was associated with the upregulation of xenobiotic efflux transporters (e.g., ABCA3, ABCC3/MRP3, ABCC10/MRP7, and ABCG2/BCRP) and amino acid transporters involved in protein synthesis (e.g., SLC1A4, SLC1A5, SLC6A9, SLC7A1, SLC7A2, SLC7A5, SLC7A11, and SLC43A1), as well as the downregulation of bile acid or xenobiotic uptake transporters (e.g., SLC10A1/NTCP, SLCO2B1 and SLCO4C1). These observations are consistent with a potential compensatory mechanism against chemical-induced injury. The authors also noted that PFDA-mediated regulation of transporters appeared to be associated with the induction of Nrf2 rather than PPARα or CAR (Lim et al., 2021). Similarly, HTS ToxCast/Tox21 assays showed PFDA-mediated induction of gene pathways associated with xenobiotic metabolism and transport (i.e., CYP1A1, CYP2C19, CYP4A11, CYP4A22, ABCC3 and ABCG2,) in HepaRG cells (see Figure E-2 and Table E-1).

The findings described above suggest that exposure to PFDA results in increased XME levels and activity in animal models, which is supported by evidence on PFDA-induced activation of the CAR/PXR signaling pathways, two key regulators of XMEs. Furthermore, evidence from experiments using null animals suggest that PPARα is important for PFDA-induced regulation of a number of XMEs and transporters involved in bile acid homeostasis (e.g., CYP450, UGT OATP, and Mrp proteins). Additional mechanisms involving Nrf2 and Kupffer cell-mediated inflammatory responses appear to also play a role in regulating the expression of hepatic transporters in response to chemical-induced toxicity. The disruption of bile acid synthesis and transport mechanisms is consistent with the observed increases in markers of hepatobiliary function/injury in mice following PFDA exposure (see synthesis on Cellular stress and Metabolic effects below). Further studies are necessary to clarify inconsistencies in the results described above and to characterize the specific role of PPARα, Nrf2 and other cell signaling pathways (e.g., CAR/PXR) in modulating XME expression and activity and associated downstream effects that could contribute to the observed hepatic effects of PFDA exposure.

Oxidative Stress

Increased production of reactive oxygen species (ROS) can lead to hepatocellular toxicity as it can result in cellular damage (e.g., increase lipid peroxidation, protein oxidation, and oxidative DNA damage) (Joshi-Barve et al., 2015; Wahlang et al., 2013) and activation of proinflammatory cell signaling cascades (Joshi-Barve et al., 2015).

Several in vivo and cell culture studies have evaluated PFDA-induced oxidative stress. In CD-1 mice, PFDA decreased the activity of antioxidant enzymes such as total superoxide dismutase (T-SOD), catalase (CAT), and glutathione peroxidase (GPx) activities, while increasing the level of hepatic oxidative markers including ROS, thiobarbituric acid reactive substances (TBARS) and malondialdehyde (MDA) in hepatic tissue (Wang et al., 2020). Likewise, PFDA exposure increased hepatic expression of ROS-responsive genes (Maher et al., 2008; Permadi et al., 1993) and

microsomal lipid peroxidation (Cai et al., 1995) in C57BL/6J mice. In Sprague Dawley and Wistar rats, PFDA exposure consistently altered expression of ROS-sensitive proteins known to respond to increased ROS including, glutathione-S-transferase, catalase, and glutathione reductase (Chen et al., 2001; Kim et al., 1998; Glauert et al., 1992; Ikeda et al., 1985). These findings are supported by the observation that PFDA exposure results in the activation of the ROS-sensitive transcription factor, Nrf2, in C57BL/6J mice (as indicated by the increase in the hepatic expression of the Nrf2 gene marker, Nqo1) (Maher et al., 2008). Studies in PPARα -null mice determined that PFDA-mediated activation of the mouse Nrf2 was independent of PPARα (Maher et al., 2008). Moreover, PFDA was associated with an increase in oxidative DNA damage in rat liver (Huang et al., 1994; Takagi et al., 1991) in studies with repeated-dose exposure up to 54 weeks, while no alterations in oxidative DNA damage (Kim et al., 1998), lipid peroxidation (Glauert et al., 1992), or changes in cellular antioxidant levels (Glauert et al., 1992) were reported in single exposure studies in rats. Notably, induction of microsomal lipid peroxidation in mice was also achieved after repeated-dose exposure to PFDA for 2 weeks (Cai et al., 1995).

PFDA exposure induced ROS levels (Ojo et al., 2021; Wielsøe et al., 2015) and reduced intracellular glutathione (GSH) (Ojo et al., 2021) in HepG2 cells but did not affect the total cellular antioxidant capacity (Wielsøe et al., 2015).

The available evidence suggests that PFDA exposure increases ROS production in animal models and in HepG2 cells and may also promote ROS-related cellular damage (e.g., DNA oxidation and lipid peroxidation) in rodent species after prolonged or repeated exposure. The specific involvement of Nrf2 and other cell signaling pathways in PFDA-induced ROS and potential effects on cellular antioxidant capacity and oxidative cellular and tissue damage with prolonged chemical exposure remains to be elucidated.

Mitochondrial Damage

Mitochondrial damage is a mechanism associated with toxicant-induced alterations in hepatocellular lipid balance (Angrish et al., 2016) and increased liver toxicity (Wahlang et al., 2013). Damage to mitochondria caused by oxidative stress, attenuation in mitochondrial transmembrane potential, and alterations in membrane permeability, electron transport and calcium fluxes are considered stimuli that induce hepatic steatosis (Kaiser et al., 2012) and mitochondrial-mediated liver cell death (Li et al., 2017; Cao et al., 2016).

Several in vivo studies using different animal species and strains have evaluated PFDA-induced responses in hepatic mitochondria. In Sprague Dawley rats, exposure to PFDA led to reduced cytochrome c oxidase activity (Harrison et al., 1988) and increased mitochondrial swelling (Harrison et al., 1988), a response that can lead to disruption of the mitochondrial membrane (Jaeschke et al., 2012). Consistent with this, PFDA exposure led to increased swelling and structural alterations in liver mitochondria in CF-1 mice, Fischer rats, Syrian hamsters, and Guinea pigs; responses varied across species with rats being most sensitive (Van Rafelghem et al., 1987). In C57BL/6J mice and Fischer rats, PFDA treatment caused alterations in mitochondrial protein

content and increased mitochondrial enzyme activity (Permadi et al., 1993); (Witzmann and Parker, 1991; Kelling et al., 1987). In vitro studies reported that isolated rat liver mitochondria exposed to PFDA display uncoupling of electron transport and oxidative phosphorylation (Langley, 1990) and induction of mitochondrial permeability transition (Wallace et al., 2013). In primary Sprague Dawley rat hepatocytes, PFDA treatment resulted in decreased mitochondrial metabolic functions (Vanden Heuvel et al., 1991). In vitro HTS data showed changes in mitochondrial mass but no effects on mitochondrial membrane potential in HepG2 cells after PFDA exposure (see Table E-1).

Overall, in vivo and in vitro studies suggest that PFDA exposure disrupts hepatic mitochondrial proteins, integrity and function, and some of the observed effects appeared to be conserved across different species of animals, including Syrian hamsters and Guinea pigs, known to be low PPARα responders compared to other rodent models (Corton et al., 2018; Hall et al., 2012). Additional studies assessing the potential mitochondrial effects of PFDA in human primary and immortalized liver cells would help clarify the potential human relevance and essentiality of the apparent PFDA-induced disruptions of mitochondrial pathways in PFDA-induced hepatotoxicity.

Inflammation

Hepatic inflammation is a mechanism associated with toxicant-induced liver injury (Angrish et al., 2016; Wahlang et al., 2013). Activated macrophages and Kupffer cells produce cytokines (e.g., TNFα, interleukin-6 [IL-6] and interleukin-10 [IL-10]) that activate hepatic stellate cells and contribute toxicant-induced liver damage (Joshi-Barve et al., 2015; Malhi and Gores, 2008).

PFDA-induced markers of hepatic inflammation and related mechanisms were evaluated in studies using rodent models. PFDA increased hepatic and/or serum protein levels of the proinflammatory cytokine TNFα in C57BL/6J mice (Maher et al., 2008), CD-1 mice (Wang et al., 2020) and Fisher-344 rats (Adinehzadeh and Reo, 1998). Induction of hepatic TNF-α levels were accompanied by increases in other proinflammatory cytokines such as IL-1β, IL-18 and IL-6 and increases in Nod-like receptor family, pyrin domain containing 3 (NLRP3) inflammasome activation markers such as NLRP3, adaptor apoptosis-associated speck-like protein (ASC) and caspase-1 in CD-1 mice (Wang et al., 2020). Maher et al. (2008) also reported that pretreatment with gadolinium chloride, an anti-inflammatory agent that suppresses Kupffer cell responses, ameliorated induction of TNFα levels in PFDA-exposed C57BL/6J mice. These results suggest that Kupffer cells may play a role in pro-inflammatory responses following PFDA exposure. Another study evaluated the involvement of PPARα on PFDA-induced responses related to hepatic inflammation. Luo et al. (2017) reported that exposure to PFDA induced anti-inflammatory responses such as increased IL-10 mRNA levels and decreased phosphorylation of NFκB in SV129 mice and that these effects did not occur in exposed PPARα-null animals. Hepatic TNFα and IL-6 mRNA levels were unaffected by exposure regardless of the genetic background of the animals. Similarly, Li et al. (2022) showed enrichment of gene pathways associated with anti-inflammatory

responses in the liver of female C57BL/6J mice exposed to PFDA. Specifically, mRNA expression of cytokines IL-1β and IL-18, caspase-1, inflammasome-related genes (NLRP1, NLRP3, and NLRC4) and key regulators of inflammasome assembly (e.g., cellular inhibitor of apoptosis 2 [cIAP2]) were suppressed. The data also showed inhibition of T helper cell type 1 (Th1) differentiation in mouse livers treated with PFDA.

The inconsistent responses on TNFα levels between Luo et al. (2017) versus Maher et al. (2008), Adinehzadeh and Reo (1998) and Wang et al. (2020) may have been due to differences in experimental design. Adinehzadeh and Reo (1998) and Maher et al. (2008) measured protein levels 24 and 48 hours, respectively, after a single dose of 50–80 mg/kg via i.p. injection, whereas Luo et al. (2017) measured transcription (i.e., mRNA levels) on day 5 after a single i.p. injection of 80 mg/kg. The negative response on TNFα in the Luo et al. (2017) study is consistent with the observed anti-inflammatory response (i.e., inhibition NFκB and IL-10) and may reflect a compensatory mechanism following initial acute hepatic injury (Luo et al., 2017). Furthermore, Wang et al. (2020) evaluated protein levels of TNFα after oral administration of PFDA (13 mg/kg) for 12 days, demonstrating induction of TNF-α and other pro-inflammatory markers with sustained PFDA exposure.

In summary, although uncertainties remain, PFDA exposure appears capable of promoting both pro- and anti-inflammatory responses in rodents, and PPARα may be involved in some of these effects.

Cellular Stress

Several in vivo studies have evaluated markers of cellular stress after exposure to PFDA. As described in the Animal Studies section for liver effects in the main assessment document (see Section 3.2.1), short-term oral exposure to PFDA has been shown to promote degenerative changes such as necrosis (Frawley et al., 2018; NTP, 2018) and increase in serum biomarkers of hepatocyte damage in Sprague Dawley rats (NTP, 2018) and CD-1 mice (Wang et al., 2020). Liver cell necrosis can promote steatohepatitis and fibrosis by exacerbating tissue damage via increased release of cellular contents which in turn trigger proinflammatory responses and death of neighboring hepatocytes (Cattley and Cullen, 2018; Joshi-Barve et al., 2015). One study using Wistar rats evaluated PFDA-induced effects on cytoskeletal proteins and reported no exposure related alterations (Witzmann and Parker, 1991). Additional effects indicative of cell damage/stress include PFDA-induced disruptions to the endoplasmic reticulum in the livers of Fischer or Sprague-Dawley rats, CD-1 mice, Syrian hamsters, and Guinea pigs (Harrison et al., 1988; Van Rafelghem et al., 1987), and dysregulation in intercellular gap junctions in Fischer rat and WB-F344 liver epithelial cells (Sovadinova et al., 2015). Wang et al. (2020) also reported increased expression of proapoptotic protein markers, Bax and cleaved caspase-3, in the liver of CD-1 mice exposed to PFDA. Furthermore, PFDA exposure was associated with increases in serum markers of hepatocyte and biliary damage (ALT, AST, and ALP) in wildtype SV129 mice that corresponded with the

activation of responses indicative of cellular stress signaling, including phosphorylation of JNK and its downstream target, ATF-2 (Luo et al., 2017). Notably, PPARα-null animals did not show these effects (Luo et al., 2017).

Cell viability and DNA damage were not affected in HepG2 cells exposed to PFDA concentrations of up to 100 μM across two studies (Rosenmai et al., 2018; Wielsøe et al., 2015) but three other studies reported that PFDA induced cytotoxicity in HepG2 cells in a concentration-dependent manner (effective concentrations causing 50% cytotoxicity [IC_{50}] were 14.10–15 μM) (Ojo et al., 2021; Ojo et al., 2020; Buhrke et al., 2013). Similarly, PFDA elevated markers of cellular stress and cytotoxicity in HTS assays conducted in HepG2 cells at higher concentrations (AC50 values ranging from 106.54 to 122.76 μM). PFDA-induced cytotoxicity was also reported in HepaRG cells ((Abe et al., 2017) and Table E-1 of the ToxCast/Tox21 data summary), primary rat and human hepatocytes (Rosen et al., 2013), immortalized human fetal liver cells (HL-7702) (Hu et al., 2014).

Overall, the available evidence suggests that PFDA exposure increases hepatocyte cytotoxicity in in vitro and in vivo animal models, including species considered less sensitive to PPARα activation (i.e., Syrian hamsters and Guinea pigs). Studies using null animals suggest that stress responses related to disruption of bile acid homeostasis in mice may be mediated, at least in part, by PPARα. However, the potential involvement of other cellular signaling pathways in PFDA-induced liver cell stress has not been investigated.

Metabolic Effects

Toxicant-induced alterations in hepatocyte function can result in abnormal metabolism and accumulation of cholesterol, fatty acids and triglycerides, and exacerbate effects caused by steatosis (Angrish et al., 2016), which in turn may increase susceptibility to other insults or progress to steatohepatitis (Yang et al., 2014; Wahlang et al., 2013).

PFDA-induced effects on liver metabolic function have been evaluated in multiple rodent models. In Wistar, Fischer, and Sprague-Dawley rats PFDA exposure was associated with alterations in lipid composition (Adinehzadeh et al., 1999; Yamamoto and Kawashima, 1997; Olson and Andersen, 1983), fatty acid transport (Vanden Heuvel et al., 1993) and metabolism (Reo et al., 1994; Davis et al., 1991); and increased fatty acid and triglyceride accumulation (Kudo and Kawashima, 2003; Adinehzadeh and Reo, 1998; Kawashima et al., 1995; Sterchele et al., 1994; Harrison et al., 1988; Van Rafelghem et al., 1988). Rat studies have also reported increased hepatic levels of cholesterol (Kawashima et al., 1995), bilirubin, and bile acids (NTP, 2018); decreased microsomal electron transport (Kawashima et al., 1995; Van Rafelghem and Andersen, 1988); alterations in hepatic cholesterol metabolism (Davis et al., 1991); glucose transport (Goecke-Flora et al., 1995) and metabolism (Goecke et al., 1994); and decreased albumin levels (NTP, 2018; Witzmann and Parker, 1991). PFDA also increases peroxisomal proliferation (Van Rafelghem et al., 1987), activity of responsive enzymes such as acyl-CoA oxidases (NTP, 2018; Kim et al., 1998; Huang et al., 1994; Borges et al., 1993; Vanden Heuvel et al., 1993; Borges et al., 1992; Glauert et al.,

1992; Intrasuksri and Feller, 1991; Kozuka et al., 1991a; Borges et al., 1990), and β-oxidation (Kudo and Kawashima, 2003; Kudo et al., 2000; Adinehzadeh et al., 1999; Kawashima et al., 1995; Kozuka et al., 1991b), which are consistent with the evidence of PPARα activation in experimental animal models (see synthesis on Molecular Initiating Events above). As mentioned previously, PPARs, including PPARα, regulate genes involved in lipid and cholesterol metabolism and promote β-oxidation of fatty acids (Xu et al., 2005). The findings from in vivo studies are supported by cell culture studies using primary rat hepatocytes that report alterations in fatty acid metabolism (Vanden Heuvel et al., 1991) and increased peroxisomal β–oxidation (Kudo et al., 2000).

Mice exposed to PFDA also demonstrate alterations in hepatic metabolic functions. PFDA exposure increased activity of fatty acid metabolizing enzymes (Permadi et al., 1993) and increased hepatic lipid accumulation in C57BL/6J mice (Brewster and Birnbaum, 1989), an initial manifestation of fatty liver disease that may progress to fibrosis (Wahlang et al., 2013). PFDA exposure caused alterations in the levels of bile acid metabolizing enzymes and transporters and increased serum levels of several indicators of cholestasis (including bile acids and their components and bilirubin) in mice (Luo et al., 2017; Maher et al., 2008) but PPARα-null animals were resistant to these effects (Luo et al., 2017). Finally, Van Rafelghem et al. (1987) reported extensive hepatic lipid vacuolization in hamsters and guinea pigs (and to a lesser extent in rats or mice) after PFDA treatment.

Studies examining PFDA-mediated liver metabolic effects in human models are mostly lacking. A study by Zhang et al. (2013) showed binding affinity towards the human liver fatty acid protein by multiple PFAS, including PFDA, which may disrupt fatty acid uptake and transport

The available evidence suggests that PFDA exposure alters liver metabolic functions across multiple rodent species, and studies using genetically modified animals suggest that PFDA-induced disruption of bile acid homeostasis is at least partially mediated by PPARα. More studies are needed to understand the specific role that PPARα and other cell signaling pathways play in PFDA-induced alterations in liver metabolic functions involving bile acid, glucose, lipid and cholesterol metabolism and under what conditions these alterations might lead to steatohepatitis and other liver pathologies in humans following prolonged chemical exposure.

D.3.3. ORGAN-LEVEL EFFECTS

Animal toxicity studies via the oral route have reported effects on histological and clinical markers and organ weight measures, which are indicative of adverse responses in the liver. These include changes in the incidence of hepatocellular necrosis, serum biomarkers of hepatobiliary and liver damage and increased liver weights (see synthesis of Animal studies). A study by (NTP, 2018) compared liver effects in rats after short-term exposure between PFDA (and other PFAS) and Wyeth-14,643, which was used as a positive control for PPARα activation. Much like PFDA, Wyeth-14,643 caused increases in liver weights, changes in liver biomarkers in the blood and hepatocyte hypertrophy; however, no evidence of necrosis or other degenerative lesions were

associated with Wyeth-14,643 exposure. The findings provide support for the hypothesis that some PFDA-induced liver responses are mediated by mechanisms independent of PPARα.

Additional evidence of PFDA-induced liver weight changes from i.p. injection studies is described herein. Several studies using rats and mice support increases in liver weight following PFDA exposure (Abe et al., 2017; Luo et al., 2017; Maher et al., 2008; Kim et al., 1998; Chen et al., 1994; Chinje et al., 1994; Borges et al., 1993; Borges et al., 1992; Kozuka et al., 1991b; Borges et al., 1990; Brewster and Birnbaum, 1989; Schramm et al., 1989; Van Rafelghem and Andersen, 1988; Kelling et al., 1987; Van Rafelghem et al., 1987; Kelling et al., 1986; Powers and Aust, 1986; Ikeda et al., 1985; Olson and Andersen, 1983). One study in particular used wild type and PPARα-null mice and reported that PFDA exposure led to increases in liver weight regardless of the genetic background of the exposed animals (Luo et al., 2017). Two other studies evaluated PFDA-induced effects in Guinea pigs and Syrian hamsters. In Guinea pigs, exposure to PFDA did not have a significant impact on relative liver weight (Chinje et al., 1994; Van Rafelghem et al., 1987), while in Syrian hamsters treatment was associated with increased liver weight (Van Rafelghem et al., 1987). As described above, Guinea pigs and Syrian hamsters are less responsive to PPARα activation when compared to other rodent models. However, the observation that PFDA exposure caused increases in liver weights in Syrian hamsters and PPARα-null mice suggests that other cell signaling pathways may be contributing to PFDA-induced hepatomegaly in hamsters.

Overall, the available evidence from in vivo studies reports that PFDA exposure results in organ-level effects, such as increases in liver weights that are consistently observed across multiple species and may be mediated, at least in part, by PPARα-independent mechanisms.

APPENDIX E. ANALYSIS OF RELEVANT HIGH-THROUGHPUT SCREENING ASSAYS FROM EPA'S CHEMICALS DASHBOARD

E.1. IN VITRO BIOACTIVITY DATA RELEVANT TO THE MECHANISMS OF PFDA-INDUCED LIVER EFFECTS

In vitro high throughput screening (HTS) assays for PFDA were downloaded from EPA's CompTox Chemicals Dashboard (https://comptox.epa.gov/dashboard) ((U.S. EPA, 2019), accessed November 3, 2022) which provides bioactivity data from the ToxCast and Tox21 collaborative projects. Available information most pertinent to the analysis of the potential mechanisms of PFDA-induced liver effects was extracted to supplement and augment mechanistic findings from studies in the peer-reviewed literature previously described. Results (active/inactive, AC50 values, and scaled activity) from in vitro assays in human hepatoma HepG2 cells and metabolically competent human hepatic progenitor cells (HepaRG) cells were obtained, filtering out background control assays and nonspecific responses from inducible reporter gene assays analyzed in the negative fitting direction relative to the control ("_dn"). Bioactivity data were analyzed based on the type of biological response or gene target using the annotation structure within the ToxCast assay summary information ((U.S. EPA, 2019), accessed November 3, 2022).

PFDA was active in 74 of 238 unique assay endpoints (~31%) in HepG2 and HepaRG cells, inducing a range of cell- and gene-specific changes (see Figure E-1 and Table E-1). PFDA was associated with cell cycle arrest and proliferation responses and induction of markers of oxidative stress and cell death (see Table E-1). Alterations in nuclear size and mitochondrial mass were also observed in HTS assays for PFDA with no apparent changes in microtubule conformation and mitochondrial membrane potential and respiration (see Table E-1). Further, PFDA caused upregulation of transcriptional activity that occurred generally at lower effective concentrations (i.e., AC50) compared to the cell-based responses (see Figure E-1). Specifically, PFDA induced the expression of CYP450 enzymes, growth factors, transporters and transcriptional factors, including several xenobiotic-sensing nuclear receptors previously implicated in the mechanisms of liver toxicity of PFDA or other PFAS (i.e., PPARα/γ, PXR, and FXR) (see Figure E-2 and Table E-1).

In summary, PFDA elicited in vitro responses in HTS assays conducted in HepG2 and HepaRG cells most consistently for cellular stress and cytotoxicity. Additionally, induction of gene target pathways corresponding to several transcriptional factor/nuclear receptor activities occurred upstream of the cell-mediated responses, albeit at similar effective concentrations.

Nuclear receptor activities were investigated more closely to provide further insights into the putative interaction of PFDA with these receptor-mediated signaling pathways in ToxCast/Tox21 assays profiling multiple endpoints (e.g., receptor binding, coregulator recruitment, and gene transactivation) and cell types (see Table E-2). As mentioned above, PFDA induced activity of specific steroid/xenobiotic sensing receptors, most notably FXR, PPAR and PXR (see Figure E-2A). PFDA interacted with the human FXR in a receptor-ligand binding assay evaluating agonist activity and in one of two independent assays measuring transcriptional activity in HepG2 cells but was inactive in four FXR-related assays in human embryonic kidney cells (HEK293T), targeting receptor/cofactor recruitment and agonist/antagonist activities (see Table E-2). Upregulation of transcriptional activity for PPARα and PPARγ but not PPARβ/δ (PPARD) was demonstrated in HepG2 cells, and PFDA was found to interact with the human PPARγ (but not human PPARα) in a receptor-ligand binding assay (see Table E-2). No activity was detected in assays conducted in HEK293T cells profiling agonist/antagonist activities for PPARγ or PPARβ/δ or receptor/cofactor recruitment for PPARγ (see Table E-2). PFDA was active in two of four assays for PXR, showing transcriptional induction in HepG2 cells (one of two independent assays) and direct binding to the human PXR but no activity in an agonist assay using HepG2 cells (see Table E-2). HNF4A, NURR1, RAR, ROR, RXR, and VDR were also targets of PFDA in reporter gene assays using HepG2 cells and antagonist activity toward ERR was reported in HEK293T cells (see Table E-2). PFDA targeted the ER and AR in in vitro HTS assays; however, overall activity for these receptors was low (refer to Appendix E.2 for additional details on the HTS results for the ER and AR). PFDA showed no appreciable activity in assays for GR, CAR, LXR, TR, and PR (Figure E-2A). Comparison of AC50 values across the nuclear receptor assays indicate that PFDA exerts the highest potency toward the human FXR with the lowest AC50 of 0.52 µM in a cell-free receptor binding assay (Figure E-2B), which is below the lower bound of the ToxCast cytotoxicity limit estimated for this chemical (7.108 µM) ((U.S. EPA, 2019), accessed November 3, 2022).

Altogether, the results of the ToxCast/Tox21 HTS analysis provide some mechanistic support for the PFDA-induced liver effects. PFDA caused upregulation of transcriptional activity in human hepatoma HepG2 cells involving multiple nuclear receptor pathways previously implicated in the MOA for PFDA-induced liver toxicity, namely PXR, FXR, and PPARα/γ. These target gene responses were associated with the induction of cellular stress/cytotoxicity. PFDA also interacted directly with the human PXR, FXR, and PPARγ in receptor binding assays, demonstrating particular sensitivity for the human FXR at concentrations below those associated with cytotoxicity and suggesting that FXR may be an important target for this chemical.

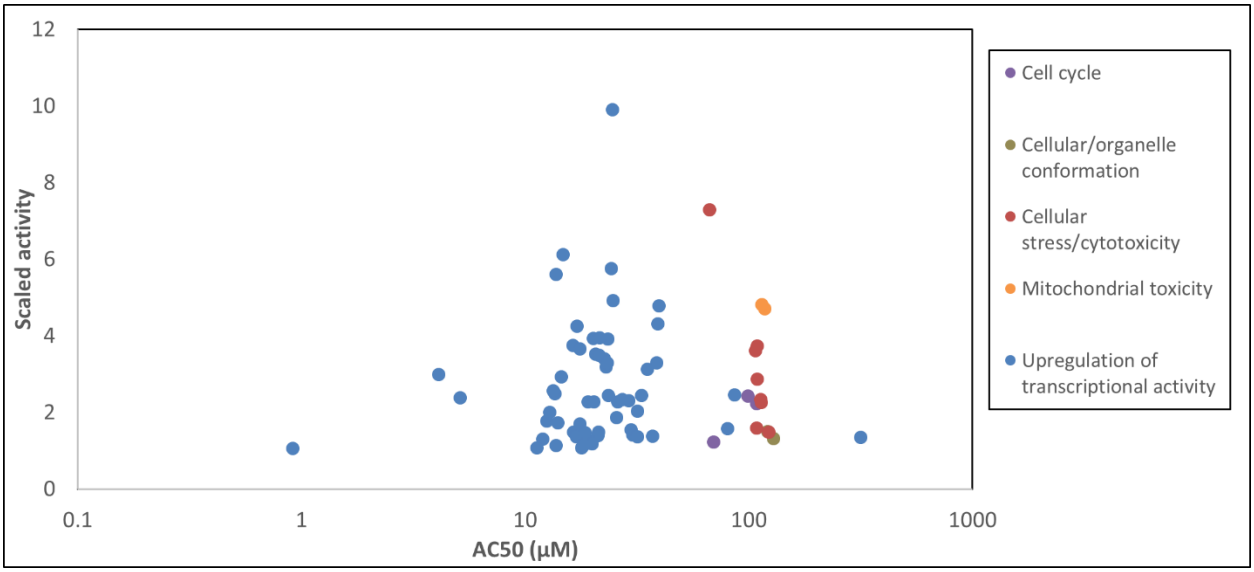

Figure E-1. Bioactivity data for PFDA from in vitro HTS ToxCast/Tox21 assays conducted in human liver cell lines (HepG2 and HepaRG cells).

Scatterplots show AC50 and scaled activity values from assays visualized according to the type of biological response. AC50 values refer to the concentration that elicits half maximal response and the scaled activity refers to the response value divided by the activity cutoff. Assays for which chemicals were inactive are not displayed. Additional information on all tested assays in HepG2 and HepaRG cells can be found in Table E-1.

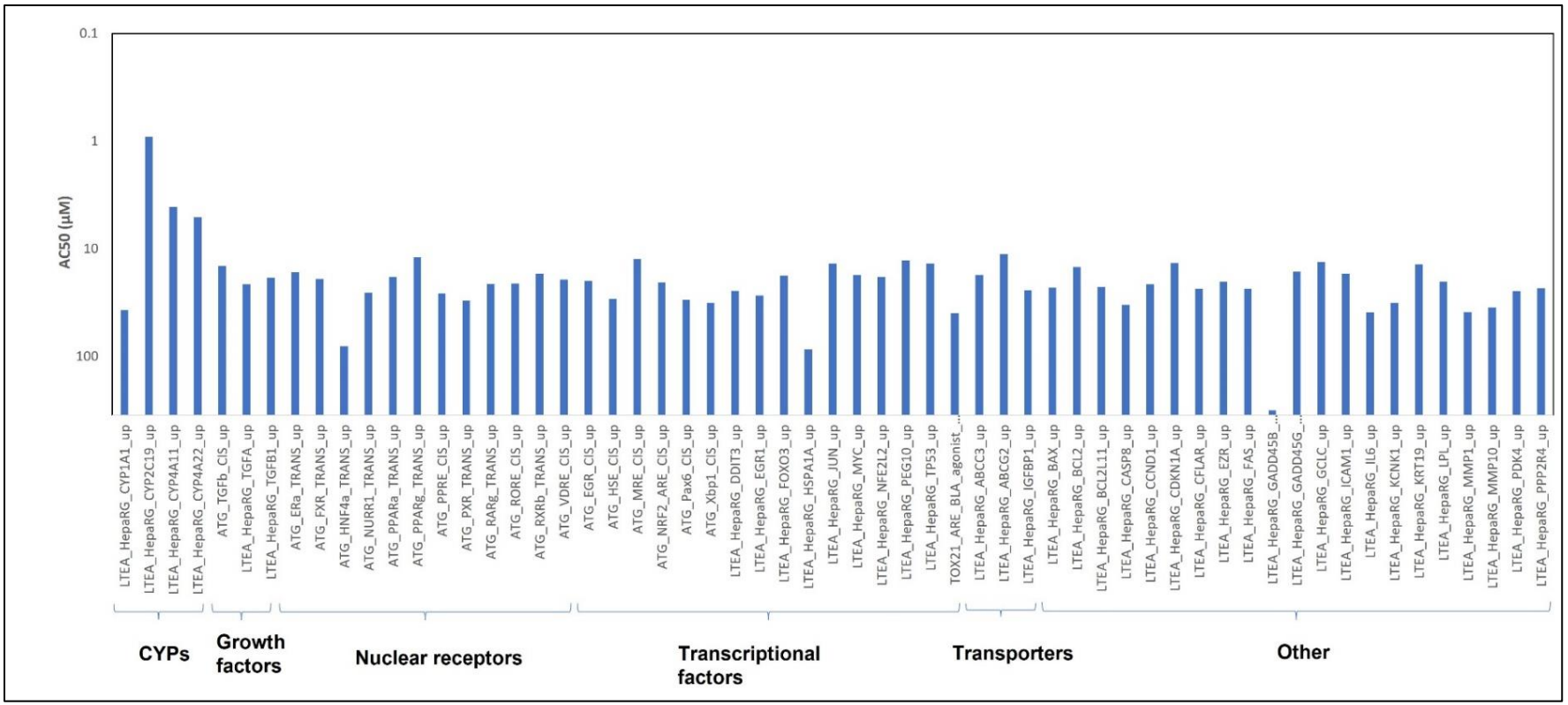

Figure E-2. Analysis of PFDA-induced upregulation of transcriptional activity in ToxCast/Tox21 assays conducted in human liver cell lines (HepG2 and HepaRG cells).

Bar graph compares AC50 values (concentration at half maximal response) for active assays. The scale for the AC50 values is shown in reverse order to visualize the most sensitive assays (the higher bar indicates a lower AC50 value). Additional information on the transcriptional activity assays can be found in Table E-1.

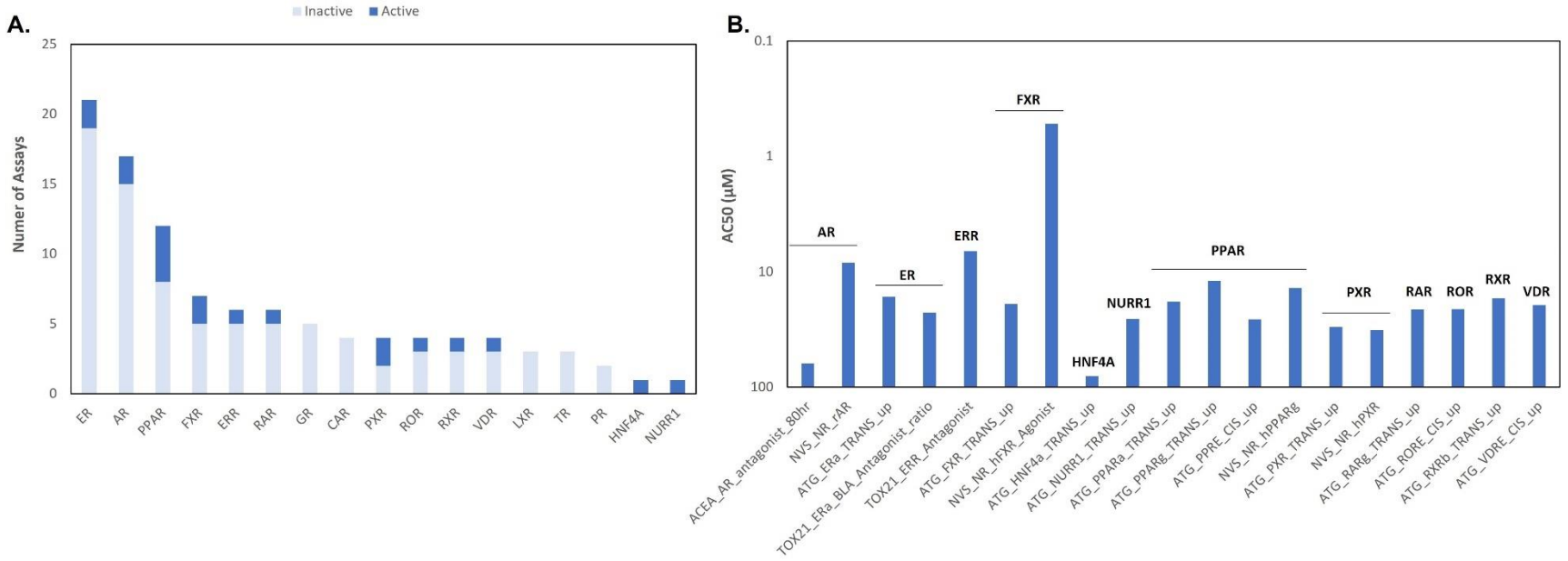

Figure E-3. Analysis of PFDA-induced nuclear receptor-related activities in ToxCast/Tox21 assays across multiple endpoints and cell types.

Panel A summarizes active/inactive calls from nuclear receptor assays mapped to specific target genes. Panel B compares AC50 values (concentration at half maximal response) for active assays. The scale for the AC50 values is shown in reverse order to visualize the most sensitive nuclear receptor activities (the higher bar indicates a lower AC50 value). Additional information on all tested nuclear receptor-related assays can be found in Table E-2.

Abbreviations: AR, androgen receptor; CAR, constitutive androgen receptor; ER, estrogen receptor; ERR, estrogen-related receptor; FXR, farnesoid X receptor; GR, glucocorticoid receptor; HNF4A, hepatocyte nuclear factors 4 alpha; LXR, liver X receptor; NURR1, nuclear receptor related-1 protein; PPAR, peroxisome proliferator-activated receptor; PXR, pregnane X receptor; RAR, retinoid acid receptor; ROR, RAR-related orphan receptor; RXR, retinoid X receptor; TR, thyroid hormone receptor; VDR, vitamin D receptor.

Table E-1. Bioactivity summary for PFDA from in vitro HTS assays from ToxCast/Tox21 conducted in human liver cell lines (HepG2 and HepaRG cells) and grouped by biological response/target[a,b]

Assay name	Activity call	Scaled activity	AC50 (μM)	Assay design	Cell line
Cell cycle					
APR_HepG2_CellCycleArrest_72h_dn	Active	1.23	69.51	morphology reporter	HepG2
APR_HepG2_MitoticArrest_24h_up	Active	2.25	107.91	morphology reporter	HepG2
APR_HepG2_MitoticArrest_72h_up	Active	2.44	98.57	morphology reporter	HepG2
APR_HepG2_CellCycleArrest_24h_dn	Inactive	NA	NA	morphology reporter	HepG2
APR_HepG2_CellCycleArrest_24h_up	Inactive	NA	NA	morphology reporter	HepG2
APR_HepG2_CellCycleArrest_72h_up	Inactive	NA	NA	morphology reporter	HepG2
APR_HepG2_MitoticArrest_24h_dn	Inactive	NA	NA	morphology reporter	HepG2
APR_HepG2_MitoticArrest_72h_dn	Inactive	NA	NA	morphology reporter	HepG2
Cellular/organelle conformation					
APR_HepG2_NuclearSize_24h_dn	Active	1.33	128.23	morphology reporter	HepG2
APR_HepG2_NuclearSize_72h_dn	Active	1.51	121.20	morphology reporter	HepG2
APR_HepG2_MicrotubuleCSK_24h_dn	Inactive	NA	NA	conformation reporter	HepG2
APR_HepG2_MicrotubuleCSK_24h_up	Inactive	NA	NA	conformation reporter	HepG2
APR_HepG2_MicrotubuleCSK_72h_dn	Inactive	NA	NA	conformation reporter	HepG2
APR_HepG2_MicrotubuleCSK_72h_up	Inactive	NA	NA	conformation reporter	HepG2
APR_HepG2_NuclearSize_24h_up	Inactive	NA	NA	morphology reporter	HepG2
APR_HepG2_NuclearSize_72h_up	Inactive	NA	NA	morphology reporter	HepG2
Cellular stress/cytotoxicity					
APR_HepG2_CellLoss_24h_dn	Active	3.75	108.88	viability reporter	HepG2
APR_HepG2_CellLoss_72h_dn	Active	3.63	106.54	viability reporter	HepG2
APR_HepG2_p53Act_24h_up	Active	1.61	107.89	viability reporter	HepG2
APR_HepG2_p53Act_72h_up	Active	2.28	113.49	viability reporter	HepG2
APR_HepG2_P-H2AX_24h_up	Active	2.35	112.97	viability reporter	HepG2
APR_HepG2_P-H2AX_72h_up	Active	2.88	108.81	viability reporter	HepG2
APR_HepG2_StressKinase_72h_up	Active	1.50	122.76	enzyme reporter	HepG2
LTEA_HepaRG_LDH_cytotoxicity	Active	7.31	66.39	viability reporter	HepaRG
APR_HepG2_CellLoss_24h_up	Inactive	NA	NA	viability reporter	HepG2
APR_HepG2_CellLoss_72h_up	Inactive	NA	NA	viability reporter	HepG2
APR_HepG2_p53Act_24h_dn	Inactive	NA	NA	viability reporter	HepG2
APR_HepG2_p53Act_72h_dn	Inactive	NA	NA	viability reporter	HepG2
APR_HepG2_P-H2AX_24h_dn	Inactive	NA	NA	viability reporter	HepG2
APR_HepG2_P-H2AX_72h_dn	Inactive	NA	NA	viability reporter	HepG2
APR_HepG2_StressKinase_24h_dn	Inactive	NA	NA	enzyme reporter	HepG2
APR_HepG2_StressKinase_24h_up	Inactive	NA	NA	enzyme reporter	HepG2
APR_HepG2_StressKinase_72h_dn	Inactive	NA	NA	enzyme reporter	HepG2
ATG_XTT_Cytotoxicity_up	Inactive	NA	NA	viability reporter	HepG2

Assay name	Activity call	Scaled activity	AC50 (μM)	Assay design	Cell line
CCTE_Simmons_MITO_viability	Inactive	NA	NA	viability reporter	HepG2
TOX21_AhR_LUC_Agonist_viability	Inactive	NA	NA	viability reporter	HepG2
TOX21_ARE_BLA_agonist_viability	Inactive	NA	NA	viability reporter	HepG2
TOX21_CAR_Agonist_viabillity	Inactive	NA	NA	viability reporter	HepG2
TOX21_CAR_Antagonist_viability	Inactive	NA	NA	viability reporter	HepG2
TOX21_CASP3_HEPG2	Inactive	NA	NA	inducible reporter	HepG2
TOX21_CASP3_HEPG2_viability	Inactive	NA	NA	viability reporter	HepG2
TOX21_MMP_viability	Inactive	NA	NA	viability reporter	HepG2
TOX21_PXR_viability	Inactive	NA	NA	viability reporter	HepG2
TOX21_RT_HEPG2_FLO_00hr_ctrl_viability	Inactive	NA	NA	viability reporter	HepG2
TOX21_RT_HEPG2_FLO_08hr_viability	Inactive	NA	NA	viability reporter	HepG2
TOX21_RT_HEPG2_FLO_16hr_ctrl_viability	Inactive	NA	NA	viability reporter	HepG2
TOX21_RT_HEPG2_FLO_24hr_viability	Inactive	NA	NA	viability reporter	HepG2
TOX21_RT_HEPG2_FLO_32hr_ctrl_viability	Inactive	NA	NA	viability reporter	HepG2
TOX21_RT_HEPG2_FLO_40hr_ctrl_viability	Inactive	NA	NA	viability reporter	HepG2
TOX21_RT_HEPG2_GLO_00hr_ctrl_viability	Inactive	NA	NA	viability reporter	HepG2
TOX21_RT_HEPG2_GLO_08hr_ctrl_viability	Inactive	NA	NA	viability reporter	HepG2
TOX21_RT_HEPG2_GLO_16hr_ctrl_viability	Inactive	NA	NA	viability reporter	HepG2
TOX21_RT_HEPG2_GLO_24hr_ctrl_viability	Inactive	NA	NA	viability reporter	HepG2
TOX21_RT_HEPG2_GLO_32hr_ctrl_viability	Inactive	NA	NA	viability reporter	HepG2
TOX21_RT_HEPG2_GLO_40hr_viability	Inactive	NA	NA	viability reporter	HepG2
Mitochondrial toxicity					
APR_HepG2_MitoMass_24h_dn	Active	4.72	117.36	morphology reporter	HepG2
APR_HepG2_MitoMass_72h_dn	Active	4.83	113.92	morphology reporter	HepG2
APR_HepG2_MitoMass_24h_up	Inactive	NA	NA	morphology reporter	HepG2
APR_HepG2_MitoMass_72h_up	Inactive	NA	NA	morphology reporter	HepG2
APR_HepG2_MitoMembPot_24h_dn	Inactive	NA	NA	membrane potential reporter	HepG2
APR_HepG2_MitoMembPot_24h_up	Inactive	NA	NA	membrane potential reporter	HepG2
APR_HepG2_MitoMembPot_72h_dn	Inactive	NA	NA	membrane potential reporter	HepG2
APR_HepG2_MitoMembPot_72h_up	Inactive	NA	NA	membrane potential reporter	HepG2
CCTE_Simmons_MITO_basal_resp_rate_OCR_dn	Inactive	NA	NA	respirometric reporter	HepG2
CCTE_Simmons_MITO_basal_resp_rate_OCR_up	Inactive	NA	NA	respirometric reporter	HepG2
CCTE_Simmons_MITO_inhib_resp_rate_OCR_dn	Inactive	NA	NA	respirometric reporter	HepG2
CCTE_Simmons_MITO_inhib_resp_rate_OCR_up	Inactive	NA	NA	respirometric reporter	HepG2
CCTE_Simmons_MITO_max_resp_rate_OCR_dn	Inactive	NA	NA	respirometric reporter	HepG2
CCTE_Simmons_MITO_max_resp_rate_OCR_up	Inactive	NA	NA	respirometric reporter	HepG2
TOX21_MMP_ratio_down	Inactive	NA	NA	membrane potential reporter	HepG2

Assay name	Activity call	Scaled activity	AC50 (μM)	Assay design	Cell line
TOX21_MMP_ratio_up	Inactive	NA	NA	membrane potential reporter	HepG2
Upregulation of transcriptional activity					
ATG_EGR_CIS_up	Active	1.19	19.92377	inducible reporter	HepG2
ATG_ERa_TRANS_up	Active	1.50	16.43561	inducible reporter	HepG2
ATG_FXR_TRANS_up	Active	2.28	18.99931	inducible reporter	HepG2
ATG_HNF4a_TRANS_up	Active	1.59	80.32058	inducible reporter	HepG2
ATG_HSE_CIS_up	Active	2.31	28.98294	inducible reporter	HepG2
ATG_MRE_CIS_up	Active	1.78	12.43083	inducible reporter	HepG2
ATG_NRF2_ARE_CIS_up	Active	3.54	20.6361	inducible reporter	HepG2
ATG_NURR1_TRANS_up	Active	1.87	25.56622	inducible reporter	HepG2
ATG_Pax6_CIS_up	Active	1.56	29.70391	inducible reporter	HepG2
ATG_PPARa_TRANS_up	Active	1.30	18.12921	inducible reporter	HepG2
ATG_PPARg_TRANS_up	Active	1.31	11.97573	inducible reporter	HepG2
ATG_PPRE_CIS_up	Active	2.29	25.89358	inducible reporter	HepG2
ATG_PXR_TRANS_up	Active	1.42	30.14653	inducible reporter	HepG2
ATG_RARg_TRANS_up	Active	1.50	21.20087	inducible reporter	HepG2
ATG_RORE_CIS_up	Active	1.41	21.068	inducible reporter	HepG2
ATG_RXRb_TRANS_up	Active	4.26	16.95397	inducible reporter	HepG2
ATG_TGFb_CIS_up	Active	2.94	14.44227	inducible reporter	HepG2
ATG_VDRE_CIS_up	Active	1.25	19.38327	inducible reporter	HepG2
ATG_Xbp1_CIS_up	Active	2.05	31.73703	inducible reporter	HepG2
LTEA_HepaRG_ABCC3_up	Active	1.71	17.53302	inducible reporter	HepaRG
LTEA_HepaRG_ABCG2_up	Active	1.08	11.2217	inducible reporter	HepaRG
LTEA_HepaRG_BAX_up	Active	3.20	22.88926	inducible reporter	HepaRG
LTEA_HepaRG_BCL2_up	Active	6.13	14.76859	inducible reporter	HepaRG
LTEA_HepaRG_BCL2L11_up	Active	3.41	22.55949	inducible reporter	HepaRG
LTEA_HepaRG_CASP8_up	Active	2.45	33.09058	inducible reporter	HepaRG
LTEA_HepaRG_CCND1_up	Active	3.50	21.35921	inducible reporter	HepaRG
LTEA_HepaRG_CDKN1A_up	Active	2.49	13.57402	inducible reporter	HepaRG
LTEA_HepaRG_CFLAR_up	Active	3.93	23.40259	inducible reporter	HepaRG
LTEA_HepaRG_CYP1A1_up	Active	1.40	37.12706	inducible reporter	HepaRG
LTEA_HepaRG_CYP2C19_up	Active	1.08	0.911362	inducible reporter	HepaRG
LTEA_HepaRG_CYP4A11_up	Active	3.00	4.084149	inducible reporter	HepaRG
LTEA_HepaRG_CYP4A22_up	Active	2.39	5.093503	inducible reporter	HepaRG
LTEA_HepaRG_DDIT3_up	Active	9.91	24.56621	inducible reporter	HepaRG
LTEA_HepaRG_EGR1_up	Active	2.35	27.13929	inducible reporter	HepaRG
LTEA_HepaRG_EZR_up	Active	2.29	20.2641	inducible reporter	HepaRG
LTEA_HepaRG_FAS_up	Active	2.46	23.51647	inducible reporter	HepaRG
LTEA_HepaRG_FOXO3_up	Active	1.08	17.79771	inducible reporter	HepaRG

Assay name	Activity call	Scaled activity	AC50 (μM)	Assay design	Cell line
LTEA_HepaRG_GADD45B_up	Active	1.37	316.2278	inducible reporter	HepaRG
LTEA_HepaRG_GADD45G_up	Active	3.77	16.26879	inducible reporter	HepaRG
LTEA_HepaRG_GCLC_up	Active	2.58	13.26529	inducible reporter	HepaRG
LTEA_HepaRG_HSPA1A_up	Active	2.48	86.07431	inducible reporter	HepaRG
LTEA_HepaRG_ICAM1_up	Active	1.37	16.93707	inducible reporter	HepaRG
LTEA_HepaRG_IGFBP1_up	Active	5.77	24.20317	inducible reporter	HepaRG
LTEA_HepaRG_IL6_up	Active	4.33	39.10404	inducible reporter	HepaRG
LTEA_HepaRG_JUN_up	Active	1.15	13.67962	inducible reporter	HepaRG
LTEA_HepaRG_KCNK1_up	Active	1.37	31.6189	inducible reporter	HepaRG
LTEA_HepaRG_KRT19_up	Active	1.75	13.95732	inducible reporter	HepaRG
LTEA_HepaRG_LPL_up	Active	3.94	20.11038	inducible reporter	HepaRG
LTEA_HepaRG_MMP1_up	Active	3.30	38.55908	inducible reporter	HepaRG
LTEA_HepaRG_MMP10_up	Active	3.14	35.00735	inducible reporter	HepaRG
LTEA_HepaRG_MYC_up	Active	3.67	17.50487	inducible reporter	HepaRG
LTEA_HepaRG_NFE2L2_up	Active	1.16	18.16403	inducible reporter	HepaRG
LTEA_HepaRG_PDK4_up	Active	4.93	24.64551	inducible reporter	HepaRG
LTEA_HepaRG_PEG10_up	Active	2.01	12.83903	inducible reporter	HepaRG
LTEA_HepaRG_PPP2R4_up	Active	3.31	23.18532	inducible reporter	HepaRG
LTEA_HepaRG_TGFA_up	Active	3.96	21.42175	inducible reporter	HepaRG
LTEA_HepaRG_TGFB1_up	Active	1.48	18.53422	inducible reporter	HepaRG
LTEA_HepaRG_TP53_up	Active	5.61	13.70365	inducible reporter	HepaRG
TOX21_ARE_BLA_agonist_ratio	Active	4.79	39.41989	inducible reporter	HepG2
ATG_Ahr_CIS_up	Inactive	NA	NA	inducible reporter	HepG2
ATG_AP_1_CIS_up	Inactive	NA	NA	inducible reporter	HepG2
ATG_AP_2_CIS_up	Inactive	NA	NA	inducible reporter	HepG2
ATG_AR_TRANS_up	Inactive	NA	NA	inducible reporter	HepG2
ATG_BRE_CIS_up	Inactive	NA	NA	inducible reporter	HepG2
ATG_C_EBP_CIS_up	Inactive	NA	NA	inducible reporter	HepG2
ATG_CAR_TRANS_up	Inactive	NA	NA	inducible reporter	HepG2
ATG_CRE_CIS_up	Inactive	NA	NA	inducible reporter	HepG2
ATG_DR4_LXR_CIS_up	Inactive	NA	NA	inducible reporter	HepG2
ATG_DR5_CIS_up	Inactive	NA	NA	inducible reporter	HepG2
ATG_E_Box_CIS_up	Inactive	NA	NA	inducible reporter	HepG2
ATG_E2F_CIS_up	Inactive	NA	NA	inducible reporter	HepG2
ATG_ERE_CIS_up	Inactive	NA	NA	inducible reporter	HepG2
ATG_ERRa_TRANS_up	Inactive	NA	NA	inducible reporter	HepG2
ATG_ERRg_TRANS_up	Inactive	NA	NA	inducible reporter	HepG2
ATG_Ets_CIS_up	Inactive	NA	NA	inducible reporter	HepG2
ATG_FoxA2_CIS_up	Inactive	NA	NA	inducible reporter	HepG2
ATG_FoxO_CIS_up	Inactive	NA	NA	inducible reporter	HepG2

Assay name	Activity call	Scaled activity	AC50 (μM)	Assay design	Cell line
ATG_GATA_CIS_up	Inactive	NA	NA	inducible reporter	HepG2
ATG_GLI_CIS_up	Inactive	NA	NA	inducible reporter	HepG2
ATG_GR_TRANS_up	Inactive	NA	NA	inducible reporter	HepG2
ATG_GRE_CIS_up	Inactive	NA	NA	inducible reporter	HepG2
ATG_HIF1a_CIS_up	Inactive	NA	NA	inducible reporter	HepG2
ATG_HNF6_CIS_up	Inactive	NA	NA	inducible reporter	HepG2
ATG_IR1_CIS_up	Inactive	NA	NA	inducible reporter	HepG2
ATG_ISRE_CIS_up	Inactive	NA	NA	inducible reporter	HepG2
ATG_LXRa_TRANS_up	Inactive	NA	NA	inducible reporter	HepG2
ATG_LXRb_TRANS_up	Inactive	NA	NA	inducible reporter	HepG2
ATG_Myb_CIS_up	Inactive	NA	NA	inducible reporter	HepG2
ATG_Myc_CIS_up	Inactive	NA	NA	inducible reporter	HepG2
ATG_NF_kB_CIS_up	Inactive	NA	NA	inducible reporter	HepG2
ATG_NFI_CIS_up	Inactive	NA	NA	inducible reporter	HepG2
ATG_NRF1_CIS_up	Inactive	NA	NA	inducible reporter	HepG2
ATG_Oct_MLP_CIS_up	Inactive	NA	NA	inducible reporter	HepG2
ATG_p53_CIS_up	Inactive	NA	NA	inducible reporter	HepG2
ATG_PBREM_CIS_up	Inactive	NA	NA	inducible reporter	HepG2
ATG_PPARd_TRANS_up	Inactive	NA	NA	inducible reporter	HepG2
ATG_PXRE_CIS_up	Inactive	NA	NA	inducible reporter	HepG2
ATG_RARa_TRANS_up	Inactive	NA	NA	inducible reporter	HepG2
ATG_RARb_TRANS_up	Inactive	NA	NA	inducible reporter	HepG2
ATG_RORb_TRANS_up	Inactive	NA	NA	inducible reporter	HepG2
ATG_RORg_TRANS_up	Inactive	NA	NA	inducible reporter	HepG2
ATG_RXRa_TRANS_up	Inactive	NA	NA	inducible reporter	HepG2
ATG_Sox_CIS_up	Inactive	NA	NA	inducible reporter	HepG2
ATG_Sp1_CIS_up	Inactive	NA	NA	inducible reporter	HepG2
ATG_SREBP_CIS_up	Inactive	NA	NA	inducible reporter	HepG2
ATG_STAT3_CIS_up	Inactive	NA	NA	inducible reporter	HepG2
ATG_TCF_b_cat_CIS_up	Inactive	NA	NA	inducible reporter	HepG2
ATG_THRa1_TRANS_up	Inactive	NA	NA	inducible reporter	HepG2
ATG_VDR_TRANS_up	Inactive	NA	NA	inducible reporter	HepG2
LTEA_HepaRG_ABCB1_up	Inactive	NA	NA	inducible reporter	HepaRG
LTEA_HepaRG_ABCB11_up	Inactive	NA	NA	inducible reporter	HepaRG
LTEA_HepaRG_ABCC2_up	Inactive	NA	NA	inducible reporter	HepaRG
LTEA_HepaRG_ACLY_up	Inactive	NA	NA	inducible reporter	HepaRG
LTEA_HepaRG_ACOX1_up	Inactive	NA	NA	inducible reporter	HepaRG
LTEA_HepaRG_ADK_up	Inactive	NA	NA	inducible reporter	HepaRG
LTEA_HepaRG_ALPP_up	Inactive	NA	NA	inducible reporter	HepaRG
LTEA_HepaRG_APOA5_up	Inactive	NA	NA	inducible reporter	HepaRG

Assay name	Activity call	Scaled activity	AC50 (μM)	Assay design	Cell line
LTEA_HepaRG_BAD_up	Inactive	NA	NA	inducible reporter	HepaRG
LTEA_HepaRG_BID_up	Inactive	NA	NA	inducible reporter	HepaRG
LTEA_HepaRG_CASP3_up	Inactive	NA	NA	inducible reporter	HepaRG
LTEA_HepaRG_CAT_up	Inactive	NA	NA	inducible reporter	HepaRG
LTEA_HepaRG_CYP1A2_up	Inactive	NA	NA	inducible reporter	HepaRG
LTEA_HepaRG_CYP24A1_1_up	Inactive	NA	NA	inducible reporter	HepaRG
LTEA_HepaRG_CYP2B6_up	Inactive	NA	NA	inducible reporter	HepaRG
LTEA_HepaRG_CYP2C8_up	Inactive	NA	NA	inducible reporter	HepaRG
LTEA_HepaRG_CYP2C9_up	Inactive	NA	NA	inducible reporter	HepaRG
LTEA_HepaRG_CYP2E1_up	Inactive	NA	NA	inducible reporter	HepaRG
LTEA_HepaRG_CYP3A4_up	Inactive	NA	NA	inducible reporter	HepaRG
LTEA_HepaRG_CYP3A5_up	Inactive	NA	NA	inducible reporter	HepaRG
LTEA_HepaRG_CYP3A7_up	Inactive	NA	NA	inducible reporter	HepaRG
LTEA_HepaRG_CYP7A1_up	Inactive	NA	NA	inducible reporter	HepaRG
LTEA_HepaRG_EGF_up	Inactive	NA	NA	inducible reporter	HepaRG
LTEA_HepaRG_FABP1_up	Inactive	NA	NA	inducible reporter	HepaRG
LTEA_HepaRG_FASN_up	Inactive	NA	NA	inducible reporter	HepaRG
LTEA_HepaRG_FMO3_up	Inactive	NA	NA	inducible reporter	HepaRG
LTEA_HepaRG_FOXO1_up	Inactive	NA	NA	inducible reporter	HepaRG
LTEA_HepaRG_GADD45A_up	Inactive	NA	NA	inducible reporter	HepaRG
LTEA_HepaRG_GSTA2_up	Inactive	NA	NA	inducible reporter	HepaRG
LTEA_HepaRG_GSTM3_up	Inactive	NA	NA	inducible reporter	HepaRG
LTEA_HepaRG_HGF_up	Inactive	NA	NA	inducible reporter	HepaRG
LTEA_HepaRG_HIF1A_up	Inactive	NA	NA	inducible reporter	HepaRG
LTEA_HepaRG_HMGCS2_up	Inactive	NA	NA	inducible reporter	HepaRG
LTEA_HepaRG_IGF1_up	Inactive	NA	NA	inducible reporter	HepaRG
LTEA_HepaRG_IL6R_up	Inactive	NA	NA	inducible reporter	HepaRG
LTEA_HepaRG_LIPC_up	Inactive	NA	NA	inducible reporter	HepaRG
LTEA_HepaRG_MIR122_up	Inactive	NA	NA	inducible reporter	HepaRG
LTEA_HepaRG_MMP3_up	Inactive	NA	NA	inducible reporter	HepaRG
LTEA_HepaRG_NFKB1_up	Inactive	NA	NA	inducible reporter	HepaRG
LTEA_HepaRG_NQO1_up	Inactive	NA	NA	inducible reporter	HepaRG
LTEA_HepaRG_PTEN_up	Inactive	NA	NA	inducible reporter	HepaRG
LTEA_HepaRG_SDHB_up	Inactive	NA	NA	inducible reporter	HepaRG
LTEA_HepaRG_SLC10A1_up	Inactive	NA	NA	inducible reporter	HepaRG
LTEA_HepaRG_SLC22A1_up	Inactive	NA	NA	inducible reporter	HepaRG
LTEA_HepaRG_SLC22A6_up	Inactive	NA	NA	inducible reporter	HepaRG
LTEA_HepaRG_SLCO1B1_up	Inactive	NA	NA	inducible reporter	HepaRG
LTEA_HepaRG_STAT3_up	Inactive	NA	NA	inducible reporter	HepaRG
LTEA_HepaRG_SULT2A1_up	Inactive	NA	NA	inducible reporter	HepaRG

Assay name	Activity call	Scaled activity	AC50 (μM)	Assay design	Cell line
LTEA_HepaRG_THRSP_up	Inactive	NA	NA	inducible reporter	HepaRG
LTEA_HepaRG_TIMP1_up	Inactive	NA	NA	inducible reporter	HepaRG
LTEA_HepaRG_TNFRSF1A_up	Inactive	NA	NA	inducible reporter	HepaRG
LTEA_HepaRG_UGT1A1_up	Inactive	NA	NA	inducible reporter	HepaRG
LTEA_HepaRG_UGT1A6_up	Inactive	NA	NA	inducible reporter	HepaRG
LTEA_HepaRG_XBP1_up	Inactive	NA	NA	inducible reporter	HepaRG
TOX21_AhR_LUC_Agonist	Inactive	NA	NA	inducible reporter	HepG2
TOX21_CAR_Agonist	Inactive	NA	NA	inducible reporter	HepG2
TOX21_CAR_Antagonist	Inactive	NA	NA	inducible reporter	HepG2
TOX21_PXR_Agonist	Inactive	NA	NA	inducible reporter	HepG2

[a]Data were sourced from EPA's CompTox Chemicals Dashboard ((U.S. EPA, 2019), accessed November 3, 2022).
[b]Background control assays and nonspecific responses from inducible reporter gene assays analyzed in the negative fitting direction relative to the control ("_dn") are not presented herein.
NA = not applicable.

Table E-2. Bioactivity summary for PFDA from in vitro HTS assays evaluating nuclear receptor-related activities from ToxCast/Tox21 across multiple endpoints and cell types[a,b,c]

Assay name	Activity call	Scaled Activity	AC50 (µM)	Biological target	Assay design	Organism	Tissue	Cell line
ATG_CAR_TRANS_up	Inactive	NA	NA	CAR (NR1I3)	inducible reporter	human	liver	HepG2
ATG_PBREM_CIS_up	Inactive	NA	NA	CAR (NR1I3)	inducible reporter	human	liver	HepG2
TOX21_CAR_Agonist	Inactive	NA	NA	CAR (NR1I3)	inducible reporter	human	liver	HepG2
TOX21_CAR_Antagonist	Inactive	NA	NA	CAR (NR1I3)	inducible reporter	human	liver	HepG2
TOX21_ERR_Antagonist	Active	1.31	6.62	ERR (ESRRA)	inducible reporter	human	kidney	HEK293T
ATG_ERRa_TRANS_up	Inactive	NA	NA	ERR (ESRRA)	inducible reporter	human	liver	HepG2
ATG_ERRg_TRANS_up	Inactive	NA	NA	ERR (ESRRA)	inducible reporter	human	liver	HepG2
TOX21_ERR_Agonist	Inactive	NA	NA	ERR (ESRRA)	inducible reporter	human	kidney	HEK293T
TOX21_PGC_ERR_Agonist	Inactive	NA	NA	ERR (ESRRA)	inducible reporter	human	kidney	HEK293T
TOX21_PGC_ERR_Antagonist	Inactive	NA	NA	ERR (ESRRG)	inducible reporter	human	kidney	HEK293T
ATG_FXR_TRANS_up	Active	2.28	19.00	FXR (NR1H4)	inducible reporter	human	liver	HepG2
NVS_NR_hFXR_Agonist	Active	5.52	0.52	FXR (NR1H4)	binding reporter	human	NA	NA
ATG_IR1_CIS_up	Inactive	NA	NA	FXR (NR1H4)	inducible reporter	human	liver	HepG2
OT_FXR_FXRSRC1_0480	Inactive	NA	NA	FXR (NR1H4)	binding reporter	human	kidney	HEK293T
OT_FXR_FXRSRC1_1440	Inactive	NA	NA	FXR (NR1H4)	binding reporter	human	kidney	HEK293T
TOX21_FXR_BLA_agonist_ratio	Inactive	NA	NA	FXR (NR1H4)	inducible reporter	human	kidney	HEK293T
TOX21_FXR_BLA_antagonist_ratio	Inactive	NA	NA	FXR (NR1H4)	inducible reporter	human	kidney	HEK293T
ATG_GR_TRANS_up	Inactive	NA	NA	GR (NR3C1)	inducible reporter	human	liver	HepG2
ATG_GRE_CIS_up	Inactive	NA	NA	GR (NR3C1)	inducible reporter	human	liver	HepG2
NVS_NR_hGR	Inactive	NA	NA	GR (NR3C1)	binding reporter	human	NA	NA
TOX21_GR_BLA_Agonist_ratio	Inactive	NA	NA	GR (NR3C1)	inducible reporter	human	cervix	HeLa
TOX21_GR_BLA_Antagonist_ratio	Inactive	NA	NA	GR (NR3C1)	inducible reporter	human	cervix	HeLa

Assay name	Activity call	Scaled Activity	AC50 (µM)	Biological target	Assay design	Organism	Tissue	Cell line
ATG_HNF4a_TRANS_up	Active	1.59	80.32	HNF4A	inducible reporter	human	liver	HepG2
ATG_LXRb_TRANS_up	Inactive	NA	NA	LXR (NR1H2)	inducible reporter	human	liver	HepG2
ATG_DR4_LXR_CIS_up	Inactive	NA	NA	LXR (NR1H2|NR1H3)	inducible reporter	human	liver	HepG2
ATG_LXRa_TRANS_up	Inactive	NA	NA	LXR (NR1H3)	inducible reporter	human	liver	HepG2
ATG_NURR1_TRANS_up	Active	1.87	25.57	NURR1 (NR4A2)	inducible reporter	human	liver	HepG2
ATG_PPARa_TRANS_up	Active	1.30	18.13	PPAR (PPARA)	inducible reporter	human	liver	HepG2
NVS_NR_hPPARa	Inactive	NA	NA	PPAR (PPARA)	binding reporter	human	NA	NA
ATG_PPARd_TRANS_up	Inactive	NA	NA	PPAR (PPARD)	inducible reporter	human	liver	HepG2
TOX21_PPARd_BLA_agonist_ratio	Inactive	NA	NA	PPAR (PPARD)	inducible reporter	human	kidney	HEK293T
TOX21_PPARd_BLA_antagonist_ratio	Inactive	NA	NA	PPAR (PPARD)	inducible reporter	human	kidney	HEK293T
ATG_PPARg_TRANS_up	Active	1.31	11.98	PPAR (PPARG)	inducible reporter	human	liver	HepG2
NVS_NR_hPPARg	Active	5.15	13.73	PPAR (PPARG)	binding reporter	human	NA	NA
OT_PPARg_PPARgSRC1_0480	Inactive	NA	NA	PPAR (PPARG)	binding reporter	human	kidney	HEK293T
OT_PPARg_PPARgSRC1_1440	Inactive	NA	NA	PPAR (PPARG)	binding reporter	human	kidney	HEK293T
TOX21_PPARg_BLA_Agonist_ratio	Inactive	NA	NA	PPAR (PPARG)	inducible reporter	human	kidney	HEK293T
TOX21_PPARg_BLA_antagonist_ratio	Inactive	NA	NA	PPAR (PPARG)	inducible reporter	human	kidney	HEK293
ATG_PPRE_CIS_up	Active	2.29	25.89	PPAR (PPARA|PPARD|PPARG)	inducible reporter	human	liver	HepG2
TOX21_PR_BLA_Agonist_ratio	Inactive	NA	NA	PR (PGR)	inducible reporter	human	kidney	HEK293T
TOX21_PR_BLA_Antagonist_ratio	Inactive	NA	NA	PR (PGR)	inducible reporter	human	kidney	HEK293T
ATG_PXR_TRANS_up	Active	1.42	30.15	PXR (NR1I2)	inducible reporter	human	liver	HepG2
NVS_NR_hPXR	Active	2.34	32.07	PXR (NR1I2)	binding reporter	human	NA	NA
ATG_PXRE_CIS_up	Inactive	NA	NA	PXR (NR1I2)	inducible reporter	human	liver	HepG2
TOX21_PXR_Agonist	Inactive	NA	NA	PXR (NR1I2)	inducible reporter	human	liver	HepG2
ATG_RARa_TRANS_up	Inactive	NA	NA	RAR (RARA)	inducible reporter	human	liver	HepG2
TOX21_RAR_LUC_Agonist	Inactive	NA	NA	RAR (RARA)	inducible reporter	mouse	embryo	C3H10T1/2

Assay name	Activity call	Scaled Activity	AC50 (µM)	Biological target	Assay design	Organism	Tissue	Cell line
TOX21_RAR_LUC_Antagonist	Inactive	NA	NA	RAR (RARA)	inducible reporter	mouse	embryo	C3H10T1/2
ATG_RARb_TRANS_up	Inactive	NA	NA	RAR (RARB)	inducible reporter	human	liver	HepG2
ATG_RARg_TRANS_up	Active	1.50	21.20	RAR (RARG)	inducible reporter	human	liver	HepG2
ATG_DR5_CIS_up	Inactive	NA	NA	RAR (RARA|RARB|RARG)	inducible reporter	human	liver	HepG2
ATG_RORb_TRANS_up	Inactive	NA	NA	ROR (RORB)	inducible reporter	human	liver	HepG2
ATG_RORg_TRANS_up	Inactive	NA	NA	ROR (RORC)	inducible reporter	human	liver	HepG2
TOX21_RORg_LUC_CHO_Antagonist	Inactive	NA	NA	ROR (RORC)	inducible reporter	Chinese hamster	ovary	CHO-K1
ATG_RORE_CIS_up	Active	1.41	21.07	ROR (RORA|RORB|RORC)	inducible reporter	human	liver	HepG2
ATG_RXRa_TRANS_up	Inactive	NA	NA	RXR (RXRA)	inducible reporter	human	liver	HepG2
OT_NURR1_NURR1RXRa_0480	Inactive	NA	NA	RXR (RXRA)	binding reporter	human	kidney	HEK293T
OT_NURR1_NURR1RXRa_1440	Inactive	NA	NA	RXR (RXRA)	binding reporter	human	kidney	HEK293T
ATG_RXRb_TRANS_up	Active	4.26	16.95	RXR (RXRB)	inducible reporter	human	liver	HepG2
ATG_THRa1_TRANS_up	Inactive	NA	NA	TR (THRA)	inducible reporter	human	liver	HepG2
TOX21_TR_LUC_GH3_Agonist	Inactive	NA	NA	TR (THRA|THRB)	inducible reporter	rat	pituitary gland	GH3
TOX21_TR_LUC_GH3_Antagonist	Inactive	NA	NA	TR (THRA|THRB)	inducible reporter	rat	pituitary gland	GH3
ATG_VDRE_CIS_up	Active	1.25	19.38	VDR	inducible reporter	human	liver	HepG2
ATG_VDR_TRANS_up	Inactive	NA	NA	VDR	inducible reporter	human	liver	HepG2
TOX21_VDR_BLA_agonist_ratio	Inactive	NA	NA	VDR	inducible reporter	human	kidney	HEK293T
TOX21_VDR_BLA_antagonist_ratio	Inactive	NA	NA	VDR	inducible reporter	human	kidney	HEK293T

[a]Data were sourced from EPA's CompTox Chemicals Dashboard ((U.S. EPA, 2019), accessed November 3, 2022).
[b]Nonspecific responses from inducible reporter gene assays analyzed in the negative fitting direction relative to the control ("_dn") are not presented herein.
[c]In vitro bioactivity data for the AR and ER are summarized in detail in Appendix E.2 and, therefore, are not presented herein.
NA = not applicable.

E.2. IN VITRO BIOACTIVITY DATA RELEVANT TO THE POTENTIAL MECHANISMS OF REPRODUCTIVE TOXICITY

HTS screening ToxCast assays profiling in vitro activities for the AR, ER and steroid hormone biosynthesis were sourced from EPA's CompTox Chemicals Dashboard ((U.S. EPA, 2019), accessed November 3, 2022) to investigate potential mechanisms of disruption of steroid hormone receptor activation and steroidogenesis that may be important for the reproductive toxicity of PFDA.

The suite of ToxCast assays and model predictions for the ER and AR encompass several endpoints in the signaling pathway of these receptors (e.g., receptor binding, receptor dimerization, cofactor recruitment, DNA binding, gene expression, and cell proliferation) across multiple in vitro models. PFDA was active in 2 of 17 AR assays (13%), demonstrating binding to the AR in rat prostrate tissue and AR-induced cell proliferation in a human prostate carcinoma cell line (22Rv1), but no activity in assays for cofactor recruitment and AR agonist/antagonist transactivation conducted primarily in human cell lines (see Table E-3). In ER assays, PFDA was active in 2 of 21 assays (11%), demonstrating activity for the ERα (ESR1) in 1 of 2 assays measuring RNA transcription in human hepatoma HepG2 cells and in an antagonist transactivation assays measuring protein expression in human embryonic kidney HEK293T cells (see Table E-3). PFDA was inactive in receptor binding assays for the ERα in human, bovine, and mouse tissues and in ER α/β assays for receptor dimerization, transcription factor-DNA binding, agonist transactivation, and ER-induced cell proliferation in different human cell lines. The AC50 values for the active ER and AR assays ranged from 8.40 to 62.3 μM, which are above the lower bound of the estimated ToxCast cytotoxicity limit (7.108 μM) ((U.S. EPA, 2019), accessed November 3, 2022). ToxCast model predictions incorporating in vitro assay results and nonspecific responses such as cytotoxicity suggest that PFDA is inactive for both ER/AR agonist and antagonist pathways (AUC = 0) (see Table E-4).

The ToxCast database also included in vitro assays related to the regulation of steroidogenesis. PFDA showed a lack of activity in a single assay measuring inhibition of transcriptional activity for the aromatase gene (CYP19A1) in human breast cancer MCF-7 cells and several assays measuring biosynthesis of steroid hormones including glucocorticoids, androgens, estrogens and progestogens in adrenal gland H295R cells (see Table E-5).

Table E-3. Bioactivity summary for PFDA from in vitro HTS assays evaluating activities for the AR, ER[a,b]

Assay name	Activity call	Scaled activity	AC50 (μM)	Biological target	Assay design	Organism	Tissue	Cell line
ACEA_AR_antagonist_80hr	Active	9.34	62.3	AR	growth reporter	human	prostate	22Rv1
NVS_NR_rAR	Active	2.47	8.40	AR	binding reporter	rat	prostate	NA
ACEA_AR_agonist_80hr	Inactive	NA	NA	AR	growth reporter	human	prostate	22Rv1
ATG_AR_TRANS_up	Inactive	NA	NA	AR	inducible reporter	human	liver	HepG2
OT_AR_ARELUC_AG_1440	Inactive	NA	NA	AR	inducible reporter	Chinese hamster	ovary	CHO-K1
OT_AR_ARSRC1_0480	Inactive	NA	NA	AR	binding reporter	human	kidney	HEK293T
OT_AR_ARSRC1_0960	Inactive	NA	NA	AR	binding reporter	human	kidney	HEK293T
TOX21_AR_BLA_Agonist_ratio	Inactive	NA	NA	AR	inducible reporter	human	kidney	HEK293T
TOX21_AR_BLA_Antagonist_ratio	Inactive	NA	NA	AR	inducible reporter	human	kidney	HEK293T
TOX21_AR_LUC_MDAKB2_Agonist	Inactive	NA	NA	AR	inducible reporter	human	breast	MDA-kb2
TOX21_AR_LUC_MDAKB2_Agonist_3uM_Nilutamide	Inactive	NA	NA	AR	inducible reporter	human	breast	MDA-kb2
TOX21_AR_LUC_MDAKB2_Antagonist_0.5nM_R1881	Inactive	NA	NA	AR	inducible reporter	human	breast	MDA-kb2
TOX21_AR_LUC_MDAKB2_Antagonist_10nM_R1881	Inactive	NA	NA	AR	inducible reporter	human	breast	MDA-kb2
UPITT_HCI_U2OS_AR_TIF2_Nucleoli_Agonist	Inactive	NA	NA	AR	binding reporter	human	bone	U2OS

Assay name	Activity call	Scaled activity	AC50 (µM)	Biological target	Assay design	Organism	Tissue	Cell line
UPITT_HCI_U2OS_AR_TIF2_Nucleoli_Antagonist	Inactive	NA	NA	AR	binding reporter	human	bone	U2OS
UPITT_HCI_U2OS_AR_TIF2_Nucleoli_Cytoplasm_Ratio_Agonist	Inactive	NA	NA	AR	binding reporter	human	bone	U2OS
UPITT_HCI_U2OS_AR_TIF2_Nucleoli_Cytoplasm_Ratio_Antagonist	Inactive	NA	NA	AR	binding reporter	human	bone	U2OS
ATG_ERa_TRANS_up	Active	1.50	16.44	ER (ESR1)	inducible reporter	human	liver	HepG2
TOX21_ERa_BLA_Antagonist_ratio	Active	3.32	22.7	ER (ESR1)	inducible reporter	human	kidney	HEK293T
ACEA_ER_80hr	Inactive	NA	NA	ER (ESR1)	growth reporter	human	breast	T47D
ATG_ERE_CIS_up	Inactive	NA	NA	ER (ESR1)	inducible reporter	human	liver	HepG2
NVS_NR_bER	Inactive	NA	NA	ER (ESR1)	binding reporter	bovine	uterus	NA
NVS_NR_hER	Inactive	NA	NA	ER (ESR1)	binding reporter	human	NA	NA
NVS_NR_mERa	Inactive	NA	NA	ER (Esr1)	binding reporter	mouse	NA	NA
OT_ER_ERaERa_0480	Inactive	NA	NA	ER (ESR1)	binding reporter	human	kidney	HEK293T
OT_ER_ERaERa_1440	Inactive	NA	NA	ER (ESR1)	binding reporter	human	kidney	HEK293T
OT_ERa_EREGFP_0120	Inactive	NA	NA	ER (ESR1)	inducible reporter	human	cervix	HeLa
OT_ERa_EREGFP_0480	Inactive	NA	NA	ER (ESR1)	inducible reporter	human	cervix	HeLa
TOX21_ERa_BLA_Agonist_ratio	Inactive	NA	NA	ER (ESR1)	inducible reporter	human	kidney	HEK293T

Assay name	Activity call	Scaled activity	AC50 (µM)	Biological target	Assay design	Organism	Tissue	Cell line
TOX21_ERa_LUC_VM7_Agonist	Inactive	NA	NA	ER (ESR1)	inducible reporter	human	ovary	VM7
TOX21_ERa_LUC_VM7_Antagonist_0.1nM_E2	Inactive	NA	NA	ER (ESR1)	inducible reporter	human	ovary	VM7
TOX21_ERa_LUC_VM7_Antagonist_0.5nM_E2	Inactive	NA	NA	ER (ESR1)	inducible reporter	human	ovary	VM7
OT_ER_ERbERb_0480	Inactive	NA	NA	ER (ESR2)	binding reporter	human	kidney	HEK293T
OT_ER_ERbERb_1440	Inactive	NA	NA	ER (ESR2)	binding reporter	human	kidney	HEK293T
TOX21_ERb_BLA_Agonist_ratio	Inactive	NA	NA	ER (ESR2)	inducible reporter	human	kidney	HEK293T
TOX21_ERb_BLA_Antagonist_ratio	Inactive	NA	NA	ER (ESR2)	inducible reporter	human	kidney	HEK293T
OT_ER_ERaERb_0480	Inactive	NA	NA	ER (ESR1|ESR2)	binding reporter	human	kidney	HEK293T
OT_ER_ERaERb_1440	Inactive	NA	NA	ER (ESR1|ESR2)	binding reporter	human	kidney	HEK293T

[a]Data were sourced from EPA's CompTox Chemicals Dashboard ((U.S. EPA, 2019), accessed November 3, 2022).
[b]Nonspecific responses from inducible reporter gene assays analyzed in the negative fitting direction relative to the control ("_dn") are not presented herein.
NA = not applicable.

Table E-4. ToxCast model predictions for the ER and AR pathways for PFDA[a]

	Agonist AUC values (95% CI)	Antagonist AUC values (95% CI)
ER pathway	0 (0–0.0051)	0 (0–0.019)
AR pathway	0 (0–0.063)	0 (0–0.00016)

[a]Data for ER and AR pathways were sourced from Judson et al. (2015) and Kleinstreuer et al. (2017), respectively.
[b]95% CI for the ER activity model were sourced from a subsequent publication to the Judson et al. (2015) study (Watt and Judson, 2018).
AUC = area under the curve score ranging from 0 to 1. An AUC value of 0 indicates that the chemical is inactive.
CI = confidence interval.

Table E-5. Bioactivity summary for PFDA from in vitro HTS assays related to steroidogenesis[a,b]

Assay name	Activity call	Scaled activity	AC50 (µM)	Biological target	Assay design	Organism	Tissue	Cell line
CEETOX_H295R_11DCORT_noMTC_dn	Inactive	NA	NA	11-Deoxycortisol	inducible reporter	human	adrenal gland	H295R
CEETOX_H295R_11DCORT_noMTC_up	Inactive	NA	NA	11-Deoxycortisol	inducible reporter	human	adrenal gland	H295R
CEETOX_H295R_ANDR_noMTC_dn	Inactive	NA	NA	Androstenedione	inducible reporter	human	adrenal gland	H295R
CEETOX_H295R_ANDR_noMTC_up	Inactive	NA	NA	Androstenedione	inducible reporter	human	adrenal gland	H295R
CEETOX_H295R_CORTIC_noMTC_dn	Inactive	NA	NA	Corticosterone	inducible reporter	human	adrenal gland	H295R
CEETOX_H295R_CORTIC_noMTC_up	Inactive	NA	NA	Corticosterone	inducible reporter	human	adrenal gland	H295R
CEETOX_H295R_CORTISOL_noMTC_dn	Inactive	NA	NA	Cortisol	inducible reporter	human	adrenal gland	H295R
CEETOX_H295R_CORTISOL_noMTC_up	Inactive	NA	NA	Cortisol	inducible reporter	human	adrenal gland	H295R
CEETOX_H295R_DOC_noMTC_dn	Inactive	NA	NA	11-Deoxycorticosterone	inducible reporter	human	adrenal gland	H295R
CEETOX_H295R_DOC_noMTC_up	Inactive	NA	NA	11-Deoxycorticosterone	inducible reporter	human	adrenal gland	H295R
CEETOX_H295R_ESTRADIOL_noMTC_dn	Inactive	NA	NA	Estradiol	inducible reporter	human	adrenal gland	H295R
CEETOX_H295R_ESTRADIOL_noMTC_up	Inactive	NA	NA	Estradiol	inducible reporter	human	adrenal gland	H295R
CEETOX_H295R_ESTRONE_noMTC_dn	Inactive	NA	NA	Estrone	inducible reporter	human	adrenal gland	H295R
CEETOX_H295R_ESTRONE_noMTC_up	Inactive	NA	NA	Estrone	inducible reporter	human	adrenal gland	H295R
CEETOX_H295R_OHPREG_noMTC_dn	Inactive	NA	NA	17alpha-hydroxypregnenolone	inducible reporter	human	adrenal gland	H295R
CEETOX_H295R_OHPREG_noMTC_up	Inactive	NA	NA	17alpha-hydroxypregnenolone	inducible reporter	human	adrenal gland	H295R
CEETOX_H295R_OHPROG_noMTC_dn	Inactive	NA	NA	17alpha-hydroxyprogesterone	inducible reporter	human	adrenal gland	H295R
CEETOX_H295R_OHPROG_noMTC_up	Inactive	NA	NA	17alpha-hydroxyprogesterone	inducible reporter	human	adrenal gland	H295R
CEETOX_H295R_PROG_noMTC_dn	Inactive	NA	NA	Progesterone	inducible reporter	human	adrenal gland	H295R
CEETOX_H295R_PROG_noMTC_up	Inactive	NA	NA	Progesterone	inducible reporter	human	adrenal gland	H295R
CEETOX_H295R_TESTO_noMTC_dn	Inactive	NA	NA	Testosterone	inducible reporter	human	adrenal gland	H295R

Assay name	Activity call	Scaled activity	AC50 (µM)	Biological target	Assay design	Organism	Tissue	Cell line
CEETOX_H295R_TESTO_noMTC_up	Inactive	NA	NA	Testosterone	inducible reporter	human	adrenal gland	H295R
TOX21_Aromatase_Inhibition	Inactive	NA	NA	CYP19A1	inducible reporter	human	breast	MCF7

[a]Data were sourced from EPA's CompTox Chemicals Dashboard (U.S. EPA, 2019), accessed November 3, 2022).
NA = not applicable.

APPENDIX F. ADDITIONAL CONFOUNDING CONSIDERATIONS

F.1. SPECIFIC PFAS CONFOUNDING CONSIDERATIONS FOR FETAL GROWTH RESTRICTION

As noted, in the PFAS protocol, the potential for bias in effect estimates due to confounding is a concern in epidemiological studies and was a focus during study evaluation. Hemodynamic changes occur during pregnancy, such as increased blood plasma volume as a result of decreased mean arterial pressure, increased cardiac output, and systemic vasodilation (Sagiv et al., 2018; Sanghavi and Rutherford, 2014; Chapman et al., 1998). These changes could lead to lower PFAS levels in plasma, due to dilution and increased renal filtration. A decrease in PFAS levels has been noted in serial measurements of some PFAS during pregnancy, namely PFOA, PFOS, and PFNA (Glynn et al., 2012). These hemodynamic changes have been proposed as a potential confounder for associations between PFDA and neonatal and early childhood growth measures. This is suggested by the association between glomerular filtration rate (GFR), a marker of renal function and, indirectly, of plasma volume expansion, and fetal growth independent of gestational age and other maternal covariates (Morken et al., 2014; Gibson, 1973). Because PFDA concentration in serum is expected to decrease during pregnancy due to plasma volume expansion, increased renal excretion, and transplacental transfer, time windows earlier in pregnancy prior to this decrease may reflect the largest insult to a developing fetus. Potential confounding is one possible explanation for the effects of pregnancy hemodynamics, but in their meta-analysis of PFOA Steenland et al. (2018) also proposed that GFR may lead to reverse causality if increased fetal growth leads to increased maternal blood expansion and glomerular filtration rate. This potential source of bias related to pregnancy hemodynamics are anticipated to be of greater concern when maternal serum PFAS samples are collected later in pregnancy. Therefore, as part of the study quality evaluations, more confidence was placed in studies that adjusted for different pregnancy hemodynamic markers or if they considered this potential source of confounding by sampling PFAS levels earlier in pregnancy. As noted in the syntheses, pattern analyses of study results were also considered according to biomarker sampling timing to determine pregnancy hemodynamics may be a source of between-study heterogeneity.

Only 1 of the 22 PFDA birth weight-related studies included in the Developmental Effects section collected and analyzed maternal hemodynamic data such as GFR and/or albumin (i.e., a marker of plasma volume expansion). Gyllenhammar et al. (2018) did not find any evidence of confounding following statistical adjustment of different GFR measures for any of the PFAS examined. Outside of one study that showed some differences in PFOA results following

adjustment for albumin, the Gyllenhammar et al. (2018) results are consistent with a lack of confounding demonstrated by either adjustment for albumin (Sagiv et al., 2018) or different GFR measures (Manzano-Salgado et al., 2017; Whitworth et al., 2012) for different PFAS examined in other studies. Nonetheless, existing meta-analyses for both PFOA (Steenland et al., 2018) and PFOS (Dzierlenga et al., 2020) only detected birth weight deficits for later trimester sampling (e.g., beyond trimester one). One limitation of these meta-analyses is that they did not have the ability to differentiate late pregnancy from post-partum measures. Only 5 of the 22 PFDA studies of mean BWT in the overall population examined any first trimester measures, which precluded a more detailed examination here. Overall, there was limited evidence of any patterns of larger birth weight associations with sample timing for PFDA. However, the ability to more fully evaluate this further was limited given the available data as well as disparate exposure measures, distributions, and contrasts being examined.

F.2. PFAS COEXPOSURE STATISTICAL APPROACHES AND CONFOUNDING DIRECTIONALITY

In general, an additional source of uncertainty in epidemiological is the potential for confounding by other PFAS (and other co-occurring contaminants). Although scientific consensus on how best to address PFAS co-exposures remains elusive, this was considered in the study quality evaluations and as part of the overall weight of evidence determination. To be a confounder, the co-occurring PFAS would need to be associated with both the PFAS of interest and the outcome, but not an intermediate in the causal pathway; such PFAS would be considered positive confounders if their effect estimate with the endpoint of interest is in the same direction as the primary PFAS of interest. If positive confounders are not accounted for, the anticipation is that any resultant bias would be away from the null.

Certain statistical approaches can help address the challenges of evaluating the associations between health endpoints and numerous (often correlated) PFAS that may be present in the environment. For example, multipollutant models (i.e., those that adjust for at least one co-occurring exposure) can provide an estimate of the independent association for specific pollutants with the endpoint of interest. However, these models may not perform well when co-occurring exposures are highly correlated. Such correlation can lead to collinearity concerns and instability of modeling results. When exposures are highly correlated and additionally subject to different potential confounding factors (which may occur, e.g., when PFAS arise from different sources), co-exposure amplification bias may be a concern (Weisskopf et al., 2018). Under this scenario, estimated associations from multi-PFAS adjusted models would be subject to greater bias compared with results from single-PFAS models. A different approach is to instead 'screen' large groups of exposures to determine which are associated with the outcome of interest and important to retain in further analyses. These dimension-reducing statistical approaches (e.g., principal component analysis, penalized modeling based on elastic net regression, Bayesian kernel machine

regression, etc.) are increasingly being used for screening large groups of chemical exposures and help prioritize specific mixtures. However, as noted by Meng et al. (2018), these approaches might be better suited as "prediction models to screen for a wide range of chemicals from different sources, and the interpretation of results might become less straightforward due to the necessary standardization of exposure values." Given these interpretation difficulties and potential for co-exposure amplification bias, it is not clear which statistical approach best represents independent effects of specific pollutants within complex PFAS mixtures.

The objective of this part of the appendix is to assess whether there is any direct evidence for confounding in the studies comparing results from multipollutant (mutually adjusted for other PFAS) models and results from single pollutant (i.e., PFDA alone with other confounders adjusted for) models. A second objective is to compare relationships between co-occurring PFAS and evaluate the extent to which these PFAS may be associated with the primary endpoints of interest (e.g., birth weight-related measures).

F.3. PFDA AND PFAS COEXPOSURE STUDY RESULTS

In general, the stronger an association between coexposures, and the larger the effect sizes seen for the coexposure of interest, the more concern there would be for potential confounding. Table F-1 shows correlations between PFAS coexposures and PFDA reported from five studies with mutually adjusted PFAS data, including four *medium* confidence (Meng et al., 2018; Woods et al., 2017; Lenters et al., 2016; Robledo et al., 2015) and one *high* confidence study (Starling et al., 2017). As shown in the PFAS Systematic Review Protocol (see Appendix A) and in Table F-1, PFNA and PFDA often co-occur (as expected given some similar anticipated sources) across studies with a consistent correlation of 0.6 or higher. These results also show that other PFAS may not consistently co-occur with PFDA, as the magnitude of these relationships can vary significantly across studies.

Table F-1. PFAS correlation coefficients in mutually adjusted studies

Reference	Study Setting	Confidence	Correlations with PFDA			
			PFOS	PFOA	PFNA	PFHxS
Woods et al. (2017)	Cincinnati, Ohio, USA	Medium	0.3	0.1	0.6	0.1
Lenters et al. (2016)	Greenland; Kharkiv, Ukraine; Warsaw, Poland	Medium	0.78	0.50	0.60	0.35
Luo et al. (2021)	Guangzhou, China	High	0.68	0.13	0.85	-0.03
Meng et al. (2018)	Denmark	Medium	0.48	0.28	0.73	0.17
Robledo et al. (2015)	Michigan and Texas, USA	Medium	N/A	N/A	N/A	N/A

Starling et al. (2017)	Colorado, USA	Low	0.49	0.56	0.65	0.27

The results for the six studies based on continuous PFDA data (expressed as change in mean birth weight per unit change in exposure) are compared and summarized below in Table F-2. Three of the studies included multiple PFAS as predictors in ordinary least squares regression models (Meng et al., 2018; Woods et al., 2017; Robledo et al., 2015). Two studies (Starling et al., 2017; Lenters et al., 2016) examined multiple PFAS using elastic net regression models. Elastic net regression is a modeling approach to select independent predictors (from an initial group of potentially correlated predictors) for inclusion in the model using penalized shrinkage methods (Lenters et al., 2016). As shown in Table F-2, two of the six studies (Luo et al., 2021; Lenters et al., 2016) reported nonsignificant birth weight deficits for PFDA from single-pollutant models. However, PFDA was not associated with birth weight changes in multipollutant models for either study. For example, Lenters et al. (2016) reported null results for PFDA in both their single-pollutant model and elastic net regression model, with only PFOA retained in the latter model. Starling et al. (2017) did not report birth weight deficits associated with PFDA based on either single-pollutant or multipollutant models nor was PFDA selected for inclusion using elastic net regression. Meng et al. (2018) reported largely null results for PFDA in single-pollutant models but detected increases in mean birth weight with adjustment for PFOS, PFOA, PFNA, perfluoroheptane sulfonic acid (PFHpS), and PFHxS. Luo et al. (2021) reported large birth weight deficits (-97 g; -178, -16 per each ln-unit PFDA increase) in single-pollutant PFDA model, but results were null in the multipollutant model. Lastly, Robledo et al. (2015) did not report results from single pollutant models (or correlations) but did find birth weight deficits associated with PFDA in female neonates only.

Given the moderate and strong correlations between PDFA and other PFAS, the magnitude of any associations may exist between these co-occurring PFAS and birth-weight related measures (and other developmental effects) may inform the potential for confounding of PFDA associations. For example, Lenters et al. (2016) reported birth weight deficits associated with increased levels of PFNA (β =−44.7 g; 95%CI: −92.0, 2.7 per each 2SD ln-unit PFDA increase), PFOS (β =−68.8 g; 95%CI: −152.9, 15.2) and PFOA (β =−78.5 g; 95%CI: −137.01, −20.0) in single-pollutant models although only PFOA (β =−63.8 g; 95%CI: −122.8, −4.7) was retained in the elastic net regression model. Although birth weight deficits were not seen for PFDA in any of the regression models used by Starling et al. (2017), there were large mean birth weight deficits associated with increased exposure evaluated in single pollutant models for both PFNA (β =−58 g; 95%CI: −104, −11 per each ln-unit PFDA increase) and PFOA (β = −51 g; 95%CI: −97, −6). These deficits were larger in multipollutant models for both PFNA (β =−92 g; 95%CI: −167, −18) and PFOA (β =−70 g; 95%CI: −148, −9) but were attenuated when included in a penalized elastic net regression model (β = −33 g and −14 g, respectively). Meng et al. (2018) reported similar deficits in birth weight associated with increased exposure to PFNA (β =−54.2 g; 95%CI: −105.8, −2.7 per each $\log_2$-unit

PFDA increase) and PFOS (β =−55.5 g; 95%CI: −145.6, 34.5) in their model containing mutually adjusted PFAS; however, effects were seen in the opposite direction (increase in mean birth weight) for PFDA (β = 48.0 g; 95%CI: −0.6, 96.5) and PFOA (β = 49.5 g; 95%CI: −8.7, 107.9) in the same model. In the Woods et al. (2017) study, none of the five PFAS examined contributed greatly to the overall changes in mean birth weight when other environmental contaminants were considered in their elastic net model. Based on their multi-pollutant model, Luo et al. (2021) reported only large birth weight deficits for PFOA (in excess of -100 g for each PFDA tertile. Finally, Robledo et al. (2015) reported that only PFOA was associated with large deficits in mean birth weight (β=−61.6 g; 95%CI: −159.2, 35.9 per each SD ln-unit PFDA increase) in girls, while among boys deficits were only seen for perfluorooctane sulfonamide (PFOSA) (β =−104.2 g; 95%CI: −194.2, −14.3) and PFDA (β =−53.4 g; 95%CI: −161.0, 54.2). In contrast, increased birth weight in boys was reported for PFNA (β = 62.7 g; 95%CI: −32.1, 157.4) and PFOS (β = 38 g; 95%CI: −73.5, 148.5).

In the six studies using mutually adjusted PFAS approaches to address coexposures, there was not consistent evidence for birth weight deficits associated with increased exposure to PFDA. Among the five studies that examined both single and multipollutant models, none of studies that showed birth weight deficits in single-pollutant models reported greater or more precise associations following statistical adjustment for other PFAS. Of the three studies showing some adverse effects (Luo et al., 2021; Lenters et al., 2016; Robledo et al., 2015), only one (Robledo et al., 2015) showed deficits in multipollutant models and this was limited to females only. Among the three studies that provided correlations among co-occurring PFAS and showed some evidence of adverse effects for any PFAS, the largest birth weight deficits were seen for PFNA (Meng et al., 2018; Starling et al., 2017), PFOA (Robledo et al., 2015), and PFOS (Luo et al., 2021). The correlation coefficients for PFDA and these three co-exposures across these studies were all at least 0.50.

As noted in the Developmental Effects section, 11 of 22 studies showed evidence of some associations with PFDA and mean birth weight in the overall population. Among these 11 studies, which included the 3 highlighted above (Luo et al., 2021; Lenters et al., 2016; Robledo et al., 2015), 7 showed deficits comparable in magnitude for PFNA and PFDA. Two studies showed larger deficits for PFDA compared to PFNA, and three studies showed larger deficits for PFNA compared to PFDA. Given these comparable results seen in most of these studies for both PFNA and PFDA and the moderately high correlations consistently reported between PFDA and PFNA, there is considerable uncertainty due to potential confounding by co-occurring PFAS in the existing literature. It remains unclear, however, if the consistency of birth weight deficits demonstrated from (categorical and continuous) results in the full set of 22 mean birth weight PFDA studies could be fully attributed to confounding by PFAS coexposures.

Table F-2. Impact of coexposure adjustment on estimated change in mean birth weight per unit change (ng/mL) in PFDA levels[a]

Reference	Study Confidence	Single PFAS Model Results (in grams) with 95%CIs[a]	Multi-PFAS Results (in grams) with 95%CIs[a]	Elastic Net Regression Results	Exposure Comparison[b]	Effect of adjustment on PFDA birth weight results	PFAS adjustments
Starling et al. (2017)	High	11.5 (−37.3, 60.4)	97.5 (31.5, 163.6)	15.7	ln-unit (ng/mL) increase	Slightly Strengthened	PFOS, PFOA, PFNA, PFHxS
Lenters et al. (2016)	Medium	−43.9 (−104.8, 17.0)	N/A	N/S	2 SD ln-unit (ng/mL) increase	Attenuated	PFOS, PFOA, PFNA, PFUnDA, PFDoDA, PFHxS
Luo et al. (2021)	High	−96.8 (−178.0, −15.5)	6.6 (95%CI: -84.2, 97.3)[b]	N/A	ln-unit () increase	Attenuated	PFOA, PFOS, PFBA, PFBS, PFHxS, PFNA, PFUnDA, PFDoDA, PFTrDA, 6:2 Cl-PFESA, 8:2 Cl-PFESA
Meng et al. (2018)	Medium	−9.0 (−43.2, 35.2)	48.0 (−0.6, 96.5)	N/A	log_2-unit (ng/mL) increase	Changed from Null to Positive	PFOS, PFOA, PFNA, PFHxS, PFHpS
Robledo et al. (2015)	Medium	N/A	−53.4 (−161.0, 54.2) Girls −1.8 (−90.6, 87.1) Boys[c]	N/A	1 SD ln-unit (ng/mL) increase	N/A	PFOA, PFOS, PFNA, PFOSA, Et-PFOSA-AcOH, Me-PFOSA-AcOH
Woods et al. (2017)	Medium	−12.6 (−56.8, 40.4)[d]	N/A	N/S	log_{10} unit (ng/mL) increase	Attenuated	PFOS, PFOA, PFNA, PFUnDA, PFDoDA, PFHxS

Abbreviations: N/A: Not available; N/S: PFAS not selected in elastic net regression model.

[a]Models were based on ordinary least squares regression.

[b]Beta and 95%CIs estimated from Figure 3 of (Luo et al., 2021).

[c]The birth weight results tabulated here are all for the overall population (i.e., male, and female neonates combined), except for Robledo, which only reported sex-specific findings.

[d]The Posterior 95% credible intervals reported for Woods et al. (2017) based on a Bayesian hierarchical linear model.

APPENDIX G. DETAILED PHARMACOKINETIC ANALYSES

This appendix provides two detailed pharmacokinetic analyses. The first is a Bayesian analysis of PFDA pharmacokinetics in laboratory animals to estimate key pharmacokinetic parameters. The second is the description and evaluation of a one-compartment PK modeling approach for estimating internal doses, evaluated against rat PFDA PK data using the mean parameter values estimated for male rats in the Bayesian estimation.

G.1. PARTIAL POOLING OF PFDA PHARMACOKINETIC DATA FOR HIERARCHICAL BAYESIAN ANALYSIS

We estimated the sex-specific pharmacokinetic parameters (half-life, volume of distribution, and clearance) of PFDA in rats by fitting one- and two-compartment models to the available concentration vs. time data. A Bayesian hierarchical methodology was developed to fit these models because of the need to pool time-course concentration data across numerous studies with varying exposure scenarios within each study. This allowed for each concentration vs. time dataset to be fit to each pharmacokinetic model where fitted parameters for each dataset are sampled from a population-level distribution which models the similarities between each dataset. In addition, the Bayesian analysis allowed for the generation of central estimates and credible intervals for the pharmacokinetic parameter of interest e.g., half-life, volume of distribution and clearance, using posterior distributions from the estimated variables. Finally, the Bayesian methodology allowed for hypothesis testing of the 1- and 2-compartment formulations to decide which model more appropriately fit the data.

G.1.1. Pharmacokinetic model

To determine pharmacokinetic parameters for PFDA, we estimated constants for both one- and two-compartment model assumptions. For a one-compartment model assumption, the following exponential decay functions were fit to the available data

$$C_{1-cmpt}^{IV}(t) = \frac{D}{V} e^{-k_e t}$$

$$C_{1-cmpt}^{oral}(t) = \frac{D}{V}\left(\frac{k_a}{k_a - k_e}\right)(e^{-k_e t} - e^{-k_a t})$$

where D represents the administered dose and V, k_e, and k_a represent the central compartment volume, elimination constant, and absorption constant (for oral only) to be fit. From these fitted constants, pharmacokinetic parameters are derived:

$$V_d = \frac{V}{BW}$$

$$t_{\frac{1}{2}} = \frac{\ln 2}{k_e}$$

$$CLC = V_d * k_e$$

where V_d, $t_{1/2}$, and CLC represent the volume of distribution, terminal half-life, and clearance respectively and BW represents the animal body weight.

For the two-compartment model assumption, the following exponential decay functions were fit to available data

$$A^{IV} = \frac{\alpha - k_{dc}}{\alpha - \beta};\ A^{oral} = k_a\left(\frac{k_{dc} - \alpha}{(k_a - \alpha)(\beta - \alpha)}\right)$$

$$B^{IV} = \frac{\beta - k_{dc}}{\beta - \alpha};\ B^{oral} = k_a\left(\frac{k_{dc} - \beta}{(k_a - \beta)(\alpha - \beta)}\right)$$

$$C^{IV}_{2-cmpt}(t) = \frac{D}{V}\left(A^{IV}e^{-\alpha t} + B^{IV}e^{-\beta t}\right)$$

$$C^{oral}_{2-cmpt}(t) = \frac{D}{V}\left(A^{oral}e^{-\alpha t} + B^{oral}e^{-\beta t} - (A^{oral} + B^{oral})e^{-k_a t}\right)$$

where D represents the administered dose and V, α, β, k_{dc}, and k_a represent central compartment volume, alpha-phase elimination constant, beta-phase elimination constant, deep-to-central compartment rate constant, and absorption constant (for oral only) to be fit. From these fitted constants, the remaining two-compartment constants (k_{cd}: central-to-deep compartment rate constant and k_e: elimination constant) and the deep compartment volume (V_{deep}) are derived by solving:

$$\alpha + \beta = k_{cd} + k_{dc} + k_e$$

$$\alpha * \beta = k_{dc} * k_e$$

$$V_d = V\frac{k_{cd}}{k_{dc}}$$

which allows for the desired pharmacokinetic parameters to be derived using the following equations:

$$V_{d-ss} = \frac{V + V_{deep}}{BW} = \frac{V}{BW}\left(\frac{k_{cd} + k_{dc}}{k_{dc}}\right)$$

$$t_{\frac{1}{2}} = \frac{\ln 2}{\beta}$$

$$CLC = \frac{V}{BW} * k_e$$

where $V_{d\text{-}ss}$, $t_{1/2}$, and CLC represent the steady-state volume of distribution, terminal half-life, and clearance respectively and BW represents the animal body weight.

G.1.2. Bayesian inference

The fitted constants for each model structure (described above) were estimated using available time-course concentration data reported in rats with parameters for each model estimated using a hierarchical Bayesian calibration approach. This hierarchical Bayesian approach pooled the time-course concentration data for male and female rats from multiple studies Ohmori et al. (2003), Kim et al. (2019), Dzierlenga et al. (2019). For the two-compartment model, to ensure parameter identifiability, α and β were constrained to be ordered such that $\alpha > \beta$. This constraint ensures the exponential terms are identifiable and don't "flip" while exploring the parameter space during Markov-chain Monte-Carlo (MCMC) sampling. Finally, priors for each pharmacokinetic parameter were chosen to be "weakly informative" based on prior knowledge of PFAS pharmacokinetics (ATSDR, 2021) with 95% equal-tailed intervals spanning multiple order of magnitude.

Priors for pharmacokinetic parameters are presented in Table G-1 with corresponding model-specific parameter prior distributions presented below. Finally, a sensitivity analysis on the model priors is shown in the *Prior sensitivity analysis* section.

Table G-1. Weakly informed prior distributions for pharmacokinetic parameters used in the Bayesian analysis

	median	mad	eti_3%	eti_97%
Half-life (d)	15	12	0.88	250
Clearance (mL/kg-d)	50	49	0.32	6,000
Vd-ss (ml/kg)	900	811	9.3	32,822

For the hierarchical approach, the concentration vs. time data comprised a population- and dataset-level for which model parameters were estimated. Here, each dataset represented each study/sex/dose concentration vs. time dataset extracted from the literature and were fit using the model

$$C_{ij} = \begin{cases} C_{1-cmpt}^{route} & \text{for 1-compartment model,} \\ C_{2-cmpt}^{route} & \text{for 2-compartment model} \end{cases}$$

$$C_{ik} \sim LN(\bar{x}_{ij}, \tilde{\sigma}_k)$$

where $\bar{x}_{ij}$ is the sample mean of the observed concentrations at time t_{ij} for dataset j and $\tilde{\sigma}_k$ is study-level log-transformed standard deviation for the relative errors based on study k. Study-level priors for $\tilde{\sigma}_k$ were determined using the average log-transformed standard deviations

$$\bar{\sigma}_{i,j}^2 = \ln\left(1 + \frac{s_{i,j}^2}{\bar{x}_{i,j}^2}\right)$$

$$\gamma_k = \frac{\sum_i \bar{\sigma}_{i,j\in k}}{n_k}$$

where $s_{i,j}$ is the sample standard deviation on the observed concentrations at time $t_{i,j}$ for study k. If s_{ij} was available, $\bar{\sigma}_{i,j}$ is the log-transformed standard deviation using the sample mean and standard deviation. For studies where sample standard deviations could not be extracted, an average of all log-transformed standard deviations was used. This allowed for study-level prior distributions on the error model log-transformed standard deviation:

$$\tilde{\sigma}_k \sim \begin{cases} \text{Exp}\left(1/\gamma_k\right) & \text{if } \gamma_k \text{ available,} \\ \text{Exp}\left(1/\gamma\right) & \text{otherwise.} \end{cases}$$

Using this model, dataset-level fitted constants were assigned priors based on a non-centered parameterization of a population-level distribution. This reparameterization of a typical hierarchical Bayesian model allows for increased sampling efficiency and can be more efficient for sampling when there is limited data (Betancourt and Girolami, 2013). Finally, non-elimination rate constants (k_a and k_{dc}) were assigned a unit normal, weakly informative prior to aid parameter identifiability (Gelman et al., 2015).

$$\ln \mu_{k_a} \sim N(0,1)$$

$$\ln \mu_V \sim N(0,1)$$

$$\ln \mu_{k_e} \sim N(-3,1.5) \; one\; compartment\; model$$

$$\ln \mu_{k_{dc}} \sim N(0,1) \text{ two compartment model}$$

$$\ln \mu_{\alpha,\beta} \sim N(-3,1.5), \mu_\beta < \mu_\alpha \; two\; compartment\; model$$

$$\sigma_{k_a,V,k_e,\alpha,\beta,k_{dc}} \sim \text{Exp}(3)$$

$$\ln(k_a, V, k_e, \alpha, \beta, k_{dc})_j \sim N\left(\mu_{k_a,V,k_e,\alpha,\beta,k_{dc}}, \sigma_{k_a,V,k_e,\alpha,\beta,k_{dc}}\right)$$

One- and two-compartment model goodness of fits were compared using the widely applicable information criteria (WAIC). Pharmacokinetic parameters from the most appropriate model, as judged by the WAIC comparison, were reported. To estimate the population-level pharmacokinetic parameters we examined posterior probability densities of the parameters from the WAIC-determined model and calculated distributional estimates of the half-life, volume of distribution, and clearance using the equations described above. The parameter space was sampled using PyMC (Salvatier et al., 2016) using four independent Markov chains run for 10,000 iterations

per chain. Posterior parameter distributions were determined using the final 5,000 iterations of each chain ensuring an effective sample size (ESS) greater than 10,000 (Kruschke, 2021). Convergence was assessed using a potential scale reduction factor with a maximum threshold of $\hat{R} = 1.05$ (Kruschke, 2021).

G.1.3. Prior sensitivity analysis

To investigate the impact of prior selection on posterior pharmacokinetic parameter estimation, we conducted a sensitivity analysis on the priors used in the Bayesian analysis. Priors were classified into three categories: weakly informed, broad, and uninformed. Weakly informed priors are defined using the half-life, clearance, and volume of distribution described above based on reported ranges of PFDA pharmacokinetics with a prior predictive check demonstrating available data for fitting fall within the prior 90% credible interval.

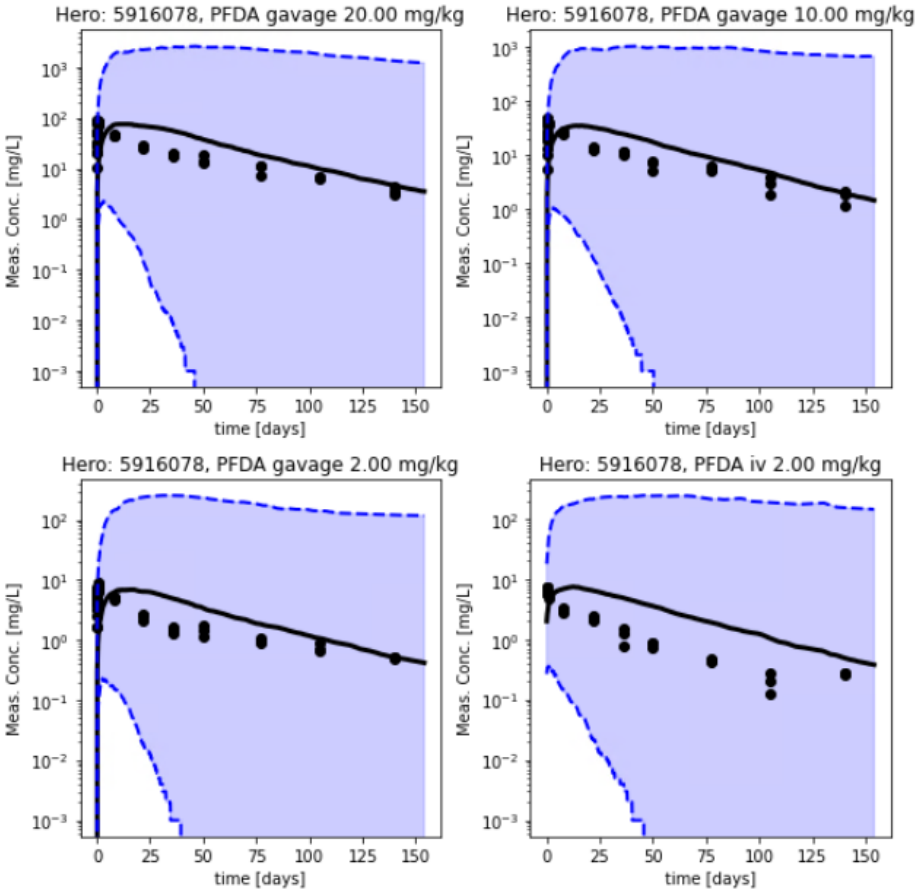

Figure G-1. Prior predictive check to ensure equal-tailed interval from prior distributions encompass the available time-course concentration data for fitting.

In addition to these weakly informed priors, we also characterized a set of broad priors, defined as uniform distributions spanning the 3% and 97% ETI from the weakly informed priors,

and completely uninformed priors, representing uniform priors spanning multiple orders of magnitude i.e., flat priors. Figure G-2 (prior sensitivity) compares these three classes of priors and their impact on the posterior pharmacokinetic parameter distributions,

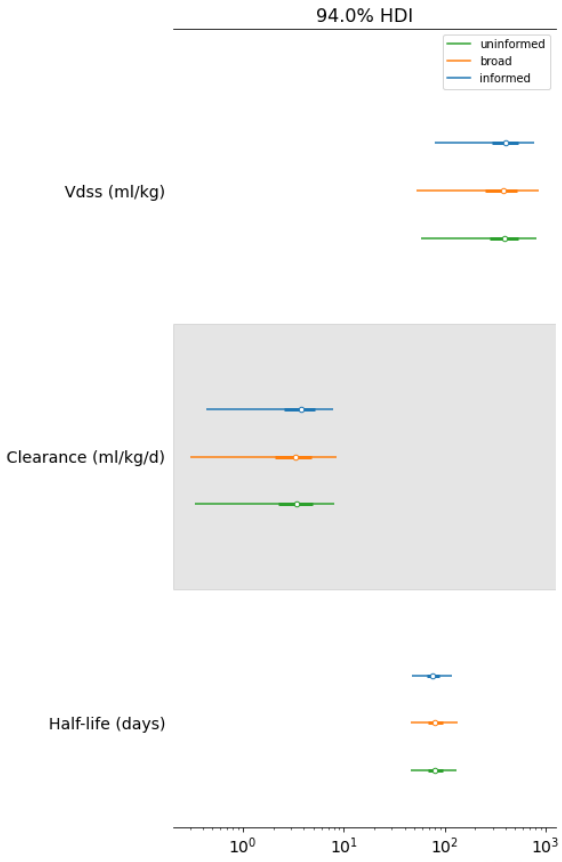

Figure G-2. Prior sensitivity on half-life, steady-state volume of distribution, and clearance to ensure weakly informed priors do not bias posterior distributions of the pharmacokinetic parameters.

Based on these findings, we used the weakly informed pharmacokinetic priors for fitting available time-course concentration data.

G.1.4. Study-specific Clearance Values and Model Fits

Three data sets were used for the sex-specific parameter estimation, which had a mixture of gavage and iv exposure routes and follow-up times extending up to 150 days (Dzierlenga et al., 2019; Kim et al., 2019; Ohmori et al., 2003). The sex-specific clearance value distribution obtained from fitting the three data sets together had a mean and 90% credible interval of 4.06 (2.05–6.05) mL/kg-day in female rats and 4.14 (0.68–7.02) mL/kg-day in male rats. For these data, a 2-compartment PK model was deemed superior. Visual inspection shows some of the data have a distinguishable distribution and excretion phase, which is appropriate for a 2-compartment model (see Figure G-3). A 2-compartment model is also able to fit data that appear linear as is evidenced in

fits to other data sets (see Figure G-4). Credible intervals for the fits to individual data sets are qualitatively small showing good model fits to the data from individual studies. The relatively large credible interval for the pooled data is due to the large variation between studies. For example, in male rats the mean clearance values for individual studies ranged from 1.51 to 7.45 mL/kg-day, and a similar range was seen in female rats.

Trends comparing the terminal clearance following IV and gavages doses appeared within studies but did not hold for the whole data set. For example, in Kim et al. (2019) IV doses resulted in smaller, but similar clearance to gavage doses (see Figure G-4). However, these clearance values were consistently smaller than clearance values calculated from the two other data sets. In the analysis of the Dzierlenga et al. (2019) dataset, IV doses resulted in clearly greater clearance than the three dose levels administered by gavage, which all had similar clearance within each sex (see Figure G-5,6). There was a difference in clearance between sexes in this study, but only for gavage doses. In this study, the gavage doses resulted in mean clearance values between 3.57 and 3.77 mL/kg-day in female rats and 5.12 and 5.74 mL/kg-day in male rats. However, the clearance calculated from the single IV dose was similar between female and male rats. Likewise, the two other studies showed similar mean clearance values for male and female rats (see Figure G-3 and Figure G-4). It is possible that most of the difference in PFDA PK between male and female rats is related to a difference in absorption, which can be moderated by active transport. Additional experiments designed to carefully evaluate these factors would be needed to resolve this question.

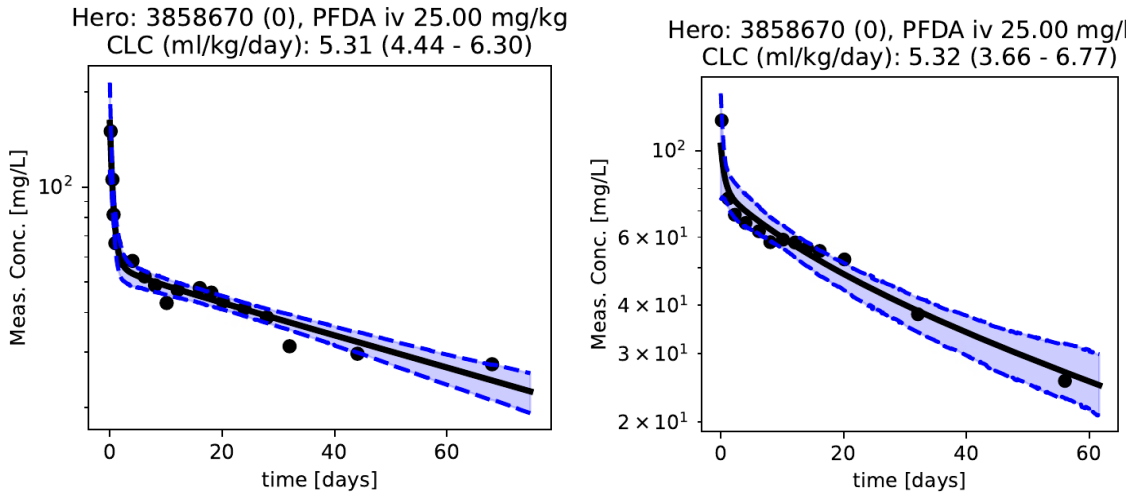

Figure G-3. Predicted (black line with blue 90% credible interval) and observed (black circles) serum time-courses for female (left) and male (right) rats after a 25 mg/kg IV bolus of PFDA. Observed data from (Ohmori et al., 2003).

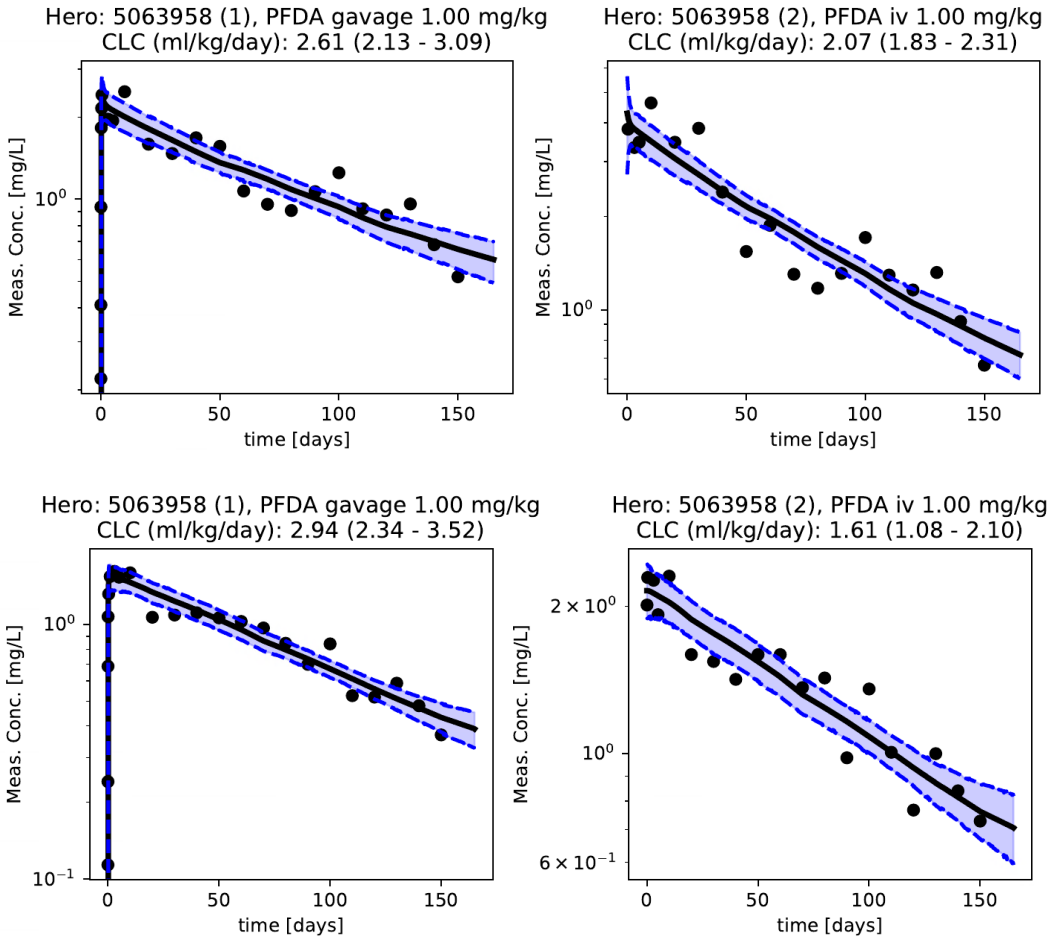

Figure G-4. Predicted (black line with blue 90% credible interval) and observed (black circles) serum time-courses for female (top 2 panels) and male (bottom 2 panels) rats after a 1 mg/kg gavage or IV bolus of PFDA. Gavage exposures are on the left, while IV exposures are on the left, while IV exposures are on the right. Observed data from (Kim et al., 2019).

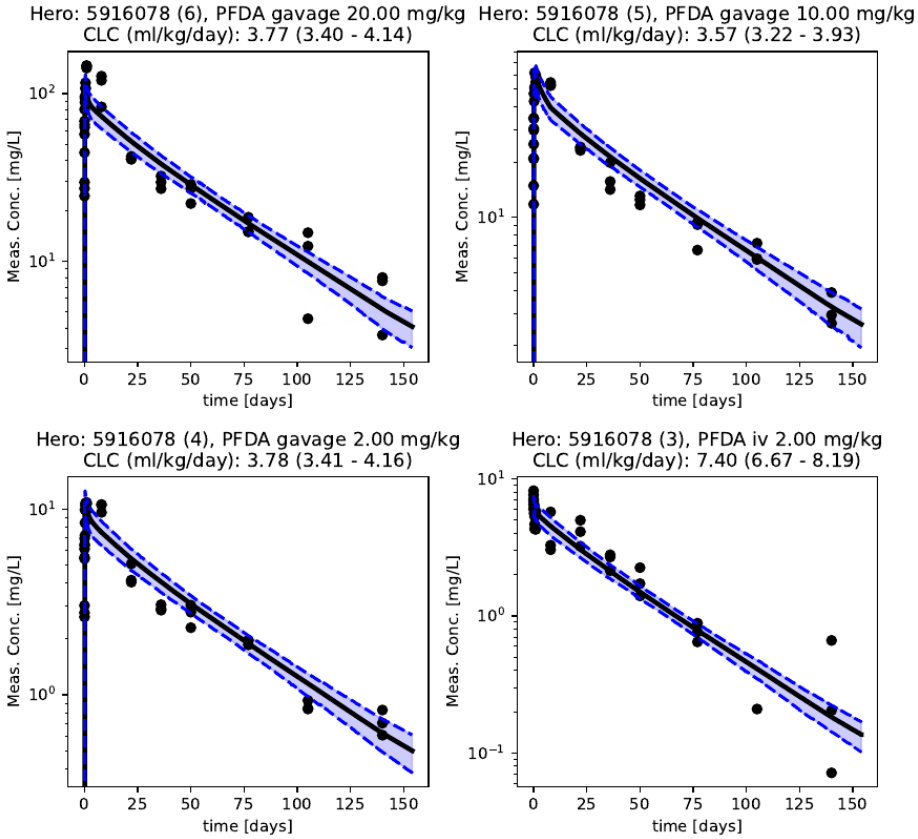

Figure G-5. Predicted (black line with blue 90% credible interval) and observed (black circles) serum time-courses for female rats after a 2 mg/kg IV or 2, 10, or 20 mg/kg gavage bolus of PFDA. Observed data from (Dzierlenga et al., 2019).

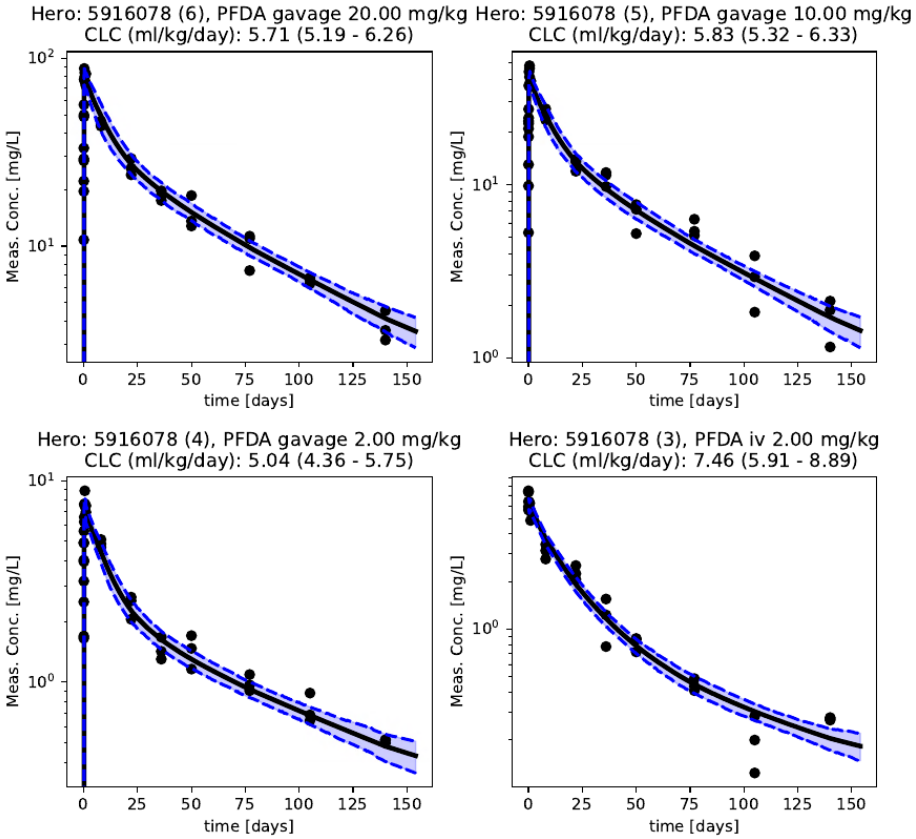

Figure G-6. Predicted (black line with blue 90% credible interval) and observed (black circles) serum time-courses for male rats after a 2 mg/kg IV or 2, 10, or 20 mg/kg gavage bolus of PFDA. Observed data from (Dzierlenga et al., 2019).

G.2. DESCRIPTION AND EVALUATION OF A SINGLE-COMPARTMENT PK APPROACH

For PFDA, the clearance values obtained in the preceding Bayesian analysis are low enough that internal doses will not reach steady-state for shorter-term studies, in particular for developmental studies where dosing may only be for a few weeks. In this case a PK model can potentially be used to account for the growth of the animal, the intrinsic elimination, and the accumulation of PFDA over the period of dosing. The single-compartment PK model is given by:

$$dA/dt = F_{abs} \times dose \times BW - CL_{tot} \times A / Vd, \quad \text{(G-1)}$$

where A is the total amount of PFDA in the animal (mg), F_{abs} is the fraction absorbed for an oral dose (bioavailability), BW is the body-weight (kg), and CL_{tot} is the total clearance, and Vd is the volume of distribution. Implicit in this model is an assumption of rapid distribution of PFDA in the body (relative to the clearance), in which case the concentration in plasma is:

$$C_{plasma} = A/ (Vd \times BW). \quad \text{(G-2)}$$

The differential equation for the amount of chemical in the body can then be re-written:

$$dA/dt = F_{abs} \times dose \times BW - CL_{tot} \times BW \times C_{plasma}, \quad \text{(G-3)}$$

which leads to the interpretation that the clearance or volume of blood cleared of the chemical per unit time per kg BW is CL_{tot}.

While F_{abs} is shown in equations (G-1) and (G-3) for completeness, the available data could not be used to identify a value for F_{abs} independent of other parameters in the Bayesian PK analysis and given the observations of generally high uptake (see the section on Absorption in the Toxicological Review) it was set to a value of 1 (i.e., 100%) for this analysis, and hence is not included in the subsequent description.

PK parameters for rats (CL_{tot}, and Vd) are taken from the preceding Bayesian analysis (values listed in Table 3-3). Given the slow clearance of PFDA, the growth of rats during toxicity studies lasting multiple weeks can be a significant factor as increases in BW dilute the body burden from earlier exposures. The highest doses tested in the NTP bioassay significantly reduced animal BW, which compounds this effect. Therefore, time-dependence in BW based on the empirical data for BW at the doses evaluated was incorporated into the model evaluation, to account for this time- and dose-dependence. For illustration, the change in male rat BW observed in the NTP bioassay (28-day exposure (NTP, 2018)) is shown in Figure G-7. Doses of 0.625 mg/kg-day and below did not significantly affect BW gain during the bioassay, but higher dose levels caused a significant decline after 7 days of exposure.

The internal dose of PFDA predicted by the PK model as a function of exposure day, normalized to the dose for comparison, is shown in Figure G-8. For example, the model simulated concentrations obtained using a dose of 0.625 mg/kg-day were divided by 0.625 before plotting. If the BW curve was the same for all doses, all the resulting normalized curves would lie on top of each other. The predicted concentration increases steadily throughout the study for all dose levels, showing no sign of saturation. However, the increase in animals receiving the highest doses becomes relatively faster after day 7, deflecting above the lower-dose curves. This occurs because the decreasing BW at these doses concentrates the PFDA already administered into a smaller total animal mass. For model simulations the dose is assumed to be adjusted continuously based on the interpolated weights as shown in Figure 3-3. (The study report states that animals were weighed daily, but only weekly values are provided there.) For example, if an animal loses weight between day 7 and 21, the daily dose is assumed to be adjusted accordingly. Since the animals were necropsied on day 29, 1 day after the final dose, the model simulations include a final day with zero exposure. Mean serum PFDA concentrations from the NTP study, collected at time of necropsy, are shown for comparison.

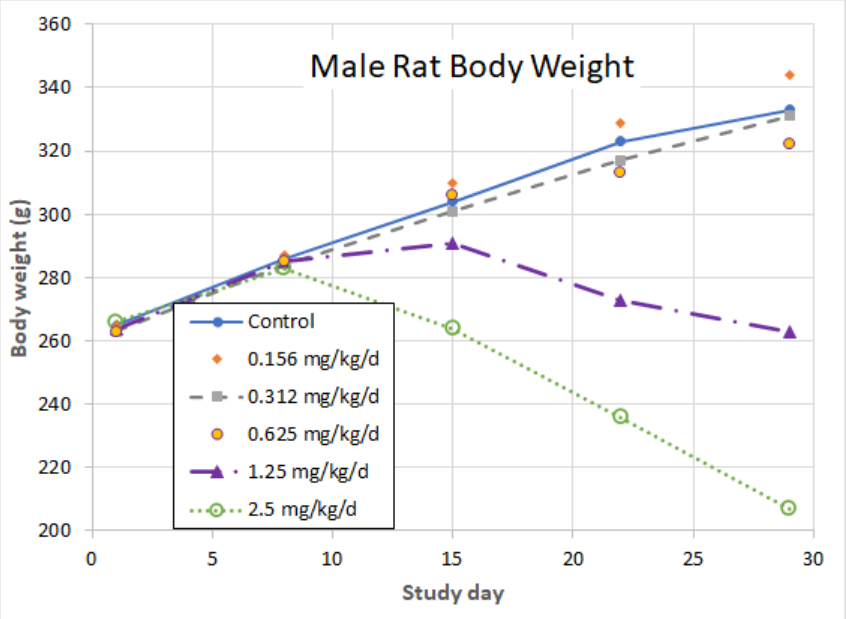

Figure G-7. Male rat body weight changes during 28-day PFDA bioassay (NTP, 2018). Data sets are identified by the dose (mg/kg-d).

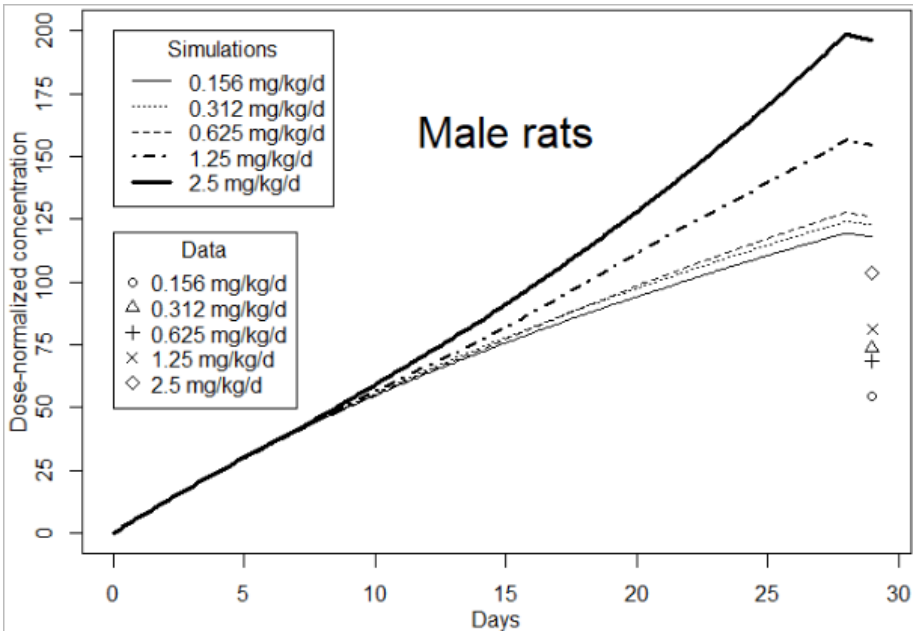

Figure G-8. Predicted accumulation and observed end-of-study of PFDA in male rats in the NTP bioassay (NTP, 2018) as a function of dose. Predicted and measured concentrations (mg/L) were normalized to respective doses (mg/kg-d).

In Figure G-8 the model consistently over-predicts the data by a factor of about 1.5. While the EPA general considers this much discrepancy acceptable for a comparison of PK model predictions to data, the fact that there is systematic bias, rather than some predictions being above and some below the data raises concern. The direction of the error indicates that the model will

over-predict internal doses in rats, and hence the corresponding HEDs. One might also note that the data point for 0.625 mg/kg-day is less than that for 0.312 mg/kg-day, whereas the model simulations show only increasing normalized concentration with dose. The pattern in the data (which points are more closely clustered vs. farther apart) is a bit different from that predicted by the model. To further evaluate the extent of nonlinearity, the end-of-study plasma concentrations from NTP (2018) are plotted against the dose in Figure G-9. The exposure-dose relationship is seen to be essentially linear for the three lowest doses (to 0.625 mg/kg-day), with some variation, and then to increase a bit faster than linear with dose above that. As indicated by the BW data in Figure G-7 and resulting simulations in Figure G-8, this upward inflection could be due to dose-related BW loses, which are predicted to concentrate the previously administered PFDA into a smaller total volume. However, there is no evidence of saturation of renal resorption, which would result in downward curvature in the exposure-dose relationship. Instead, the discrepancy between the NTP data and the model simulations can be mostly explained if rat clearance is about three times higher than estimated from the PK studies.

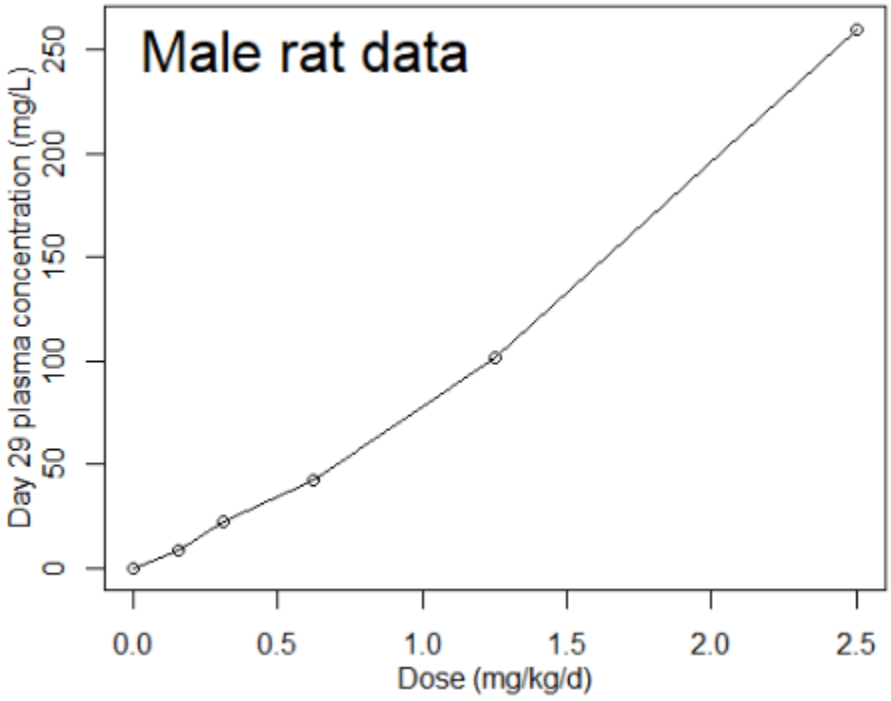

Figure G-9. Measured end-of-study of PFDA in male rats in the NTP bioassay (NTP, 2018) as a function of dose.

APPENDIX H. SUMMARY OF PUBLIC AND EXTERNAL PEER REVIEW COMMENTS AND EPA'S DISPOSITION

1

APPENDIX I. QUALITY ASSURANCE FOR THE IRIS TOXICOLOGICAL REVIEW OF PERFLUORODECANOIC ACID AND RELATED SALTS

This assessment is prepared under the auspices of the U.S. Environmental Protection Agency's (EPA's) Integrated Risk Information System (IRIS) Program. The IRIS Program is housed within the Office of Research and Development (ORD) in the Center for Public Health and Environmental Assessment (CPHEA). EPA has an agency-wide quality assurance (QA) policy that is outlined in the *EPA Quality Manual for Environmental Programs* (see CIO 2105-P-01.1) and follows the specifications outlined in EPA Order CIO 2105.1.

As required by CIO 2105.1, ORD maintains a Quality Management Program, which is documented in an internal Quality Management Plan (QMP). The latest version was developed in 2013 using Guidance for Developing Quality Systems for Environmental Programs (QA/G-1). An NCEA/CPHEA-specific QMP was also developed in 2013 as an appendix to the ORD QMP. Quality assurance for products developed within CPHEA is managed under the ORD QMP and applicable appendices.

The IRIS Toxicological Review of Perfluorodecanoic acid (PFDA) is designated as Influential Scientific Information (ISI) and is classified as QA Category A. Category A designations require reporting of all critical QA activities, including audits. The development of IRIS assessments is done through a seven-step process. Documentation of this process is available on the IRIS website: https://www.epa.gov/iris/basic-information-about-integrated-risk-information-system#process.

Specific management of quality assurance within the IRIS Program is documented in a Programmatic Quality Assurance Project Plan (PQAPP). A PQAPP is developed using the EPA Guidance for Quality Assurance Project Plans (QA/G-5). All IRIS assessments follow the IRIS PQAPP, and all assessment leads and team members are required to receive QA training on the IRIS PQAPP. During assessment development, additional QAPPs may be applied for quality assurance management. They include:

Title	Document number	Date
Program Quality Assurance Project Plan (PQAPP) for the Integrated Risk Information System (IRIS) Program	L-CPAD-0030729-QP-1-5	June 2022
An Umbrella Quality Assurance Project Plan (QAPP) for Dosimetry and Mechanism-Based Models (PBPK)	L-CPAD-0032188-QP-1-2	December 2020

Quality Assurance Project Plan (QAPP) for Enhancements to Benchmark Dose Software (BMDS)	L-HEEAD-0032189-QP-1-2	October 2020
Umbrella Quality Assurance Project Plan for CPHEA PFAS Toxicity Assessments	L-CPAD-0031652-QP-1-5	February 2023

During assessment development, this project undergoes four quality audits during assessment development including:

Date	Type of audit	Major findings	Actions taken
August 2019	Technical system audit	None	None
August 2020	Technical system audit	None	None
July 2021	Technical system audit	None	None
August 2022	Technical system audit	None	None

During Step 3 and Step 6 of the IRIS process, the IRIS toxicological review is subjected to external reviews by other federal agency partners, including the Executive Offices of the White House. Comments during these IRIS process steps are available in the Docket EPA-HQ-ORD-2019-0287 on http://www.regulations.gov.

REFERENCES

Abe, T; Takahashi, M; Kano, M; Amaike, Y; Ishii, C; Maeda, K; Kudoh, Y; Morishita, T; Hosaka, T; Sasaki, T; Kodama, S; Matsuzawa, A; Kojima, H; Yoshinari, K. (2017). Activation of nuclear receptor CAR by an environmental pollutant perfluorooctanoic acid. Arch Toxicol 91: 2365-2374. http://dx.doi.org/10.1007/s00204-016-1888-3.

Adinehzadeh, M; Reo, NV. (1998). Effects of peroxisome proliferators on rat liver phospholipids: sphingomyelin degradation may be involved in hepatotoxic mechanism of perfluorodecanoic acid. Chem Res Toxicol 11: 428-440. http://dx.doi.org/10.1021/tx970155t.

Adinehzadeh, M; Reo, NV; Jarnot, BM; Taylor, CA; Mattie, DR. (1999). Dose-response hapatotoxicity of the peroxisome proliferator, perfluorodecanoic acid and the relationship to phospholipid metabolism in rats. Toxicology 134: 179-195. http://dx.doi.org/10.1016/S0300-483X(99)00038-4.

Al Sharif, M; Alov, P; Vitcheva, V; Pajeva, I; Tsakovska, I. (2014). Modes-of-action related to repeated dose toxicity: tissue-specific biological roles of PPAR γ ligand-dependent dysregulation in nonalcoholic fatty liver disease [Review]. PPAR Research 2014: 432647. http://dx.doi.org/10.1155/2014/432647.

Angrish, MM; Kaiser, JP; Mcqueen, CA; Chorley, BN. (2016). Tipping the balance: Hepatotoxicity and the 4 apical key events of hepatic steatosis [Review]. Toxicol Sci 150: 261-268. http://dx.doi.org/10.1093/toxsci/kfw018.

Arand, M; Coughtrie, MW; Burchell, B; Oesch, F; Robertson, LW. (1991). Selective induction of bilirubin UDP-glucuronosyl-transferase by perfluorodecanoic acid. Chem Biol Interact 77: 97-105. http://dx.doi.org/10.1016/0009-2797(91)90008-U.

ATSDR (Agency for Toxic Substances and Disease Registry). (2018). Toxicological profile for perfluoroalkyls. Draft for public comment [ATSDR Tox Profile]. Atlanta, GA: U.S. Department of Health and Human Services, Centers for Disease Control and Prevention. https://www.atsdr.cdc.gov/toxprofiles/tp200.pdf.

ATSDR (Agency for Toxic Substances and Disease Registry). (2021). Toxicological profile for perfluoroalkyls [ATSDR Tox Profile]. Atlanta, GA: U.S. Department of Health and Human Services, Public Health Service. http://dx.doi.org/10.15620/cdc:59198.

Barish, GD; Narkar, VA; Evans, RM. (2006). PPAR delta: a dagger in the heart of the metabolic syndrome. J Clin Invest 116: 590-597. http://dx.doi.org/10.1172/JCI27955.

Betancourt, MJ; Girolami, M. (2013). Hamiltonian monte carlo for hierarchical models. Betancourt, MJ; Girolami, M. http://dx.doi.org/10.48550/arXiv.1312.0906.

Boobis, AR; Doe, JE; Heinrich-Hirsch, B; Meek, ME; Munn, S; Ruchirawat, M; Schlatter, J; Seed, J; Vickers, C. (2008). IPCS framework for analyzing the relevance of a noncancer mode of action for humans [Review]. Crit Rev Toxicol 38: 87-96. http://dx.doi.org/10.1080/10408440701749421.

Borges, T; Glauert, HP; Chen, LC; Chow, CK; Robertson, LW. (1990). Effect of the peroxisome proliferator perfluorodecanoic acid on growth and lipid metabolism in Sprague Dawley rats fed three dietary levels of selenium. Arch Toxicol 64: 26-30. http://dx.doi.org/10.1007/BF01973372.

Borges, T; Glauert, HP; Robertson, LW. (1993). Perfluorodecanoic acid noncompetitively inhibits the peroxisomal enzymes enoyl-CoA hydratase and 3-hydroxyacyl-CoA dehydrogenase. Toxicol Appl Pharmacol 118: 8-15. http://dx.doi.org/10.1006/taap.1993.1003.

Borges, T; Robertson, LW; Peterson, RE; Glauert, HP. (1992). Dose-related effects of perfluorodecanoic acid on growth, feed intake and hepatic peroxisomal beta-oxidation. Arch Toxicol 66: 18-22. http://dx.doi.org/10.1007/BF02307265.

Brewster, DW; Birnbaum, LS. (1989). The biochemical toxicity of perfluorodecanoic acid in the mouse is different from that of 2,3,7,8-tetrachlorodibenzo-p-dioxin. Toxicol Appl Pharmacol 99: 544-554. http://dx.doi.org/10.1016/0041-008X(89)90161-0.

Budtz-Jørgensen, E; Grandjean, P. (2018a). Application of benchmark analysis for mixed contaminant exposures: Mutual adjustment of perfluoroalkylate substances associated with immunotoxicity. PLoS ONE 13: e0205388. http://dx.doi.org/10.1371/journal.pone.0205388.

Budtz-Jørgensen, E; Grandjean, P. (2018b). Computational details for the paper "Application of benchmark analysis for mixed contaminant exposures: Mutual adjustment of perfluoroalkylate substances associated with immunotoxicity".

Buhrke, T; Kibellus, A; Lampen, A. (2013). In vitro toxicological characterization of perfluorinated carboxylic acids with different carbon chain lengths. Toxicol Lett 218: 97-104. http://dx.doi.org/10.1016/j.toxlet.2013.01.025.

Butenhoff, JL; Bjork, JA; Chang, SC; Ehresman, DJ; Parker, GA; Das, K; Lau, C; Lieder, PH; van Otterdijk, FM; Wallace, KB. (2012). Toxicological evaluation of ammonium perfluorobutyrate in rats: twenty-eight-day and ninety-day oral gavage studies. Reprod Toxicol 33: 513-530. http://dx.doi.org/10.1016/j.reprotox.2011.08.004.

Cai, Y; Appelkvist, EL; Depierre, JW. (1995). Hepatic oxidative stress and related defenses during treatment of mice with acetylsalicylic acid and other peroxisome proliferators. J Biochem Toxicol 10: 87-94. http://dx.doi.org/10.1002/jbt.2570100205.

Cao, L; Quan, XB; Zeng, WJ; Yang, XO; Wang, MJ. (2016). Mechanism of hepatocyte apoptosis [Review]. Journal of Cell Death 9: 19-29. http://dx.doi.org/10.4137/JCD.S39824.

Cattley, RC; Cullen, JM. (2018). Chapter 8. Liver and gall bladder. In MA Wallig; WM Haschek; CG Rousseaux; B Bolon (Eds.), Fundamentals of toxicologic pathology (3rd ed., pp. 125-151). Cambridge, MA: Academic Press. http://dx.doi.org/10.1016/B978-0-12-809841-7.00008-3.

Cellesi, C; Michelangeli, C; Rossolini, GM; Giovannoni, F; Rossolini, A. (1989). Immunity to diphtheria, six to 15 years after a basic three-dose immunization schedule. Journal of Biological Standardization 17: 29-34. http://dx.doi.org/10.1016/0092-1157(89)90025-5.

Chapman, AB; Abraham, WT; Zamudio, S; Coffin, C; Merouani, A; Young, D; Johnson, A; Osorio, F; Goldberg, C; Moore, LG; Dahms, T; Schrier, RW. (1998). Temporal relationships between hormonal and hemodynamic changes in early human pregnancy. Kidney Int 54: 2056-2063. http://dx.doi.org/10.1046/j.1523-1755.1998.00217.x.

Chen, H; Huang, CY; Wilson, MW; Lay, LT; Robertson, LW; Chow, CK; Glauert, HP. (1994). Effect of the peroxisome proliferators ciprofibrate and perfluorodecanoic acid on hepatic cell proliferation and toxicity in Sprague-Dawley rats. Carcinogenesis 15: 2847-2850. http://dx.doi.org/10.1093/carcin/15.12.2847.

Chen, LC; Tatum, V; Glauert, HP; Chow, CK. (2001). Peroxisome proliferator perfluorodecanoic acid alters glutathione and related enzymes. J Biochem Mol Toxicol 15: 107-113. http://dx.doi.org/10.1002/jbt.6.

Cheng, X; Klaassen, CD. (2008a). Critical role of PPAR-alpha in perfluorooctanoic acid- and perfluorodecanoic acid-induced downregulation of Oatp uptake transporters in mouse livers. Toxicol Sci 106: 37-45. http://dx.doi.org/10.1093/toxsci/kfn161.

Cheng, X; Klaassen, CD. (2008b). Perfluorocarboxylic acids induce cytochrome P450 enzymes in mouse liver through activation of PPAR-alpha and CAR transcription factors. Toxicol Sci 106: 29-36. http://dx.doi.org/10.1093/toxsci/kfn147.

Chinje, E; Kentish, P; Jarnot, B; George, M; Gibson, G. (1994). Induction of the CYP4A subfamily by perfluorodecanoic acid: The rat and the guinea pig as susceptible and non-susceptible species. Toxicol Lett 71: 69-75. http://dx.doi.org/10.1016/0378-4274(94)90200-3.

Christenson, B; Böttiger, M. (1986). Serological immunity to diphtheria in Sweden in 1978 and 1984. Scand J Infect Dis 18: 227-233. http://dx.doi.org/10.3109/00365548609032331.

Collier, RJ. (1975). Diphtheria toxin: Mode of action and structure [Review]. Bacteriol Rev 39: 54-85. http://dx.doi.org/10.1128/br.39.1.54-85.1975.

Corton, JC; Peters, JM; Klaunig, JE. (2018). The PPARα-dependent rodent liver tumor response is not relevant to humans: addressing misconceptions [Review]. Arch Toxicol 92: 83-119. http://dx.doi.org/10.1007/s00204-017-2094-7.

Crump, KS. (1995). Calculation of benchmark doses from continuous data. Risk Anal 15: 79-89. http://dx.doi.org/10.1111/j.1539-6924.1995.tb00095.x.

Davis, JW; Vanden Heuvel, JP; Peterson, RE. (1991). Effects of perfluorodecanoic acid on de novo fatty acid and cholesterol synthesis in the rat. Lipids 26: 857-859. http://dx.doi.org/10.1007/BF02536170.

Derbel, M; Hosokawa, M; Satoh, T. (1996). Differences in the induction of carboxylesterase RL4 in rat liver microsomes by various perfluorinated fatty acids, metabolically inert derivatives of fatty acids. Biol Pharm Bull 19: 765-767. http://dx.doi.org/10.1248/bpb.19.765.

Division of Environmental Epidemiology, I, forRAS; Portengen, L; Rignell-Hydbom, A; Jönsson, B, oAG; Lindh, CH; Piersma, AH; Toft, G; Bonde, JP; Heederik, D; Rylander, L; Vermeulen, R. (2016). Prenatal Phthalate, Perfluoroalkyl Acid, and Organochlorine Exposures and Term Birth Weight in Three Birth Cohorts: Multi-Pollutant Models Based on Elastic Net Regression. Environ Health Perspect 124: 365-372.

Dzierlenga, AL; Robinson, VG; Waidyanatha, S; Devito, MJ; Eifrid, MA; Gibbs, ST; Granville, CA; Blystone, CR. (2019). Toxicokinetics of perfluorohexanoic acid (PFHxA), perfluorooctanoic acid (PFOA) and perfluorodecanoic acid (PFDA) in male and female Hsd:Sprague dawley SD rats following intravenous or gavage administration. Xenobiotica 50: 1-11. http://dx.doi.org/10.1080/00498254.2019.1683776.

Dzierlenga, M, .W.; Crawford, L, .; Longnecker, M, .P. (2020). Birth weight and perfluorooctane sulfonic acid: a random-effects meta-regression analysis. Environmental Epidemiology 4: e095. http://dx.doi.org/10.1097/EE9.0000000000000095.

Edwards, SW; Tan, YM; Villeneuve, DL; Meek, ME; McQueen, CA. (2016). Adverse outcome pathways—Organizing toxicological information to improve decision making [Review]. J Pharmacol Exp Ther 356: 170-181. http://dx.doi.org/10.1124/jpet.115.228239.

Frawley, RP; Smith, M; Cesta, MF; Hayes-Bouknight, S; Blystone, C; Kissling, GE; Harris, S; Germolec, D. (2018). Immunotoxic and hepatotoxic effects of perfluoro-n-decanoic acid (PFDA) on female Harlan Sprague-Dawley rats and B6C3F1/N mice when administered by oral gavage for 28 days. J Immunotoxicol 15: 41-52. http://dx.doi.org/10.1080/1547691X.2018.1445145.

Galazka, A; Kardymowicz, B. (1989). Immunity against diphtheria in adults in Poland. Epidemiol Infect 103: 587-593. http://dx.doi.org/10.1017/s0950268800030983.

Galazka, AM; Milstien, JB; Robertson, SE; Cutts, FT. (1993). The immunological basis for immunization module 2 : Diphtheria. (WHO/EPI/Gen/93.11-18). Galazka, AM; Milstien, JB; Robertson, SE; Cutts, FT. http://apps.who.int/iris/bitstream/handle/10665/58891/WHO-EPI-GEN-93.12-mod2-eng.pdf?sequence=38&isAllowed=y.

Gelman, A; Lee, D; Guo, L. (2015). Stan: a probabilistic programming language for bayesian inference and optimization. American Educational Research Journal 40. http://dx.doi.org/10.3102/1076998615606113.

Gibson, H, .M. (1973). Plasma volume and glomerular filtration rate in pregnancy and their relation to differences in fetal growth. Br J Obstet Gynaecol 80: 1067-1074. http://dx.doi.org/10.1111/j.1471-0528.1973.tb02981.x.

Glauert, HP; Srinivasan, S; Tatum, VL; Chen, LC; Saxon, DM; Lay, LT; Borges, T; Baker, M; Chen, LH; Robertson, LW; Chow, CK. (1992). Effects of the peroxisome proliferators ciprofibrate and perfluorodecanoic acid on hepatic cellular antioxidants and lipid peroxidation in rats. Biochem Pharmacol 43: 1353-1359. http://dx.doi.org/10.1016/0006-2952(92)90513-I.

Glynn, A; Berger, U; Bignert, A; Ullah, S; Aune, M; Lignell, S; Darnerud, PO. (2012). Perfluorinated alkyl acids in blood serum from primiparous women in Sweden: serial sampling during pregnancy and nursing, and temporal trends 1996-2010. Environ Sci Technol 46: 9071-9079. http://dx.doi.org/10.1021/es301168c.

Goecke-Flora, CM; Wyman, JF; Jarnot, BM; Reo, NV. (1995). Effect of the peroxisome proliferator perfluoro-n-decanoic acid on glucose transport in the isolated perfused rat liver. Chem Res Toxicol 8: 77-81. http://dx.doi.org/10.1021/tx00043a010.

Goecke, CM; Jarnot, BM; Reo, NV. (1994). Effects of the peroxisome proliferator perfluoro-n-decanoic acid on hepatic gluconeogenesis and glycogenesis: a 13C NMR investigation. Chem Res Toxicol 7: 15-22. http://dx.doi.org/10.1021/tx00037a003.

Grandjean, P; Andersen, EW; Budtz-Jørgensen, E; Nielsen, F; Mølbak, K; Weihe, P; Heilmann, C. (2012). Serum vaccine antibody concentrations in children exposed to perfluorinated compounds. JAMA 307: 391-397. http://dx.doi.org/10.1001/jama.2011.2034.

Grandjean, P; Bateson, T. (2021). RE: Benchmark analysis for PFAS immunotoxicity. Available online at (accessed

Grandjean, P; Heilmann, C; Weihe, P; Nielsen, F; Mogensen, UB; Timmermann, A; Budtz-Jørgensen, E. (2017). Estimated exposures to perfluorinated compounds in infancy predict attenuated vaccine antibody concentrations at age 5-years. J Immunotoxicol 14: 188-195. http://dx.doi.org/10.1080/1547691X.2017.1360968.

Gyllenhammar, I; Diderholm, B; Gustafsson, J; Berger, U; Ridefelt, P; Benskin, JP; Lignell, S; Lampa, E; Glynn, A. (2018). Perfluoroalkyl acid levels in first-time mothers in relation to offspring weight gain and growth. Environ Int 111: 191-199. http://dx.doi.org/10.1016/j.envint.2017.12.002.

Hack, M; Klein, NK; Taylor, HG. (1995). Long-term developmental outcomes of low birth weight infants [Review]. Future Child 5: 176-196. http://dx.doi.org/10.2307/1602514.

Hall, AP; Elcombe, CR; Foster, JR; Harada, T; Kaufmann, W; Knippel, A; Küttler, K; Malarkey, DE; Maronpot, RR; Nishikawa, A; Nolte, T; Schulte, A; Strauss, V; York, MJ. (2012). Liver hypertrophy: a review of adaptive (adverse and non-adverse) changes--conclusions from the 3rd International ESTP Expert Workshop [Review]. Toxicol Pathol 40: 971-994. http://dx.doi.org/10.1177/0192623312448935.

Han, CY. (2018). Update on FXR Biology: Promising Therapeutic Target? International Journal of Molecular Sciences 19. http://dx.doi.org/10.3390/ijms19072069.

Harris, MW; Birnbaum, LS. (1989). Developmental toxicity of perfluorodecanoic acid in C57BL/6N mice. Fundam Appl Toxicol 12: 442-448. http://dx.doi.org/10.1016/0272-0590(89)90018-3.

Harrison, EH; Lane, JS; Luking, S; Van Rafelghem, MJ; Andersen, ME. (1988). Perfluoro-n-decanoic acid: Induction of peroxisomal beta-oxidation by a fatty acid with dioxin-like toxicity. Lipids 23: 115-119. http://dx.doi.org/10.1007/BF02535290.

Hu, J; Li, J; Wang, J; Zhang, A; Dai, J. (2014). Synergistic effects of perfluoroalkyl acids mixtures with J-shaped concentration-responses on viability of a human liver cell line. Chemosphere 96: 81-88. http://dx.doi.org/10.1016/j.chemosphere.2013.07.033.

Huang, CY; Wilson, MW; Lay, LT; Chow, CK; Robertson, LW; Glauert, HP. (1994). Increased 8-hydroxydeoxyguanosine in hepatic DNA of rats treated with the peroxisome proliferators ciprofibrate and perfluorodecanoic acid. Cancer Lett 87: 223-228. http://dx.doi.org/10.1016/0304-3835(94)90226-7.

Ikeda, T; Aiba, K; Fukuda, K; Tanaka, M. (1985). The induction of peroxisome proliferation in rat liver by perfluorinated fatty acids, metabolically inert derivatives of fatty acids. J Biochem 98: 475-482. http://dx.doi.org/10.1093/oxfordjournals.jbchem.a135302.

Intrasuksri, U; Feller, DR. (1991). Comparison of the effects of selected monocarboxylic, dicarboxylic and perfluorinated fatty acids on peroxisome proliferation in primary cultured rat hepatocytes. Biochem Pharmacol 42: 184-188. http://dx.doi.org/10.1016/0006-2952(91)90698-5.

IPCS (International Programme on Chemical Safety). (2007). Harmonization project document no. 4: Part 2: IPCS framework for analysing the relevance of a non-cancer mode of action for humans. Geneva, Switzerland: World Health Organization. http://www.who.int/ipcs/methods/harmonization/areas/cancer_mode.pdf?ua=1.

Ishibashi, H; Hirano, M; Kim, EY; Iwata, H. (2019). In vitro and in silico evaluations of binding affinities of perfluoroalkyl substances to baikal seal and human peroxisome proliferator-activated receptor α. Environ Sci Technol 53: 2181-2188. http://dx.doi.org/10.1021/acs.est.8b07273.

Jaeschke, H; Mcgill, MR; Ramachandran, A. (2012). Oxidant stress, mitochondria, and cell death mechanisms in drug-induced liver injury: lessons learned from acetaminophen hepatotoxicity [Review]. Drug Metab Rev 44: 88-106. http://dx.doi.org/10.3109/03602532.2011.602688.

Johnson, DR; Klaassen, CD. (2002). Regulation of rat multidrug resistance protein 2 by classes of prototypical microsomal enzyme inducers that activate distinct transcription pathways. Toxicol Sci 67: 182-189. http://dx.doi.org/10.1093/toxsci/67.2.182.

Joshi-Barve, S; Kirpich, I; Cave, MC; Marsano, LS; McClain, CJ. (2015). Alcoholic, nonalcoholic, and toxicant-associated steatohepatitis: Mechanistic similarities and differences [Review]. CMGH 1: 356-367. http://dx.doi.org/10.1016/j.jcmgh.2015.05.006.

Judson, RS; Magpantay, FM; Chickarmane, V; Haskell, C; Tania, N; Taylor, J; Xia, M; Huang, R; Rotroff, DM; Filer, DL; Houck, KA; Martin, MT; Sipes, N; Richard, AM; Mansouri, K; Setzer, RW; Knudsen, TB; Crofton, KM; Thomas, RS. (2015). Integrated model of chemical perturbations of a biological pathway using 18 in vitro high throughput screening assays for the estrogen receptor. Toxicol Sci 148: 137-154. http://dx.doi.org/10.1093/toxsci/kfv168.

Kaiser, JP; Lipscomb, JC; Wesselkamper, SC. (2012). Putative mechanisms of environmental chemical-induced steatosis. Int J Toxicol 31: 551-563. http://dx.doi.org/10.1177/1091581812466418.

Kawashima, Y; Kobayashi, H; Miura, H; Kozuka, H. (1995). Characterization of hepatic responses of rat to administration of perfluorooctanoic and perfluorodecanoic acids at low levels. Toxicology 99: 169-178. http://dx.doi.org/10.1016/0300-483X(95)03027-D.

Kelling, CK; Van Rafelghem, MJ; Drake, RL; Menahan, LA; Peterson, RE. (1986). Regulation of hepatic malic enzyme by perfluorodecanoic acid. J Biochem Toxicol 1: 23-37. http://dx.doi.org/10.1002/jbt.2570010304.

Kelling, CK; Van Rafelghem, MJ; Menahan, LA; Peterson, RE. (1987). Effects of perfluorodecanoic acid on hepatic indices of thyroid status in the rat. Biochem Pharmacol 36: 1337-1344. http://dx.doi.org/10.1016/0006-2952(87)90091-8.

Kim, SC; Hong, JT; Jang, SJ; Kang, WS; Yoo, HS; Yun, YP. (1998). Formation of 8-oxodeoxyguanosine in liver DNA and hepatic injury by peroxisome proliferator clofibrate and perfluorodecanoic acid in rats. J Toxicol Sci 23: 113-119. http://dx.doi.org/10.2131/jts.23.2_113.

Kim, SJ; Choi, EJ; Choi, GW; Lee, YB; Cho, HY. (2019). Exploring sex differences in human health risk assessment for PFNA and PFDA using a PBPK model. Arch Toxicol 93: 311-330. http://dx.doi.org/10.1007/s00204-018-2365-y.

Kleinstreuer, NC; Ceger, P; Watt, ED; Martin, M; Houck, K; Browne, P; Thomas, RS; Casey, WM; Dix, DJ; Allen, D; Sakamuru, S; Xia, M; Huang, R; Judson, R. (2017). Development and validation of a computational model for androgen receptor activity. Chem Res Toxicol 30: 946-964. http://dx.doi.org/10.1021/acs.chemrestox.6b00347.

Kozuka, H; Watanabe, T; Horie, S; Yamada, J; Suga, T; Ikeda, T. (1991a). Characteristics of peroxisome proliferation: co-induction of peroxisomal fatty acid oxidation-related enzymes with microsomal laurate hydroxylase. Chem Pharm Bull (Tokyo) 39: 1267-1271. http://dx.doi.org/10.1248/cpb.39.1267.

Kozuka, H; Yamada, J; Horie, S; Watanabe, T; Suga, T; Ikeda, T. (1991b). Characteristics of induction of peroxisomal fatty acid oxidation-related enzymes in rat liver by drugs:Relationships between structure and inducing activity. Biochem Pharmacol 41: 617-623. http://dx.doi.org/10.1016/0006-2952(91)90635-I.

Kruschke, JK. (2021). Bayesian analysis reporting guidelines. Nat Hum Behav 5: 1282-1291. http://dx.doi.org/10.1038/s41562-021-01177-7.

Kudo, N; Bandai, N; Suzuki, E; Katakura, M; Kawashima, Y. (2000). Induction by perfluorinated fatty acids with different carbon chain length of peroxisomal beta-oxidation in the liver of rats. Chem Biol Interact 124: 119-132. http://dx.doi.org/10.1016/S0009-2797(99)00150-7.

Kudo, N; Kawashima, Y. (2003). Induction of triglyceride accumulation in the liver of rats by perfluorinated fatty acids with different carbon chain lengths: Comparison with induction of peroxisomal beta-oxidation. Biol Pharm Bull 26: 47-51. http://dx.doi.org/10.1248/bpb.26.47.

Langley, AE. (1990). Effects of perfluoro-n-decanoic acid on the respiratory activity of isolated rat liver mitochondria. J Toxicol Environ Health 29: 329-336. http://dx.doi.org/10.1080/15287399009531395.

Lenters, V; Portengen, L; Rignell-Hydbom, A; Jönsson, BA; Lindh, CH; Piersma, AH; Toft, G; Bonde, JP; Heederik, D; Rylander, L; Vermeulen, R. (2016). Prenatal phthalate, perfluoroalkyl acid, and organochlorine exposures and term birth weight in three birth cohorts: multi-pollutant models based on elastic net regression. Environ Health Perspect 124: 365-372. http://dx.doi.org/10.1289/ehp.1408933.

Li, C; Ren, X; Cao, L; Qin, W; Guo, LH. (2019). Investigation of binding and activity of perfluoroalkyl substances to the human peroxisome proliferator-activated receptor β/δ. Environ Sci Process Impacts 21: 1908-1914. http://dx.doi.org/10.1039/c9em00218a.

Li, K; Gao, P; Xiang, P; Zhang, X; Cui, X; Ma, LQ. (2017). Molecular mechanisms of PFOA-induced toxicity in animals and humans: Implications for health risks [Review]. Environ Int 99: 43-54. http://dx.doi.org/10.1016/j.envint.2016.11.014.

Li, KM; Zhao, Q; Fan, ZY; Jia, SY; Liu, Q; Liu, FY; Liu, SL. (2022). The toxicity of perfluorodecanoic acid is mainly manifested as a deflected immune function. Mol Biol Rep 49: 4365-4376. http://dx.doi.org/10.1007/s11033-022-07272-w.

Li, T; Yu, RT; Atkins, AR; Downes, M; Tukey, RH; Evans, RM. (2012). Targeting the pregnane X receptor in liver injury [Review]. Expert Opin Ther Targets 16: 1075-1083. http://dx.doi.org/10.1517/14728222.2012.715634.

Liang, JL; Tiwari, T; Moro, P; Messonnier, NE; Reingold, A; Sawyer, M; Clark, TA. (2018). Prevention of pertussis, tetanus, and diphtheria with vaccines in the United States: Recommendations of the Advisory Committee on Immunization Practices (ACIP). MMWR Recomm Rep 67: 1-44. http://dx.doi.org/10.15585/mmwr.rr6702a1.

Lim, JJ; Suh, Y; Faustman, EM; Cui, JY. (2021). Regulation of transporters by perfluorinated carboxylic acids in HepaRG cells. Drug Metab Dispos 50: 1396-1413. http://dx.doi.org/10.1124/dmd.121.000477.

Long, M; Ghisari, M; Bonefeld-Jørgensen, EC. (2013). Effects of perfluoroalkyl acids on the function of the thyroid hormone and the aryl hydrocarbon receptor. Environ Sci Pollut Res Int 20: 8045-8056. http://dx.doi.org/10.1007/s11356-013-1628-7.

Luo, D; Wu, WX; Pan, YA; Du, BB; Shen, MJ; Zeng, LX. (2021). Associations of prenatal exposure to per- and polyfluoroalkyl substances with the neonatal birth size and hormones in the growth hormone/insulin-like growth factor axis. Environ Sci Technol 55: 11859-11873. http://dx.doi.org/10.1021/acs.est.1c02670.

Luo, M; Tan, Z; Dai, M; Song, D; Lin, J; Xie, M; Yang, J; Sun, L; Wei, D; Zhao, J; Gonzalez, FJ; Liu, A. (2017). Dual action of peroxisome proliferator-activated receptor alpha in perfluorodecanoic acid-induced hepatotoxicity. Arch Toxicol 91: 897-907. http://dx.doi.org/10.1007/s00204-016-1779-7.

Ma, K; Saha, PK; Chan, L; Moore, DD. (2006). Farnesoid X receptor is essential for normal glucose homeostasis. J Clin Invest 116: 1102-1109. http://dx.doi.org/10.1172/JCI25604.

Ma, Y; Sachdeva, K; Liu, J; Song, X; Li, Y; Yang, D; Deng, R; Chichester, CO; Yan, B. (2005). Clofibrate and perfluorodecanoate both upregulate the expression of the pregnane X receptor but oppositely affect its ligand-dependent induction on cytochrome P450 3A23. Biochem Pharmacol 69: 1363-1371. http://dx.doi.org/10.1016/j.bcp.2005.02.011.

Mackowiak, B; Hodge, J; Stern, S; Wang, H. (2018). The roles of xenobiotic receptors: Beyond chemical disposition [Review]. Drug Metab Dispos 46: 1361-1371. http://dx.doi.org/10.1124/dmd.118.081042.

Maher, JM; Aleksunes, LM; Dieter, MZ; Tanaka, Y; Peters, JM; Manautou, JE; Klaassen, CD. (2008). Nrf2- and PPAR alpha-mediated regulation of hepatic Mrp transporters after exposure to perfluorooctanoic acid and perfluorodecanoic acid. Toxicol Sci 106: 319-328. http://dx.doi.org/10.1093/toxsci/kfn177.

Malhi, H; Gores, GJ. (2008). Cellular and molecular mechanisms of liver injury [Review]. Gastroenterology 134: 1641-1654. http://dx.doi.org/10.1053/j.gastro.2008.03.002.

Manzano-Salgado, CB; Casas, M; Lopez-Espinosa, MJ; Ballester, F; Iñiguez, C; Martinez, D; Costa, O; Santa-Marina, L; Pereda-Pereda, E; Schettgen, T; Sunyer, J; Vrijheid, M. (2017). Prenatal exposure to perfluoroalkyl substances and birth outcomes in a Spanish birth cohort. Environ Int 108: 278-284. http://dx.doi.org/10.1016/j.envint.2017.09.006.

Meek, ME; Boobis, A; Cote, I; Dellarco, V; Fotakis, G; Munn, S; Seed, J; Vickers, C. (2014). New developments in the evolution and application of the WHO/IPCS framework on mode of action/species concordance analysis [Review]. J Appl Toxicol 34: 1-18. http://dx.doi.org/10.1002/jat.2949.

Mellor, CL; Steinmetz, FP; Cronin, MT. (2016). The identification of nuclear receptors associated with hepatic steatosis to develop and extend adverse outcome pathways [Review]. Crit Rev Toxicol 46: 138-152. http://dx.doi.org/10.3109/10408444.2015.1089471.

Meng, Q; Inoue, K; Ritz, B; Olsen, J; Liew, Z. (2018). Prenatal exposure to perfluoroalkyl substances and birth outcomes; an updated analysis from the danish national birth

cohort. Int J Environ Res Public Health 15: 1832. http://dx.doi.org/10.3390/ijerph15091832.

Morken, NH; Travlos, GS; Wilson, RE; Eggesbø, M; Longnecker, MP. (2014). Maternal glomerular filtration rate in pregnancy and fetal size. PLoS ONE 9: e101897. http://dx.doi.org/10.1371/journal.pone.0101897.

NTP (National Toxicology Program). (2018). 28-day evaluation of the toxicity (C20615) of perfluorodecanoic acid (PFDA) (335-76-2) on Harlan Sprague-Dawley rats exposed via gavage [NTP]. U.S. Department of Health and Human Services. http://dx.doi.org/10.22427/NTP-DATA-002-02652-0004-0000-1.

Oguro, T; Hayashi, M; Nakajo, S; Numazawa, S; Yoshida, T. (1998). The expression of heme oxygenase-1 gene responded to oxidative stress produced by phorone, a glutathione depletor, in the rat liver; the relevance to activation of c-jun n-terminal kinase. J Pharmacol Exp Ther 287: 773-778.

Ohmori, K; Kudo, N; Katayama, K; Kawashima, Y. (2003). Comparison of the toxicokinetics between perfluorocarboxylic acids with different carbon chain length. Toxicology 184: 135-140. http://dx.doi.org/10.1016/S0300-483X(02)00573-5.

Ojo, AF; Peng, C; Ng, JC. (2020). Combined effects and toxicological interactions of perfluoroalkyl and polyfluoroalkyl substances mixtures in human liver cells (HepG2). Environ Pollut 263: 114182. http://dx.doi.org/10.1016/j.envpol.2020.114182.

Ojo, AF; Xia, Q; Peng, C; Ng, JC. (2021). Evaluation of the individual and combined toxicity of perfluoroalkyl substances to human liver cells using biomarkers of oxidative stress. Chemosphere 281: 130808. http://dx.doi.org/10.1016/j.chemosphere.2021.130808.

Olson, CT; Andersen, ME. (1983). The acute toxicity of perfluorooctanoic and perfluorodecanoic acids in male rats and effects on tissue fatty acids. Toxicol Appl Pharmacol 70: 362-372. http://dx.doi.org/10.1016/0041-008x(83)90154-0.

Passen, EL; Andersen, BR. (1986). Clinical tetanus despite a protective level of toxin-neutralizing antibody [Case Report]. JAMA 255: 1171-1173. http://dx.doi.org/10.1001/jama.1986.03370090093029.

Patel, JC; Mehta, BC. (1999). Tetanus: Study of 8,697 cases. Indian J Med Sci 53: 393-401.

Permadi, H; Lundgren, B; Andersson, K; Sundberg, C; Depierre, JW. (1993). Effects of perfluoro fatty acids on peroxisome proliferation and mitochondrial size in mouse liver: dose and time factors and effect of chain length. Xenobiotica 23: 761-770. http://dx.doi.org/10.3109/00498259309166782.

Powers, RH; Aust, SD. (1986). The effects of nonadecafluoro-n-decanoic acid on serum retinol and hepatic retinyl palmitate hydrolase activity in male Sprague-Dawley rats. J Biochem Toxicol 1: 27-42. http://dx.doi.org/10.1002/jbt.2570010204.

Reo, NV; Goecke, CM; Narayanan, L; Jarnot, BM. (1994). Effects of perfluoro-n-octanoic acid, perfluoro-n-decanoic acid, and clofibrate on hepatic phosphorus metabolism in rats and guinea pigs in vivo. Toxicol Appl Pharmacol 124: 165-173. http://dx.doi.org/10.1006/taap.1994.1020.

Reyes, L; Mañalich, R. (2005). Long-term consequences of low birth weight [Review]. Kidney Int Suppl 68: S107-S111. http://dx.doi.org/10.1111/j.1523-1755.2005.09718.x.

Robledo, CA; Yeung, E; Mendola, P; Sundaram, R; Maisog, J; Sweeney, AM; Barr, DB; Louis, GM. (2015). Preconception maternal and paternal exposure to persistent organic pollutants and birth size: the LIFE study. Environ Health Perspect 123: 88-94. http://dx.doi.org/10.1289/ehp.1308016.

Rosen, MB; Das, KP; Wood, CR; Wolf, CJ; Abbott, BD; Lau, C. (2013). Evaluation of perfluoroalkyl acid activity using primary mouse and human hepatocytes. Toxicology 308: 129-137. http://dx.doi.org/10.1016/j.tox.2013.03.011.

Rosenmai, AK; Ahrens, L; le Godec, T; Lundqvist, J; Oskarsson, A. (2018). Relationship between peroxisome proliferator-activated receptor alpha activity and cellular concentration of 14 perfluoroalkyl substances in HepG2 cells. J Appl Toxicol 38: 219-226. http://dx.doi.org/10.1002/jat.3515.

Roth, RA; Jaeschke, H; Luyendyk, JP. (2019). Chapter 13: Toxic responses of the liver. In CD Klaassen (Ed.), Casarett & Doull's toxicology: The basic science of poisons (9th ed., pp. 719-766). New York, NY: McGraw Hill.

Routti, H; Berg, MK; Lille-Langøy, R; Øygarden, L; Harju, M; Dietz, R; Sonne, C; Goksøyr, A. (2019). Environmental contaminants modulate the transcriptional activity of polar bear (Ursus maritimus) and human peroxisome proliferator-activated receptor alpha (PPARA). Sci Rep 9: 6918. http://dx.doi.org/10.1038/s41598-019-43337-w.

Russell, DW. (2003). The enzymes, regulation, and genetics of bile acid synthesis [Review]. Annu Rev Biochem 72: 137-174. http://dx.doi.org/10.1146/annurev.biochem.72.121801.161712.

Sagiv, SK; Rifas-Shiman, SL; Fleisch, AF; Webster, TF; Calafat, AM; Ye, X; Gillman, MW; Oken, E. (2018). Early Pregnancy Perfluoroalkyl Substance Plasma Concentrations and Birth Outcomes in Project Viva: Confounded by Pregnancy Hemodynamics? Am J Epidemiol 187: 793-802. http://dx.doi.org/10.1093/aje/kwx332.

Salvatier, J; Wiecki, TV; Fonnesbeck, C. (2016). Probabilistic programming in Python using PyMC3. PeerJ Computer Science 2: e55. http://dx.doi.org/10.7717/peerj-cs.55.

Sanghavi, M; Rutherford, JD. (2014). Cardiovascular physiology of pregnancy. Circulation 130: 1003-1008. http://dx.doi.org/10.1161/CIRCULATIONAHA.114.009029.

Schramm, H; Friedberg, T; Robertson, LW; Oesch, F; Kissel, W. (1989). Perfluorodecanoic acid decreases the enzyme activity and the amount of glutathione S-transferases proteins and mRNAs in vivo. Chem Biol Interact 70: 127-143. http://dx.doi.org/10.1016/0009-2797(89)90068-9.

Selgrade, MK. (2007). Immunotoxicity: The risk is real [Review]. Toxicol Sci 100: 328-332. http://dx.doi.org/10.1093/toxsci/kfm244.

Sovadinova, I; Babica, P; Böke, H; Kumar, E; Wilke, A; Park, JS; Trosko, JE; Upham, BL. (2015). Phosphatidylcholine Specific PLC-Induced Dysregulation of Gap Junctions, a Robust Cellular Response to Environmental Toxicants, and Prevention by Resveratrol in a Rat Liver Cell Model. PLoS ONE 10: e0124454. http://dx.doi.org/10.1371/journal.pone.0124454.

Starling, AP; Adgate, JL; Hamman, RF; Kechris, K; Calafat, AM; Ye, X; Dabelea, D. (2017). Perfluoroalkyl substances during pregnancy and offspring weight and adiposity at birth:

Examining mediation by maternal fasting glucose in the healthy start study. Environ Health Perspect 125: 067016. http://dx.doi.org/10.1289/EHP641.

Steenland, K; Barry, V; Savitz, D. (2018). Serum perfluorooctanoic acid and birthweight: an updated meta-analysis with bias analysis. Epidemiology 29: 765-776. http://dx.doi.org/10.1097/EDE.0000000000000903.

Sterchele, PF; Sun, H; Peterson, RE; Vanden Heuvel, JP. (1996). Regulation of peroxisome proliferator-activated receptor-alpha mRNA in rat liver. Arch Biochem Biophys 326: 281-289. http://dx.doi.org/10.1006/abbi.1996.0077.

Sterchele, PF; Vanden Heuvel, JP; Davis, JW; Shrago, E; Knudsen, J; Peterson, RE. (1994). Induction of hepatic acyl-CoA-binding protein and liver fatty acid-binding protein by perfluorodecanoic acid in rats. Lack of correlation with hepatic long-chain acyl-CoA levels. Biochem Pharmacol 48: 955-966. http://dx.doi.org/10.1016/0006-2952(94)90366-2.

Takacs, ML; Abbott, BD. (2007). Activation of mouse and human peroxisome proliferator-activated receptors (alpha, beta/delta, gamma) by perfluorooctanoic acid and perfluorooctane sulfonate. Toxicol Sci 95: 108-117. http://dx.doi.org/10.1093/toxsci/kfl135.

Takagi, A; Sai, K; Umemura, T; Hasegawa, R; Kurokawa, Y. (1991). Short-term exposure to the peroxisome proliferators, perfluorooctanoic acid and perfluorodecanoic acid, causes significant increase of 8-hydroxydeoxyguanosine in liver DNA of rats. Cancer Lett 57: 55-60. http://dx.doi.org/10.1016/0304-3835(91)90063-N.

Takahashi, S; Tanaka, N; Golla, S; Fukami, T; Krausz, KW; Polunas, MA; Weig, BC; Masuo, Y; Xie, C; Jiang, C; Gonzalez, FJ. (2017). Editor's highlight: farnesoid X receptor protects against low-dose carbon tetrachloride-induced liver injury through the taurocholate-JNKpathway. Toxicol Sci 158: 334–346. http://dx.doi.org/10.1093/toxsci/kfx094.

Tian, M, .; Reichetzeder, C, .; Li, J, .; Hocher, B, . (2019). Low birth weight, a risk factor for diseases in later life, is a surrogate of insulin resistance at birth. J Hypertens 37: 2123-2134. http://dx.doi.org/10.1097/HJH.0000000000002156.

U.S. EPA (U.S. Environmental Protection Agency). (2012). Benchmark dose technical guidance [EPA Report]. (EPA100R12001). Washington, DC: U.S. Environmental Protection Agency, Risk Assessment Forum. https://www.epa.gov/risk/benchmark-dose-technical-guidance.

U.S. EPA (U.S. Environmental Protection Agency). (2016a). Health effects support document for perfluorooctane sulfonate (PFOS) [EPA Report]. (EPA 822-R-16-002). Washington, DC: U.S. Environmental Protection Agency, Office of Water, Health and Ecological Criteria Division. https://www.epa.gov/sites/production/files/2016-05/documents/pfos_hesd_final_508.pdf.

U.S. EPA (U.S. Environmental Protection Agency). (2016b). Health effects support document for perfluorooctanoic acid (PFOA) [EPA Report]. (EPA 822-R-16-003). Washington, DC: U.S. Environmental Protection Agency, Office of Water, Health and Ecological Criteria Division. https://www.epa.gov/sites/production/files/2016-05/documents/pfoa_hesd_final-plain.pdf.

U.S. EPA (U.S. Environmental Protection Agency). (2019). CompTox Chemicals Dashboard [Database]. Research Triangle Park, NC. Retrieved from https://comptox.epa.gov/dashboard

Valvi, D; Oulhote, Y; Weihe, P; Dalgård, C; Bjerve, KS; Steuerwald, U; Grandjean, P. (2017). Gestational diabetes and offspring birth size at elevated environmental pollutant exposures. Environ Int 107: 205-215. http://dx.doi.org/10.1016/j.envint.2017.07.016.

van Otterdijk, FM. (2007). Repeated dose 90-day oral toxicity study with MTDID 8391 by daily gavage in the rat followed by a 3-week recovery period. (Study Number 06-398). Maplewood, MN: 3M.

Van Rafelghem, MJ; Andersen, ME. (1988). The effects of perfluorodecanoic acid on hepatic stearoyl-coenzyme A desaturase and mixed function oxidase activities in rats. Fundam Appl Toxicol 11: 503-510. http://dx.doi.org/10.1016/0272-0590(88)90114-5.

Van Rafelghem, MJ; Mattie, DR; Bruner, RH; Andersen, ME. (1987). Pathological and hepatic ultrastructural effects of a single dose of perfluoro-n-decanoic acid in the rat, hamster, mouse, and guinea pig. Fundam Appl Toxicol 9: 522-540. http://dx.doi.org/10.1016/0272-0590(87)90034-0.

Van Rafelghem, MJ; Vanden Heuvel, JP; Menahan, LA; Peterson, RE. (1988). Perfluorodecanoic acid and lipid metabolism in the rat. Lipids 23: 671-678. http://dx.doi.org/10.1007/BF02535666.

Vanden Heuvel, JP; Kuslikis, BI; Shrago, E; Peterson, RE. (1991). Inhibition of long-chain acyl-CoA synthetase by the peroxisome proliferator perfluorodecanoic acid in rat hepatocytes. Biochem Pharmacol 42: 295-302. http://dx.doi.org/10.1016/0006-2952(91)90716-I.

Vanden Heuvel, JP; Sterchele, PF; Nesbit, DJ; Peterson, RE. (1993). Coordinate induction of acyl-CoA binding protein, fatty acid binding protein and peroxisomal beta-oxidation by peroxisome proliferators. Biochim Biophys Acta 1177: 183-190. http://dx.doi.org/10.1016/0167-4889(93)90039-R.

Wahlang, B; Beier, JI; Clair, HB; Bellis-Jones, HJ; Falkner, K; Mcclain, CJ; Cave, MC. (2013). Toxicant-associated steatohepatitis [Review]. Toxicol Pathol 41: 343-360. http://dx.doi.org/10.1177/0192623312468517.

Wallace, KB; Kissling, GE; Melnick, RL; Blystone, CR. (2013). Structure-activity relationships for perfluoroalkane-induced in vitro interference with rat liver mitochondrial respiration. Toxicol Lett 222: 257-264. http://dx.doi.org/10.1016/j.toxlet.2013.07.025.

Wang, D; Gao, Q; Wang, T; Kan, Z; Li, X; Hu, L; Peng, CY; Qian, F; Wang, Y; Granato, D. (2020). Green tea polyphenols and epigallocatechin-3-gallate protect against perfluorodecanoic acid induced liver damage and inflammation in mice by inhibiting NLRP3 inflammasome activation. Food Res Int 127: 108628. http://dx.doi.org/10.1016/j.foodres.2019.108628.

Wang, YM; Chai, SC; Brewer, CT; Chen, T. (2014). Pregnane X receptor and drug-induced liver injury [Review]. Expert Opin Drug Metab Toxicol 10: 1521-1532. http://dx.doi.org/10.1517/17425255.2014.963555.

Watt, ED; Judson, RS. (2018). Uncertainty quantification in ToxCast high throughput screening. PLoS ONE 13: e0196963. http://dx.doi.org/10.1371/journal.pone.0196963.

Weisskopf, MG; Seals, RM; Webster, TF. (2018). Bias amplification in epidemiologic analysis of exposure to mixtures. Environ Health Perspect 126. http://dx.doi.org/10.1289/EHP2450.

Weisskopf, MG; Webster, TF. (2017). Trade-offs of personal versus more proxy exposure measures in environmental epidemiology. Epidemiology 28: 635-643. http://dx.doi.org/10.1097/EDE.0000000000000686.

Whitworth, KW; Haug, LS; Baird, DD; Becher, G; Hoppin, JA; Skjaerven, R; Thomsen, C; Eggesbo, M; Travlos, G; Wilson, R; Longnecker, MP. (2012). Perfluorinated compounds and subfecundity in pregnant women. Epidemiology 23: 257-263. http://dx.doi.org/10.1097/EDE.0b013e31823b5031.

Wielsøe, M; Long, M; Ghisari, M; Bonefeld-Jørgensen, EC. (2015). Perfluoroalkylated substances (PFAS) affect oxidative stress biomarkers in vitro. Chemosphere 129: 239-245. http://dx.doi.org/10.1016/j.chemosphere.2014.10.014.

Wikström, S; Lin, PI; Lindh, CH; Shu, H; Bornehag, CG. (2020). Maternal serum levels of perfluoroalkyl substances in early pregnancy and offspring birth weight. Pediatr Res 87: 1093-1099. http://dx.doi.org/10.1038/s41390-019-0720-1.

Witzmann, F; Coughtrie, M; Fultz, C; Lipscomb, J. (1996). Effect of structurally diverse peroxisome proliferators on rat hepatic sulfotransferase. Chem Biol Interact 99: 73-84. http://dx.doi.org/10.1016/0009-2797(95)03661-X.

Witzmann, FA; Parker, DN. (1991). Hepatic protein pattern alterations following perfluorodecanoic acid exposure in rats. Toxicol Lett 57: 29-36. http://dx.doi.org/10.1016/0378-4274(91)90116-N.

Wolf, CJ; Schmid, JE; Lau, C; Abbott, BD. (2012). Activation of mouse and human peroxisome proliferator-activated receptor-alpha (PPARα) by perfluoroalkyl acids (PFAAs): further investigation of C4-C12 compounds. Reprod Toxicol 33: 546-551. http://dx.doi.org/10.1016/j.reprotox.2011.09.009.

Wolf, CJ; Takacs, ML; Schmid, JE; Lau, C; Abbott, BD. (2008). Activation of mouse and human peroxisome proliferator-activated receptor alpha by perfluoroalkyl acids of different functional groups and chain lengths. Toxicol Sci 106: 162-171. http://dx.doi.org/10.1093/toxsci/kfn166.

Woods, MM; Lanphear, BP; Braun, JM; McCandless, LC. (2017). Gestational exposure to endocrine disrupting chemicals in relation to infant birth weight: A Bayesian analysis of the HOME Study. Environ Health 16: 115. http://dx.doi.org/10.1186/s12940-017-0332-3.

Xu, K; Guidez, F; Glasow, A; Chung, D; Petrie, K; Stegmaier, K; Wang, KK; Zhang, J; Jing, Y; Zelent, A; Waxman, S. (2005). Benzodithiophenes potentiate differentiation of acute promyelocytic leukemia cells by lowering the threshold for ligand-mediated corepressor/coactivator exchange with retinoic acid receptor alpha and enhancing changes in all-trans-retinoic acid-regulated gene expression. Cancer Res 65: 7856-7865. http://dx.doi.org/10.1158/0008-5472.CAN-05-1056.

Yamamoto, A; Kawashima, Y. (1997). Perfluorodecanoic acid enhances the formation of oleic acid in rat liver. Biochem J 325 (Pt 2): 429-434. http://dx.doi.org/10.1042/bj3250429.

Yang, X; Schnakenberg, LK; Shi, Q; Salminen, WF. (2014). Hepatic toxicity biomarkers. In RC Gupta (Ed.), Biomarkers in Toxicology (pp. 241-259). New York, NY: Academic Press. http://dx.doi.org/10.1016/B978-0-12-404630-6.00013-0.

Yao, Q; Gao, Y; Zhang, Y; Qin, K; Liew, Z; Tian, Y. (2021). Associations of paternal and maternal per- and polyfluoroalkyl substances exposure with cord serum reproductive hormones, placental steroidogenic enzyme and birth weight. Chemosphere 285: 131521. http://dx.doi.org/10.1016/j.chemosphere.2021.131521.

Zhang, L; Ren, XM; Guo, LH. (2013). Structure-based investigation on the interaction of perfluorinated compounds with human liver fatty acid binding protein. Environ Sci Technol 47: 11293-11301. http://dx.doi.org/10.1021/es4026722.

Zhang, LY; Ren, XM; Wan, B; Guo, LH. (2014). Structure-dependent binding and activation of perfluorinated compounds on human peroxisome proliferator-activated receptor γ. Toxicol Appl Pharmacol 279: 275-283. http://dx.doi.org/10.1016/j.taap.2014.06.020.

Zhang, YM; Dong, XY; Fan, LJ; Zhang, ZL; Wang, Q; Jiang, N; Yang, XS. (2017). Poly- and perfluorinated compounds activate human pregnane X receptor. Toxicology 380: 23-29. http://dx.doi.org/10.1016/j.tox.2017.01.012.